CALIBRATION OF LINEAR IMAGER CAMERA FOR RELATIVE POSE ESTIMATION

A Thesis

by

ROSHAN SURESH KUMAR

Submitted to the Office of Graduate and Professional Studies of
Texas A&M University
in partial fulfillment of the requirements for the degree of

MASTER OF SCIENCE

Co-Chairs of Committee,	John Junkins
	Manoranjan Majji
Committee Members,	Srikanth Saripalli
Head of Department,	Rodney Bowersox

May 2019

Major Subject: Aerospace Engineering

ABSTRACT

The process of camera calibration is of paramount importance in order to employ any vision based sensor for relative navigation purposes. Understanding and quantifying the physical process that converts the external electromagnetic stimulus into an image inside a camera is key to relating the position of a body in an image to its pose in the real world. Both camera calibration and relative navigation are extensively explored topics. In the topic of camera calibration, various algorithms have been proposed that model the image formation process in different ways. This research utilizes the Homography approach proposed by Zhang [1] along with two distortion models: Brown's nonlinear Distortion Model and the Geometric Distortion Model in order to model the intrinsic distortion and discrete image formation process. The idea of this research is to utilize the intrinsic parameters estimated using the homography optimization approach for the estimation of the relative pose of an object in the camera's field of view. A nonlinear optimization based approach is presented for this purpose. The camera used here is the Phasespace Motion Capture camera [2] which utilizes linear imagers to form a fictitious image plane. Hence, the applicability of the two distortion models is tested through multiple datasets. Through testing with three datasets, it is found that neither distortion model is adequate to describe the distortion and image formation process in the Phasespace camera. A further test is conducted in order to validate the efficacy of the optimization based approach for relative pose estimation.

DEDICATION

To my parents, friends, teachers throughout my years of education and most importantly, to the vast immeasurable void we call space, and also omniscience.

ACKNOWLEDGMENTS

A long time ago in a smoky dusty city far far away, a scrawny, wheatish complexioned kid looked up to the sky and swore, in the presence of all the omniscient, omnipresent and omnipotent entities commonly given the name "Gods", that he shall endeavor to contribute significantly to mankind's efforts to further explore and understand the frontiers of space. Fifteen years have passed since then, and he now finds himself in one of the foremost institutions that imparts the knowledge he requires and indeed proudly wields to realize his dreams. He now stands at the altar, eager to prove his worth and achieve a key milestone in his academic career. Texas A&M University will always hold a special place in my heart.

The journey has an uneasy but memorable one. It all started at home with my parents encouraging free thought and exploration of my career possibilities, something that I cannot thank them enough for. They have been a steady pillar of support and a non judgmental wall for me to rant away my grievances of the day. My grandfather has been an especially humble source of inspiration for me. The heights he achieved in his career only serve to motivate me further. All the relatives in my extended family also deserve a shout out, especially my cousins, most of whom are pursuing careers in non conventional fields such as journalism. Every conversation with any of them expands the vistas of my outlook on life, serving to put my academic achievements in perspective, keeping me grounded.

My advisors Drs. John Junkins and Manoranjan Majji have been invaluable sources of inspiration in my effort to navigate through graduate academic life. They have been extremely helpful during discussions in giving some direction for my work. I cannot thank them both enough.

I consider myself extremely fortunate to be surrounded by a group of friends who I can unquestionably say are my equals, if not superiors, in intellectual wealth, academic knowledge and ambition. They constantly serve as a measure against complacency and arrogance.

CONTRIBUTORS AND FUNDING SOURCES

Contributors

This work was supervised by a thesis committee consisting of Professors John Junkins and Manoranjan Majji of the Department of Aerospace Engineering and Professor Srikanth Saripalli of the Department of Mechanical Engineering.

All other work conducted for the thesis was completed by the student, under the advisement of Drs. John Junkins and Manoranjan Majji of the Department of Aerospace Engineering. Valuable insights were provided by Dr. Nagavenkat Adurthi of the Department of Aerospace Engineering. Experiments were conducted at the Land, Air and Space Robotics (LASR) Lab at Texas A&M University.

Funding Sources

There are no outside funding contributions to acknowledge related to the research and compilation of this document.

NOMENCLATURE

s	Scaling factor in pinhole projection model
$\tilde{\boldsymbol{m}}$	Beacon Image Plane coordinates (=$\begin{bmatrix} u & v & 1 \end{bmatrix}^T$)
$\tilde{\boldsymbol{M}}$	Beacon Inertial Frame coordinates (=$\begin{bmatrix} X & Y & 1 \end{bmatrix}^T$)
A	Camera Intrinsic Parameter matrix
R	Rotation matrix from Camera frame to Inertial frame
$\boldsymbol{t}$	Translation vector from Camera frame to Inertial frame
α	Focal length in the $\hat{\boldsymbol{u}}$ direction of the image plane
β	Focal length in the $\hat{\boldsymbol{v}}$ direction of the image plane
c	skewness factor
u_0	Principal Offset in the $\hat{\boldsymbol{u}}$ direction of the image plane
v_0	Principal Offset in the $\hat{\boldsymbol{v}}$ direction of the image plane
H	Homography matrix
J	Scalar cost function for nonlinear least squares algorithm
Q	Skew symmetric matrix associated with the Classical Rodrigues Parameters (CRP)
$\boldsymbol{q}$	CRP vector
U	Matrix of left singular vectors of R
V	Matrix of right singular vectors of R
S	Diagonal singular values matrix of R
$\hat{\boldsymbol{d}}_{\mathbf{0}}$	Unit vector along detector 0
$\hat{\boldsymbol{d}}_{\mathbf{1}}$	Unit vector along detector 1
$\hat{\boldsymbol{u}}$	Unit vector along image plane x-axis

$\hat{\boldsymbol{v}}$	Unit vector along image plane y-axis
$\boldsymbol{k}$	Vector of distortion coefficients for Brown's Distortion Model (=$\begin{bmatrix} k_1 & k_2 & k_3 & p_1 & p_2 \end{bmatrix}^T$)
$\boldsymbol{k_x}$	Vector of distortion coefficients in the $\hat{\boldsymbol{u}}$ direction of the image plane (=$\begin{bmatrix} k_{x1} & k_{x2} & k_{x3} \end{bmatrix}^T$)
$\boldsymbol{k_y}$	Vector of distortion coefficients in the $\hat{\boldsymbol{v}}$ direction of the image plane (=$\begin{bmatrix} k_{y1} & k_{y2} & k_{y3} \end{bmatrix}^T$)
σ_a	Uncertainty bound magnitude of the quantity a

TABLE OF CONTENTS

Page

ABSTRACT ii

DEDICATION iii

ACKNOWLEDGMENTS iv

CONTRIBUTORS AND FUNDING SOURCES v

NOMENCLATURE vi

TABLE OF CONTENTS viii

LIST OF FIGURES x

LIST OF TABLES xiv

1. INTRODUCTION AND LITERATURE REVIEW 1

    1.1 Camera Calibration 1
    1.2 Vision based GNC 2

2. HOMOGRAPHY EXPLANATION 6

3. PHASESPACE MOTION CAPTURE CAMERA 12

    3.1 Overview 12
    3.2 Coordinate System Determination 13
        3.2.1 Basis Vectors Test 13
        3.2.2 Range Test 23
        3.2.3 Standard Deviation Test 24

4. ESTIMATION OF THE EXTRINSICS USING NONLINEAR LEAST SQUARES 29

5. DISTORTION INCORPORATED ESTIMATION 36

    5.1 Brown's Distortion Model 36
        5.1.1 Bouguet Toolbox Dataset 38
        5.1.2 Zhang's Dataset 45
    5.2 Geometric Distortion Model 49
        5.2.1 Bouguet Toolbox Dataset 50
        5.2.2 Zhang's Dataset 58

6. EXPERIMENTAL RESULTS 62

6.1 Dataset 1 62
6.1.1 Brown's Distortion Model 65
6.1.2 Geometric Distortion Model 74
6.2 Dataset 2 82
6.2.1 Brown's Distortion model 83
6.2.2 Geometric Distortion model 90
6.3 Dataset 3 99
6.3.1 Brown's Distortion Model 100
6.3.2 Geometric Distortion model 107
6.4 Dataset 4 116
6.5 Intrinsic Parameter analysis 129

7. CONCLUSIONS AND FUTURE WORK 132

REFERENCES 133

APPENDIX A. COMBINED DISTORTION INCORPORATED ESTIMATION PROCEDURE 136

APPENDIX B. EXTRINSICS ESTIMATION USING NONLINEAR LEAST SQUARES - JACOBIAN 151

APPENDIX C. GEOMETRIC DISTORTION INCORPORATED ESTIMATION 154

APPENDIX D. EXTRINSIC PROJECTIONS FOR ALL DATASETS 164

LIST OF FIGURES

Figure Page

2.1 The Homography Problem as shown in the paper[3] 6

3.1 The orientation of the two linear detectors in the Phasespace camera is shown. The orange line represents detector 0 and blue line represents detector 1. Original image taken from [2] 12

3.2 The beacon arrangement on the checkerboard pattern is shown. The number next to each beacon denotes its assigned reference number in the Phasespace SDK 14

3.3 The direction of increasing position values for both detectors is shown, as inferred from Table 3.1. The orange arrow shows the direction of increasing position values for Detector 0 and the blue line shows the direction of increasing position values for Detector 1 16

3.4 The inertial coordinate system with beacon positions. "O" is the origin and "OX" and "OY" represent the inertial planar axes. 17

3.5 Plots of translation vector elements in inches against frame number 19

3.6 Plots of CRP vector elements against frame number 19

3.7 Extrinsic Projections of all frames combined and shown with respect to the inertial frame 20

3.8 Comparison between the inertial frame projections (shown on the left) and the image plane projections (shown on the right) for each case. The top two images are for Case 1, the middle two images are for Case 2 and the bottom two images are for Case 3 22

3.9 Normalized beacon positions from the Range Test 23

3.10 Image plane projections of each pose of the board as seen through the Phasespace Viewer. The frames are ordered from the top left to the bottom right. 26

3.11 The physical alignment of the board with respect to the camera corresponding to each image plane projection shown in Figure 3.10. The frames are ordered from the top left to the bottom right. 27

3.12 Extrinsic Projections as computed using Zhang's Homography algorithm corresponding to each image plane projection shown in Figure 3.10. The distances are provided in inches. The frames are ordered from the top left to the bottom right..... 28

6.1 Beacon Arrangement on the checkerboard pattern is shown. The numbers next to the beacons indicate their number assignment in the Phasespace system. The origin O, the inertial x-axis X and inertial y-axis Y are also shown..... 63

6.2 Image plane projections of each pose of the board as seen through the Phasespace Viewer. The frames are ordered from the top left to the bottom right. 65

6.3 Extrinsic projections of all well-conditioned frames for Dataset 1 are shown together with respect to the inertial frame. Brown's distortion model is employed in the optimization process. 71

6.4 Plots of translation vector elements in inches against frame number for Dataset 1. These frame numbers are for the "non-noisy" frames where the noisy frame numbers are replaced by the next successive frame. Brown's distortion model is employed in the optimization process. 72

6.5 Plots of CRP vector elements against frame number for Dataset 1. These frame numbers are for the "non-noisy" frames where the noisy frame numbers are replaced by the next successive frame. Brown's distortion model is employed in the optimization process..... 73

6.6 Extrinsic projections of all frames for Dataset 1 are shown together with respect to the inertial frame. Geometric distortion model is employed in the optimization process. 79

6.7 Plots of translation vector elements in inches against frame number for Dataset 1. These frame numbers are for the "non-noisy" frames where the noisy frame numbers are replaced by the next successive frame. Geometric distortion function is employed in the optimization process 80

6.8 Plots of CRP vector elements against frame number for Dataset 1. These frame numbers are for the "non-noisy" frames where the noisy frame numbers are replaced by the next successive frame. Geometric distortion function is employed in the optimization process 81

6.9 Beacon Arrangement on the checkerboard pattern is shown. The numbers next to the beacons indicate their number assignment in the Phasespace system. The origin O, the inertial x-axis X and inertial y-axis Y are also shown..... 82

6.10 Image plane projections of each pose of the board as seen through the Phasespace Viewer. The frames are ordered from the top left to the bottom right. 84

6.11 Extrinsic projections of all frames for Dataset 2 are shown together with respect to the inertial frame. Brown's distortion model is employed in the optimization process. 89

6.12 Plots of translation vector elements in inches against frame number for Dataset 2. Brown's distortion model is employed in the optimization process. 90

6.13 Plots of CRP vector elements against frame number for Dataset 2. Brown's distortion model is employed in the optimization process. 91

6.14 Extrinsic projections of all frames for Dataset 2 are shown together with respect to the inertial frame. Geometric Distortion Model is employed to obtain these results .. 97

6.15 Plots of translation vector elements in inches against frame number for Dataset 2. Geometric distortion model is employed in the optimization process. 98

6.16 Plots of CRP vector elements against frame number for Dataset 2. Geometric distortion model is employed in the optimization process. 99

6.17 Image plane projections of each pose of the board as seen through the Phasespace Viewer. The frames are ordered from the top left to the bottom right. 100

6.18 Extrinsic projections of all frames for Dataset 3 are shown together with respect to the inertial frame. Brown's Distortion Model is employed to obtain these results 106

6.19 Plots of translation vector elements in inches against frame number for Dataset 3. Brown's distortion model is employed in the optimization process. 107

6.20 Plots of CRP vector elements against frame number for Dataset 3. Brown's distortion model is employed in the optimization process. 108

6.21 Extrinsic projections of all frames are shown together with respect to the inertial frame for Dataset 3. Geometric distortion model is employed in the optimization process. 113

6.22 Plots of translation vector elements in inches against frame number for Dataset 3. Geometric distortion model is employed in the optimization process. 114

6.23 Plots of CRP vector elements against frame number for Dataset 3. Geometric distortion model is employed in the optimization process. 115

6.24 Beacon Arrangement on the checkerboard pattern is shown. The numbers next to the beacons indicate their number assignment in the Phasespace system. The origin O, the inertial x-axis X and inertial y-axis Y are also shown. 116

6.25 Image plane projections of each pose of the board as seen through the Phasespace Viewer. The frames are ordered from the top left to the bottom right. 118

6.26 Physical alignment of the board with respect to the camera corresponding to each frame in Figure 6.25. The frames are numbered successively starting from the top left frame being numbered as zero. 119

6.27 Combined Extrinsic Projections with respect to the first frame as computed from the Homography optimization algorithm for Dataset 4 125

6.28 Combined Extrinsic Projections with respect to the first frame as computed from Wong's algorithm for Dataset 4 126

6.29 Difference between the translation elements of each frame with respect to the first frame, expressed in the first frame, as computed using Wong's algorithm and Homography optimization algorithm for Dataset 4 127

6.30 Difference between the CRP elements of each frame with respect to the first frame, expressed in the first frame, as computed using Wong's algorithm and Homography optimization algorithm for Dataset 4 128

D.1 Extrinsic Projections as computed using the Homography optimization algorithm corresponding to each image plane projection shown in Figure 6.2 for Dataset 1. The distances are provided in inches. Brown's distortion is employed in the optimization process. The frames are ordered from the top left to the bottom right. 165

D.2 Extrinsic Projections as computed using the Homography optimization algorithm corresponding to each image plane projection shown in Figure 6.2 for Dataset 1. The distances are provided in inches. Geometric distortion is employed in the optimization process. The frames are ordered from the top left to the bottom right. . . 166

D.3 Extrinsic Projections as computed using the Homography optimization algorithm corresponding to each image plane projection shown in Figure 6.10 for Dataset 2. The distances are provided in inches. Brown distortion is employed in the optimization process. The frames are ordered from the top left to the bottom right. . . 167

D.4 Extrinsic Projections as computed using the Homography optimization algorithm corresponding to each image plane projection shown in Figure 6.10 for Dataset 2. The distances are provided in inches. Geometric distortion is employed in the optimization process. The frames are ordered from the top left to the bottom right. . . 168

D.5 Extrinsic Projections as computed using the Homography optimization algorithm corresponding to each image plane projection shown in Figure 6.17 for Dataset 3. The distances are provided in inches. Brown's distortion is employed in the optimization process. The frames are ordered from the top left to the bottom right. . . 169

D.6 Extrinsic Projections as computed using the Homography optimization algorithm corresponding to each image plane projection shown in Figure 6.17 for Dataset 3. The distances are provided in inches. Geometric distortion is employed in the optimization process. The frames are ordered from the top left to the bottom right. . . 170

LIST OF TABLES

Table Page

3.1 The recorded positions of each beacon in both detectors and for all alignment groups they lie in are shown. 15

3.2 Inertial coordinates of each beacon given as [X-coordinate,Y-coordinate], s=49/16 inches 17

3.3 Maximum and minimum recorded normalized position values for both detectors 24

3.4 Standard Deviation values sorted beacon-wise for the first iteration of the Standard Deviation Test. d_0 and d_1 pertain to positions in detectors 0 and 1 respectively. 24

3.5 Standard Deviation values sorted beacon-wise for the second iteration of the Standard Deviation Test. d_0 and d_1 pertain to positions in detectors 0 and 1 respectively.. 25

5.1 Intrinsic parameters and distortion coefficients for the Bouguet Toolbox dataset are shown. The initial values, computed using Homography, are used for Nonlinear Optimization. The corresponding parameter values from the Bouguet Toolbox are shown for comparison. Brown's Distortion Model is used in the optimization process 39

5.2 The rotation matrices for the first 7 frames of the Bouguet Toolbox dataset are shown. The initial values, computed by Homography, are used for nonlinear optimization. The results from Bouguet Toolbox are shown for comparison. Brown's Distortion function is used in the optimization process 40

5.3 The rotation matrices for the frames 8 through 14 of the Bouguet Toolbox dataset are shown. The initial values, computed by Homography, are used for nonlinear optimization. The results from Bouguet Toolbox are shown for comparison.Brown's Distortion function is used in the optimization process 41

5.4 The rotation matrices for the frames 15 through 20 of the Bouguet Toolbox dataset are shown. The initial values, computed by Homography, are used for nonlinear optimization. The results from Bouguet Toolbox are shown for comparison.Brown's Distortion function is used in the optimization process 42

5.5 The translation vectors for the first 12 frames of the Bouguet Toolbox dataset are shown. The initial values, computed by Homography, are used for nonlinear optimization. The results from Bouguet Toolbox are shown for comparison. Brown's Distortion function is used in the optimization process 43

5.6 The translation vectors for the frames 13 through 20 of the Bouguet Toolbox dataset are shown. The initial values, computed by Homography, are used for nonlinear optimization. The results from Bouguet Toolbox are shown for comparison. Brown's Distortion function is used in the optimization process 44

5.7 Intrinsic parameters and distortion coefficients for the Zhang dataset are shown. The initial values, computed using Homography, are used for Nonlinear Optimization. The corresponding parameter values from the Bouguet Toolbox are shown for comparison. Brown's Distortion function is used in the optimization process..... 45

5.8 The rotation matrices for the frames of the Zhang dataset are shown. The initial values, computed by Homography, are used for nonlinear optimization. The results from Bouguet Toolbox are shown for comparison. Brown's Distortion function is used in the optimization process..... 47

5.9 The translation vectors for the frames of the Zhang dataset are shown. The initial values, computed by Homography, are used for nonlinear optimization. The results from Bouguet Toolbox are shown for comparison. Brown's Distortion function is used in the optimization process..... 48

5.10 Family of Polynomial and Rational Distortion Functions as presented in Ma et [4] .. 49

5.11 The intrinsic parameters for the Bouguet Toolbox dataset are shown. The optimized values are shown in the second column in comparison with the values obtained from Bouguet's Toolbox. Geometric Distortion function is used in the optimization process..... 50

5.12 The rotation matrices for the first 7 frames of the Bouguet Toolbox dataset are shown. The initial values, computed by Homography, are used for nonlinear optimization. The results from Bouguet Toolbox are shown for comparison. Geometric Distortion function is used in the optimization process 52

5.13 The rotation matrices for the frames 8 through 14 of the Bouguet Toolbox dataset are shown. The initial values, computed by Homography, are used for nonlinear optimization. The results from Bouguet Toolbox are shown for comparison. Geometric Distortion function is used in the optimization process 53

5.14 The rotation matrices for the frames 15 through 20 of the Bouguet Toolbox dataset are shown. The initial values, computed by Homography, are used for nonlinear optimization. The results from Bouguet Toolbox are shown for comparison. Geometric Distortion function is used in the optimization process 54

5.15 The translation vectors for the first 12 frames of the Bouguet Toolbox dataset are shown. The initial values, computed by Homography, are used for nonlinear optimization. The results from Bouguet Toolbox are shown for comparison. Geometric Distortion function is used in the optimization process 56

5.16 The translation vectors for the frames 13 through 20 of the Bouguet Toolbox dataset are shown. The initial values, computed by Homography, are used for nonlinear optimization. The results from Bouguet Toolbox are shown for comparison. Geometric Distortion function is used in the optimization process 57

5.17 The intrinsic parameters for the Zhang dataset are shown. The optimized values are shown in the second column in comparison with the values obtained from Bouguet's Toolbox. Geometric Distortion function is used in the optimization process 58

5.18 The rotation matrices for the frames of the Zhang dataset are shown. The initial values, computed by Homography, are used for nonlinear optimization. The results from Bouguet Toolbox are shown for comparison. Geometric Distortion function is used in the optimization process 60

5.19 The translation vectors for the frames of the Zhang dataset are shown. The initial values, computed by Homography, are used for nonlinear optimization. The results from Bouguet Toolbox are shown for comparison. Geometric Distortion function is used in the optimization process 61

6.1 Inertial coordinates of each beacon given as [X-coordinate,Y-coordinate], s=2.95 inches 64

6.2 The intrinsic parameters and distortion coefficients for Dataset 1, as computed by the Homography algorithm and the optimization scheme are shown. Brown's Distortion Model is employed in the optimization process 66

6.3 The CRPs for the first 12 well-conditioned frames for Dataset 1 is presented. The initialization values computed by Homography are juxtaposed with the optimized values for comparison. Brown's distortion model is employed in the optimization process. 67

6.4 The CRPs for the remaining well-conditioned frames for Dataset 1 is presented. The initialization values computed by Homography are juxtaposed with the optimized values for comparison. Brown's distortion model is employed in the optimization process. 68

6.5 The Translation vectors (in inches) corresponding to the firt 12 well-conditioned frames for Dataset 1 is presented. The initialization values computed by Homography are shown along with the optimized values for comparison,Brown's distortion model is employed in the optimization process. 69

6.6 The Translation vectors (in inches) corresponding to the remaining well-conditioned frame for Dataset 1 is presented. The initialization values computed by Homography are shown along with the optimized values for comparison.Brown's distortion model is employed in the optimization process. 70

6.7 The intrinsic parameters and distortion coefficients for Dataset 1, as computed by the Homography algorithm and the optimization scheme are shown. Geometric Distortion Model is employed in the optimization process 74

6.8 The CRPs for the first 12 well-conditioned frames for Dataset 1 is presented. The initialization values computed by Homography are juxtaposed with the optimized values for comparison. Geometric distortion model is employed in the optimization process. 75

6.9 The CRPs for the remaining well-conditioned frames for Dataset 1 is presented. The initialization values computed by Homography are juxtaposed with the optimized values for comparison. Geometric distortion model is employed in the optimization process..... 76

6.10 The translations for the first 12 well-conditioned frames for Dataset 1 is presented. The initialization values computed by Homography are juxtaposed with the optimized values for comparison. Geometric distortion model is employed in the optimization process..... 77

6.11 The translations for the remaining well-conditioned frames for Dataset 1 is presented. The initialization values computed by Homography are juxtaposed with the optimized values for comparison. Geometric distortion model is employed in the optimization process. 78

6.12 Inertial coordinates of each beacon given as [X-coordinate,Y-coordinate], s=2.95 inches 83

6.13 The intrinsic parameters and the distortion coefficients for Dataset 2, as computed by the Homography algorithm and optimized using nonlinear optimization are shown. Brown's distortion model is employed in the optimization process..... 84

6.14 The CRPs for the first 12 well-conditioned frames for Dataset 2 are presented. The initialization values computed by Homography are juxtaposed with the optimized values for comparison. Brown's distortion model is employed in the optimization process. 85

6.15 The CRPs for the remaining well-conditioned frames for Dataset 2 are presented. The initialization values computed by Homography are juxtaposed with the optimized values for comparison.Brown's distortion model is employed in the optimization process..... 86

6.16 The Translation vectors (in inches) corresponding to the first 12 well-conditioned frames for Dataset 2 is presented. The initialization values computed by Homography are shown along with the optimized values for comparison. Brown's distortion model is employed in the optimization process..... 87

6.17 The Translation vectors (in inches) corresponding to the remaining well-conditioned frame for Dataset 2 is presented. The initialization values computed by Homography are shown along with the optimized values for comparison. Brown's distortion model is employed in the optimization process. 88

6.18 The intrinsic parameters and the distortion coefficients for Dataset 2, as computed by the Homography algorithm and optimized are shown. Geometric distortion model is employed in the optimization process. 92

6.19 The CRPs corresponding to the first 12 well-conditioned frames for Dataset 2 is presented. The initialization values computed by Homography are shown along with the optimized values for comparison. Geometric distortion model is employed in the optimization process. 93

6.20 The CRPs corresponding to the remaining well-conditioned frame for Dataset 2 is presented. The initialization values computed by Homography are shown along with the optimized values for comparison. Geometric distortion model is employed in the optimization process. 94

6.21 The Translation vectors (in inches) corresponding to the first 12 well-conditioned frame for Dataset 2 is presented. The initialization values computed by Homography are shown along with the optimized values for comparison. Geometric distortion model is employed in the optimization process. 95

6.22 The Translation vectors (in inches) corresponding to the remaining well-conditioned frame for Dataset 2 is presented. The initialization values computed by Homography are shown along with the optimized values for comparison. Geometric distortion model is employed in the optimization process. 96

6.23 The intrinsic parameters and the distortion coefficients for Dataset 3, as computed by the Homography algorithm and optimized are shown. Brown's distortion model is employed in the optimization process. 101

6.24 The CRPs corresponding to the first 12 well-conditioned frame for Dataset 3 is presented. The initialization values computed by Homography are shown along with the optimized values for comparison. Brown's distortion model is employed in the optimization process. 102

6.25 The CRPs corresponding to the remaining well-conditioned frame for Dataset 3 is presented. The initialization values computed by Homography are shown along with the optimized values for comparison. Brown's distortion model is employed in the optimization process. 103

6.26 The Translation vectors (in inches) corresponding to the first 12 well-conditioned frame for Dataset 3 is presented. The initialization values computed by Homography are shown along with the optimized values for comparison. Brown's distortion model is employed in the optimization process. 104

6.27 The Translation vectors (in inches) corresponding to the remaining well-conditioned frame for Dataset 3 is presented. The initialization values computed by Homography are shown along with the optimized values for comparison. Brown's distortion model is employed in the optimization process. 105

6.28 The intrinsic parameters and the distortion coefficients for Dataset 3, as computed by the Homography algorithm and optimized are shown. Geometric distortion model is employed in the optimization process. 108

6.29 The CRPs corresponding to the first 12 well-conditioned frame for Dataset 3 is presented. The initialization values computed by Homography are shown along with the optimized values for comparison. Geometric distortion model is employed in the optimization process. 109

6.30 The CRPs corresponding to the remaining well-conditioned frame for Dataset 3 is presented. The initialization values computed by Homography are shown along with the optimized values for comparison. Geometric distortion model is employed in the optimization process. 110

6.31 The Translation vectors (in inches) corresponding to the first 12 well-conditioned frame for Dataset 3 is presented. The initialization values computed by Homography are shown along with the optimized values for comparison. Geometric distortion model is employed in the optimization process. 111

6.32 The Translation vectors (in inches) corresponding to the remaining well-conditioned frame for Dataset 3 is presented. The initialization values computed by Homography are shown along with the optimized values for comparison. Geometric distortion model is employed in the optimization process. 112

6.33 Inertial coordinates of each beacon given as [X-coordinate,Y-coordinate], s=49/16 inches 117

6.34 The CRPs corresponding to the first 12 well-conditioned frames for Dataset 4 is presented. The optimized values are shown along with the values from Wong's algorithm for comparison. Brown's distortion model is used here. 120

6.35 The CRPs corresponding to the remaining well-conditioned frames for Dataset 4 is presented. The optimized values are shown along with the values from Wong's algorithm for comparison. Brown's distortion model is used here. 121

6.36 The Translation elements (in inches) corresponding to the first 12 well-conditioned frames for Dataset 4 is presented. The optimized values are shown along with the values from Wong's algorithm for comparison. Brown's distortion model is used here. 122

6.37 The Translation elements (in inches) corresponding to the remaining well-conditioned frames for Dataset 4 is presented. The optimized values are shown along with the values from Wong's algorithm for comparison. Brown's distortion model is used here. 123

6.38 Intrinsic parameter matrices and Distortion Coefficient Vectors computed from datasets 1 to 3 using the combined estimation approach with Brown's Distortion Model 130

6.39 Intrinsic parameter matrices and Distortion Coefficient Vectors computed from datasets 1 to 3 using the combined estimation approach with Brown's Distortion model 130

6.40 Intrinsic parameter matrices and Distortion Coefficient Vectors computed from datasets 1 to 3 using the combined estimation approach with Geometric Distortion Model 131

6.41 Intrinsic parameter matrices and Distortion Coefficient Vectors computed from datasets 1 to 3 using the combined estimation approach with Geometric Distortion Model 131

1. INTRODUCTION AND LITERATURE REVIEW

The advent of practical semiconductor technology in the early 1970's has ushered in the age of sensor technology that is inexpensive and can be mass produced. As a result electronic instrumentation for niche fields of research, which otherwise would have been restricted to organizations and individuals with exceptional financial backing, has been made easier to obtain and inexpensive to use. This has led to a boon in research within disciplines involving heavy use of application-specific electronic equipment. A good example of such a discipline is Machine Vision. The introduction of CMOS integrated vision sensors has resulted in a brighter spotlight on research involving Vision based guidance and navigation.

1.1 Camera Calibration

The first step in the utilization of any sensor is its calibration. Once the inherent biases of the sensor are known, additional corrections can be applied either physically to the experiment or digitally in order to obtain accurate measurements. For vision based sensors, the calibration procedure is conducted in order to quantify the parameters that model the formation of the image from an external electromagnetic stimulus, whether it be part of the visible or invisible electromagnetic spectrum. Camera calibration has been extensively researched since the early 1960s under the name of "Photogrammetry". The early photogrammetry algorithms were developed assuming the idealised pinhole model with the focal length and principa point offsets being the only parameters of the image plane to estimate. However, the idealised pinhole model was not sufficiently precise so distortion models were developed in order to capture the additional nonlinear effects in the image capturing process. Seminal work in the field of photogrammetry by Magill [5], Cox [6] and many others led to the nascent formulations that would lay the groundwork for many researches like Brown [7] and Kenefick [8] to come up with some of the first camera distortion estimation algorithms. Although Brown's camera calibration algorithm was created to be used on images stored in photographic plates, the same distortion formulation is applicable to CCD/CMOS cameras.

With the introduction of CCD/CMOS cameras, various algorithms were developed by Zhang [1], Heikkila et al [9] and Tsai [10] that sought to combine the image distortion concepts developed by Brown with a nonlinear optimization based approach to estimate the intrinsic parameters of the camera and the relative pose of the object being viewed. The standard calibration procedure for a digital off-the-shelf camera is to employ Zhang's Homography algorithm and Brown's distortion algorithm to optimize over the intrinsic parameters and the relative pose of the body. However, the image distortion process can be modelled in various ways. Ma et al [4] proposed a set of geometric distortion models where the distortion function has various nonlinear forms that can be used for a wide range of cameras depending on the degree of distortion that manifests on the image. This research utilizes Zhang's Homography algorithm to generate the starting guesses for the nonlinear optimization algorithm. The image distortion is modelled using both Brown's model and the Geometric distortion model to see if the constant intrinsic camera parameters and distortion coefficients can be computed across different datasets.

1.2 Vision based GNC

With the semiconductor-based sensors being made cheap and ubiquitous, many off-the-shelf consumer products employ the use of inexpensive vision sensing technologies. Microsoft's Kinect[11] and Nintendo's Wii[12] are examples of vision based sensors that detect invisible electromagnetic radiation for relative pose estimation purposes. The Kinect uses an Infrared camera to capture a set of infrared features in the scene projected onto its sensor array. Triangulation is then utilized to obtain the coordinates of these features in the object space. As the ball is pushed further in terms of increasing computational ability with decreasing size, wearable technology has also been on the rise, both in the commercial market and among researchers. Vision Tape[13], for example, utilizes eight photodiodes for fast image acquisition and dense optical flow detection at great speeds. Research on similar devices developed by Placer and Kovacic[14], Hung and Suh[15], Do and Suh[16] and many more prove that the interest in developing systems for machine learning with the vision sensors playing a pivotal role in data acquisition will only rise in the future.

All vision based guidance and navigation applications can be divided into two categories. The

first category can employ the use of reference points at known locations in the object space to facilitate relative navigation in a cooperative manner. Autonomous aerial refueling[17], aircraft and spacecraft relative navigation[18], [19] and autonomous aircraft landing on ships and aircraft carriers are instances of the first category. The second category requires the development of navigation systems in an uncooperative manner (i.e. non reliance on the presence of reference points in the workspace). Examples of this category include, but are not limited to, path planning for robots [20], planetary exploration[21], planetary reentry navigation [22] and proximity operations [23]. Vision based navigation systems provide robust 6 degree-of-freedom (DOF) relative navigation solutions driven by the geometry of the problem.

Proximity based operations use high speed, high resolution cameras along with a slew of other sensors to monitor various parameters pertaining to the relative pose and pose rates between the target and the manipulator. Recently, some systems have been developed as alternatives to the CCD/CMOS camera-incorporated sensor suites being used to provide 6 DOF relative pose estimates of a target. An example of this is the VISNAV system developed by Gunnam et al[24] and Junkins et al[25]. VISNAV is an analog system that uses a position sensitive diode (PSD) to measure camera space positions of active beacons in the scene; with four or more imagd beacons, least squares "resection" permits accurate estimates of the VISNAV sensor relative to an object space reference frame. In this case the PSD behaves like a high speed CCD/CMOS array, providing fictitious image plane coordinates with respect to a coordinate system, defined by the normalized imbalance of four voltage values. The analog nature of the VISNAV system means high effective frame rates but a significant amount of expertise in analog electro-optical systems is required to operate and troubleshoot the system. An alternative to the analog VISNAV system is the development of a digital counterpart to it, as done in Wong et al[3]. This all digital system is much eaier to design, engineer and acquire data from, and harnesses the capability of recent advances in data transfer solutions and high processing power of embedded computer systems to provide robust 6 DOF relative pose estimates relatively at high rates. Although this system uses a conventional CCD camera as its optical sensor, the novel approach is the utilization of a set of LED beacons which are

programmed to strobe at different frequencies (motivated by the original analog VISNAV patent). This allows for the isolation and identification of each beacon independently. Commercial motion capture technologies like Vicon[26] and Phasespace[2] employ similar arrangements of beacons in the workspace with multiple cameras to identify and track them to provide 6 DOF relative pose estimates. The beacons are passive in the case of Vicon and active in the case of Phasespace and are attached to a target body to estimate its relative pose in respect to their internal coordinate system. Vicon leverages the known positions of its infrared beacons to estimate the relative pose of a target body. Phasespace harnesses the fact that each of its LED beacons strobe with a different frequency to isolate and group four or more specific beacons together in order to estimate the relative pose of a body.

The Phasespace camera uses optical elements to focus the light emanating from the active LED beacons to two orthogonal linear detectors. One vertical linear detector images the collapsed left-right field of view (thus capturing the x-coordinates of the beacons) and the other horizontal linear detector images the collapsed up-down field of view (thus capturing the y-coordinates of the beacons). The frame rate of the camera is 960 Hz. This allows for a high rate of beacon coordinate computation (around 200 Hz). The faster frame rate is used to capture the unique beacon frequency of modulation to uniquely associate the measured coordinates with the corresponding beacon. The Phasespace system is conventionally designed to operate o thebeacon coordinates and compute and output the three dimensional line of sight vector for each beacon with respect to its internal precalibrated coordinate system using the linear detector positions from each camera. In this research, a single Phasespace camera is employed as the optical sensor. The linear detector values are used to compute uncalibrated coordinates of the beacons in the fictitious image plane whose bases are taken to be the two linear detectors.

This research presents, in addition to the calibration results of the Phasespace camera, a nonlinear optimization algorithm that can be implemented online to estimate the relative pose of an uncooperative target equipped with the compatible beacons. The first chapter discusses Zhang's homography algorithm. A key contribution is the alternate formulation of the matrix B dependent

on the intrinsic parameter matrix which mitigates the effects of data noise on the intrinsics estimation process. The second chapter provides details of the Phasespace motion capture camera used in this research along with some tests that provide some insight about its parameters. The third chapter discusses in depth the two distortion models tried in this work, with some more algorithmic description in the Appendices. The fourth chapter presents the nonlinear optimization based approach that can be implemented once the constant intrinsic camera parameters and distortion coefficients are estimated to estimate the relative pose of an uncooperative target equipped with the requisite number of compatible LED beacons. Experimental results are then presented that determine the applicability of the two distortion models to the Phasespace camera and the efficacy of the algorithm presented in the previous chapter in estimation of the relative pose. The final chapter details the conclusions and possible avenues for future research in this area.

2. HOMOGRAPHY EXPLANATION

A detailed dicussion of the utilization of Homography for the calibration of a CCD/CMOS camera is presented in Zhang[1].

According to Zhang, the pinhole projection model is represented by 2.1.

$$s\tilde{\boldsymbol{m}} = A \begin{bmatrix} R & \boldsymbol{t} \end{bmatrix} \tilde{\boldsymbol{M}} \tag{2.1}$$

where s is a scaling factor, $\tilde{\boldsymbol{M}}$ is a beacon coordinate in the target frame, $\tilde{\boldsymbol{m}}$ is the corresponding image plane projection of $\tilde{\boldsymbol{M}}$, R and $\boldsymbol{t}$ are the Rotation matrix and translation vector pertaining to the transformation from the target frame to the camera frame and A is the intrinsic parameter matrix is given by $A = \begin{bmatrix} \alpha & c & u_0 \\ 0 & \beta & v_0 \\ 0 & 0 & 1 \end{bmatrix}$, the scaling parameters in the x and y directions in the image plane are given by α and β respectively, the skewness metric is given by c and the principal point offset is given by $\begin{bmatrix} u_0 & v_0 \end{bmatrix}^T$.

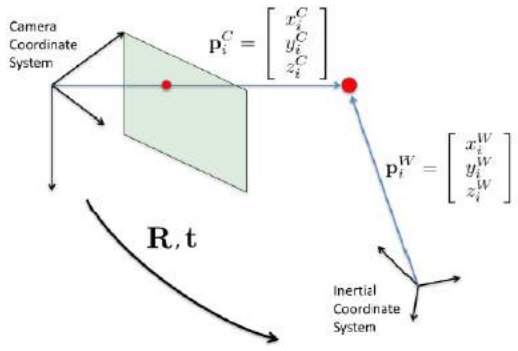

Figure 2.1: The Homography Problem as shown in the paper[3]

The figure 2.1 illustrates the geometry of the perspective problem that Zhang's paper serves to

find a computational solution for.

4.2 can be further expanded as 2.2 since without any loss of generality, we can set Z=0.

$$\begin{bmatrix} u \\ v \\ 1 \end{bmatrix} = A \begin{bmatrix} \boldsymbol{r_1} & \boldsymbol{r_2} & \boldsymbol{r_3} & \boldsymbol{t} \end{bmatrix} \begin{bmatrix} X \\ Y \\ 0 \\ 1 \end{bmatrix} = A \begin{bmatrix} \boldsymbol{r_1} & \boldsymbol{r_2} & \boldsymbol{t} \end{bmatrix} \begin{bmatrix} X \\ Y \\ 1 \end{bmatrix} \tag{2.2}$$

For notational conciseness, let us define

$$H = A \begin{bmatrix} \boldsymbol{r_1} & \boldsymbol{r_2} & \boldsymbol{t} \end{bmatrix}$$

The first step is the estimation of the homography matrix H. 2.2 is rewritten as

$$\begin{bmatrix} \tilde{\boldsymbol{M}}^T & \boldsymbol{0}^T & -u\tilde{\boldsymbol{M}}^T \\ \boldsymbol{0}^T & \tilde{\boldsymbol{M}}^T & -v\tilde{\boldsymbol{M}}^T \end{bmatrix} \boldsymbol{x} = \boldsymbol{0} \tag{2.3}$$

where $\boldsymbol{x}$ is the columns of H arranged into a column vector.

For *n* points in the image there will be *n* such equations that can be stacked.

This sequence of steps is carried out for multiple frames. In each case, if $L = \begin{bmatrix} \tilde{\boldsymbol{M}}^T & \boldsymbol{0}^T & -u\tilde{\boldsymbol{M}}^T \\ \boldsymbol{0}^T & \tilde{\boldsymbol{M}}^T & -v\tilde{\boldsymbol{M}}^T \end{bmatrix}$, the solution $\boldsymbol{x}$ is the singular vector of L corresponding to the smallest singular value of L.

This result can now be used as an initial guess to solve the nonlinear least squares problem given by 2.4.

$$J = \sum_i ||\boldsymbol{m_i} - \hat{\boldsymbol{m}}_{\boldsymbol{i}}||^2 \tag{2.4}$$

where $\hat{\boldsymbol{m}}_{\boldsymbol{i}} = \frac{1}{\tilde{\boldsymbol{h_3}}^T \boldsymbol{M_i}} \begin{bmatrix} \tilde{\boldsymbol{h_1}}^T \boldsymbol{M_i} \\ \tilde{\boldsymbol{h_2}}^T \boldsymbol{M_i} \end{bmatrix}$

With H estimated for all frames, the next step is to calculate intrinsic and extrinsic parameters.

Zhang's paper defines a matrix B as given in 2.5.

$$B = A^{-T}A^{-1} \tag{2.5}$$

The motivation behind the definition of B stems from the following development. The estimation of the homography matrix calculated earlier can be written as the following.

$$\begin{bmatrix} \boldsymbol{h_1} & \boldsymbol{h_2} & \boldsymbol{h_3} \end{bmatrix} = \lambda A \begin{bmatrix} \boldsymbol{r_1} & \boldsymbol{r_2} & \boldsymbol{t} \end{bmatrix} \tag{2.6}$$

Now, using two known fundamental properties of the rotation matrix, i.e. orthonormality of the basis vectors with respect to each other and the equality of magnitude for each direction, the next two equations can be developed.

$$\begin{aligned} \boldsymbol{h_1}^T A^{-T}A^{-1}\boldsymbol{h_2} &= 0 \\ \boldsymbol{h_1}^T A^{-T}A^{-1}\boldsymbol{h_1} &= \boldsymbol{h_2}^T A^{-T}A^{-1}\boldsymbol{h_2} \end{aligned} \tag{2.7}$$

The occurence of $A^{-T}A^{-1}$ in both equations suggests its analysis.

Substitution of the A matrix enables the determination of B in terms of the intrinsic camera parameters.

$$B = \begin{bmatrix} \frac{1}{\alpha^2} & -\frac{c}{\alpha^2\beta} & \frac{cv_0-u_0\beta}{\alpha^2\beta} \\ -\frac{c}{\alpha^2\beta} & \frac{c^2}{\alpha^2\beta^2}+\frac{1}{\beta^2} & -\frac{c(cv_0-u_0\beta)}{\alpha^2\beta^2}-\frac{v_0}{\beta^2} \\ \frac{cv_0-u_0\beta}{\alpha^2\beta} & -\frac{c(cv_0-u_0\beta)}{\alpha^2\beta^2}-\frac{v_0}{\beta^2} & \frac{(cv_0-u_0\beta)^2}{\alpha^2\beta^2}+\frac{v_0^2}{\beta^2}+1 \end{bmatrix} \tag{2.8}$$

Now,since B is a symmetric matrix, it can be represented as a vector of its six distinct elements.

$$\boldsymbol{b} = \begin{bmatrix} B_{11} & B_{12} & B_{22} & B_{13} & B_{23} & B_{33} \end{bmatrix}^T \tag{2.9}$$

The vector $\boldsymbol{b}$ describes the image of the absolute conic, which is a concept innate to the process of self calibration.

The definition of B, defined in either 2.8 or 2.13, allows for the representation of 2.7 in the following manner.

$$\begin{bmatrix} \boldsymbol{v_{12}}^T \\ (\boldsymbol{v_{11}} - \boldsymbol{v_{22}})^T \end{bmatrix} \boldsymbol{b} = \mathbf{0} \tag{2.10}$$

where $\boldsymbol{v_{ij}} = \begin{bmatrix} h_{i1}h_{j1} & h_{i1}h_{j2} + h_{i2}h_{j1} & h_{i2}h_{j2} & h_{i3}h_{j1} + h_{i1}h_{j3} & h_{i3}h_{j2} + h_{i2}h_{j3} & h_{i3}h_{j3} \end{bmatrix}^T$ So, if we have n images, they can be stacked in order to have a $2nx6$ matrix V, which gives the following equation.

$$V\boldsymbol{b} = \mathbf{0} \tag{2.11}$$

The solution to the above equation is the singular vector of V associated with the smallest singular value of V.

Once, $\boldsymbol{b}$ is estimated, we can compute the intrinsic parameters of the A matrix using the following formulas.

$$\begin{aligned} v_0 &= \frac{B_{12}B_{13} - B_{11}B_{23}}{B_{11}B_{22} - B_{12}^2} \\ \lambda &= B_{33} - \frac{B_{13}^2 + v_0(B_{12}B_{13} - B_{11}B_{23})}{B_1 1} \\ \alpha &= \sqrt{\frac{\lambda}{B_{11}}} \\ \beta &= \sqrt{\frac{\lambda B_{11}}{B_{11}B_{22} - B_{12}^2}} \\ c &= -\frac{B_{12}\alpha^2\beta}{\lambda} \\ u_0 &= \frac{cv_0}{\alpha} - \frac{B_{13}\alpha^2}{\lambda} \end{aligned} \tag{2.12}$$

A novel contribution by this research is the reformulation of B as follows.

$$B = A^{-1}A^{-T} \tag{2.13}$$

As a result, B has the following form.

$$B^T = A^{-1}A^{-T} = \begin{bmatrix} \frac{1}{\alpha^2} + \frac{c^2}{\alpha^2\beta^2} + (\frac{cv_0-\beta u_0}{\alpha\beta})^2 & -\frac{c}{\alpha\beta^2} - \frac{cv_0-\beta u_0}{\alpha\beta}\frac{v_0}{\beta} & \frac{cv_0-\beta u_0}{\alpha\beta} \\ -\frac{c}{\alpha\beta^2} - \frac{cv_0-\beta u_0}{\alpha\beta}\frac{v_0}{\beta} & \frac{1}{\beta^2} + \frac{v_0^2}{\beta^2} & -\frac{v_0}{\beta} \\ \frac{cv_0-\beta u_0}{\alpha\beta} & -\frac{v_0}{\beta} & 1 \end{bmatrix} \tag{2.14}$$

It is noteworthy that since B_{33} is one as opposed to $\frac{(cv_0-u_0\beta)^2}{\alpha^2\beta^2} + \frac{v_0^2}{\beta^2} + 1$ in 2.8, there in no need for normalization with respect to B_{33} in the case of 2.13. This allows for less contribution of the formulation of B towards the errors in the estimation of the intrinsic camera parameters.

If B^T is used, the intrinsic parameters are computed as so.

$$\begin{aligned} \beta &= \frac{1}{B_{22} - B_{23}^2} \\ v_0 &= -B_{23}\beta \\ \alpha &= \left(B_{11} - B_{31}^2 - \frac{B_{21} - B_{31}B_{32}}{B_{22} - B_{23}^2}\right)^{-\frac{1}{2}} \\ c &= -(B_{12} - B_{13}B_{23})\alpha\beta^2 \\ u_0 &= \frac{cv_0 - \alpha\beta B_{31}}{\beta} \end{aligned} \tag{2.15}$$

Once A is known, the definition of the homography matrix can be used to compute the extrinsic parameters for each image. From 2.6, we have.

$$\begin{aligned} \boldsymbol{r_1} &= \lambda A^{-1}\boldsymbol{h_1} \\ \boldsymbol{r_2} &= \lambda A^{-1}\boldsymbol{h_2} \\ \boldsymbol{r_3} &= \boldsymbol{r_1} \times \boldsymbol{r_2} \\ \boldsymbol{t} &= \lambda A^{-1}\boldsymbol{h_3} \end{aligned} \tag{2.16}$$

where $\lambda = \frac{1}{\|A^{-1}\boldsymbol{h_1}\|} = \frac{1}{\|A^{-1}\boldsymbol{h_2}\|}$. Because of noise in the data, $\boldsymbol{h_1}$ never equals $\boldsymbol{h_2}$, as a result using $\boldsymbol{h_1}$ and $\boldsymbol{h_2}$ will result in different extrinsic parameters. A key clue to this fact is the observation that the smallest singular value associated with L, defined in 2.3, is never zero, irrespective of

frame. Another adverse effect of noise in the data is that rotation matrix thus computed from the Homography matrix and intrinsic parameters does not in general satisfy the properties of a rotation matrix. There are many ways to estimate the best rotation matrix from the given rotation matrix. Zhang provides a solution S such that the $R - S$ has the least Frobenius norm. This research utilizes a solution to the Orthogonal Procrustes Problem to compute the best rotation matrix.

The normalisation variable λ (refer Equation 2.16) will be different depending on the choice of either $\boldsymbol{r_1}$ or $\boldsymbol{r_2}$, due to some noise in the calculations as introduced by the SVD analysis for the estimation of the Homography matrix and measurement noise. As a result, the estimated rotation matrix will not satisfy the orthogonality constraint or the unit determinant constraint. Out of the many possible algorithms that could be harnessed to estimate the best possible rotation matrix, the solution to the Orthogonal Procrustes problem is utilized.

If R is the estimated rotation matrix for a frame, let us say that the Singular Value Decomposition of R gives us matrix of left singular vectors U, matrix of right singular vectors V and the diagonal singular values matrix S. (i.e. $svd(R) = USV^T$,assuming R has real entries). In that case the best possible rotation matrix is given by $\hat{R}_{best} = UV^T$.

The Classical Rodrigues Parameters (CRPs) are obtained from the rotation matrix using the Cayley Transform.

$$Q = (I - \hat{R}_{best}^{-1})(I + \hat{R}_{best}) \tag{2.17}$$

where Q is the skew-symmetric matrix associated with the CRP vector $\begin{bmatrix} q_1 & q_2 & q_3 \end{bmatrix}^T$.

3. PHASESPACE MOTION CAPTURE CAMERA

3.1 Overview

This research uses the camera from the Phasespace Impulse X2E Motion Capture System as the structured light sensor. The uniqueness of the camera lies in the fact that instead of using a CCD/CMOS array, it utilizes two linear detectors to capture light information from the scene. The orientation of the detectors is shown in Figure 3.1. It is to be noted that both linear detectors are aligned perpendicular to each other. The camera frame rate is 960 Hz but the data display rate is about 200 Hz.

Figure 3.1: The orientation of the two linear detectors in the Phasespace camera is shown. The orange line represents detector 0 and blue line represents detector 1. Original image taken from [2]

The detectors are assigned values 0 and 1 according to their manner of reference in the Phasespace SDK package. Facing the front face of the camera, Detector 0 starts from the centre on the top edge and ends at the bottom right corner whereas Detector 1 starts from the centre of the top edge and ends at the bottom left corner. The actual physical position of the detectors is somewhere

away from the front face of the camera, at a distance which is not known to the author at the time of writing.

Each LED beacon that falls within the field of view of the camera is identified using a proprietary algorithm which isolates beacons based on their strobing frequency. The light rays emanating from each beacon are directed onto each detector using optical instruments such as lenses. The footprint left by the light rays from each beacon is treated as a Gaussian and an internal algorithm computes its width, normalized position and amplitude on each detector. These values can be accessed through the Phasespace SDK and the structure associated with the footprint of the light rays from each beacon on each detector is called "Peaks".

The mutually perpendicular orientation of the linear detectors in the camera make them viable candidates as basis vectors for the fictitious 2D image plane. A number of tests were conducted in order to determine the ideal direction for the chosen basis vectors, the standard deviation for the position of a stationary beacon and the range of both detector positions before a definitive coordinate system was assigned to the fictitious image plane.

3.2 Coordinate System Determination

3.2.1 Basis Vectors Test

This test was conducted in order to determine the direction of increase in position for each detector. For this purpose, 8 beacons are affixed to a checkerboard pattern at known positions (corners of certain squares on the checkerboard) in the shape of an "F". This arrangement is shown in Figure 3.2.

Figure 3.2: The beacon arrangement on the checkerboard pattern is shown. The number next to each beacon denotes its assigned reference number in the Phasespace SDK

The camera was mounted on a Manfrotto table top tripod, tilted so as to align Detector 0 with the vertical lines of the checkerboard pattern and Detector 1 with the horizontal lines of the checkerboard pattern and positioned at a distance from the board. The camera and board are kept stationary, the system is turned on and the positions of the beacons are acquired. Three alignment categories are defined.

1. Horizontal alignment: There are 3 groups each beacon can be sorted under.
    - Horizontal line 1(Lh1): Consisting of beacons 4,7,6 and 0
    - Horizontal line 2(Lh2): Consisting of beacons 5,1 and 2
    - Horizontal line 3(Lh3): Consisting of beacon 3
2. Vertical alignment: There are 4 groups each beacon can be sorted under.
    - Vertical line 1(Lv1): Consisting of beacons 4,5 and 3
    - Vertical line 2(Lv2): Consisting of beacons 7 and 1
    - Vertical line 3(Lv3): Consisting of beacons 6 and 2

- Vertical line 4(Lv4): Consisting of beacon 0

3. Individual: The light from each beacon is captured individually by blocking out the radiation from the other beacons.

Data is acquired by allowing light from a certain category of beacons to be captured by obscuring the other beacons. For example, the Lh1 data is acquired by only allowing light from beacons 4,7,6 and 0 to be captured by the camera. The recorded normalized positions are shown in Table 3.1.

Beacon No.	**Detector 0 normalized position**	**Detector 1 normalized position**
0	Lh1 = 0.525 Individual = 0.527	Lh1 = 0.348 Individual = 0.354
1	Lh2 = 0.572 Lv2 = 0.572 Individual = 0.572	Lh2 = 0.458 Lv2 = 0.458 Individual = 0.458
2	Lh2 = 0.575 Lv3 = 0.575 Individual = 0.575	Lh2 = 0.408 Lv3 = 0.408 Individual = 0.408
3	Lv1 = 0.619 Individual = 0.619	Lv1 = 0.512 Individual = 0.512
4	Lh1 = 0.514 Lv1 = 0.517 Individual = 0.517	Lh1 = 0.499 Lv1 = 0.506 Individual = 0.506
5	Lh2 = 0.568 Lv1 = 0.568 Individual = 0.568	Lh2 = 0.509 Lv1 = 0.509 Individual = 0.509
6	Lh1 = 0.522 Lv3 = 0.524 Individual = 0.524	Lh1 = 0.398 Lv3 = 0.404 Individual = 0.404
7	Lh1 = 0.519 Lv2 = 0.521 Individual = 0.521	Lh1 = 0.448 Lv2 = 0.455 Individual = 0.455

Table 3.1: The recorded positions of each beacon in both detectors and for all alignment groups they lie in are shown.

For beacons 0,4,6 and 7 there is a slight difference between the detector normalized positions for different alignment categories. This can be attributed to the fact that the values in the Table 3.1

pertain to one timestep chosen for which position values for all beacons and detectors are available.

When the detector position values of each beacon are compared to the beacon's corresponding position on the board, it can be inferred that the direction of increase of normalized position for both detectors would be as shown in Figure 3.3.

Figure 3.3: The direction of increasing position values for both detectors is shown, as inferred from Table 3.1. The orange arrow shows the direction of increasing position values for Detector 0 and the blue line shows the direction of increasing position values for Detector 1

Figure 3.3 forces a change in the perception of the coordinate system of the image plane from the conventional $\begin{bmatrix} d_0 & d_1 \end{bmatrix}$ to $\begin{bmatrix} d_{1max} - d_1 & d_0 \end{bmatrix}$. Where d_0 is the normalized position for detector 0, d_1 is the normalized position for detector 1 and d_{1max} is the maximum normalized position physically observed for detector 1. So, the x axis of the fictitious image plane is in the opposite direction of the blue arrow in Figure 3.3, the y axis is in the direction of the orange arrow and the z axis comes out of the front face on the camera.

A calibration test was conducted ,with the camera in the tilted alignment, with the goal to ascertain the choice of coordinates from the detector position values so as to obtain a near-parallel image plane alignment with the inertial plane. The same beacon arrangement as shown in Figure 3.1 is used. The position of the origin, in addition to the beacon positions, is shown in Figure 3.4.

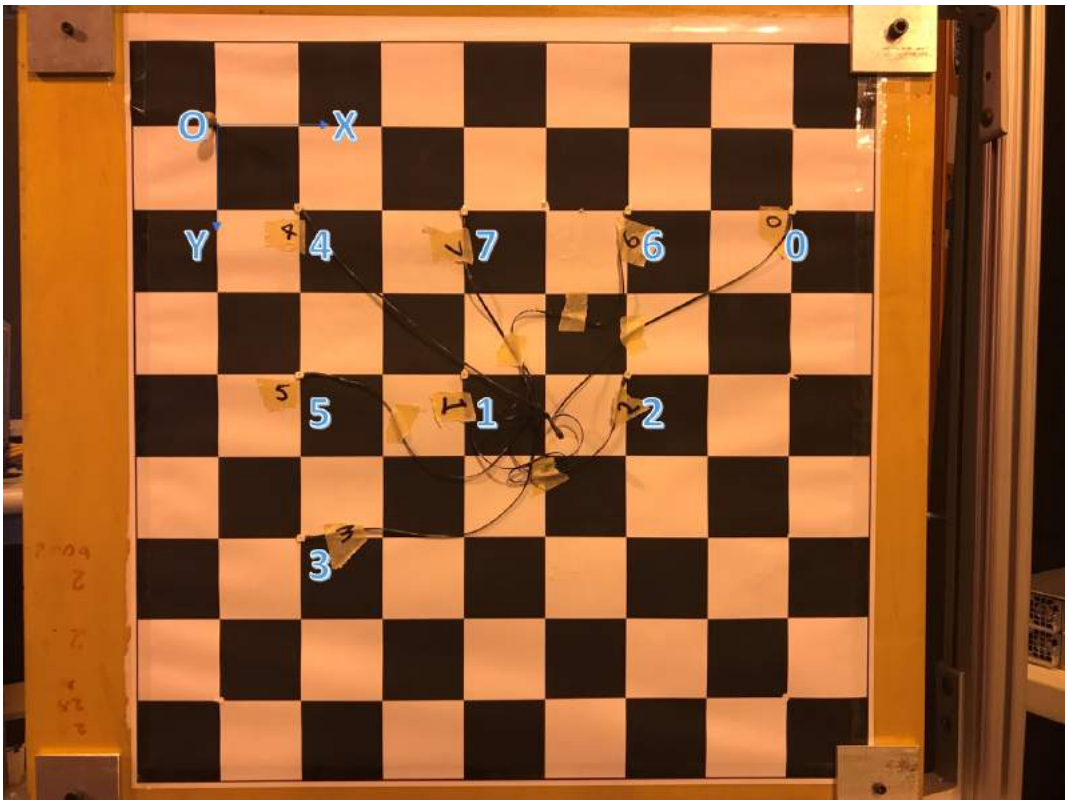

Figure 3.4: The inertial coordinate system with beacon positions. "O" is the origin and "OX" and "OY" represent the inertial planar axes.

The inertial frame coordinates of each beacon are shown in Table 3.2.

Beacon No.	**Inertial Position**
0	$[7s,s]$
1	$[3s,3s]$
2	$[5s,3s]$
3	$[s,5s]$
4	$[s,s]$
5	$[s,3s]$
6	$[5s,s]$
7	$[3s,s]$

Table 3.2: Inertial coordinates of each beacon given as [X-coordinate,Y-coordinate], s=49/16 inches

The image plane projections for each pose of the board as seen from the Phasespace Viewer are shown in 3.10 and their corresponding physical setup images can be seen in Figure 3.11.

The extrinsic projections of each frame as computed from Zhang's[1] homography algorithm is shown in Figure 3.12. The projections have been shown from the board's perspective. For aesthetic purposes, the figures have been moved to the end of the Chapter.

For the purpose of simple verification, consider the first figure and the last two figures. These three figures are fronto-parallel board orientations at different distances from the camera. The increasing order of frames by distance is Frame 1, Frame 23 and Frame 24. The extrinsic projections of these frames as seen in Figure 3.12 provide two conclusions:

- The inter-planar distance between the inertial and the frame coordinate system also increases from Frame 1 to Frame 24 through Frame 23.
- The planar axes are nearly aligned to each other, as is expected for the fronto-parallel orientation.

The translation and CRP plots against frame number are given in Figures 3.5 and 3.6 respectively.

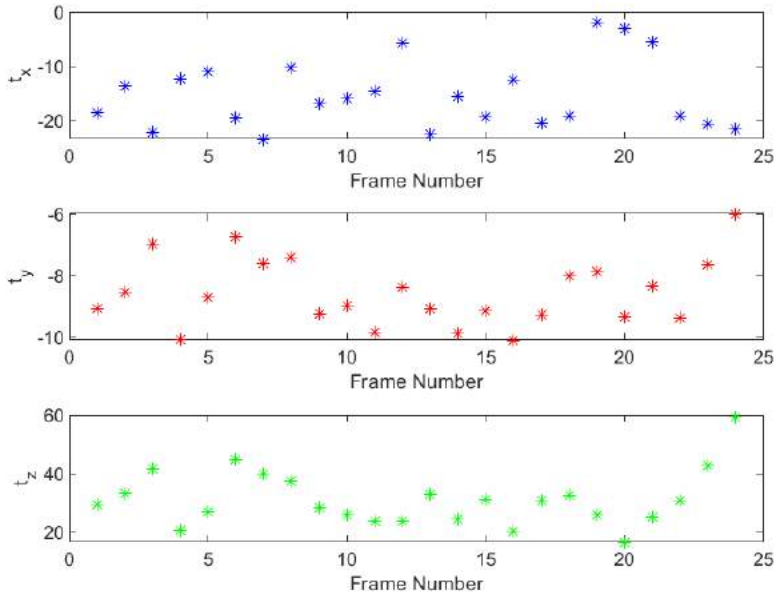

Figure 3.5: Plots of translation vector elements in inches against frame number

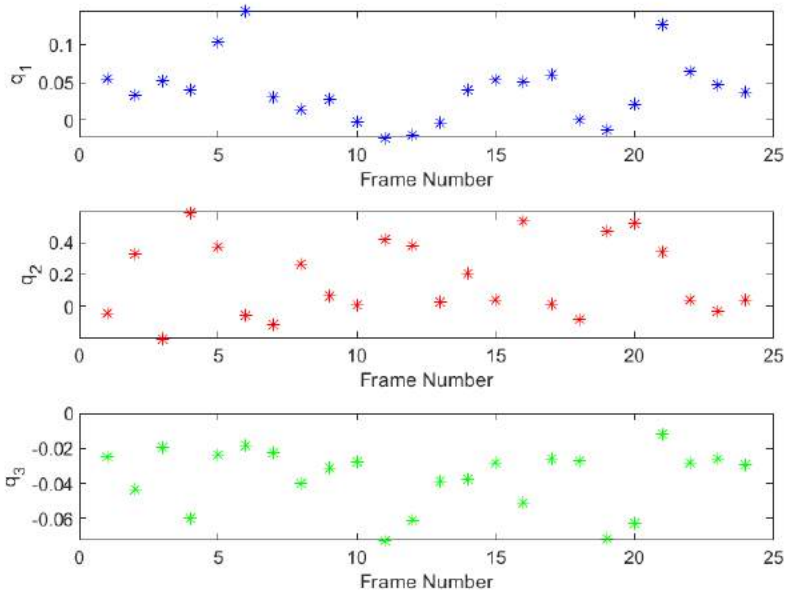

Figure 3.6: Plots of CRP vector elements against frame number

The z-coordinate of the translation vectors for all frames are positive, which lends credibility to the solution. All CRPs for all the frames are below 1. The extrinsic projections of all frames with respect to the inertial frame are shown in Figure 3.7.

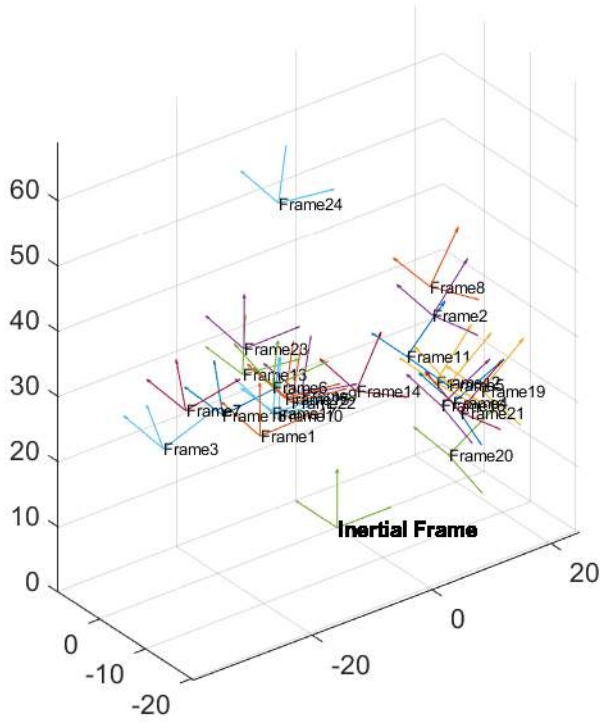

Figure 3.7: Extrinsic Projections of all frames combined and shown with respect to the inertial frame

The choice of image plane coordinates, as related to the position values from the two linear detectors, to obtain nearly aligned planar axes of the image plane and the inertial plane was determined by undergoing cases for assignment of the detectors as the two axes of the image plane and finding the right assignment. If $\hat{\boldsymbol{u}}$ and $\hat{\boldsymbol{v}}$ are the two fictitious image plane axes and $\hat{\boldsymbol{d}}_{\mathbf{0}}$ and $\hat{\boldsymbol{d}}_{\mathbf{1}}$ are the unit vectors associated with detectors 0 and 1 respectively, the following cases were tested.

- Case 1: -$\hat{\boldsymbol{d}}_{\mathbf{0}} \parallel \hat{\boldsymbol{u}}$ and $\hat{\boldsymbol{d}}_{\mathbf{1}} \parallel \hat{\boldsymbol{v}}$
- Case 2: $\hat{\boldsymbol{d}}_{\mathbf{1}} \parallel \hat{\boldsymbol{u}}$ and $\hat{\boldsymbol{d}}_{\mathbf{0}} \parallel \hat{\boldsymbol{v}}$
- Case 3: -$\hat{\boldsymbol{d}}_{\mathbf{1}} \parallel \hat{\boldsymbol{u}}$ and $\hat{\boldsymbol{d}}_{\mathbf{0}} \parallel \hat{\boldsymbol{v}}$

The negative detector axes coordinates were represented as $d_{nmax} - d_n$, where $n \in [0, 1]$. d_{nmax} was calculated using the range test, discussed in the next subsection.

The image plane projections plotted by Matlab, were compared with the inertial frame projections plotted by Matlab. These are shown in Figure 3.8.

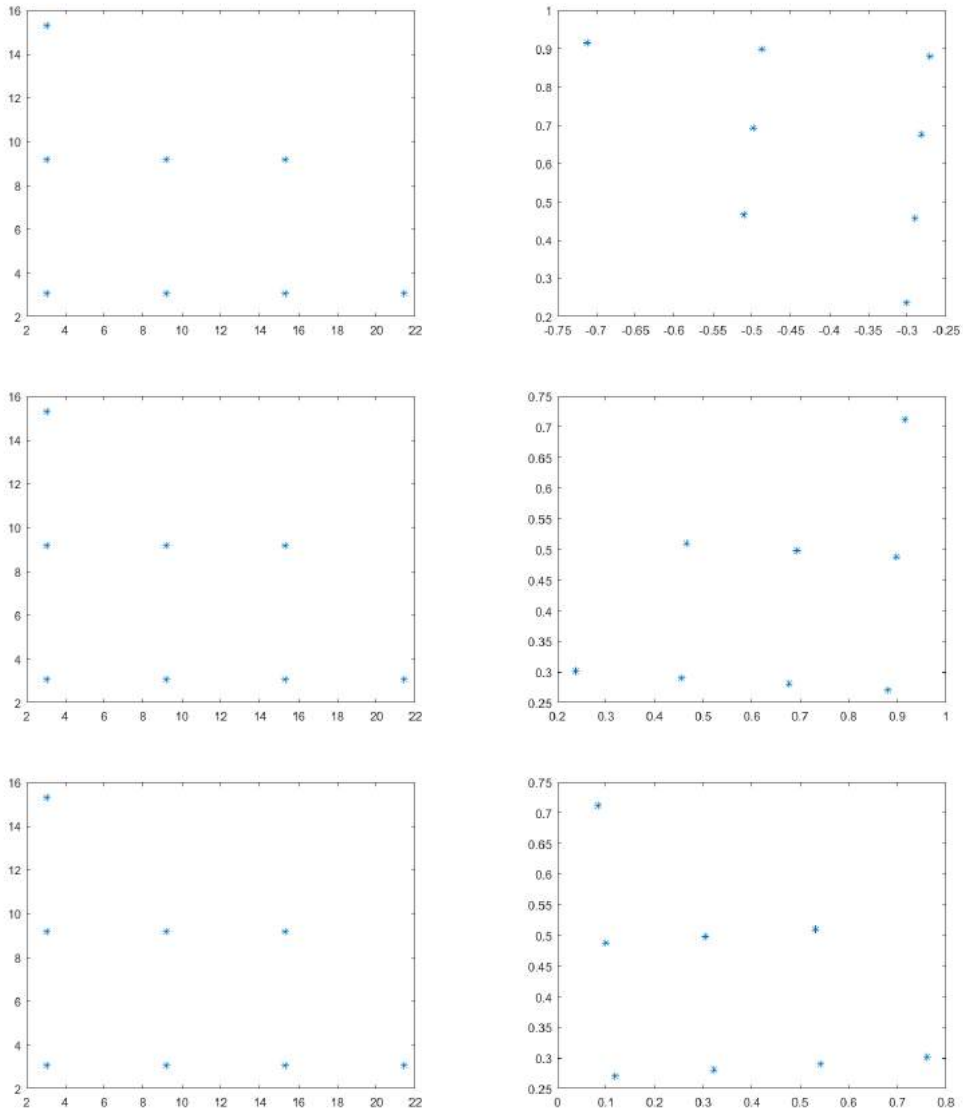

Figure 3.8: Comparison between the inertial frame projections (shown on the left) and the image plane projections (shown on the right) for each case. The top two images are for Case 1, the middle two images are for Case 2 and the bottom two images are for Case 3

It can be seen from Figure 3.8 that for Case 3, the two plot match nearly perfectly. This implies that the sense of the image plane for the Phasespace Camera is indeed as seen in Figure 3.3.

3.2.2 Range Test

The next test was to determine the range of normalized position values for both detectors. The main reason for this test was to determine the value of d_{1max}. This test was performed by keeping the board stationary and moving the camera around so as to capture various positions of the beacons covering as much of the workspace of the camera's field of view as possible. There were beacon registration errors when the camera was brought too close to the board so data was acquired in three stages with the camera being set at three different pitch angles. These three levels are named upper, centre and lower. Figure 3.9 shows the various positions each beacon occupied at all timesteps and for all three camera pitch angle configurations.

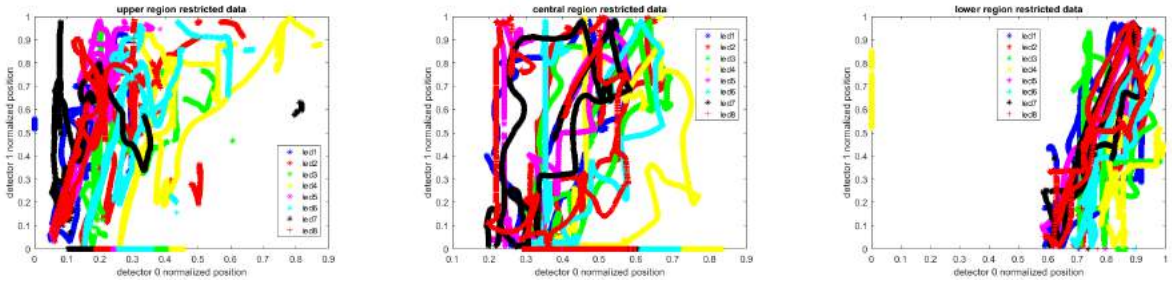

(a) Normalized positions of all beacons for the upper pitch angle camera configuration

(b) Normalized positions of all beacons for the centre pitch angle camera configuration

(c) Normalized positions of all beacons for the lower pitch angle camera configuration

Figure 3.9: Normalized beacon positions from the Range Test

From the position data obtained, the maximum and minimum normalized position values for both detectors across all three pitch angle camera configurations were determined. Table 3.3 shows the same.

Out of the values shown in Table 3.3, the one of most importance is d_{1max} since it will be used to determine the y coordinate of a beacon in the fictitious image plane, as discussed in the previous subsection.

Detector max/min	Value
Detector 0 max	0.991708
Detector 0 min	0
Detector 1 max	0.99814
Detector 1 min	0

Table 3.3: Maximum and minimum recorded normalized position values for both detectors

3.2.3 Standard Deviation Test

In order to be aware of the deviation in position that can be expected from the camera's sensor, the standard deviation test was conducted. The main inspiration for this test came from the results of the basis vectors test for beacons 0,4,6 and 7 shown in Table 3.1.

The test was conducted by keeping the board and the camera stationary with a certain distance between them and acquiring data for about 20 seconds. Two iterations of this test were conducted. The results of the first iteration are provided in Table 3.4 and the results of the second iteration are provide in Table 3.5. The results are tabulated beacon-wise to shine light on the influence of specific beacons on the uncertainty of their positions.

Beacon No.	Standard Deviation for d_0	Standard Deviation for d_1
0	0.0059247	0.0000019
1	0.0064068	0.0000015
2	0.0000019	0.0000064
3	0.0000053	0.0075424
4	0.0000021	0.0000020
5	0.0000037	0.0000017
6	0.0000015	0.0000085
7	0.0000019	0.0046924

Table 3.4: Standard Deviation values sorted beacon-wise for the first iteration of the Standard Deviation Test. d_0 and d_1 pertain to positions in detectors 0 and 1 respectively.

Out of all the standard deviation values observed in both tables, the maximum standard deviation value observed is 0.0075424. Looking at the variation in position values for beacons 0,4,6 and

Beacon No.	**Standard Deviation for d_0**	**Standard Deviation for d_1**
0	0.0000119	0.0000025
1	0.0000037	0.0073923
2	0.0000020	0.0065174
3	0.0000052	0.0000142
4	0.0000021	0.0000018
5	0.0000037	0.0058451
6	0.0000014	0.0045665
7	0.0000019	0.0051810

Table 3.5: Standard Deviation values sorted beacon-wise for the second iteration of the Standard Deviation Test. d_0 and d_1 pertain to positions in detectors 0 and 1 respectively.

7 in Table 3.1, all variations lie within 0.0075424. So those measurements are acceptable. Also, the fact that both iterations show different standard deviations for both detectors for different beacons shows that the standard deviation for any beacon at any day cannot be certainly determined.

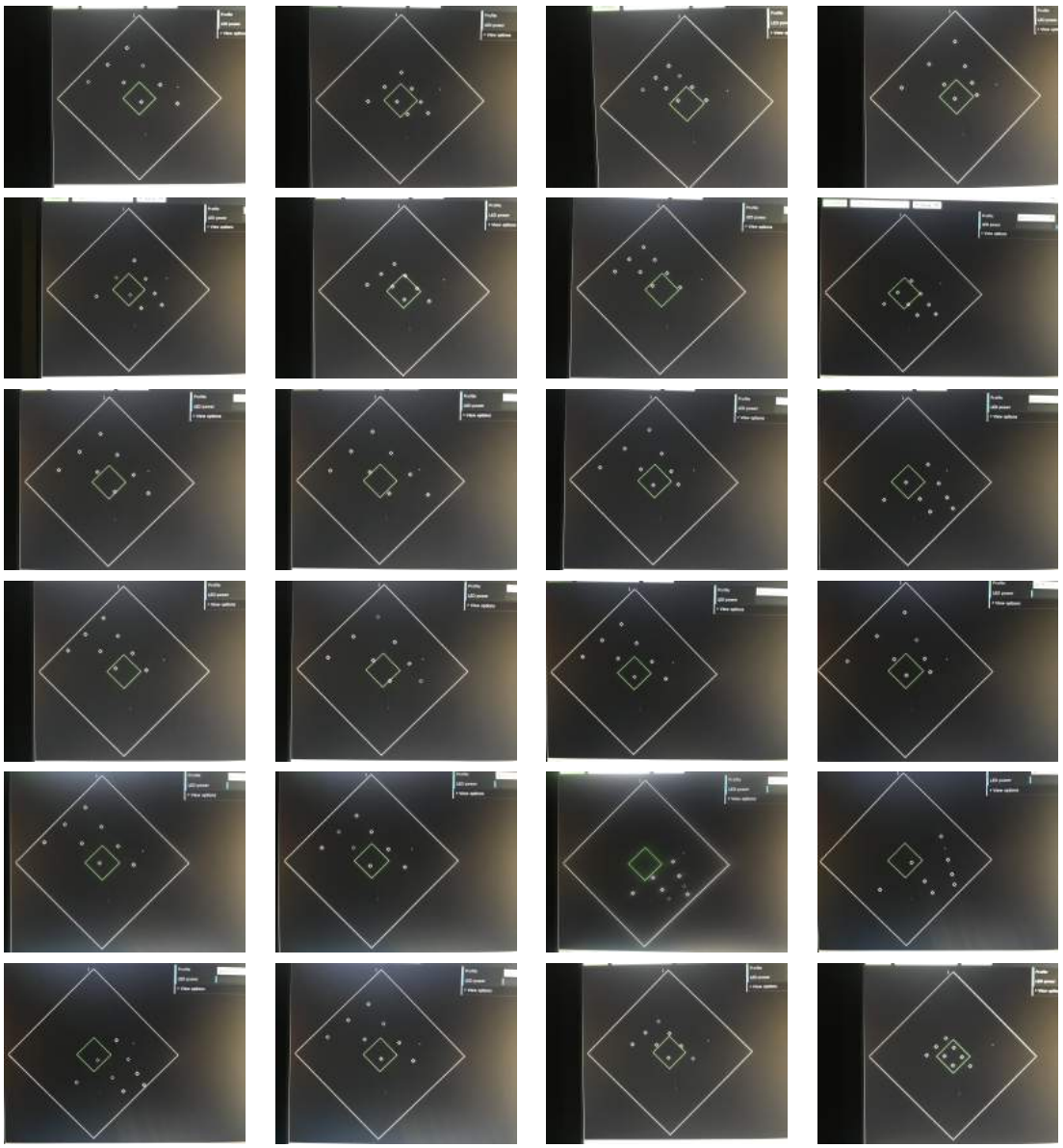

Figure 3.10: Image plane projections of each pose of the board as seen through the Phasespace Viewer. The frames are ordered from the top left to the bottom right.

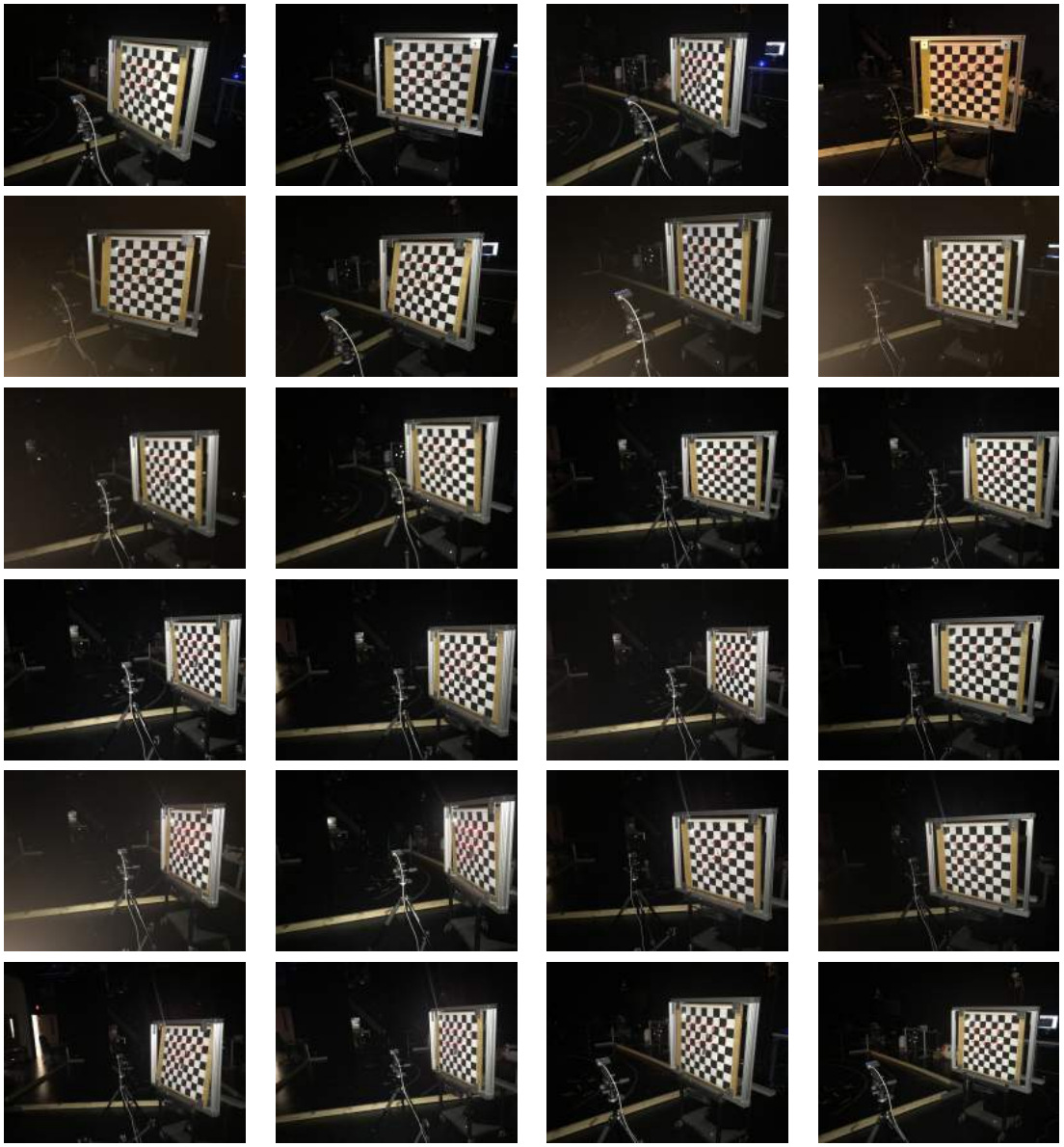

Figure 3.11: The physical alignment of the board with respect to the camera corresponding to each image plane projection shown in Figure 3.10. The frames are ordered from the top left to the bottom right.

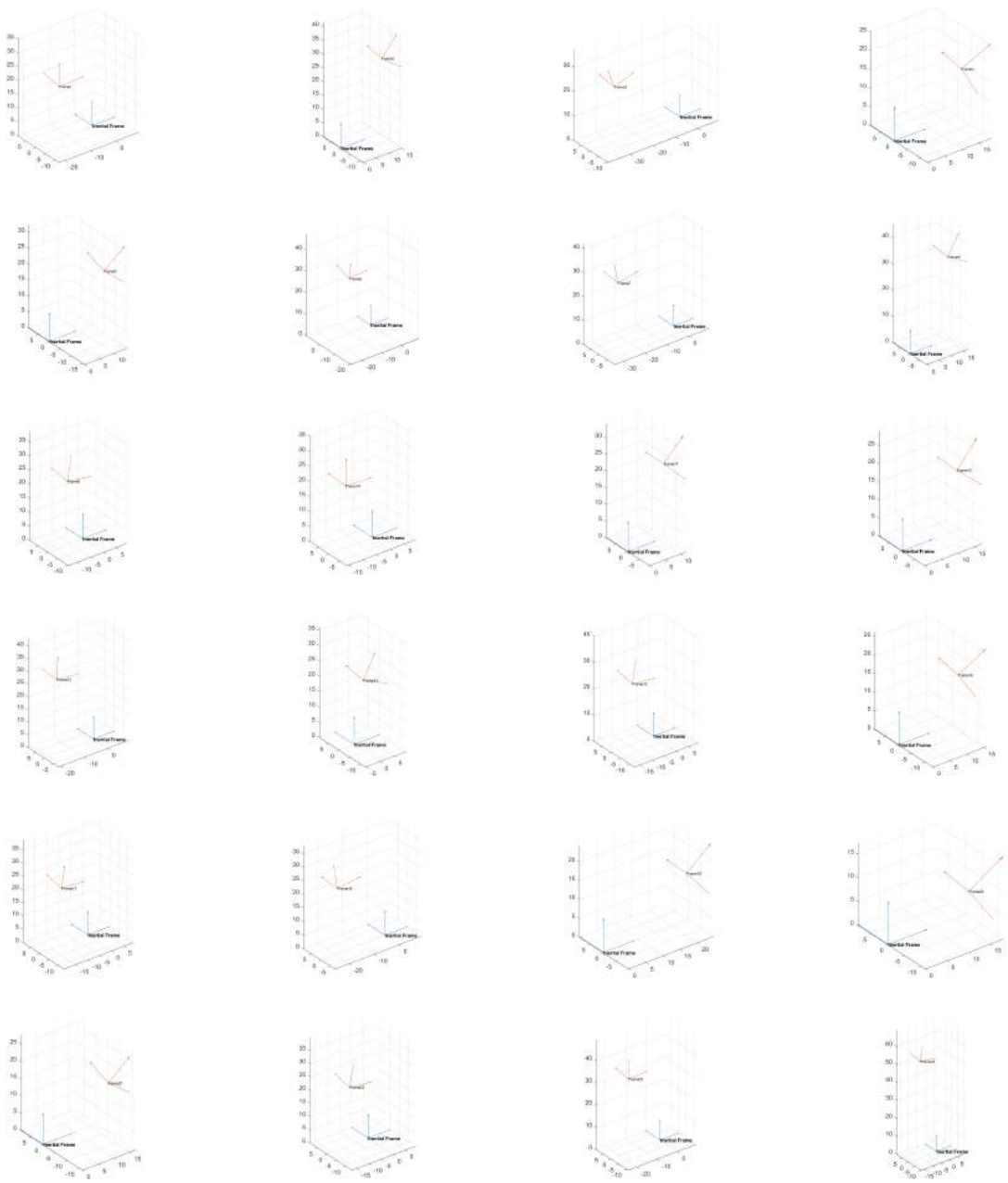

Figure 3.12: Extrinsic Projections as computed using Zhang's Homography algorithm corresponding to each image plane projection shown in Figure 3.10. The distances are provided in inches. The frames are ordered from the top left to the bottom right.

4. ESTIMATION OF THE EXTRINSICS USING NONLINEAR LEAST SQUARES[1]

As stated before, Wong et al[3] presents an batch algorithm to estimate the relative pose of the camera with respect to the target given the intrinsic parameters and the distortion coefficients. The estimation of the pose rates is not performed and instantaneous beacon positions in the image plane are used to estimate instantaneous relative pose of the camera. It is noteworthy that the planar assumption for the beacons in the target centred frame is not required for this algorithm, but the camera must be calibrated.

The objective is to obtain expressions relating the image coordinates of the beacons to their inertial coordinates using the notions of homography and rigid body motion. 4.1 represents rigid body motion and 4.2 represents the pinhole camera model without distortion.

$$\boldsymbol{p_i^C} = R\boldsymbol{p_i^W} + \boldsymbol{t} \tag{4.1}$$

$$\begin{aligned} u_i &= u_0 + f_x \frac{x_i^C}{z_i^C} \\ v_i &= v_0 + f_y \frac{y_i^C}{z_i^C} \end{aligned} \tag{4.2}$$

where $\boldsymbol{p_i^W}$ is the inertial frame coordinate of the ith beacon, $\boldsymbol{p_i^C} = \begin{bmatrix} x_i^C & y_i^C & z_i^C \end{bmatrix}^T$ is the 3D camera frame coordinate of $\boldsymbol{p_i^W}$ and $\begin{bmatrix} u_i & v_i \end{bmatrix}^T$ is the image plane projection associated with $\boldsymbol{p_i^W}$. Principal offset vector $\begin{bmatrix} u_i & v_i \end{bmatrix}^T$ and focal length vector $\begin{bmatrix} f_x & f_y \end{bmatrix}^T$ are the camera intrinsic parameters along with the skewness factor c, not shown here. If the rotation matrix and translation vector are written as $R = \begin{bmatrix} r_{11} & r_{12} & r_{13} \\ r_{21} & r_{22} & r_{23} \\ r_{31} & r_{32} & r_{33} \end{bmatrix}$ and $\boldsymbol{t} = \begin{bmatrix} t_1 \\ t_2 \\ t_3 \end{bmatrix}$ respectively and substituted into 4.2, 4.3

[1]Rewritten with permission from "A Structured Light System for Relative Navigation Applications" by Wong and Majji in IEEE Sensors Journal 16.17 (2016): 6662-6679 ©2011 IEEE

would be obtained.

$$\begin{aligned} u_i &= u_0 + f_x \frac{r_{11}x_i^W + r_{12}y_i^W + r_{13}z_i^W + t_1}{r_{31}x_i^W + r_{32}y_i^W + r_{33}z_i^W + t_3} \\ v_i &= v_0 + f_y \frac{r_{21}x_i^W + r_{22}y_i^W + r_{23}z_i^W + t_2}{r_{31}x_i^W + r_{32}y_i^W + r_{33}z_i^W + t_3} \end{aligned} \tag{4.3}$$

If auxilliary variables u_i' and v_i' are defined as in 4.4, 4.3 would reduce to 4.5. u_i' and v_i' are the normalised camera space coordinates.

$$\begin{bmatrix} u_i' \\ v_i' \\ 1 \end{bmatrix} = A^{-1} \begin{bmatrix} u_i \\ v_i \\ 1 \end{bmatrix} \tag{4.4}$$

$$\begin{aligned} u_i`(r_{31}x_i^W + r_{32}y_i^W + r_{33}z_i^W + t_3) &= r_{11}x_i^W + r_{12}y_i^W + r_{13}z_i^W + t_1 \\ v_i`(r_{31}x_i^W + r_{32}y_i^W + r_{33}z_i^W + t_3) &= r_{21}x_i^W + r_{22}y_i^W + r_{23}z_i^W + t_2 \end{aligned} \tag{4.5}$$

Here, A is the intrinsic parameter matrix. 4.5 pertains to each beacon in each frame. If there are n beacons in each frames, the $2n$ condition equations can be stacked and rearranged in order to form 4.6.

$$\begin{bmatrix} A_1 & A_2 \end{bmatrix} \begin{bmatrix} \boldsymbol{r} \\ \boldsymbol{t} \end{bmatrix} = \mathbf{0} \tag{4.6}$$

where

$$A_1 = \begin{bmatrix} x_1^W & 0 & -u_1'x_i^W & y_1^W & 0 & -u_1'y_1^W & z_1^W & 0 & -u_1'z_1^W \\ 0 & x_1^W & -v_1'x_i^W & 0 & y_1^W & -v_1'y_i^W & 0 & z_1^W & -v_1'z_1^W \\ \vdots & \vdots & \vdots & \vdots & \vdots & \vdots & \vdots & \vdots & \vdots \\ x_n^W & 0 & -u_n'x_n^W & y_n^W & 0 & -u_n'y_n^W & z_n^W & 0 & -u_n'z_n^W \\ 0 & x_n^W & -v_n'x_i^W & 0 & y_n^W & -v_n'y_n^W & 0 & z_n^W & -v_n'z_n^W \end{bmatrix}$$

,

$$A_2 = \begin{bmatrix} 1 & 0 & -u'_1 \\ 0 & 1 & -v'_1 \\ \vdots & \vdots & \vdots \\ 1 & 0 & -u'_n \\ 0 & 1 & -v'_n \end{bmatrix}$$

, $\boldsymbol{r} = \begin{bmatrix} r_{11} & r_{21} & r_{31} & r_{12} & r_{22} & r_{32} & r_{13} & r_{23} & r_{33} \end{bmatrix}^T$ and $\boldsymbol{t}$ is defined earlier. In this research, the A_1 matrix has been modified to accommodate the fact that all beacons lie on a plane in the target centred frame.

$$A_1 = \begin{bmatrix} x_1^W & 0 & -u'_1 x_i^W & y_1^W & 0 & -u'_1 y_1^W & 0 & 0 & 0 \\ 0 & x_1^W & -v'_1 x_i^W & 0 & y_1^W & -v'_1 y_i^W & 0 & 0 & 0 \\ \vdots & \vdots & \vdots & \vdots & \vdots & \vdots & \vdots & \vdots & \vdots \\ x_n^W & 0 & -u'_n x_n^W & y_n^W & 0 & -u'_n y_n^W & 0 & 0 & 0 \\ 0 & x_n^W & -v'_n x_i^W & 0 & y_n^W & -v'_n y_n^W & 0 & 0 & 0 \end{bmatrix} \tag{4.7}$$

The last three columns in 4.7 can be truncated during computation. On substitution into 4.6, it is clear that the last column of the rotation matrix gets eliminated from the computational process. This highlights the similarity of this configuration with the homography algorithm discussed in Zhang[1].

$\boldsymbol{r}$ and $\boldsymbol{t}$ can be found by solving the linear algebra problem outlined by 4.6.

Now, $\boldsymbol{t}$ can be computed in terms of $\boldsymbol{r}$ in accordance with 4.8.

$$\hat{\boldsymbol{t}} = -(A_2^T A_2)^{-1} A_2^T A_1 \boldsymbol{r} \tag{4.8}$$

Since A_2 is column rank deficient, the pseudo-inverse of A_2 is used to compute the translation vector. Also, due to the errors associated with the pseudo-inverse process 4.8 does not deterministically obtain $\boldsymbol{t}$ but only estimates it, therefore the notation of $\hat{\boldsymbol{t}}$ is used to represent the translation vector.

On resubstituting 4.8 into 4.6, the null space problem to solve for $\boldsymbol{r}$ is obtained.

$$(A_1 - A_2(A_2^T A_2)^{-1} A_2^T A_1)\boldsymbol{r} = K\boldsymbol{r} = 0 \tag{4.9}$$

Noting the modified definition of A_1 as shown in 4.7, the projection matrix K will have a distinct form wherein the last three columns will be zeros, owing to the fact that $K = SA_1$ where $S = I - A_2(A_2^T A_2)^{-1} A_2^T$. This again reinforces the fact that only $\boldsymbol{r_1}$ and $\boldsymbol{r_2}$ are begin estimated, thus reaffirming the similarity with the homography algorithm in Zhang[1]. Two challenges are associated with the null space solution.

- There is scale ambiguity in the solution, thus precluding the direct estimation of the orthogonal matrix.
- In the presence of noise, small changes in parameters of K can cause large variations in the null space vector.

To alleviate some of these challenges, the rotation matrix is parameterized in terms of CRPs. The use of CRPs has the following advantages.

- Reduction of dimensionality of the pose estimation problem to 6.
- Each row of the $K\boldsymbol{r} = 0$ equation is a quadratic in the CRPs, assuring global convergence and facilitating the formulation of the problem into a nonlinear least squares problem.

If we define, $K\boldsymbol{r}$ as $\boldsymbol{f}(u, v, \boldsymbol{P^T}, \hat{\boldsymbol{q}})$, then we have the following.

$$\boldsymbol{y} = f(u, v, \boldsymbol{P^T}, \boldsymbol{q}) = \boldsymbol{0} \tag{4.10}$$

Here, $\boldsymbol{P^T}$ is the beacon coordinates in the target centred frame stacked on top of each other. The actual measurements will have some errors, therefore

$$\tilde{\boldsymbol{y}} = f(u, v, \boldsymbol{P^T}, \hat{\boldsymbol{q}}) + \boldsymbol{e} \tag{4.11}$$

The cost function to be minimized is 4.12

$$J = \frac{1}{2}\boldsymbol{e^T} W \boldsymbol{e} = \frac{1}{2}[\boldsymbol{f}(\hat{\boldsymbol{q}})]^{\boldsymbol{T}} W [\boldsymbol{f}(\hat{\boldsymbol{q}})] \tag{4.12}$$

After linearizing about the current estimate of CRPs, the closed form optimal corrections are given by 4.13

$$\Delta q = -(H^T W H)^{-1} H^T W \boldsymbol{f}(\hat{(\boldsymbol{q})}) \tag{4.13}$$

Where $H = \frac{\partial f}{\partial q}_{\hat{q}}$ is the Jacobian Matrix. The linearization process is carried out iteratively by updating the current estimate $\hat{q} = \hat{q} + \Delta q$. The derivation and form of H are discussed in Appendix B.

For the purpose of linear covariance analysis, it is assumed that the image space measurements are corrupted by zero mean Gaussian white noise. This is represented by 4.14.

$$\begin{aligned} \tilde{\boldsymbol{u}} &= \boldsymbol{u} + \boldsymbol{\epsilon_u} \\ \tilde{\boldsymbol{v}} &= \boldsymbol{v} + \boldsymbol{\epsilon_v} \end{aligned} \tag{4.14}$$

where $\boldsymbol{\epsilon_u}$ and $\boldsymbol{\epsilon_v}$ represent the independent identically distributed zero mean white noise vectors with covariances Σ_u and Σ_v respectively. Σ_u and Σ_v are diagonal matrices whose iith element is given by σ_{ui}^2 and σ_{vi}^2 respectively. Similarly beacon location uncertainty in the inertial coordinate system is captured using a similar assumption.

$$\tilde{\boldsymbol{P}} = \boldsymbol{P} + \boldsymbol{\epsilon_P} \tag{4.15}$$

with $\boldsymbol{\epsilon_P} = \begin{bmatrix} \boldsymbol{\epsilon_{p1}} & \boldsymbol{\epsilon_{p2}} & \dots & \boldsymbol{\epsilon_{pn}} \end{bmatrix}^T$ and Σ_P is a $3n \times 3n$ diagonal matrix whose ith diagonal element corresponds to position uncertainty in the corresponding beacon coordinate.

The Taylor Series expansion of $\boldsymbol{f}(u, v, \boldsymbol{P^T}, \hat{\boldsymbol{q}})$ is given by 4.16.

$$\boldsymbol{f}(\boldsymbol{u}, \boldsymbol{v}, \boldsymbol{P}, \boldsymbol{q}) = \boldsymbol{f}(\tilde{\boldsymbol{u}}, \tilde{\boldsymbol{v}}, \tilde{\boldsymbol{P}}, \hat{\boldsymbol{q}}) + \left[\frac{\partial \boldsymbol{f}}{\partial \boldsymbol{q}}\right]_{\tilde{\boldsymbol{u}}, \tilde{\boldsymbol{v}}, \tilde{\boldsymbol{P}}, \hat{\boldsymbol{q}}} \delta \boldsymbol{q} + \left[\frac{\partial \boldsymbol{f}}{\partial \boldsymbol{u}}\right]_{\tilde{\boldsymbol{u}}, \tilde{\boldsymbol{v}}, \tilde{\boldsymbol{P}}, \hat{\boldsymbol{q}}} \boldsymbol{\epsilon_u} + \left[\frac{\partial \boldsymbol{f}}{\partial \boldsymbol{v}}\right]_{\tilde{\boldsymbol{u}}, \tilde{\boldsymbol{v}}, \tilde{\boldsymbol{P}}, \hat{\boldsymbol{q}}} \boldsymbol{\epsilon_v} + \left[\frac{\partial \boldsymbol{f}}{\partial \boldsymbol{P}}\right]_{\tilde{\boldsymbol{u}}, \tilde{\boldsymbol{v}}, \tilde{\boldsymbol{P}}, \hat{\boldsymbol{q}}} \boldsymbol{\epsilon_P} + H.O.T \quad (4.16)$$

On ignoring the higher order terms and combining the error contributions by $\boldsymbol{u}$, $\boldsymbol{v}$ and $\boldsymbol{P}$ into a single vector $\boldsymbol{\nu}$, 4.16 reduces to 4.17.

$$\boldsymbol{f}(\boldsymbol{u}, \boldsymbol{v}, \boldsymbol{P}, \boldsymbol{q}) = \boldsymbol{f}(\tilde{\boldsymbol{u}}, \tilde{\boldsymbol{v}}, \tilde{\boldsymbol{P}}, \hat{\boldsymbol{q}}) + H\delta \boldsymbol{q} + G(\tilde{\boldsymbol{u}}, \tilde{\boldsymbol{v}}, \tilde{\boldsymbol{P}}, \hat{\boldsymbol{q}})\boldsymbol{\nu} \quad (4.17)$$

where G is the nonlinear influence matrix that captures the influence of the sensitivities of the function with respect to the image space and inertial space coordinates of the beacons on the errors in the estimation process. The Jacobian Matrix H is evaluated at the converged CRP estimate $\hat{\boldsymbol{q}}$. It can be inferred that the random vector $\boldsymbol{\nu}$ is Gaussian with statistics $(\mathbf{0}, S)$. The covariance matrix S is given by 4.18.

$$S = \begin{bmatrix} \Sigma_u & 0 & 0 \\ 0 & \Sigma_v & 0 \\ 0 & 0 & \Sigma_P \end{bmatrix} \quad (4.18)$$

The CRP estimation error is given by $\boldsymbol{\delta q} = \hat{\boldsymbol{q}} - \boldsymbol{q}$. Keeping in mind that $\boldsymbol{f}(\boldsymbol{u}, \boldsymbol{v}, \boldsymbol{P}, \boldsymbol{q}) = \mathbf{0}$ and utilizing the linear error theory of least squares estimation[27], the CRP error covariance can be computed.

$$P_q = E(\delta \boldsymbol{q} \delta \boldsymbol{q}^T) = (H^T (GSG^T)^{-1} H)^{-1} \quad (4.19)$$

A key assumption in the error quantification in 4.19 is that the least squares estimate $\tilde{\boldsymbol{q}}$ is obtained by using a weighted least squares approach with the weight matrix $W = (GSG^T)^{-1}$.

For linear convariance analysis of the translation error, the relationship between the translation vector and the rotation vector, represented by 4.8, is revisited albeit in a modified form wherein the

weight matrix W has been added. The translation error is given by the following.

$$\delta \boldsymbol{t} = -((A_2^T W A_2)^{-1} A_2^T W A_1)(\boldsymbol{r}(\boldsymbol{q}) - \boldsymbol{r}(\hat{\boldsymbol{q}}) = C(\boldsymbol{r}(\boldsymbol{q}) - \boldsymbol{r}(\hat{\boldsymbol{q}})) \tag{4.20}$$

The nonlinear relationship between the translation error and rotation error shown in 4.20 can be linearized by linearizing $\boldsymbol{r}(\boldsymbol{q})$ about the current CRP estimate $\hat{\boldsymbol{q}}$.

$$\boldsymbol{r}(\boldsymbol{q}) = \boldsymbol{r}(\hat{\boldsymbol{q}}) + \left[\frac{\partial \boldsymbol{r}}{\partial \boldsymbol{q}}\right]_{\hat{\boldsymbol{q}}} \delta \boldsymbol{q}$$

On substituting the linearized rotation vector into 4.20, an approximate expression for translation error convariance can be obtained.

$$P_t = E(\delta \boldsymbol{t} \delta \boldsymbol{t}^T) \approx C \left[\frac{\partial \boldsymbol{r}}{\partial \boldsymbol{q}}\right]_{\hat{\boldsymbol{q}}} E(\delta \boldsymbol{q} \delta \boldsymbol{q}^T) \left[\frac{\partial \boldsymbol{r}}{\partial \boldsymbol{q}}\right]_{\hat{\boldsymbol{q}}}^T C^T \tag{4.21}$$

The Jacobian Matrix $\left[\frac{\partial \boldsymbol{r}}{\partial \boldsymbol{q}}\right]_{\hat{\boldsymbol{q}}}$ is a linear function in the current CRP estimate.

The incorporation of different sources of uncertainty in the image space and inertial space beacon coordinates makes the above outlined process robust to real world sources of error. For example, in the case of occlusion or oblique viewpoints, i.e. where the geometry of observation is poor, the related uncertainty in the acquired data will introduce large errors in the estimation process which will manifest in the large value of error covariance.

5. DISTORTION INCORPORATED ESTIMATION

The Homography algorithm described in Chapter 2 does not assume any distortion in the image plane of the camera. Hence, to estimate the distortion coefficients in addition to the intrinsic and extrinsic parameters, a nonlinear optimization strategy is employed. The nonlinear optimization algorithm of choice is the Levenberg Marquardt [28] algorithm and is carried out using the $lsqnonlin$ function in MatLab. In literature, the most common function used to model the image plane distortions is the Brown's Distortion model[7]. This is because Brown's distortion model was created with Photogrammetric plates in mind and the same model was found to be applicable to modern CCD/CMOS array cameras with rectangular pixels. But to the best knowledge of the author, no distortion model has been implemented on a Phasespace camera or a similar linear imager based camera. So, this section discusses two distortion models:

- Brown's Distortion Model
- Geometric Distortion Model presented by Ma et al[4]

To validate the two distortion models, two known CCD camera datasets are used and the nonlinear optimization algorithm is implemented on both and compared with their known results. Bouguet Toolbox dataset consists of 20 frames capturing a checkerboard pattern with 156 inner corners whereas Zhang's dataset consists of 5 frames capturing a grid of squares pattern with 256 features.

5.1 Brown's Distortion Model

The conventional formulation of distortion most commonly used to undistort CCD/CMOS cameras is given by Brown[7] in Equation 5.1.

$$\begin{aligned} x_d &= x_u + x_u(k_1 r^2 + k_2 r^4 + ...) + (p_1(r^2 + 2x_d^2) + 2p_2 x_u y_u)(1 + p_3 r^2 + p_4 r^4 + ...) \\ y_d &= y_u + y_u(k_1 r^2 + k_2 r^4 + ...) + (2p_1 x_u y_u + p_2(r^2 + 2y_d^2))(1 + p_3 r^2 + p_4 r^4 + ...) \end{aligned} \tag{5.1}$$

where $\begin{bmatrix} x_u & y_u \end{bmatrix}^T$ is the undistorted normalised camera plane coordinate, $\begin{bmatrix} x_d & y_d \end{bmatrix}^T$ is the corresponding distorted normalised camera plane coordinate, $r = \sqrt{x_u^2 + y_u^2}$ is the radial distance, k_i is the ith radial distortion coefficient and p_i is the ith tangential distortion coefficient.

An alternate realization of the relationship between the undistorted and distorted normalised camera plane coordinates, shown in Equation 5.2, can also be employed.

$$\begin{aligned} x_u &= x_d + x_d(k_1 r^2 + k_2 r^4 + ...) + (p_1(r^2 + 2x_d^2) + 2p_2 x_d y_d)(1 + p_3 r^2 + p_4 r^4 + ...) \\ y_u &= y_d + y_d(k_1 r^2 + k_2 r^4 + ...) + (2p_1 x_u y_d + p_2(r^2 + 2y_d^2))(1 + p_3 r^2 + p_4 r^4 + ...) \end{aligned} \tag{5.2}$$

Here, $r = \sqrt{x_d^2 + y_d^2}$.

Since both the distortion models use infinite radial and tangential distortion coefficients, choice of the number of coefficients to use is left to the user.

Zhang[1] utilizes a simplified version of Brown's distortion model wherein only the first two radial distortion parameters are considered and develops a linear least squares solution to obtain their estimates.

Since a linear imager is being discussed, both radial and tangential distortion must be taken into consideration. For the purposes of this research, three radial and two tangential distortion coefficients are considered. Thus the simplified Brown's distortion model corresponding to Equation 5.1 is given below. This is the model used in this research.

$$\begin{aligned} x_d &= x_u + x_u(k_1 r^2 + k_2 r^4 + k_3 r^6) + p_1(r^2 + 2x_u^2) + 2p_2 x_u y_u \\ y_d &= y_u + y_u(k_1 r^2 + k_2 r^4 + k_3 r^6) + 2p_1 x_u y_u + p_2(r^2 + 2y_u^2) \end{aligned} \tag{5.3}$$

With the lens distortion taken into consideration, Brown's model is utilized to estimate the distorted image plane coordinates for comparison with the measured image plane coordinates. It must be noted that Equations 5.1 and 5.2 represent the relationship between the undistorted and

distorted beacon coordinates in the normalised camera frame.

Brown's distortion model represented by Equation 5.3 is tested with the Bouguet's Camera Calibration Toolbox[29] dataset and Zhang's [1] dataset.

Henceforth, the process of optimizing over the intrinsics, extrinsics and the distortion coefficients will be referred to as the "Combined Estimation Approach". The Combined Estimation Approach can employ either the Brown's distortion model or the Geometric distortion model.

5.1.1 Bouguet Toolbox Dataset

The results of applying the combined estimation approach to the Bouguet Toolbox[29] Dataset are compared to the results of application of the Toolbox itself. Below is the comparitive study of the same.

The initialization values from Homography are optimized using the combined estimation approach, whereas the initialization values in Bouguet's Toolbox are optimized using the Steepest Gradient Descent algorithm. After optimization, the comparison of results are shown in the Tables that follow.

Table 5.1 shows the optimized intrinsics as computed by both the combined estimation approach and Steepest Gradient Descent side by side. The initial value shown in the Table are computed using Homgraphy.

It can be seen from the Table 5.1 that the converged intrinsics in both cases are extremely close to each other. Tables 5.2, 5.3 and 5.4 show the rotation matrices as computed from the converged parameters of rotation (CRPs in the case of the combined estimation approach and principal rotation vector in the case of the Bouguet Toolbox) next to each other for comparison. Tables 5.5 and 5.6 shows the translation vectors. The initial values shown in the tables are computed using homography.

Parameter	Initial Values	Optimized Values	Bouguet Toolbox Values
α	652.0965121	657.5199781	657.5199789
β	660.1095416	657.8880139	657.8880141
c	0.708048876	0.330929654	0.330929792
u_0	279.780234	302.6640633	302.6640606
v_0	225.9629734	242.434325	242.4343209
k_1	0	-0.261286314	-0.261286377
k_2	0	0.176867237	0.176867826
k_3	0	-0.122710594	-0.122712115
p_1	0	0.0000623	0.0000623
p_2	0	-0.000226054	-0.000226055

Table 5.1: Intrinsic parameters and distortion coefficients for the Bouguet Toolbox dataset are shown. The initial values, computed using Homography, are used for Nonlinear Optimization. The corresponding parameter values from the Bouguet Toolbox are shown for comparison. Brown's Distortion Model is used in the optimization process

Rotation Matrix			
Frame	Initial Values	Optimized Values	Bouguet Toolbox Values
1	$\begin{bmatrix} 0.044 & 0.991 & 0.120 \\ 0.638 & 0.064 & -0.767 \\ -0.768 & 0.111 & -0.630 \end{bmatrix}$	$\begin{bmatrix} 0.054 & 0.992 & 0.112 \\ 0.633 & 0.052 & -0.772 \\ -0.772 & 0.113 & -0.625 \end{bmatrix}$	$\begin{bmatrix} 0.054 & 0.992 & 0.112 \\ 0.633 & 0.052 & -0.772 \\ -0.772 & 0.113 & -0.625 \end{bmatrix}$
2	$\begin{bmatrix} -0.0004 & 0.991 & 0.137 \\ 0.861 & 0.069 & -0.503 \\ -0.508 & 0.117 & -0.853 \end{bmatrix}$	$\begin{bmatrix} 0.005 & 0.992 & 0.120 \\ 0.860 & 0.056 & -0.505 \\ -0.508 & 0.106 & -0.854 \end{bmatrix}$	$\begin{bmatrix} 0.005 & 0.992 & 0.120 \\ 0.860 & 0.056 & -0.505 \\ -0.508 & 0.106 & -0.854 \end{bmatrix}$
3	$\begin{bmatrix} -0.162 & 0.983 & 0.077 \\ 0.847 & 0.179 & -0.499 \\ -0.505 & -0.015 & -0.862 \end{bmatrix}$	$\begin{bmatrix} -0.158 & 0.985 & 0.057 \\ 0.848 & 0.166 & -0.502 \\ -0.504 & -0.030 & -0.862 \end{bmatrix}$	$\begin{bmatrix} -0.158 & 0.985 & 0.057 \\ 0.848 & 0.166 & -0.502 \\ -0.504 & -0.030 & -0.862 \end{bmatrix}$
4	$\begin{bmatrix} -0.252 & 0.917 & -0.307 \\ 0.782 & 0.006 & -0.622 \\ -0.568 & -0.397 & -0.720 \end{bmatrix}$	$\begin{bmatrix} -0.255 & 0.901 & -0.349 \\ 0.802 & -0.004 & -0.596 \\ -0.539 & -0.433 & -0.722 \end{bmatrix}$	$\begin{bmatrix} -0.255 & 0.901 & -0.349 \\ 0.802 & -0.004 & -0.596 \\ -0.539 & -0.433 & -0.722 \end{bmatrix}$
5	$\begin{bmatrix} -0.246 & 0.768 & 0.590 \\ 0.575 & 0.605 & -0.548 \\ -0.779 & 0.204 & -0.592 \end{bmatrix}$	$\begin{bmatrix} -0.225 & 0.766 & 0.601 \\ 0.584 & 0.600 & -0.545 \\ -0.779 & 0.228 & -0.583 \end{bmatrix}$	$\begin{bmatrix} -0.225 & 0.766 & 0.601 \\ 0.584 & 0.600 & -0.545 \\ -0.779 & 0.228 & -0.583 \end{bmatrix}$
6	$\begin{bmatrix} -0.130 & 0.990 & 0.043 \\ 0.734 & 0.067 & 0.675 \\ 0.666 & 0.119 & -0.735 \end{bmatrix}$	$\begin{bmatrix} -0.140 & 0.989 & 0.041 \\ 0.733 & 0.076 & 0.675 \\ 0.664 & 0.125 & -0.736 \end{bmatrix}$	$\begin{bmatrix} -0.140 & 0.989 & 0.041 \\ 0.733 & 0.076 & 0.675 \\ 0.664 & 0.125 & -0.736 \end{bmatrix}$
7	$\begin{bmatrix} -0.145 & 0.798 & 0.584 \\ 0.851 & -0.199 & 0.484 \\ 0.503 & 0.568 & -0.650 \end{bmatrix}$	$\begin{bmatrix} -0.153 & 0.786 & 0.597 \\ 0.846 & -0.207 & 0.490 \\ 0.510 & 0.581 & -0.634 \end{bmatrix}$	$\begin{bmatrix} -0.153 & 0.786 & 0.597 \\ 0.846 & -0.207 & 0.490 \\ 0.510 & 0.581 & -0.634 \end{bmatrix}$

Table 5.2: The rotation matrices for the first 7 frames of the Bouguet Toolbox dataset are shown. The initial values, computed by Homography, are used for nonlinear optimization. The results from Bouguet Toolbox are shown for comparison. Brown's Distortion function is used in the optimization process

Rotation Matrix			
Frame	Initial Values	Optimized Values	Bouguet Toolbox Values
8	$\begin{bmatrix} -0.113 & 0.768 & 0.629 \\ 0.866 & -0.232 & 0.441 \\ 0.485 & 0.595 & -0.639 \end{bmatrix}$	$\begin{bmatrix} -0.132 & 0.729 & 0.671 \\ 0.863 & -0.247 & 0.439 \\ 0.486 & 0.638 & -0.597 \end{bmatrix}$	$\begin{bmatrix} -0.132 & 0.729 & 0.671 \\ 0.863 & -0.247 & 0.439 \\ 0.486 & 0.638 & -0.597 \end{bmatrix}$
9	$\begin{bmatrix} -0.206 & 0.750 & -0.627 \\ 0.895 & 0.403 & 0.188 \\ 0.394 & -0.523 & -0.755 \end{bmatrix}$	$\begin{bmatrix} -0.200 & 0.718 & -0.666 \\ 0.892 & 0.414 & 0.178 \\ 0.404 & -0.558 & -0.723 \end{bmatrix}$	$\begin{bmatrix} -0.200 & 0.718 & -0.666 \\ 0.892 & 0.414 & 0.178 \\ 0.404 & -0.558 & -0.723 \end{bmatrix}$
10	$\begin{bmatrix} -0.231 & 0.854 & -0.465 \\ 0.930 & 0.334 & 0.152 \\ 0.285 & -0.397 & -0.871 \end{bmatrix}$	$\begin{bmatrix} -0.215 & 0.835 & -0.505 \\ 0.912 & 0.356 & 0.199 \\ 0.347 & -0.418 & -0.839 \end{bmatrix}$	$\begin{bmatrix} -0.215 & 0.835 & -0.505 \\ 0.912 & 0.356 & 0.199 \\ 0.347 & -0.418 & -0.839 \end{bmatrix}$
11	$\begin{bmatrix} -0.122 & 0.991 & -0.045 \\ 0.893 & 0.129 & 0.430 \\ 0.432 & 0.012 & -0.901 \end{bmatrix}$	$\begin{bmatrix} -0.127 & 0.990 & -0.049 \\ 0.867 & 0.135 & 0.478 \\ 0.481 & 0.018 & -0.876 \end{bmatrix}$	$\begin{bmatrix} -0.127 & 0.990 & -0.049 \\ 0.867 & 0.135 & 0.478 \\ 0.481 & 0.018 & -0.876 \end{bmatrix}$
12	$\begin{bmatrix} -0.124 & 0.991 & 0.023 \\ 0.891 & 0.101 & 0.440 \\ 0.434 & 0.076 & -0.897 \end{bmatrix}$	$\begin{bmatrix} -0.127 & 0.991 & 0.004 \\ 0.880 & 0.110 & 0.461 \\ 0.457 & 0.062 & -0.886 \end{bmatrix}$	$\begin{bmatrix} -0.127 & 0.991 & 0.004 \\ 0.880 & 0.110 & 0.461 \\ 0.457 & 0.062 & -0.886 \end{bmatrix}$
13	$\begin{bmatrix} -0.118 & 0.985 & 0.119 \\ 0.901 & 0.056 & 0.431 \\ 0.418 & 0.158 & -0.894 \end{bmatrix}$	$\begin{bmatrix} -0.121 & 0.987 & 0.103 \\ 0.897 & 0.064 & 0.437 \\ 0.425 & 0.146 & -0.893 \end{bmatrix}$	$\begin{bmatrix} -0.121 & 0.987 & 0.103 \\ 0.897 & 0.064 & 0.437 \\ 0.425 & 0.146 & -0.893 \end{bmatrix}$
14	$\begin{bmatrix} -0.109 & 0.983 & 0.144 \\ 0.911 & 0.041 & 0.408 \\ 0.396 & 0.176 & -0.901 \end{bmatrix}$	$\begin{bmatrix} -0.108 & 0.986 & 0.120 \\ 0.909 & 0.050 & 0.412 \\ 0.401 & 0.154 & -0.902 \end{bmatrix}$	$\begin{bmatrix} -0.108 & 0.986 & 0.120 \\ 0.909 & 0.050 & 0.412 \\ 0.401 & 0.154 & -0.902 \end{bmatrix}$

Table 5.3: The rotation matrices for the frames 8 through 14 of the Bouguet Toolbox dataset are shown. The initial values, computed by Homography, are used for nonlinear optimization. The results from Bouguet Toolbox are shown for comparison.Brown's Distortion function is used in the optimization process

Rotation Matrix			
Frame	Initial Values	Optimized Values	Bouguet Toolbox Values
15	$\begin{bmatrix} -0.081 & 0.985 & 0.149 \\ 0.966 & 0.041 & 0.254 \\ 0.244 & 0.165 & -0.955 \end{bmatrix}$	$\begin{bmatrix} -0.089 & 0.975 & 0.203 \\ 0.970 & 0.039 & 0.237 \\ 0.223 & 0.218 & -0.949 \end{bmatrix}$	$\begin{bmatrix} -0.089 & 0.975 & 0.203 \\ 0.970 & 0.039 & 0.237 \\ 0.223 & 0.218 & -0.949 \end{bmatrix}$
16	$\begin{bmatrix} -0.203 & 0.970 & 0.133 \\ 0.964 & 0.221 & -0.140 \\ -0.166 & 0.100 & -0.981 \end{bmatrix}$	$\begin{bmatrix} -0.207 & 0.977 & 0.030 \\ 0.962 & 0.210 & -0.172 \\ -0.174 & -0.006 & -0.984 \end{bmatrix}$	$\begin{bmatrix} -0.207 & 0.977 & 0.030 \\ 0.962 & 0.210 & -0.172 \\ -0.174 & -0.006 & -0.984 \end{bmatrix}$
17	$\begin{bmatrix} -0.102 & 0.966 & -0.235 \\ 0.807 & 0.218 & 0.547 \\ 0.581 & -0.134 & -0.802 \end{bmatrix}$	$\begin{bmatrix} -0.104 & 0.958 & -0.264 \\ 0.809 & 0.236 & 0.538 \\ 0.578 & -0.157 & -0.800 \end{bmatrix}$	$\begin{bmatrix} -0.104 & 0.958 & -0.264 \\ 0.809 & 0.236 & 0.538 \\ 0.578 & -0.157 & -0.800 \end{bmatrix}$
18	$\begin{bmatrix} 0.045 & 0.856 & -0.513 \\ 0.657 & 0.361 & 0.660 \\ 0.752 & -0.367 & -0.547 \end{bmatrix}$	$\begin{bmatrix} 0.023 & 0.862 & -0.505 \\ 0.639 & 0.375 & 0.670 \\ 0.768 & -0.338 & -0.543 \end{bmatrix}$	$\begin{bmatrix} 0.023 & 0.862 & -0.505 \\ 0.639 & 0.375 & 0.670 \\ 0.768 & -0.338 & -0.543 \end{bmatrix}$
19	$\begin{bmatrix} -0.170 & 0.834 & 0.523 \\ 0.739 & -0.243 & 0.628 \\ 0.651 & 0.493 & -0.575 \end{bmatrix}$	$\begin{bmatrix} -0.186 & 0.824 & 0.533 \\ 0.715 & -0.258 & 0.648 \\ 0.673 & 0.503 & -0.542 \end{bmatrix}$	$\begin{bmatrix} -0.186 & 0.824 & 0.533 \\ 0.715 & -0.258 & 0.648 \\ 0.673 & 0.503 & -0.542 \end{bmatrix}$
20	$\begin{bmatrix} -0.095 & 0.625 & 0.774 \\ 0.852 & -0.349 & 0.387 \\ 0.513 & 0.697 & -0.499 \end{bmatrix}$	$\begin{bmatrix} -0.114 & 0.584 & 0.803 \\ 0.847 & -0.364 & 0.386 \\ 0.518 & 0.724 & -0.453 \end{bmatrix}$	$\begin{bmatrix} -0.114 & 0.584 & 0.803 \\ 0.847 & -0.364 & 0.386 \\ 0.518 & 0.724 & -0.453 \end{bmatrix}$

Table 5.4: The rotation matrices for the frames 15 through 20 of the Bouguet Toolbox dataset are shown. The initial values, computed by Homography, are used for nonlinear optimization. The results from Bouguet Toolbox are shown for comparison.Brown's Distortion function is used in the optimization process

Translation Vector in meters			
Frame	Initial Values	Optimized Values	Bouguet Toolbox Values
1	$\begin{bmatrix} -512.529 \\ -213.933 \\ 2957.725 \end{bmatrix}$	$\begin{bmatrix} -590.490 \\ -278.347 \\ 2844.169 \end{bmatrix}$	$\begin{bmatrix} -590.490 \\ -278.347 \\ 2844.169 \end{bmatrix}$
2	$\begin{bmatrix} -435.655 \\ -472.869 \\ 2588.268 \end{bmatrix}$	$\begin{bmatrix} -515.180 \\ -530.558 \\ 2526.353 \end{bmatrix}$	$\begin{bmatrix} -515.180 \\ -530.558 \\ 2526.353 \end{bmatrix}$
3	$\begin{bmatrix} -330.695 \\ -520.868 \\ 2636.163 \end{bmatrix}$	$\begin{bmatrix} -416.035 \\ -581.429 \\ 2585.814 \end{bmatrix}$	$\begin{bmatrix} -416.035 \\ -581.429 \\ 2585.814 \end{bmatrix}$
4	$\begin{bmatrix} -121.676 \\ -448.102 \\ 2598.821 \end{bmatrix}$	$\begin{bmatrix} -213.229 \\ -515.445 \\ 2597.414 \end{bmatrix}$	$\begin{bmatrix} -213.229 \\ -515.445 \\ 2597.414 \end{bmatrix}$
5	$\begin{bmatrix} -220.317 \\ -701.434 \\ 2506.850 \end{bmatrix}$	$\begin{bmatrix} -306.0125 \\ -763.341 \\ 2456.339 \end{bmatrix}$	$\begin{bmatrix} -306.0125 \\ -763.341 \\ 2456.339 \end{bmatrix}$
6	$\begin{bmatrix} -437.360 \\ -222.515 \\ 1483.488 \end{bmatrix}$	$\begin{bmatrix} -495.461 \\ -265.076 \\ 1483.323 \end{bmatrix}$	$\begin{bmatrix} -495.461 \\ -265.076 \\ 1483.323 \end{bmatrix}$
7	$\begin{bmatrix} -224.688 \\ -219.971 \\ 1477.794 \end{bmatrix}$	$\begin{bmatrix} -275.520 \\ -258.636 \\ 1466.863 \end{bmatrix}$	$\begin{bmatrix} -275.520 \\ -258.636 \\ 1466.863 \end{bmatrix}$
8	$\begin{bmatrix} -514.237 \\ -302.501 \\ 1594.624 \end{bmatrix}$	$\begin{bmatrix} -565.929 \\ -344.657 \\ 1539.911 \end{bmatrix}$	$\begin{bmatrix} -565.929 \\ -344.657 \\ 1539.911 \end{bmatrix}$
9	$\begin{bmatrix} 83.415 \\ -688.332 \\ 2455.271 \end{bmatrix}$	$\begin{bmatrix} -4.652 \\ -749.999 \\ 2429.836 \end{bmatrix}$	$\begin{bmatrix} -4.652 \\ -749.999 \\ 2429.836 \end{bmatrix}$
10	$\begin{bmatrix} 7.971 \\ -944.286 \\ 2991.082 \end{bmatrix}$	$\begin{bmatrix} -96.757 \\ -1000.853 \\ 2868.444 \end{bmatrix}$	$\begin{bmatrix} -96.757 \\ -1000.853 \\ 2868.444 \end{bmatrix}$
11	$\begin{bmatrix} -428.546 \\ -737.311 \\ 2466.929 \end{bmatrix}$	$\begin{bmatrix} -501.981 \\ -783.902 \\ 2349.344 \end{bmatrix}$	$\begin{bmatrix} -501.981 \\ -783.902 \\ 2349.344 \end{bmatrix}$
12	$\begin{bmatrix} -375.588 \\ -540.580 \\ 2064.899 \end{bmatrix}$	$\begin{bmatrix} -443.646 \\ -590.187 \\ 2016.517 \end{bmatrix}$	$\begin{bmatrix} -443.646 \\ -590.187 \\ 2016.517 \end{bmatrix}$

Table 5.5: The translation vectors for the first 12 frames of the Bouguet Toolbox dataset are shown. The initial values, computed by Homography, are used for nonlinear optimization. The results from Bouguet Toolbox are shown for comparison. Brown's Distortion function is used in the optimization process

Translation Vector in meters			
Frame	Initial Values	Optimized Values	Bouguet Toolbox Values
13	$\begin{bmatrix} -377.325 \\ -429.319 \\ 1836.644 \end{bmatrix}$	$\begin{bmatrix} -441.138 \\ -477.987 \\ 1815.721 \end{bmatrix}$	$\begin{bmatrix} -441.138 \\ -477.987 \\ 1815.721 \end{bmatrix}$
14	$\begin{bmatrix} -352.664 \\ -412.441 \\ 1653.253 \end{bmatrix}$	$\begin{bmatrix} -410.927 \\ -456.646 \\ 1636.024 \end{bmatrix}$	$\begin{bmatrix} -410.927 \\ -456.646 \\ 1636.024 \end{bmatrix}$
15	$\begin{bmatrix} -607.843 \\ -401.109 \\ 1640.103 \end{bmatrix}$	$\begin{bmatrix} -662.720 \\ -447.929 \\ 1583.183 \end{bmatrix}$	$\begin{bmatrix} -662.720 \\ -447.929 \\ 1583.183 \end{bmatrix}$
16	$\begin{bmatrix} 29.911 \\ -510.901 \\ 2322.697 \end{bmatrix}$	$\begin{bmatrix} -51.881 \\ -567.232 \\ 2318.755 \end{bmatrix}$	$\begin{bmatrix} -51.881 \\ -567.232 \\ 2318.755 \end{bmatrix}$
17	$\begin{bmatrix} -387.156 \\ -413.882 \\ 1630.930 \end{bmatrix}$	$\begin{bmatrix} -449.816 \\ -462.815 \\ 1634.470 \end{bmatrix}$	$\begin{bmatrix} -449.816 \\ -462.815 \\ 1634.470 \end{bmatrix}$
18	$\begin{bmatrix} -566.599 \\ -484.396 \\ 1540.649 \end{bmatrix}$	$\begin{bmatrix} -617.070 \\ -525.711 \\ 1471.745 \end{bmatrix}$	$\begin{bmatrix} -617.070 \\ -525.711 \\ 1471.745 \end{bmatrix}$
19	$\begin{bmatrix} -321.373 \\ -240.456 \\ 1169.700 \end{bmatrix}$	$\begin{bmatrix} -354.435 \\ -264.843 \\ 1113.610 \end{bmatrix}$	$\begin{bmatrix} -354.435 \\ -264.843 \\ 1113.610 \end{bmatrix}$
20	$\begin{bmatrix} -435.696 \\ -257.575 \\ 1374.484 \end{bmatrix}$	$\begin{bmatrix} -478.522 \\ -292.999 \\ 1320.395 \end{bmatrix}$	$\begin{bmatrix} -478.522 \\ -292.999 \\ 1320.395 \end{bmatrix}$

Table 5.6: The translation vectors for the frames 13 through 20 of the Bouguet Toolbox dataset are shown. The initial values, computed by Homography, are used for nonlinear optimization. The results from Bouguet Toolbox are shown for comparison. Brown's Distortion function is used in the optimization process

The similarity in the values of the converged intrinsics and extrinsics lends credibility to the current implementation of the combined estimation approach using Brown's distortion model as developed in this research.

5.1.2 Zhang's Dataset

Zhang's[1] dataset was also used to verify the credibility of the combined estimation approach with Brown's distortion model. The results of the combined estimation approach are compared with the corresponding results from Bouguet's Toolbox.

After optimization of the initialization values using the homography optimization algorithm and the Steepest Gradient Descent algorithm in Bouguet's Toolbox, the results are compared in the subsequent tables. Table 5.7 compares the converged intrinsics from both algorithms. The initial values shown in the Table are computed using Homography.

Parameter	Initial Values	Optimized Values	Bouguet Toolbox Values
α	871.3640761	833.0034588	833.0034437
β	871.071365	832.9376039	832.9375887
c	0.216330799	0.211020284	0.21101857
u_0	300.7357847	304.0043788	304.0044236
v_0	220.9411681	208.8753372	208.8753452
k_1	0	-0.222263498	-0.222264505
k_2	0	0.086958529	0.086971646
k_3	0	0.364852766	0.364804933
p_1	0	0.0000566	0.0000566
p_2	0	0.001058611	0.00105861

Table 5.7: Intrinsic parameters and distortion coefficients for the Zhang dataset are shown. The initial values, computed using Homography, are used for Nonlinear Optimization. The corresponding parameter values from the Bouguet Toolbox are shown for comparison. Brown's Distortion function is used in the optimization process

The intrinsics and distortion parameters computed using the homography optimization algorithm are in good agreement with the intrinsics and distortion parameters as computed using Bouguet's Toolbox. Table 5.8 shows the rotation matrices as computed from the converged pa-

rameters of rotation (CRPs in the case of the combined estimation approach and principal rotation vector in the case of the Bouguet Toolbox) next to each other for comparison. Table 5.9 shows the translation vectors. The initial values shown in the tables are computed using homography.

Rotation Matrix			
Frame	Initial Values	Optimized Values	Bouguet Toolbox Values
1	$\begin{bmatrix} 0.990 & -0.027 & 0.135 \\ 0.015 & 0.995 & 0.092 \\ -0.137 & -0.089 & 0.986 \end{bmatrix}$	$\begin{bmatrix} 0.992 & -0.026 & 0.117 \\ 0.014 & 0.994 & 0.101 \\ -0.119 & -0.099 & 0.987 \end{bmatrix}$	$\begin{bmatrix} 0.992 & -0.026 & 0.117 \\ 0.014 & 0.994 & 0.101 \\ -0.119 & -0.099 & 0.987 \end{bmatrix}$
2	$\begin{bmatrix} 0.996 & -0.002 & 0.087 \\ 0.020 & 0.979 & -0.201 \\ -0.085 & 0.202 & 0.975 \end{bmatrix}$	$\begin{bmatrix} 0.997 & -0.004 & 0.071 \\ 0.017 & 0.983 & -0.181 \\ -0.069 & 0.181 & 0.980 \end{bmatrix}$	$\begin{bmatrix} 0.997 & -0.004 & 0.071 \\ 0.017 & 0.983 & -0.181 \\ -0.069 & 0.181 & 0.980 \end{bmatrix}$
3	$\begin{bmatrix} 0.914 & -0.036 & 0.402 \\ -0.002 & 0.995 & 0.095 \\ -0.404 & -0.087 & 0.910 \end{bmatrix}$	$\begin{bmatrix} 0.915 & -0.035 & 0.401 \\ -0.007 & 0.994 & 0.104 \\ -0.403 & -0.098 & 0.909 \end{bmatrix}$	$\begin{bmatrix} 0.915 & -0.035 & 0.401 \\ -0.007 & 0.994 & 0.104 \\ -0.403 & -0.098 & 0.909 \end{bmatrix}$
4	$\begin{bmatrix} 0.986 & -0.017 & -0.164 \\ 0.031 & 0.996 & 0.084 \\ 0.162 & -0.088 & 0.982 \end{bmatrix}$	$\begin{bmatrix} 0.986 & -0.017 & -0.162 \\ 0.033 & 0.995 & 0.094 \\ 0.159 & -0.098 & 0.982 \end{bmatrix}$	$\begin{bmatrix} 0.986 & -0.017 & -0.162 \\ 0.033 & 0.995 & 0.094 \\ 0.159 & -0.098 & 0.982 \end{bmatrix}$
5	$\begin{bmatrix} 0.967 & -0.197 & -0.155 \\ 0.188 & 0.979 & -0.069 \\ 0.166 & 0.037 & 0.985 \end{bmatrix}$	$\begin{bmatrix} 0.967 & -0.197 & -0.158 \\ 0.191 & 0.980 & -0.052 \\ 0.165 & 0.020 & 0.986 \end{bmatrix}$	$\begin{bmatrix} 0.967 & -0.197 & -0.158 \\ 0.191 & 0.980 & -0.052 \\ 0.165 & 0.020 & 0.986 \end{bmatrix}$

Table 5.8: The rotation matrices for the frames of the Zhang dataset are shown. The initial values, computed by Homography, are used for nonlinear optimization. The results from Bouguet Toolbox are shown for comparison. Brown's Distortion function is used in the optimization process

Translation Vector in meters			
Frame	Initial Values	Optimized Values	Bouguet Toolbox Values
1	$\begin{bmatrix} -3.784 \\ 3.423 \\ 13.676 \end{bmatrix}$	$\begin{bmatrix} -3.840 \\ 3.615 \\ 12.812 \end{bmatrix}$	$\begin{bmatrix} -3.840 \\ 3.615 \\ 12.812 \end{bmatrix}$
2	$\begin{bmatrix} -3.663 \\ 3.538 \\ 14.111 \end{bmatrix}$	$\begin{bmatrix} -3.717 \\ 3.731 \\ 13.217 \end{bmatrix}$	$\begin{bmatrix} -3.717 \\ 3.731 \\ 13.217 \end{bmatrix}$
3	$\begin{bmatrix} -2.886 \\ 3.531 \\ 15.108 \end{bmatrix}$	$\begin{bmatrix} -2.944 \\ 3.736 \\ 14.265 \end{bmatrix}$	$\begin{bmatrix} -2.944 \\ 3.736 \\ 14.265 \end{bmatrix}$
4	$\begin{bmatrix} -3.355 \\ 3.418 \\ 13.302 \end{bmatrix}$	$\begin{bmatrix} -3.407 \\ 3.601 \\ 12.475 \end{bmatrix}$	$\begin{bmatrix} -3.407 \\ 3.601 \\ 12.475 \end{bmatrix}$
5	$\begin{bmatrix} -4.016 \\ 2.962 \\ 15.280 \end{bmatrix}$	$\begin{bmatrix} -4.073 \\ 3.170 \\ 14.364 \end{bmatrix}$	$\begin{bmatrix} -4.073 \\ 3.170 \\ 14.364 \end{bmatrix}$

Table 5.9: The translation vectors for the frames of the Zhang dataset are shown. The initial values, computed by Homography, are used for nonlinear optimization. The results from Bouguet Toolbox are shown for comparison. Brown's Distortion function is used in the optimization process

The comparison of the converged rotation matrices and translation vectors from both algorithms proves that the combined estimation approach with Brown's distortion model has verified credibility for estimation of the intrinsics, extrinsics and distortion coefficients. However, it must be noted that the two datasets used to test the combined estimation approach are obtained using conventional CMOS cameras. It remains to be seen whether this approach can be extended to the linear imagers. The subsequent chapter presents and discusses the results from the employment of the combined estimation approach with Brown's distortion model to the Phasespace camera datasets.

Now the Geometric Distortion Model is introduced, discussed and tested with the Bouguet Toolbox dataset and Zhang dataset in the subsequent section.

5.2 Geometric Distortion Model

Ma et al[4] discusses a family of polynomial and rational distortion functions as viable substitutes to Brown's distortion model. These distortion functions are lumped models that take into account all nonlinear distortion effects. The family of functions presented in the paper are given in Table 5.10.

No.	Function
1	$1 + k_1 r$
2	$1 + k_1 r^2$
3	$1 + k_1 r + k_2 r^2$
4	$1 + k_1 r^2 + k_2 r^4$
5	$\frac{1}{1+k_1 r}$
6	$\frac{1}{1+k_1 r^2}$
7	$\frac{1+k_1 r}{1+k_2 r^2}$
8	$\frac{1}{1+k_1 r+k_2 r^2}$
9	$\frac{1+k_1 r}{1+k_2 r+k_3 r^2}$
10	$\frac{1+k_1 r^2}{1+k_2 r+k_3 r^2}$

Table 5.10: Family of Polynomial and Rational Distortion Functions as presented in Ma et [4]

Function 4 is the same form as the purely radial distortion function in Brown's distortion model with two coefficients. Out of the ten distortion functions defined, the function chosen for this research is presented in Equation 5.4.

$$\begin{aligned} x_d &= x_u \left(\frac{1 + k_{x1} r^2}{1 + k_{x2} r + k_{x3} r^2} \right) \\ y_d &= y_u \left(\frac{1 + k_{y1} r^2}{1 + k_{y2} r + k_{y3} r^2} \right) \end{aligned} \tag{5.4}$$

It is worth mentioning that the above equation is a slightly modified version of the expression 10 in Table 5.10 presented in Ma et al. Different distortion coefficients are defined for the two camera plane basis directions. Equation 5.4 represents the geometric distortion function that has

the most modularity in choice of distortion coefficients and the rational nature of the function means that both radial and tangential distortion effects can be captured.

The geometric distortion process using nonlinear optimization is discussed in detail in Appendix C.

The distortion function defined above is tested on the two datasets used for Brown's distortion function, namely the Bouguet Toolbox dataset and the Zhang's dataset. The intrinsic parameters, distortion coefficients and the extrinsic parameters are compared with the known results as was done in the previous subsection.

5.2.1 Bouguet Toolbox Dataset

Table 5.11 compares the intrinsic parameters for the Bouguet Toolbox dataset as found using the nonlinear optimization with the results from Bouguet's Toolbox. Bouguet's Toolbox does not accomodate different distortion models, so only the intrinsic parameters are compared.

Parameter	Initial Value	Optimized Value	Bouguet Toolbox Value
α	652.0965121	657.7444023	657.5199789
β	660.1095416	657.5920104	657.8880141
c	0.708048876	0.310112494	0.330929792
u_0	279.780234	302.5256425	302.6640606
v_0	225.9629734	242.8550007	242.4343209

Table 5.11: The intrinsic parameters for the Bouguet Toolbox dataset are shown. The optimized values are shown in the second column in comparison with the values obtained from Bouguet's Toolbox. Geometric Distortion function is used in the optimization process

The intrinsics as computed using the Combined Estimation procedure are in reasonable agreement with the corresponding values from Bouguet's Toolbox. Slightly different values are to be expected since a different funtion is being minimised by the combined estimation procedure as compared to Bouguet's Toolbox.

The optimized distortion parameters came out to be

$$\boldsymbol{k_x} = \begin{bmatrix} 0.278948587 & 0.004673147 & 0.526391265 \end{bmatrix}$$

and

$$\boldsymbol{k_y} = \begin{bmatrix} 0.456400351 & -0.003967398 & 0.726773159 \end{bmatrix}$$

.

The extrinsic parameters for each frame, as computed using the homography optimization algorithm and Bouguet's Toolbox, are presented below. Tables 5.12, 5.13 and 5.14 show the rotation matrices whereas Tables 5.15 and 5.16 shows the translation vectors.

Rotation Matrix			
Frame	Initial Values	Optimized Values	Bouguet Toolbox Values
1	$\begin{bmatrix} 0.044 & 0.991 & 0.120 \\ 0.638 & 0.064 & -0.767 \\ -0.768 & 0.111 & -0.630 \end{bmatrix}$	$\begin{bmatrix} 0.054 & 0.992 & 0.112 \\ 0.633 & 0.052 & -0.771 \\ -0.771 & 0.113 & -0.625 \end{bmatrix}$	$\begin{bmatrix} 0.054 & 0.992 & 0.112 \\ 0.633 & 0.052 & -0.772 \\ -0.772 & 0.113 & -0.625 \end{bmatrix}$
2	$\begin{bmatrix} -0.0004 & 0.990 & 0.136 \\ 0.861 & 0.069 & -0.503 \\ -0.507 & 0.117 & -0.853 \end{bmatrix}$	$\begin{bmatrix} 0.005 & 0.992 & 0.120 \\ 0.861 & 0.056 & -0.505 \\ -0.508 & 0.106 & -0.854 \end{bmatrix}$	$\begin{bmatrix} 0.005 & 0.992 & 0.120 \\ 0.860 & 0.056 & -0.505 \\ -0.508 & 0.106 & -0.854 \end{bmatrix}$
3	$\begin{bmatrix} -0.162 & 0.983 & 0.077 \\ 0.847 & 0.179 & -0.499 \\ -0.505 & -0.015 & -0.862 \end{bmatrix}$	$\begin{bmatrix} -0.158 & 0.985 & 0.057 \\ 0.848 & 0.166 & -0.501 \\ -0.504 & -0.030 & -0.863 \end{bmatrix}$	$\begin{bmatrix} -0.158 & 0.985 & 0.057 \\ 0.848 & 0.166 & -0.502 \\ -0.504 & -0.030 & -0.862 \end{bmatrix}$
4	$\begin{bmatrix} -0.252 & 0.917 & -0.307 \\ 0.782 & 0.006 & -0.622 \\ -0.568 & -0.397 & -0.720 \end{bmatrix}$	$\begin{bmatrix} -0.255 & 0.901 & -0.350 \\ 0.802 & -0.003 & -0.596 \\ -0.538 & -0.433 & -0.722 \end{bmatrix}$	$\begin{bmatrix} -0.255 & 0.901 & -0.349 \\ 0.802 & -0.004 & -0.596 \\ -0.539 & -0.433 & -0.722 \end{bmatrix}$
5	$\begin{bmatrix} -0.246 & 0.768 & 0.590 \\ 0.575 & 0.605 & -0.548 \\ -0.779 & 0.204 & -0.592 \end{bmatrix}$	$\begin{bmatrix} -0.225 & 0.766 & 0.601 \\ 0.585 & 0.600 & -0.545 \\ -0.778 & 0.229 & -0.583 \end{bmatrix}$	$\begin{bmatrix} -0.225 & 0.766 & 0.601 \\ 0.584 & 0.600 & -0.545 \\ -0.779 & 0.228 & -0.583 \end{bmatrix}$
6	$\begin{bmatrix} -0.130 & 0.990 & 0.043 \\ 0.734 & 0.067 & 0.675 \\ 0.666 & 0.119 & -0.735 \end{bmatrix}$	$\begin{bmatrix} -0.140 & 0.989 & 0.041 \\ 0.733 & 0.075 & 0.675 \\ 0.665 & 0.125 & -0.735 \end{bmatrix}$	$\begin{bmatrix} -0.140 & 0.989 & 0.041 \\ 0.733 & 0.076 & 0.675 \\ 0.664 & 0.125 & -0.736 \end{bmatrix}$
7	$\begin{bmatrix} -0.145 & 0.798 & 0.584 \\ 0.851 & -0.199 & 0.484 \\ 0.503 & 0.568 & -0.650 \end{bmatrix}$	$\begin{bmatrix} -0.153 & 0.787 & 0.597 \\ 0.845 & -0.207 & 0.491 \\ 0.510 & 0.580 & -0.633 \end{bmatrix}$	$\begin{bmatrix} -0.153 & 0.786 & 0.597 \\ 0.846 & -0.207 & 0.490 \\ 0.510 & 0.581 & -0.634 \end{bmatrix}$

Table 5.12: The rotation matrices for the first 7 frames of the Bouguet Toolbox dataset are shown. The initial values, computed by Homography, are used for nonlinear optimization. The results from Bouguet Toolbox are shown for comparison. Geometric Distortion function is used in the optimization process

Rotation Matrix			
Frame	Initial Values	Optimized Values	Bouguet Toolbox Values
8	$\begin{bmatrix} -0.113 & 0.768 & 0.629 \\ 0.866 & -0.232 & 0.441 \\ 0.485 & 0.595 & -0.639 \end{bmatrix}$	$\begin{bmatrix} -0.132 & 0.729 & 0.671 \\ 0.863 & -0.247 & 0.439 \\ 0.486 & 0.637 & -0.597 \end{bmatrix}$	$\begin{bmatrix} -0.132 & 0.729 & 0.671 \\ 0.863 & -0.247 & 0.439 \\ 0.486 & 0.638 & -0.597 \end{bmatrix}$
9	$\begin{bmatrix} -0.206 & 0.750 & -0.627 \\ 0.895 & 0.403 & 0.188 \\ 0.394 & -0.523 & -0.755 \end{bmatrix}$	$\begin{bmatrix} -0.201 & 0.718 & -0.666 \\ 0.892 & 0.415 & 0.178 \\ 0.405 & -0.558 & -0.723 \end{bmatrix}$	$\begin{bmatrix} -0.201 & 0.718 & -0.666 \\ 0.892 & 0.414 & 0.178 \\ 0.404 & -0.558 & -0.723 \end{bmatrix}$
10	$\begin{bmatrix} -0.231 & 0.854 & -0.465 \\ 0.930 & 0.334 & 0.152 \\ 0.285 & -0.397 & -0.871 \end{bmatrix}$	$\begin{bmatrix} -0.215 & 0.835 & -0.506 \\ 0.912 & 0.356 & 0.200 \\ 0.347 & -0.418 & -0.838 \end{bmatrix}$	$\begin{bmatrix} -0.215 & 0.835 & -0.505 \\ 0.912 & 0.356 & 0.199 \\ 0.347 & -0.418 & -0.839 \end{bmatrix}$
11	$\begin{bmatrix} -0.122 & 0.991 & -0.045 \\ 0.893 & 0.129 & 0.430 \\ 0.432 & 0.012 & -0.901 \end{bmatrix}$	$\begin{bmatrix} -0.127 & 0.990 & -0.049 \\ 0.867 & 0.135 & 0.479 \\ 0.481 & 0.018 & -0.876 \end{bmatrix}$	$\begin{bmatrix} -0.127 & 0.990 & -0.049 \\ 0.867 & 0.135 & 0.478 \\ 0.481 & 0.018 & -0.876 \end{bmatrix}$
12	$\begin{bmatrix} -0.124 & 0.991 & 0.023 \\ 0.891 & 0.101 & 0.440 \\ 0.434 & 0.076 & -0.897 \end{bmatrix}$	$\begin{bmatrix} -0.127 & 0.991 & 0.004 \\ 0.879 & 0.110 & 0.462 \\ 0.458 & 0.062 & -0.886 \end{bmatrix}$	$\begin{bmatrix} -0.127 & 0.991 & 0.004 \\ 0.880 & 0.110 & 0.461 \\ 0.457 & 0.062 & -0.886 \end{bmatrix}$
13	$\begin{bmatrix} -0.118 & 0.985 & 0.119 \\ 0.900 & 0.056 & 0.431 \\ 0.418 & 0.158 & -0.894 \end{bmatrix}$	$\begin{bmatrix} -0.121 & 0.987 & 0.103 \\ 0.896 & 0.063 & 0.438 \\ 0.425 & 0.146 & -0.892 \end{bmatrix}$	$\begin{bmatrix} -0.121 & 0.987 & 0.103 \\ 0.897 & 0.064 & 0.437 \\ 0.425 & 0.146 & -0.893 \end{bmatrix}$
14	$\begin{bmatrix} -0.109 & 0.983 & 0.144 \\ 0.911 & 0.041 & 0.408 \\ 0.396 & 0.176 & -0.901 \end{bmatrix}$	$\begin{bmatrix} -0.108 & 0.986 & 0.120 \\ 0.909 & 0.049 & 0.413 \\ 0.402 & 0.154 & -0.902 \end{bmatrix}$	$\begin{bmatrix} -0.108 & 0.986 & 0.120 \\ 0.909 & 0.050 & 0.412 \\ 0.401 & 0.154 & -0.902 \end{bmatrix}$

Table 5.13: The rotation matrices for the frames 8 through 14 of the Bouguet Toolbox dataset are shown. The initial values, computed by Homography, are used for nonlinear optimization. The results from Bouguet Toolbox are shown for comparison. Geometric Distortion function is used in the optimization process

Rotation Matrix			
Frame	Initial Values	Optimized Values	Bouguet Toolbox Values
15	$\begin{bmatrix} -0.081 & 0.985 & 0.149 \\ 0.966 & 0.041 & 0.254 \\ 0.244 & 0.165 & -0.955 \end{bmatrix}$	$\begin{bmatrix} -0.089 & 0.975 & 0.203 \\ 0.970 & 0.038 & 0.238 \\ 0.224 & 0.218 & -0.949 \end{bmatrix}$	$\begin{bmatrix} -0.089 & 0.975 & 0.203 \\ 0.970 & 0.039 & 0.237 \\ 0.223 & 0.218 & -0.949 \end{bmatrix}$
16	$\begin{bmatrix} -0.203 & 0.970 & 0.133 \\ 0.964 & 0.221 & -0.140 \\ -0.166 & 0.100 & -0.981 \end{bmatrix}$	$\begin{bmatrix} -0.207 & 0.977 & 0.030 \\ 0.962 & 0.209 & -0.171 \\ -0.173 & -0.006 & -0.984 \end{bmatrix}$	$\begin{bmatrix} -0.207 & 0.977 & 0.030 \\ 0.962 & 0.210 & -0.172 \\ -0.174 & -0.006 & -0.984 \end{bmatrix}$
17	$\begin{bmatrix} -0.102 & 0.966 & -0.235 \\ 0.807 & 0.218 & 0.547 \\ 0.581 & -0.134 & -0.802 \end{bmatrix}$	$\begin{bmatrix} -0.104 & 0.958 & -0.264 \\ 0.808 & 0.236 & 0.538 \\ 0.579 & -0.157 & -0.799 \end{bmatrix}$	$\begin{bmatrix} -0.104 & 0.958 & -0.264 \\ 0.809 & 0.236 & 0.538 \\ 0.578 & -0.157 & -0.800 \end{bmatrix}$
18	$\begin{bmatrix} 0.045 & 0.856 & -0.513 \\ 0.657 & 0.361 & 0.660 \\ 0.752 & -0.367 & -0.547 \end{bmatrix}$	$\begin{bmatrix} 0.023 & 0.862 & -0.505 \\ 0.639 & 0.375 & 0.671 \\ 0.768 & -0.338 & -0.542 \end{bmatrix}$	$\begin{bmatrix} 0.023 & 0.862 & -0.505 \\ 0.639 & 0.375 & 0.670 \\ 0.768 & -0.338 & -0.543 \end{bmatrix}$
19	$\begin{bmatrix} -0.170 & 0.834 & 0.523 \\ 0.739 & -0.243 & 0.628 \\ 0.651 & 0.493 & -0.575 \end{bmatrix}$	$\begin{bmatrix} -0.186 & 0.825 & 0.533 \\ 0.715 & -0.258 & 0.649 \\ 0.673 & 0.502 & -0.541 \end{bmatrix}$	$\begin{bmatrix} -0.186 & 0.824 & 0.533 \\ 0.715 & -0.258 & 0.648 \\ 0.673 & 0.503 & -0.542 \end{bmatrix}$
20	$\begin{bmatrix} -0.095 & 0.625 & 0.774 \\ 0.852 & -0.349 & 0.387 \\ 0.513 & 0.697 & -0.499 \end{bmatrix}$	$\begin{bmatrix} -0.114 & 0.584 & 0.803 \\ 0.846 & -0.365 & 0.386 \\ 0.519 & 0.724 & -0.453 \end{bmatrix}$	$\begin{bmatrix} -0.114 & 0.584 & 0.803 \\ 0.847 & -0.364 & 0.386 \\ 0.518 & 0.724 & -0.453 \end{bmatrix}$

Table 5.14: The rotation matrices for the frames 15 through 20 of the Bouguet Toolbox dataset are shown. The initial values, computed by Homography, are used for nonlinear optimization. The results from Bouguet Toolbox are shown for comparison. Geometric Distortion function is used in the optimization process

The rotation matrices as computed by both the combined estimation procedure and Bouguet's Toolbox are in good agreement with each other. The values do not match to the extent that they did when Brown's Distortion Model was used since the optimized values, as computed using the Geometric Distortion Model, are compared with the optimized values from Bouguet's Toolbox which uses Brown's Distortion Model. But the compared Rotation Matrices are very close to each other nonetheless. Similar observations can be made for the translation vectors, shown subsequently.

Translation Vector in meters			
Frame	Initial Values	Optimized Values	Bouguet Toolbox Values
1	$\begin{bmatrix} -512.529 \\ -213.933 \\ 2957.725 \end{bmatrix}$	$\begin{bmatrix} -589.890 \\ -280.170 \\ 2843.999 \end{bmatrix}$	$\begin{bmatrix} -590.490 \\ -278.347 \\ 2844.169 \end{bmatrix}$
2	$\begin{bmatrix} -435.655 \\ -472.869 \\ 2588.268 \end{bmatrix}$	$\begin{bmatrix} -514.648 \\ -532.192 \\ 2526.029 \end{bmatrix}$	$\begin{bmatrix} -515.180 \\ -530.558 \\ 2526.353 \end{bmatrix}$
3	$\begin{bmatrix} -330.695 \\ -520.868 \\ 2636.163 \end{bmatrix}$	$\begin{bmatrix} -415.489 \\ -583.102 \\ 2585.442 \end{bmatrix}$	$\begin{bmatrix} -416.035 \\ -581.429 \\ 2585.814 \end{bmatrix}$
4	$\begin{bmatrix} -121.676 \\ -448.102 \\ 2598.821 \end{bmatrix}$	$\begin{bmatrix} -212.652 \\ -517.105 \\ 2596.969 \end{bmatrix}$	$\begin{bmatrix} -213.229 \\ -515.445 \\ 2597.414 \end{bmatrix}$
5	$\begin{bmatrix} -220.317 \\ -701.434 \\ 2506.850 \end{bmatrix}$	$\begin{bmatrix} -305.506 \\ -764.944 \\ 2455.771 \end{bmatrix}$	$\begin{bmatrix} -306.012 \\ -763.341 \\ 2456.339 \end{bmatrix}$
6	$\begin{bmatrix} -437.360 \\ -222.515 \\ 1483.488 \end{bmatrix}$	$\begin{bmatrix} -495.155 \\ -266.034 \\ 1483.129 \end{bmatrix}$	$\begin{bmatrix} -495.461 \\ -265.0765 \\ 1483.323 \end{bmatrix}$
7	$\begin{bmatrix} -224.688 \\ -219.971 \\ 1477.794 \end{bmatrix}$	$\begin{bmatrix} -275.234 \\ -259.586 \\ 1466.721 \end{bmatrix}$	$\begin{bmatrix} -275.520 \\ -258.636 \\ 1466.863 \end{bmatrix}$
8	$\begin{bmatrix} -514.237 \\ -302.500 \\ 1594.624 \end{bmatrix}$	$\begin{bmatrix} -565.663 \\ -345.745 \\ 1539.913 \end{bmatrix}$	$\begin{bmatrix} -565.929 \\ -344.657 \\ 1539.911 \end{bmatrix}$
9	$\begin{bmatrix} 83.415 \\ -688.332 \\ 2455.271 \end{bmatrix}$	$\begin{bmatrix} -4.151 \\ -751.594 \\ 2429.302 \end{bmatrix}$	$\begin{bmatrix} -4.652 \\ -749.999 \\ 2429.836 \end{bmatrix}$
10	$\begin{bmatrix} 7.971 \\ -944.286 \\ 2991.082 \end{bmatrix}$	$\begin{bmatrix} -96.153 \\ -1002.728 \\ 2867.556 \end{bmatrix}$	$\begin{bmatrix} -96.757 \\ -1000.853 \\ 2868.444 \end{bmatrix}$
11	$\begin{bmatrix} -428.546 \\ -737.311 \\ 2466.929 \end{bmatrix}$	$\begin{bmatrix} -501.487 \\ -785.450 \\ 2348.703 \end{bmatrix}$	$\begin{bmatrix} -501.981 \\ -783.902 \\ 2349.344 \end{bmatrix}$
12	$\begin{bmatrix} -375.588 \\ -540.580 \\ 2064.899 \end{bmatrix}$	$\begin{bmatrix} -443.226 \\ -591.477 \\ 2015.965 \end{bmatrix}$	$\begin{bmatrix} -443.646 \\ -590.187 \\ 2016.517 \end{bmatrix}$

Table 5.15: The translation vectors for the first 12 frames of the Bouguet Toolbox dataset are shown. The initial values, computed by Homography, are used for nonlinear optimization. The results from Bouguet Toolbox are shown for comparison. Geometric Distortion function is used in the optimization process

Translation Vector in meters			
Frame	Initial Values	Optimized Values	Bouguet Toolbox Values
13	$\begin{bmatrix} -377.325 \\ -429.319 \\ 1836.644 \end{bmatrix}$	$\begin{bmatrix} -440.766 \\ -479.143 \\ 1815.288 \end{bmatrix}$	$\begin{bmatrix} -441.138 \\ -477.987 \\ 1815.721 \end{bmatrix}$
14	$\begin{bmatrix} -352.664 \\ -412.441 \\ 1653.253 \end{bmatrix}$	$\begin{bmatrix} -410.594 \\ -457.678 \\ 1635.589 \end{bmatrix}$	$\begin{bmatrix} -410.927 \\ -456.646 \\ 1636.024 \end{bmatrix}$
15	$\begin{bmatrix} -607.843 \\ -401.109 \\ 1640.103 \end{bmatrix}$	$\begin{bmatrix} -662.425 \\ -448.987 \\ 1583.056 \end{bmatrix}$	$\begin{bmatrix} -662.720 \\ -447.9298 \\ 1583.183 \end{bmatrix}$
16	$\begin{bmatrix} 29.911 \\ -510.901 \\ 2322.697 \end{bmatrix}$	$\begin{bmatrix} -51.414 \\ -568.745 \\ 2318.415 \end{bmatrix}$	$\begin{bmatrix} -51.881 \\ -567.232 \\ 2318.755 \end{bmatrix}$
17	$\begin{bmatrix} -387.156 \\ -413.882 \\ 1630.930 \end{bmatrix}$	$\begin{bmatrix} -449.482 \\ -463.849 \\ 1634.037 \end{bmatrix}$	$\begin{bmatrix} -449.816 \\ -462.815 \\ 1634.470 \end{bmatrix}$
18	$\begin{bmatrix} -566.599 \\ -484.396 \\ 1540.649 \end{bmatrix}$	$\begin{bmatrix} -616.767 \\ -526.667 \\ 1471.393 \end{bmatrix}$	$\begin{bmatrix} -617.070 \\ -525.711 \\ 1471.745 \end{bmatrix}$
19	$\begin{bmatrix} -321.373 \\ -240.456 \\ 1169.700 \end{bmatrix}$	$\begin{bmatrix} -354.210 \\ -265.588 \\ 1113.423 \end{bmatrix}$	$\begin{bmatrix} -354.435 \\ -264.843 \\ 1113.610 \end{bmatrix}$
20	$\begin{bmatrix} -435.696 \\ -257.575 \\ 1374.484 \end{bmatrix}$	$\begin{bmatrix} -478.283 \\ -293.929 \\ 1320.355 \end{bmatrix}$	$\begin{bmatrix} -478.522 \\ -292.999 \\ 1320.395 \end{bmatrix}$

Table 5.16: The translation vectors for the frames 13 through 20 of the Bouguet Toolbox dataset are shown. The initial values, computed by Homography, are used for nonlinear optimization. The results from Bouguet Toolbox are shown for comparison. Geometric Distortion function is used in the optimization process

The translation vectors as computed by both the combined estimation procedure and Bouguet's Toolbox are in good agreement with each other.

Now Zhang's dataset is used to further verify the credibility of the combined estimation procedure with Geometric Distortion. The results are presented in the following subsection.

5.2.2 Zhang's Dataset

The intrinsics computed using the combined estimation algorithm are compared with the values from Bouguet's Toolbox and shown in Table 5.17

Parameter	Initial Values	Optimized Values	Bouguet Toolbox Values
α	871.3640761	831.2620159	833.0034437
β	871.071365	832.1551532	832.9375887
c	0.216330799	0.204244578	0.21101857
u_0	300.7357847	303.9740639	304.0044236
v_0	220.9411681	206.6143399	208.8753452

Table 5.17: The intrinsic parameters for the Zhang dataset are shown. The optimized values are shown in the second column in comparison with the values obtained from Bouguet's Toolbox. Geometric Distortion function is used in the optimization process

The two sets of intrinsics show greater deviation as compared to the Bouguet Toolbox dataset, but the deviation is still within acceptable levels. Slightly different values are to be expected since a different funtion is being minimised by the combined estimation procedure as compared to Bouguet's Toolbox.

The optimized distortion parameters came out to be

$$\boldsymbol{k_x} = \begin{bmatrix} 1.31669588 & -0.015991552 & 1.593088424 \end{bmatrix}$$

and

$$\boldsymbol{k_y} = \begin{bmatrix} 1.223246055 & -0.007448986 & 1.483151141 \end{bmatrix}$$

.

The extrinsic parameters for each frame, as computed using the homography optimization algorithm and Bouguet's Toolbox, are presented below. Tables 5.18 and 5.19 show the rotation matrices and the translation vectors as computed using the combined estimation approach in comparison with the results from Bouguet's Toolbox.

Rotation Matrix			
Frame	Initial Values	Optimized Values	Bouguet Toolbox Values
1	$\begin{bmatrix} 0.990 & -0.027 & 0.135 \\ 0.015 & 0.995 & 0.092 \\ -0.137 & -0.089 & 0.986 \end{bmatrix}$	$\begin{bmatrix} 0.992 & -0.026 & 0.117 \\ 0.013 & 0.994 & 0.105 \\ -0.119 & -0.102 & 0.987 \end{bmatrix}$	$\begin{bmatrix} 0.992 & -0.026 & 0.117 \\ 0.014 & 0.994 & 0.101 \\ -0.119 & -0.099 & 0.987 \end{bmatrix}$
2	$\begin{bmatrix} 0.996 & -0.002 & 0.087 \\ 0.020 & 0.979 & -0.201 \\ -0.085 & 0.202 & 0.975 \end{bmatrix}$	$\begin{bmatrix} 0.997 & -0.004 & 0.071 \\ 0.017 & 0.984 & -0.177 \\ -0.069 & 0.178 & 0.981 \end{bmatrix}$	$\begin{bmatrix} 0.997 & -0.004 & 0.071 \\ 0.017 & 0.983 & -0.181 \\ -0.069 & 0.181 & 0.980 \end{bmatrix}$
3	$\begin{bmatrix} 0.914 & -0.036 & 0.402 \\ -0.002 & 0.995 & 0.095 \\ -0.404 & -0.087 & 0.910 \end{bmatrix}$	$\begin{bmatrix} 0.915 & -0.035 & 0.401 \\ -0.008 & 0.994 & 0.106 \\ -0.402 & -0.100 & 0.909 \end{bmatrix}$	$\begin{bmatrix} 0.915 & -0.035 & 0.401 \\ -0.007 & 0.994 & 0.104 \\ -0.403 & -0.098 & 0.909 \end{bmatrix}$
4	$\begin{bmatrix} 0.986 & -0.017 & -0.164 \\ 0.031 & 0.996 & 0.084 \\ 0.162 & -0.088 & 0.982 \end{bmatrix}$	$\begin{bmatrix} 0.986 & -0.017 & -0.162 \\ 0.033 & 0.994 & 0.097 \\ 0.159 & -0.102 & 0.981 \end{bmatrix}$	$\begin{bmatrix} 0.986 & -0.017 & -0.162 \\ 0.033 & 0.995 & 0.094 \\ 0.159 & -0.098 & 0.982 \end{bmatrix}$
5	$\begin{bmatrix} 0.967 & -0.197 & -0.155 \\ 0.188 & 0.979 & -0.069 \\ 0.166 & 0.037 & 0.985 \end{bmatrix}$	$\begin{bmatrix} 0.967 & -0.196 & -0.158 \\ 0.191 & 0.980 & -0.048 \\ 0.164 & 0.016 & 0.986 \end{bmatrix}$	$\begin{bmatrix} 0.967 & -0.197 & -0.158 \\ 0.191 & 0.980 & -0.052 \\ 0.165 & 0.020 & 0.986 \end{bmatrix}$

Table 5.18: The rotation matrices for the frames of the Zhang dataset are shown. The initial values, computed by Homography, are used for nonlinear optimization. The results from Bouguet Toolbox are shown for comparison. Geometric Distortion function is used in the optimization process

The rotation matrices as computed using both the combined estimation procedure and Bouguet's Toolbox are in good agreement with each other.

Translation Vector in meters			
Frame	Initial Values	Optimized Values	Bouguet Toolbox Values
1	$\begin{bmatrix} -3.784 \\ 3.423 \\ 13.676 \end{bmatrix}$	$\begin{bmatrix} -3.840 \\ 3.651 \\ 12.790 \end{bmatrix}$	$\begin{bmatrix} -3.840 \\ 3.615 \\ 12.812 \end{bmatrix}$
2	$\begin{bmatrix} -3.663 \\ 3.538 \\ 14.111 \end{bmatrix}$	$\begin{bmatrix} -3.717 \\ 3.768 \\ 13.196 \end{bmatrix}$	$\begin{bmatrix} -3.717 \\ 3.731 \\ 13.217 \end{bmatrix}$
3	$\begin{bmatrix} -2.886 \\ 3.531 \\ 15.108 \end{bmatrix}$	$\begin{bmatrix} -2.944 \\ 3.776 \\ 14.244 \end{bmatrix}$	$\begin{bmatrix} -2.944 \\ 3.736 \\ 14.265 \end{bmatrix}$
4	$\begin{bmatrix} -3.355 \\ 3.418 \\ 13.302 \end{bmatrix}$	$\begin{bmatrix} -3.407 \\ 3.635 \\ 12.454 \end{bmatrix}$	$\begin{bmatrix} -3.407 \\ 3.601 \\ 12.475 \end{bmatrix}$
5	$\begin{bmatrix} -4.016 \\ 2.962 \\ 15.280 \end{bmatrix}$	$\begin{bmatrix} -4.072 \\ 3.209 \\ 14.343 \end{bmatrix}$	$\begin{bmatrix} -4.073 \\ 3.170 \\ 14.364 \end{bmatrix}$

Table 5.19: The translation vectors for the frames of the Zhang dataset are shown. The initial values, computed by Homography, are used for nonlinear optimization. The results from Bouguet Toolbox are shown for comparison. Geometric Distortion function is used in the optimization process

The translation vectors as computed using both the combined estimation procedure and Bouguet's Toolbox are in good agreement with each other.

The comparison of the converged rotation matrices and translation vectors from both algorithms proves that the combined estimation approach with Geometric distortion model has verified credibility for estimation of the intrinsics, extrinsics and distortion coefficients. However, it must be noted that the two datasets used to test the combined estimation approach are obtained using conventional CMOS cameras. It remains to be seen whether this approach can be extended to the linear imagers. The subsequent chapter presents and discusses the results from the employment of the combined estimation approach with Geometric distortion model to the Phasespace datasets.

6. EXPERIMENTAL RESULTS

A total of 4 experiments were conducted with different goals for 4 of them. The various experiments and the goals for each are outlined below. In each experiment, the image plane coordinates found using the coordinate system determination procedure discussed in the previous Chapter. The distortion incorporated estimation is carried out using the two distortion models defined in the previous Chapter. In the end, the intrinsics as computed using the distortion incorporated estimation are collected into a table for comparison and further inferences.

- Dataset 1 - This experiment used an arrangement of 8 beacons arranged on a checkerboard. A total of 29 frames were captured, out of which 22 frames were deemed viable. This was the first experiment conducted with the Phasespace camera.

- Dataset 2 - This experiment used an arrangement of 14 beacons arranged on a checkerboard. A total of 20 frames were captured and all frames were deemed viable. The goal of this experiment was to ascertain whether the addition of extra beacons improved the estimation of the intrinsics and extrinsics.

- Dataset 3 - This experiment is similar to the one in Dataset 2, the only difference is that the board was placed farther away from the camera as compared to Dataset 2. For this case, 19 frames were captured and all frames were deemed viable.

- Dataset 4 - This experiment used an arrangement of 8 beacons on a checkerboard. 16 frames were captured out of which 15 were deemed viable. The goal of this test was to compare the algorithm developed in Wong et al[3] with the Combined Estimation approach.

6.1 Dataset 1

The arrangement of the 8 beacons on the checkerboard pattern is shown in Figure 6.1.

The inertial coordinates of the beacons are given in Table 6.1.

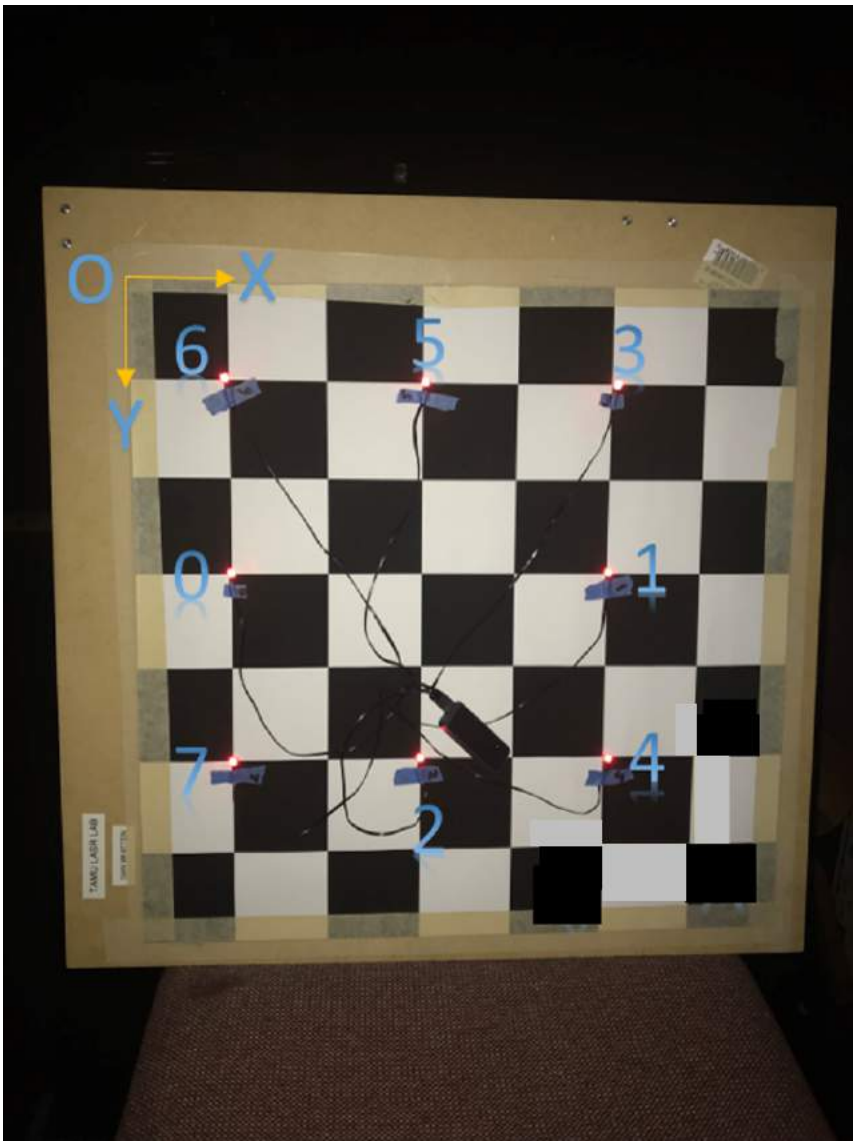

Figure 6.1: Beacon Arrangement on the checkerboard pattern is shown. The numbers next to the beacons indicate their number assignment in the Phasespace system. The origin O, the inertial x-axis X and inertial y-axis Y are also shown.

During the estimation of the rows of the Homography matrix, discussed in Chapter 2 after the Equation 2.3, a condition used to eliminate certain noisy frames was the difference in order of the last two singular values of the L matrix. If this difference was less than 2, that frame was eliminated. Using this criterion, frame numbers 1,2,8,9,13,14 and 18 were eliminated out of the total of 30 frames.

Beacon No.	Inertial Position
0	$[s,3s]$
1	$[5s,3s]$
2	$[3s,5s]$
3	$[5s,s]$
4	$[5s,5s]$
5	$[3s,s]$
6	$[s,s]$
7	$[s,5s]$

Table 6.1: Inertial coordinates of each beacon given as [X-coordinate,Y-coordinate], s=2.95 inches

The image plane projections of the 30 frames as seen from the Phasespace Viewer are shown in Figure 6.2.

The checkerboard was hand held at various poses in order to leverage the full extent of all three available rotational degrees of freedom. The physical alignment images are omitted here for aesthetic purposes.

After the noisy frames are eliminated, the remaining 22 frames are inputted to Zhang's Homography algorithm to generate the starting guess values for nonlinear optimization. Optimization over the entire set of intrinsics, distortion coefficients and extrinsics is carried out using both the Brown's and Geometric distortion models and compared. The next subsection discusses the results of the Combined Estimation Approach using Brown's Distortion model.

Figure 6.2: Image plane projections of each pose of the board as seen through the Phasespace Viewer. The frames are ordered from the top left to the bottom right.

6.1.1 Brown's Distortion Model

The combined estimation approach was employed using Brown's distortion model to compute the modified intrinsics and extrinsics, along with the distortion coefficients. The initialization values for the nonlinear optimization algorithm, as computed by the Homography algorithm, are shown in the subsequent tables. Table 6.2 shows the values of the intrinsics and the distortion

coefficients used to initialize the optimization along with the optimized values.

Parameter	Initial Values	Optimized Values
α	0.841908008	0.866387157
β	0.829096978	0.862603651
c	-0.0070489	-0.005218412
u_0	0.485247568	0.490403937
v_0	0.519056646	0.525072226
k_1	0	0.26381864
k_2	0	-2.017524534
k_3	0	4.043408479
p_1	0	-0.000291855
p_2	0	-0.004889833

Table 6.2: The intrinsic parameters and distortion coefficients for Dataset 1, as computed by the Homography algorithm and the optimization scheme are shown. Brown's Distortion Model is employed in the optimization process

Tables 6.3 and 6.4 show the values of the CRPs for each of the viable frames, used to initialize the optimization algorithm along with the optimized values. Tables 6.5 and 6.6 show the values of the translation vectors for each of the viable frames, used to initialize the optimization algorithm along with the optimized values. It must be noted that due to the relatively high values of the optimized distortion coefficients (k_2 and k_3 are greater than 1), the optimization process has resulted in some considerable shift in the CRPs from the initialization values.

CRP Vector		
Frame Number	Initial Values	Optimized Values
3	$\begin{bmatrix} 0.02991096 \\ 0.043638853 \\ 0.028073138 \end{bmatrix}$	$\begin{bmatrix} 0.035937617 \\ 0.036847763 \\ 0.027532273 \end{bmatrix}$
4	$\begin{bmatrix} 0.105988989 \\ -0.015933864 \\ 0.071895756 \end{bmatrix}$	$\begin{bmatrix} 0.124213864 \\ -0.016919857 \\ 0.071489333 \end{bmatrix}$
5	$\begin{bmatrix} 0.185184762 \\ -0.028428785 \\ 0.32020879 \end{bmatrix}$	$\begin{bmatrix} 0.19344956 \\ -0.055296271 \\ 0.319258323 \end{bmatrix}$
6	$\begin{bmatrix} 0.050246534 \\ 0.025129132 \\ 0.082927686 \end{bmatrix}$	$\begin{bmatrix} 0.061964251 \\ 0.025598324 \\ 0.082731903 \end{bmatrix}$
7	$\begin{bmatrix} 0.002072254 \\ 0.1099547 \\ 0.068403649 \end{bmatrix}$	$\begin{bmatrix} -0.000271134 \\ 0.105667424 \\ 0.067819018 \end{bmatrix}$
10	$\begin{bmatrix} 0.177189158 \\ 0.119815081 \\ -0.051259389 \end{bmatrix}$	$\begin{bmatrix} 0.194802537 \\ 0.120261913 \\ -0.050306007 \end{bmatrix}$
11	$\begin{bmatrix} 0.139948791 \\ 0.059635804 \\ -0.123214466 \end{bmatrix}$	$\begin{bmatrix} 0.144150784 \\ 0.053355134 \\ -0.123618903 \end{bmatrix}$
12	$\begin{bmatrix} 0.094516439 \\ 0.087920611 \\ 0.079243484 \end{bmatrix}$	$\begin{bmatrix} 0.10323508 \\ 0.083811965 \\ 0.079590542 \end{bmatrix}$
15	$\begin{bmatrix} 0.049147363 \\ 0.1979902 \\ 1.130415568 \end{bmatrix}$	$\begin{bmatrix} 0.037173343 \\ 0.237608894 \\ 1.125967843 \end{bmatrix}$
16	$\begin{bmatrix} 0.388164132 \\ 0.436643359 \\ 1.206453323 \end{bmatrix}$	$\begin{bmatrix} 0.386020046 \\ 0.452019204 \\ 1.209135731 \end{bmatrix}$
17	$\begin{bmatrix} 0.045857046 \\ 0.075203812 \\ 1.846815069 \end{bmatrix}$	$\begin{bmatrix} 0.053900234 \\ 0.119728093 \\ 1.839080158 \end{bmatrix}$
19	$\begin{bmatrix} -0.003279004 \\ 0.172057085 \\ 1.317186304 \end{bmatrix}$	$\begin{bmatrix} -0.016959774 \\ 0.188321965 \\ 1.316199775 \end{bmatrix}$

Table 6.3: The CRPs for the first 12 well-conditioned frames for Dataset 1 is presented. The initialization values computed by Homography are juxtaposed with the optimized values for comparison. Brown's distortion model is employed in the optimization process.

CRP Vector		
Frame Number	Initial Values	Optimized Values
20	$\begin{bmatrix} 0.40476222 \\ 0.203149278 \\ 2.084352626 \end{bmatrix}$	$\begin{bmatrix} 0.382720489 \\ 0.219342128 \\ 2.079250607 \end{bmatrix}$
21	$\begin{bmatrix} -0.388103136 \\ 0.620951344 \\ 5.000170263 \end{bmatrix}$	$\begin{bmatrix} -0.42392612 \\ 0.689722208 \\ 5.008010035 \end{bmatrix}$
22	$\begin{bmatrix} -4.840497133 \\ 8.427993488 \\ 47.76243114 \end{bmatrix}$	$\begin{bmatrix} -5.720055552 \\ 9.660896344 \\ 51.38153013 \end{bmatrix}$
23	$\begin{bmatrix} 0.264498193 \\ 0.280761042 \\ -3.094710111 \end{bmatrix}$	$\begin{bmatrix} 0.251500185 \\ 0.257636873 \\ -3.107211331 \end{bmatrix}$
24	$\begin{bmatrix} 0.264303944 \\ 0.033691856 \\ -2.082786826 \end{bmatrix}$	$\begin{bmatrix} 0.27005813 \\ 0.043110116 \\ -2.083548451 \end{bmatrix}$
25	$\begin{bmatrix} 0.093672494 \\ -0.064410833 \\ -1.865584561 \end{bmatrix}$	$\begin{bmatrix} 0.100142867 \\ -0.079133069 \\ -1.867101825 \end{bmatrix}$
26	$\begin{bmatrix} -0.01976325 \\ 0.313837849 \\ -1.94368138 \end{bmatrix}$	$\begin{bmatrix} -0.01546419 \\ 0.315655754 \\ -1.94890649 \end{bmatrix}$
27	$\begin{bmatrix} 0.739213029 \\ 1.723353966 \\ -9.496175852 \end{bmatrix}$	$\begin{bmatrix} 0.747529513 \\ 1.841881907 \\ -9.592860698 \end{bmatrix}$
28	$\begin{bmatrix} 0.780647426 \\ -0.661721708 \\ -4.598393165 \end{bmatrix}$	$\begin{bmatrix} 0.729751143 \\ -0.782096151 \\ -4.622532882 \end{bmatrix}$
29	$\begin{bmatrix} 0.019295929 \\ 0.018930625 \\ -2.204920811 \end{bmatrix}$	$\begin{bmatrix} 0.025363381 \\ 0.002657687 \\ -2.209155417 \end{bmatrix}$

Table 6.4: The CRPs for the remaining well-conditioned frames for Dataset 1 is presented. The initialization values computed by Homography are juxtaposed with the optimized values for comparison. Brown's distortion model is employed in the optimization process.

Translation Vector in inches		
Frame Number	Initial Values	Optimized Values
3	$\begin{bmatrix} -7.762311787 \\ -8.500610405 \\ 18.22250514 \end{bmatrix}$	$\begin{bmatrix} -7.912057505 \\ -8.654166474 \\ 19.24266878 \end{bmatrix}$
4	$\begin{bmatrix} -9.953222873 \\ -5.682780367 \\ 20.00738712 \end{bmatrix}$	$\begin{bmatrix} -10.08826911 \\ -5.849024098 \\ 21.069837 \end{bmatrix}$
5	$\begin{bmatrix} -10.8393115 \\ -2.705561396 \\ 22.63006525 \end{bmatrix}$	$\begin{bmatrix} -11.2328536 \\ -2.896955591 \\ 24.37896734 \end{bmatrix}$
6	$\begin{bmatrix} -10.64087904 \\ -5.518017708 \\ 18.81037454 \end{bmatrix}$	$\begin{bmatrix} -10.78294979 \\ -5.694744 \\ 19.77615673 \end{bmatrix}$
7	$\begin{bmatrix} -9.959092178 \\ -9.052910818 \\ 16.73048544 \end{bmatrix}$	$\begin{bmatrix} -10.17281902 \\ -9.235966416 \\ 17.62883334 \end{bmatrix}$
10	$\begin{bmatrix} -9.032348263 \\ -8.836486597 \\ 22.3150677 \end{bmatrix}$	$\begin{bmatrix} -9.191426042 \\ -8.9379167 \\ 23.48053051 \end{bmatrix}$
11	$\begin{bmatrix} -5.119518061 \\ -12.96189442 \\ 21.8860909 \end{bmatrix}$	$\begin{bmatrix} -5.27975731 \\ -13.02340957 \\ 22.86631775 \end{bmatrix}$
12	$\begin{bmatrix} -7.549475282 \\ -5.274623827 \\ 18.87942188 \end{bmatrix}$	$\begin{bmatrix} -7.690737799 \\ -5.460972255 \\ 20.01444074 \end{bmatrix}$
15	$\begin{bmatrix} -3.382881326 \\ 12.18971112 \\ 17.86126769 \end{bmatrix}$	$\begin{bmatrix} -3.631727771 \\ 11.98448534 \\ 18.11440752 \end{bmatrix}$
16	$\begin{bmatrix} -7.3302737 \\ 6.756214675 \\ 15.29382849 \end{bmatrix}$	$\begin{bmatrix} -7.447396732 \\ 6.598375373 \\ 15.90838632 \end{bmatrix}$
17	$\begin{bmatrix} 0.144211512 \\ 13.60224588 \\ 18.07307045 \end{bmatrix}$	$\begin{bmatrix} -0.165868617 \\ 13.53480562 \\ 18.57435661 \end{bmatrix}$
19	$\begin{bmatrix} -6.906484812 \\ 11.83491822 \\ 15.17360283 \end{bmatrix}$	$\begin{bmatrix} -7.325085676 \\ 11.85288227 \\ 15.99467435 \end{bmatrix}$

Table 6.5: The Translation vectors (in inches) corresponding to the firt 12 well-conditioned frames for Dataset 1 is presented. The initialization values computed by Homography are shown along with the optimized values for comparison,Brown's distortion model is employed in the optimization process.

Translation Vector in inches		
Frame Number	Initial Values	Optimized Values
20	$\begin{bmatrix} -2.94547048 \\ 12.0932697 \\ 16.93234077 \end{bmatrix}$	$\begin{bmatrix} -3.182598713 \\ 12.08953487 \\ 17.89852945 \end{bmatrix}$
21	$\begin{bmatrix} 5.893452865 \\ 9.508393454 \\ 18.77061919 \end{bmatrix}$	$\begin{bmatrix} 5.763470099 \\ 9.305069226 \\ 19.48738318 \end{bmatrix}$
22	$\begin{bmatrix} 7.920619454 \\ 4.213062962 \\ 19.99184029 \end{bmatrix}$	$\begin{bmatrix} 7.766142757 \\ 3.977737465 \\ 20.81951134 \end{bmatrix}$
23	$\begin{bmatrix} 16.01782847 \\ 2.715592203 \\ 23.23644919 \end{bmatrix}$	$\begin{bmatrix} 15.82001518 \\ 2.513381805 \\ 23.79821164 \end{bmatrix}$
24	$\begin{bmatrix} 12.79967916 \\ -1.677976743 \\ 22.76452623 \end{bmatrix}$	$\begin{bmatrix} 12.80924474 \\ -1.741408896 \\ 23.85050575 \end{bmatrix}$
25	$\begin{bmatrix} 12.37279547 \\ -1.374218359 \\ 19.73510863 \end{bmatrix}$	$\begin{bmatrix} 12.41828913 \\ -1.428800484 \\ 20.64446824 \end{bmatrix}$
26	$\begin{bmatrix} 13.29555651 \\ -1.566020162 \\ 20.22382799 \end{bmatrix}$	$\begin{bmatrix} 13.30124863 \\ -1.699990753 \\ 21.14585008 \end{bmatrix}$
27	$\begin{bmatrix} 11.60742707 \\ 6.902934209 \\ 24.40542288 \end{bmatrix}$	$\begin{bmatrix} 11.44540926 \\ 6.711236881 \\ 25.36077472 \end{bmatrix}$
28	$\begin{bmatrix} 15.10883122 \\ 3.694289173 \\ 21.96332176 \end{bmatrix}$	$\begin{bmatrix} 15.03698046 \\ 3.607362283 \\ 22.44841037 \end{bmatrix}$
29	$\begin{bmatrix} 13.17579131 \\ 0.0814697 \\ 18.85063227 \end{bmatrix}$	$\begin{bmatrix} 13.23649347 \\ 0.012017178 \\ 19.69547226 \end{bmatrix}$

Table 6.6: The Translation vectors (in inches) corresponding to the remaining well-conditioned frame for Dataset 1 is presented. The initialization values computed by Homography are shown along with the optimized values for comparison.Brown's distortion model is employed in the optimization process.

The converged intrinsics and extrinsics are slightly different as compared to the corresponding values computed using Homography. However, the converged extrinsics remain close enough to the extrinsics as computed using Homography to be just as justifiable.

The extrinsic projections of the 22 frames are shown in order from frame 3 through frame 30 after the removal of the noisy frames in Figure D.1 in Appendix D for aesthetic purposes.

The combined extrinsic projections of all viable frames is shown in Figure 6.3.

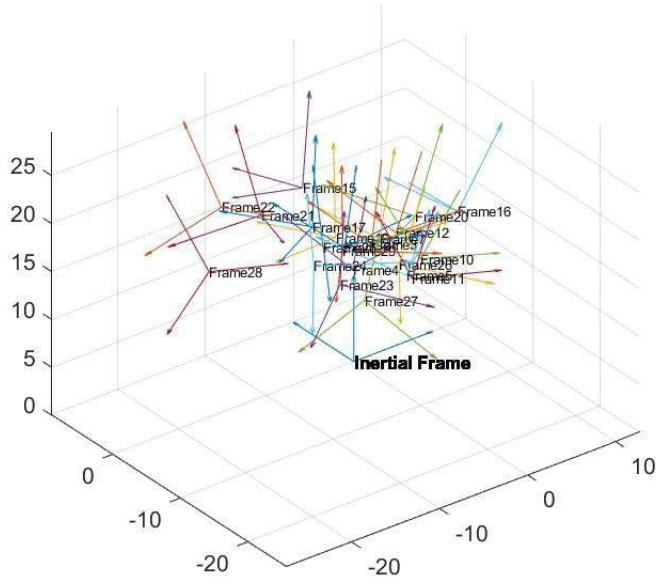

Figure 6.3: Extrinsic projections of all well-conditioned frames for Dataset 1 are shown together with respect to the inertial frame. Brown's distortion model is employed in the optimization process.

An observation of the translation and CRP vector plots, shown in Figures 6.4 and 6.5 respectively, reveal that the CRPs for most frames are well behaved, i.e. below 1 and the translation in the inertial z-direction are positive for all frames. This adds to the trust in the Homography algorithm.

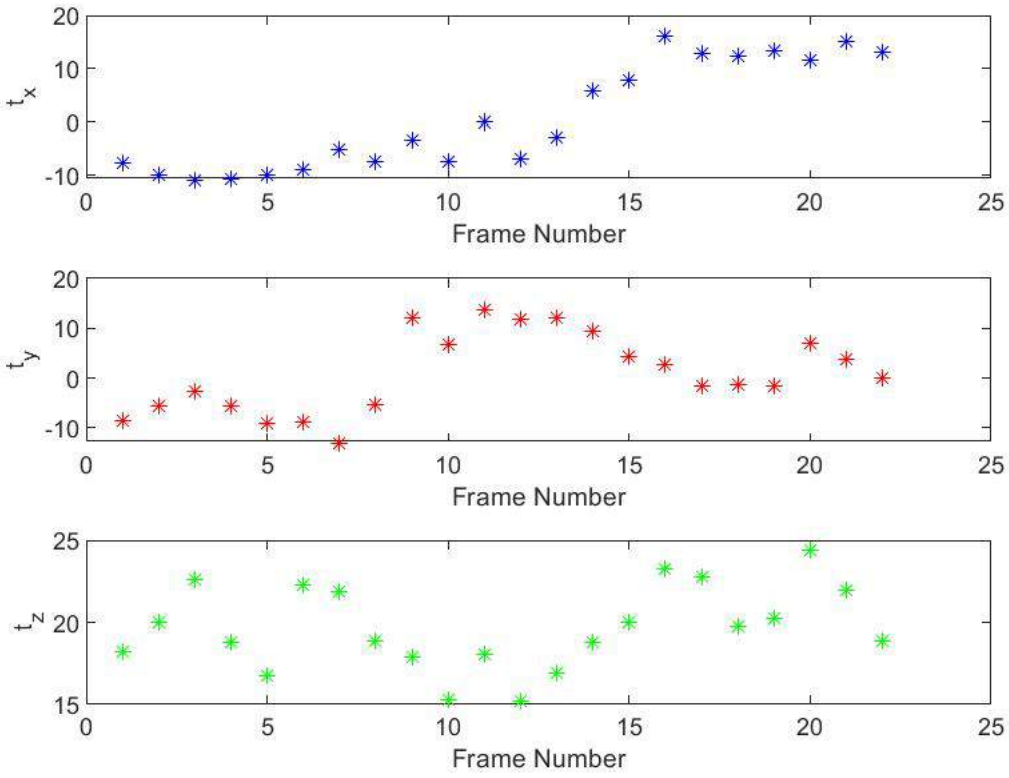

Figure 6.4: Plots of translation vector elements in inches against frame number for Dataset 1. These frame numbers are for the "non-noisy" frames where the noisy frame numbers are replaced by the next successive frame. Brown's distortion model is employed in the optimization process.

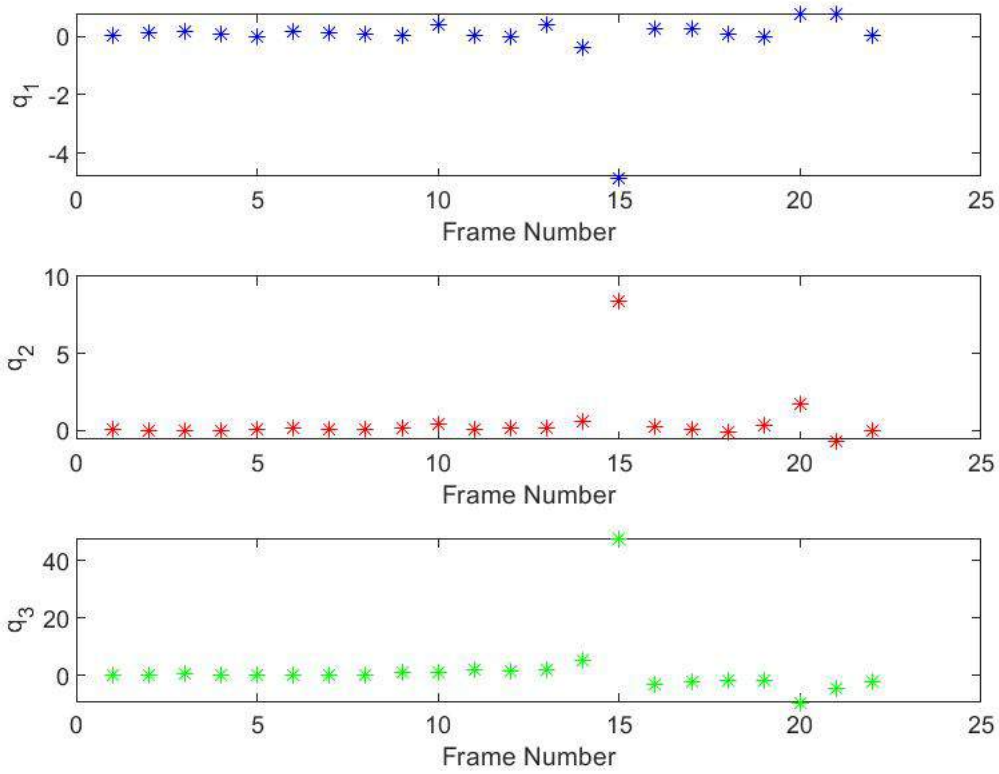

Figure 6.5: Plots of CRP vector elements against frame number for Dataset 1. These frame numbers are for the "non-noisy" frames where the noisy frame numbers are replaced by the next successive frame. Brown's distortion model is employed in the optimization process.

6.1.2 Geometric Distortion Model

The combined estimation approach was employed using the Geometric distortion model to compute the modified intrinsics and extrinsics, along with the distortion coefficients. The initialization values for the nonlinear optimization algorithm, as computed by the Homography algorithm, are shown in the subsequent tables. Table 6.7 shows the initialized (by Homography) and optimized values of the intrinsics and the distortion coefficients.

Parameter	Initial Values	Optimized Values
α	0.841908008	1.096397663
β	0.829096978	0.910222153
c	-0.0070489	-0.004898774
u_0	0.485247568	0.499829903
v_0	0.519056646	0.525091343
k_{x1}	0	140.4243102
k_{x2}	0	1.652147076
k_{x3}	0	170.0546221
k_{y1}	0	-3.062907908
k_{y2}	0	0.117087602
k_{y3}	0	-3.26737133

Table 6.7: The intrinsic parameters and distortion coefficients for Dataset 1, as computed by the Homography algorithm and the optimization scheme are shown. Geometric Distortion Model is employed in the optimization process

Tables 6.8 and 6.9 show the values of the CRPs for each of the viable frames, used to initialize the optimization algorithm along with the optimized values. Tables 6.10 and 6.11 show the initialized (by Homography) and optimized values of the translation vectors for each of the viable frames.

CRP Vector		
Frame Number	Initial Values	Optimized Values
3	$\begin{bmatrix} 0.02991096 \\ 0.043638853 \\ 0.028073138 \end{bmatrix}$	$\begin{bmatrix} 0.030372832 \\ 0.041078138 \\ 0.027732892 \end{bmatrix}$
4	$\begin{bmatrix} 0.105988989 \\ -0.015933864 \\ 0.071895756 \end{bmatrix}$	$\begin{bmatrix} 0.118937648 \\ -0.014564567 \\ 0.071872566 \end{bmatrix}$
5	$\begin{bmatrix} 0.185184762 \\ -0.028428785 \\ 0.32020879 \end{bmatrix}$	$\begin{bmatrix} 0.19201199 \\ -0.052779531 \\ 0.320257321 \end{bmatrix}$
6	$\begin{bmatrix} 0.050246534 \\ 0.025129132 \\ 0.082927686 \end{bmatrix}$	$\begin{bmatrix} 0.055845543 \\ 0.029029486 \\ 0.082756555 \end{bmatrix}$
7	$\begin{bmatrix} 0.002072254 \\ 0.1099547 \\ 0.068403649 \end{bmatrix}$	$\begin{bmatrix} -0.002521789 \\ 0.11023421 \\ 0.067523504 \end{bmatrix}$
10	$\begin{bmatrix} 0.177189158 \\ 0.119815081 \\ -0.051259389 \end{bmatrix}$	$\begin{bmatrix} 0.194532732 \\ 0.125683487 \\ -0.049542569 \end{bmatrix}$
11	$\begin{bmatrix} 0.139948791 \\ 0.059635804 \\ -0.123214466 \end{bmatrix}$	$\begin{bmatrix} 0.14481668 \\ 0.057143008 \\ -0.122824127 \end{bmatrix}$
12	$\begin{bmatrix} 0.094516439 \\ 0.087920611 \\ 0.079243484 \end{bmatrix}$	$\begin{bmatrix} 0.103395313 \\ 0.08257183 \\ 0.079740954 \end{bmatrix}$
15	$\begin{bmatrix} 0.049147363 \\ 0.1979902 \\ 1.130415568 \end{bmatrix}$	$\begin{bmatrix} 0.042490871 \\ 0.238102581 \\ 1.133127634 \end{bmatrix}$
16	$\begin{bmatrix} 0.388164132 \\ 0.436643359 \\ 1.206453323 \end{bmatrix}$	$\begin{bmatrix} 0.384799084 \\ 0.461803211 \\ 1.213568878 \end{bmatrix}$
17	$\begin{bmatrix} 0.045857046 \\ 0.075203812 \\ 1.846815069 \end{bmatrix}$	$\begin{bmatrix} 0.04755963 \\ 0.107275001 \\ 1.840308703 \end{bmatrix}$
19	$\begin{bmatrix} -0.003279004 \\ 0.172057085 \\ 1.317186304 \end{bmatrix}$	$\begin{bmatrix} -0.019773133 \\ 0.192325351 \\ 1.315658519 \end{bmatrix}$

Table 6.8: The CRPs for the first 12 well-conditioned frames for Dataset 1 is presented. The initialization values computed by Homography are juxtaposed with the optimized values for comparison. Geometric distortion model is employed in the optimization process.

CRP Vector		
Frame Number	Initial Values	Optimized Values
20	$\begin{bmatrix} 0.40476222 \\ 0.203149278 \\ 2.084352626 \end{bmatrix}$	$\begin{bmatrix} 0.376076345 \\ 0.220556625 \\ 2.082422256 \end{bmatrix}$
21	$\begin{bmatrix} -0.388103136 \\ 0.620951344 \\ 5.000170263 \end{bmatrix}$	$\begin{bmatrix} -0.446161384 \\ 0.693090664 \\ 5.023639444 \end{bmatrix}$
22	$\begin{bmatrix} -4.840497133 \\ 8.427993488 \\ 47.76243114 \end{bmatrix}$	$\begin{bmatrix} -6.810105399 \\ 10.36108328 \\ 55.53339153 \end{bmatrix}$
23	$\begin{bmatrix} 0.264498193 \\ 0.280761042 \\ -3.094710111 \end{bmatrix}$	$\begin{bmatrix} 0.262870511 \\ 0.281124981 \\ -3.108223285 \end{bmatrix}$
24	$\begin{bmatrix} 0.264303944 \\ 0.033691856 \\ -2.082786826 \end{bmatrix}$	$\begin{bmatrix} 0.271380287 \\ 0.052803094 \\ -2.08342371 \end{bmatrix}$
25	$\begin{bmatrix} 0.093672494 \\ -0.064410833 \\ -1.865584561 \end{bmatrix}$	$\begin{bmatrix} 0.094646537 \\ -0.070115938 \\ -1.86644062 \end{bmatrix}$
26	$\begin{bmatrix} -0.01976325 \\ 0.313837849 \\ -1.94368138 \end{bmatrix}$	$\begin{bmatrix} -0.010882594 \\ 0.331883557 \\ -1.952505487 \end{bmatrix}$
27	$\begin{bmatrix} 0.739213029 \\ 1.723353966 \\ -9.496175852 \end{bmatrix}$	$\begin{bmatrix} 0.788166419 \\ 1.905802188 \\ -9.678618501 \end{bmatrix}$
28	$\begin{bmatrix} 0.780647426 \\ -0.661721708 \\ -4.598393165 \end{bmatrix}$	$\begin{bmatrix} 0.750822372 \\ -0.756656356 \\ -4.589069561 \end{bmatrix}$
29	$\begin{bmatrix} 0.019295929 \\ 0.018930625 \\ -2.204920811 \end{bmatrix}$	$\begin{bmatrix} 0.026142407 \\ 0.019066381 \\ -2.210154153 \end{bmatrix}$

Table 6.9: The CRPs for the remaining well-conditioned frames for Dataset 1 is presented. The initialization values computed by Homography are juxtaposed with the optimized values for comparison. Geometric distortion model is employed in the optimization process.

Translation Vector in inches		
Frame Number	Initial Values	Optimized Values
3	$\begin{bmatrix} -7.762311787 \\ -8.500610405 \\ 18.22250514 \end{bmatrix}$	$\begin{bmatrix} -8.116477698 \\ -8.666778405 \\ 19.48400817 \end{bmatrix}$
4	$\begin{bmatrix} -9.953222873 \\ -5.682780367 \\ 20.00738712 \end{bmatrix}$	$\begin{bmatrix} -10.30073856 \\ -5.865329077 \\ 21.35813238 \end{bmatrix}$
5	$\begin{bmatrix} -10.8393115 \\ -2.705561396 \\ 22.63006525 \end{bmatrix}$	$\begin{bmatrix} -11.47681053 \\ -2.904477855 \\ 24.72192571 \end{bmatrix}$
6	$\begin{bmatrix} -10.64087904 \\ -5.518017708 \\ 18.81037454 \end{bmatrix}$	$\begin{bmatrix} -10.98122836 \\ -5.705158587 \\ 20.04567117 \end{bmatrix}$
7	$\begin{bmatrix} -9.959092178 \\ -9.052910818 \\ 16.73048544 \end{bmatrix}$	$\begin{bmatrix} -10.34573234 \\ -9.265556718 \\ 17.8914225 \end{bmatrix}$
10	$\begin{bmatrix} -9.032348263 \\ -8.836486597 \\ 22.3150677 \end{bmatrix}$	$\begin{bmatrix} -9.434023559 \\ -8.951054191 \\ 23.87492361 \end{bmatrix}$
11	$\begin{bmatrix} -5.119518061 \\ -12.96189442 \\ 21.8860909 \end{bmatrix}$	$\begin{bmatrix} -5.523816131 \\ -13.04193459 \\ 23.21784796 \end{bmatrix}$
12	$\begin{bmatrix} -7.549475282 \\ -5.274623827 \\ 18.87942188 \end{bmatrix}$	$\begin{bmatrix} -7.915639508 \\ -5.459420237 \\ 20.49816093 \end{bmatrix}$
15	$\begin{bmatrix} -3.382881326 \\ 12.18971112 \\ 17.86126769 \end{bmatrix}$	$\begin{bmatrix} -3.808946724 \\ 11.99077339 \\ 18.71323313 \end{bmatrix}$
16	$\begin{bmatrix} -7.3302737 \\ 6.756214675 \\ 15.29382849 \end{bmatrix}$	$\begin{bmatrix} -7.61802486 \\ 6.553424076 \\ 16.19163929 \end{bmatrix}$
17	$\begin{bmatrix} 0.144211512 \\ 13.60224588 \\ 18.07307045 \end{bmatrix}$	$\begin{bmatrix} -0.385090011 \\ 13.55623817 \\ 19.19740522 \end{bmatrix}$
19	$\begin{bmatrix} -6.906484812 \\ 11.83491822 \\ 15.17360283 \end{bmatrix}$	$\begin{bmatrix} -7.515267668 \\ 11.83076441 \\ 16.3571757 \end{bmatrix}$

Table 6.10: The translations for the first 12 well-conditioned frames for Dataset 1 is presented. The initialization values computed by Homography are juxtaposed with the optimized values for comparison. Geometric distortion model is employed in the optimization process.

Translation Vector in inches		
Frame Number	Initial Values	Optimized Values
20	$\begin{bmatrix} -2.94547048 \\ 12.0932697 \\ 16.93234077 \end{bmatrix}$	$\begin{bmatrix} -3.373170824 \\ 12.08316236 \\ 18.34971011 \end{bmatrix}$
21	$\begin{bmatrix} 5.893452865 \\ 9.508393454 \\ 18.77061919 \end{bmatrix}$	$\begin{bmatrix} 5.556473215 \\ 9.284499528 \\ 19.94873446 \end{bmatrix}$
22	$\begin{bmatrix} 7.920619454 \\ 4.213062962 \\ 19.99184029 \end{bmatrix}$	$\begin{bmatrix} 7.579975067 \\ 3.980387587 \\ 21.40262387 \end{bmatrix}$
23	$\begin{bmatrix} 16.01782847 \\ 2.715592203 \\ 23.23644919 \end{bmatrix}$	$\begin{bmatrix} 15.55708523 \\ 2.477667812 \\ 24.42218181 \end{bmatrix}$
24	$\begin{bmatrix} 12.79967916 \\ -1.677976743 \\ 22.76452623 \end{bmatrix}$	$\begin{bmatrix} 12.57131327 \\ -1.766681916 \\ 24.33227454 \end{bmatrix}$
25	$\begin{bmatrix} 12.37279547 \\ -1.374218359 \\ 19.73510863 \end{bmatrix}$	$\begin{bmatrix} 12.20100225 \\ -1.444749019 \\ 21.05937225 \end{bmatrix}$
26	$\begin{bmatrix} 13.29555651 \\ -1.566020162 \\ 20.22382799 \end{bmatrix}$	$\begin{bmatrix} 13.07955302 \\ -1.720058268 \\ 21.64084475 \end{bmatrix}$
27	$\begin{bmatrix} 11.60742707 \\ 6.902934209 \\ 24.40542288 \end{bmatrix}$	$\begin{bmatrix} 11.17627488 \\ 6.663292779 \\ 25.89225683 \end{bmatrix}$
28	$\begin{bmatrix} 15.10883122 \\ 3.694289173 \\ 21.96332176 \end{bmatrix}$	$\begin{bmatrix} 14.80507735 \\ 3.592964601 \\ 23.10739558 \end{bmatrix}$
29	$\begin{bmatrix} 13.17579131 \\ 0.0814697 \\ 18.85063227 \end{bmatrix}$	$\begin{bmatrix} 13.02605915 \\ 0.005608303 \\ 20.18740126 \end{bmatrix}$

Table 6.11: The translations for the remaining well-conditioned frames for Dataset 1 is presented. The initialization values computed by Homography are juxtaposed with the optimized values for comparison. Geometric distortion model is employed in the optimization process.

The converged intrinsics and extrinsics are slightly different as compared to the corresponding values computed using Homography. However, the converged extrinsics remain close enough to the extrinsics as computed using Homography to be just as justifiable.

The extrinsic projections of the 22 frames are shown in order from frame 3 through frame 30 after the removal of the noisy frames in Figure D.2 in Appendix D for aesthetic purposes.

The combined extrinsic projections of all viable frames is shown in Figure 6.6.

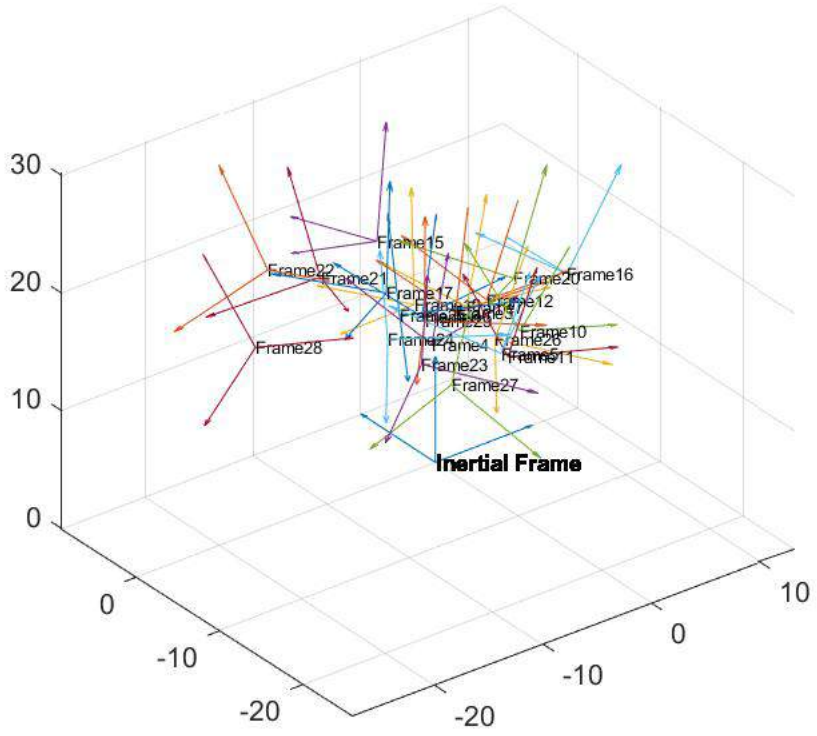

Figure 6.6: Extrinsic projections of all frames for Dataset 1 are shown together with respect to the inertial frame. Geometric distortion model is employed in the optimization process.

An observation of the translation and CRP vector plots, shown in Figures 6.7 and 6.8 respectively, reveal that the CRPs for most frames are well behaved, i.e. below 1 and the translation in the inertial z-direction are positive for all frames. This adds to the trust in the Homography algorithm.

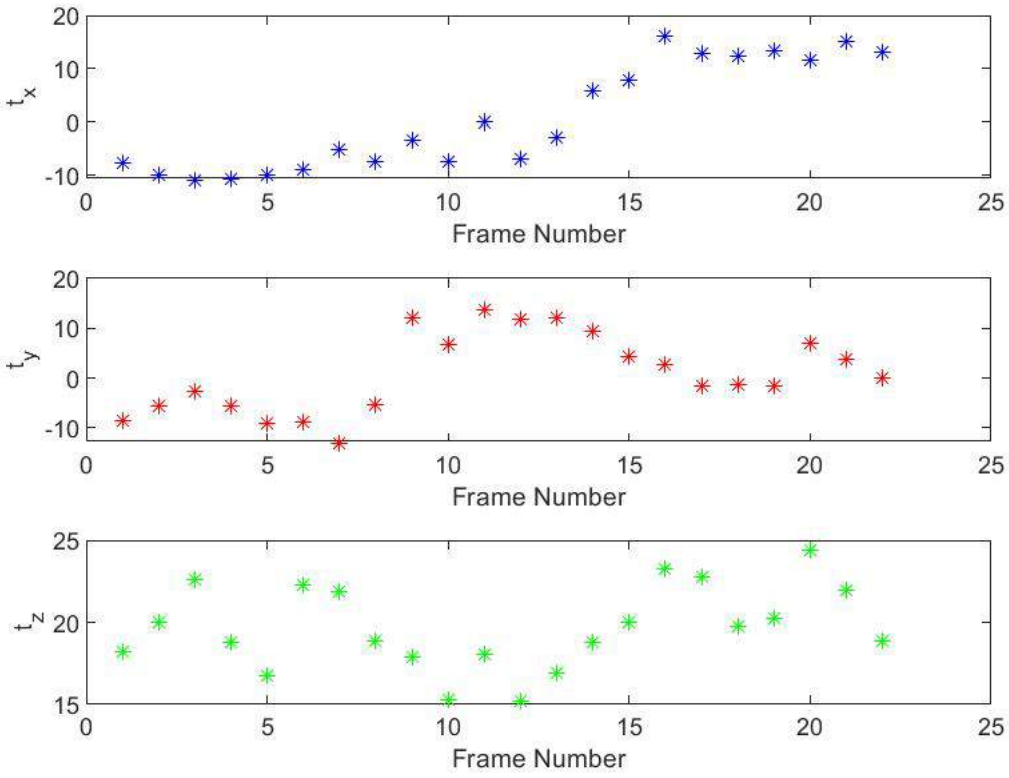

Figure 6.7: Plots of translation vector elements in inches against frame number for Dataset 1. These frame numbers are for the "non-noisy" frames where the noisy frame numbers are replaced by the next successive frame. Geometric distortion function is employed in the optimization process

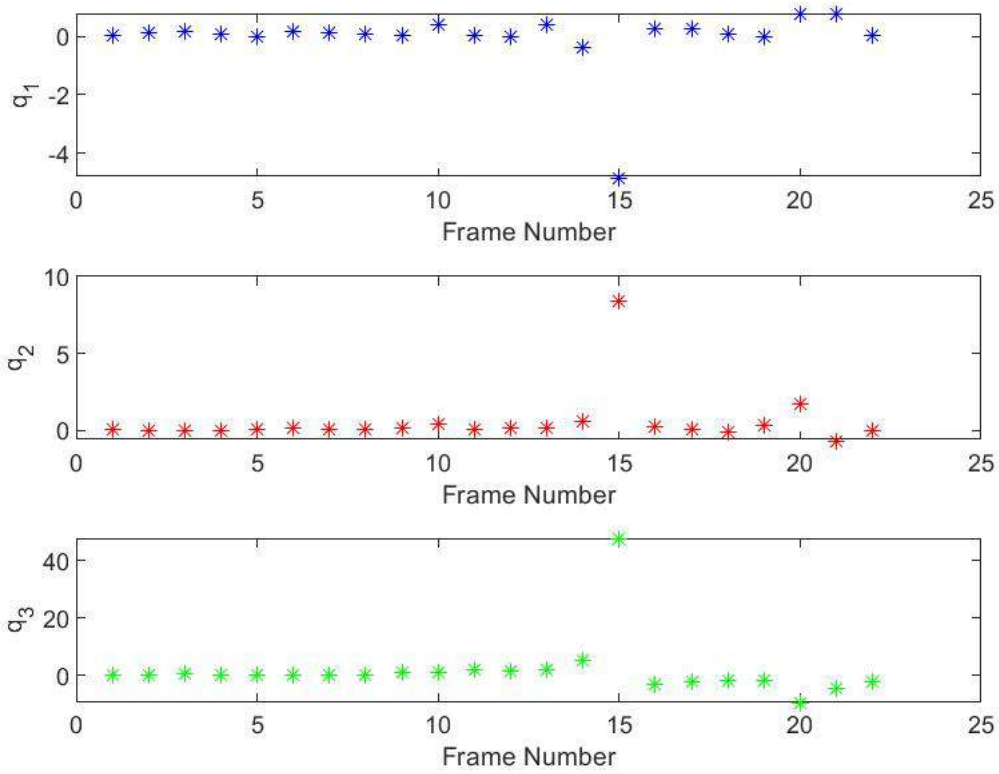

Figure 6.8: Plots of CRP vector elements against frame number for Dataset 1. These frame numbers are for the "non-noisy" frames where the noisy frame numbers are replaced by the next successive frame. Geometric distortion function is employed in the optimization process

6.2 Dataset 2

The arrangement of the 14 beacons on the checkerboard pattern is shown in Figure 6.9. The number of beacons was supposed to be 16 but two beacons failed to initialize after they were glued to the board.

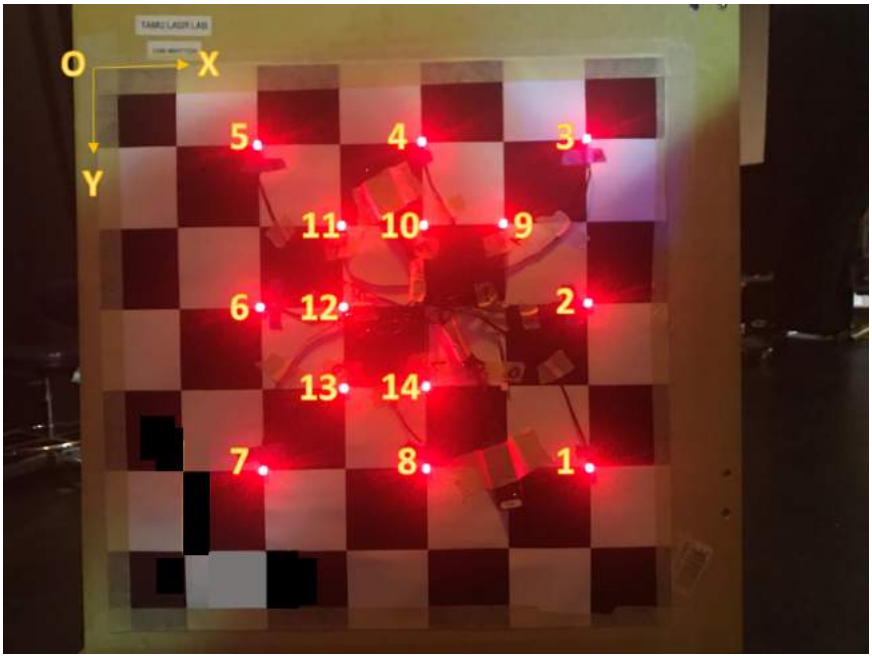

Figure 6.9: Beacon Arrangement on the checkerboard pattern is shown. The numbers next to the beacons indicate their number assignment in the Phasespace system. The origin O, the inertial x-axis X and inertial y-axis Y are also shown.

The inertial coordinates of the beacons are given in Table 6.12.

All 20 frames satisfied the criterion of the difference in order to last two singular values of the L matrix being two or greater. So no frames were eliminated as noisy.

The image plane projections of the 20 frames as seen from the Phasespace Viewer are shown in Figure 6.10.

The checkerboard was hand held at various poses in order to leverage the full extent of all three available rotational degrees of freedom. The physical alignment images are omitted here.

Beacon No.	Inertial Position
1	[$6s$,$5s$]
2	[$6s$,$3s$]
3	[$6s$,s]
4	[$4s$,s]
5	[$2s$,s]
6	[$2s$,$3s$]
7	[$2s$,$5s$]
8	[$4s$,$5s$]
9	[$5s$,$2s$]
10	[$4s$,$2s$]
11	[$3s$,$2s$]
12	[$3s$,$3s$]
13	[$3s$,$4s$]
14	[$4s$,$4s$]

Table 6.12: Inertial coordinates of each beacon given as [X-coordinate,Y-coordinate], s=2.95 inches

The intrinsic parameters and distortion coefficients will be shown at a later section to highlight a different noteworthy point.

6.2.1 Brown's Distortion model

The combined estimation approach was employed using Brown's distortion model to compute the modified intrinsics and extrinsics, along with the distortion coefficients. The initialization values for the nonlinear optimization algorithm, as computed by the Homography algorithm, are shown in the subsequent tables. Table 6.13 shows the values of the intrinsics and the distortion coefficients used to initialize the optimization along with the optimized values.

Tables 6.14 and 6.15 show the values of the CRPs for each of the viable frames, used to initialize the optimization algorithm along with the optimized values. Tables 6.16 and 6.17 show the values of the translation vectors for each of the viable frames, used to initialize the optimization algorithm along with the optimized values.

The extrinsic projections of the 20 frames are shown in Figure D.3 in Appendix D for aesthetic purposes.

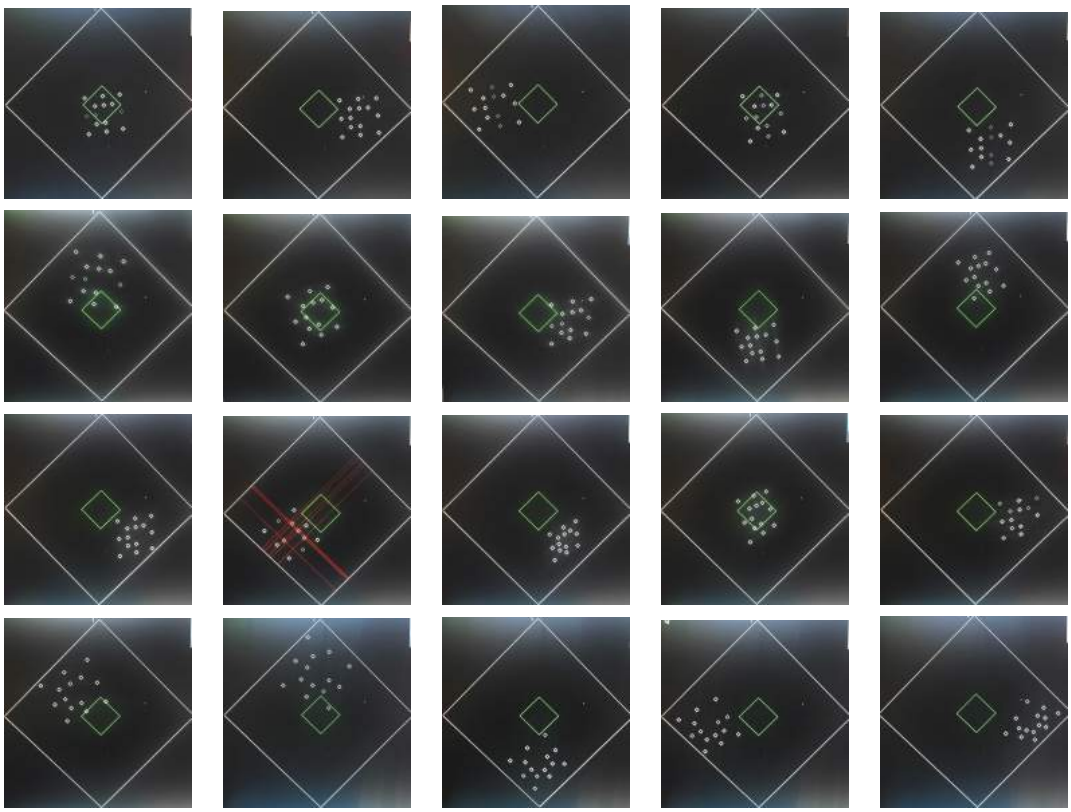

Figure 6.10: Image plane projections of each pose of the board as seen through the Phasespace Viewer. The frames are ordered from the top left to the bottom right.

Parameter	Initial Values	Optimized Values
α	1.157687557	1.033197839
β	1.228225441	1.049048926
c	0.038390921	-0.013443215
u_0	0.74216295	0.580530016
v_0	0.372623487	0.486606025
k_1	0	-0.26838847
k_2	0	0.407314863
k_3	0	-0.30403853
p_1	0	0.0000723
p_2	0	-0.012106003

Table 6.13: The intrinsic parameters and the distortion coefficients for Dataset 2, as computed by the Homography algorithm and optimized using nonlinear optimization are shown. Brown's distortion model is employed in the optimization process.

CRP Vector		
Frame Number	Initial Values	Optimized Values
1	$\begin{bmatrix} 0.023347867 \\ 0.134875443 \\ 0.469764129 \end{bmatrix}$	$\begin{bmatrix} 0.052713346 \\ 0.142780599 \\ 0.483414932 \end{bmatrix}$
2	$\begin{bmatrix} 0.058589106 \\ 0.064839454 \\ 0.471290649 \end{bmatrix}$	$\begin{bmatrix} 0.037216304 \\ -0.027530658 \\ 0.478948538 \end{bmatrix}$
3	$\begin{bmatrix} 0.157898381 \\ 0.164745831 \\ 0.548605368 \end{bmatrix}$	$\begin{bmatrix} 0.20745862 \\ 0.206261602 \\ 0.563730476 \end{bmatrix}$
4	$\begin{bmatrix} 0.273106239 \\ 0.377291341 \\ 0.512009173 \end{bmatrix}$	$\begin{bmatrix} 0.218649137 \\ 0.315739625 \\ 0.503145699 \end{bmatrix}$
5	$\begin{bmatrix} -0.192482166 \\ 0.239400098 \\ 0.437794263 \end{bmatrix}$	$\begin{bmatrix} -0.058815892 \\ 0.204189534 \\ 0.466437356 \end{bmatrix}$
6	$\begin{bmatrix} -0.0128827 \\ 0.11925558 \\ 0.327708288 \end{bmatrix}$	$\begin{bmatrix} -0.03013514 \\ 0.166359345 \\ 0.348797707 \end{bmatrix}$
7	$\begin{bmatrix} 0.110680406 \\ 0.503884266 \\ 0.613505727 \end{bmatrix}$	$\begin{bmatrix} 0.089655715 \\ 0.429787476 \\ 0.618042983 \end{bmatrix}$
8	$\begin{bmatrix} -0.177197626 \\ 0.403946394 \\ 0.458456281 \end{bmatrix}$	$\begin{bmatrix} -0.162594184 \\ 0.288534156 \\ 0.49653559 \end{bmatrix}$
9	$\begin{bmatrix} -0.288518115 \\ 0.041790808 \\ 0.49816919 \end{bmatrix}$	$\begin{bmatrix} -0.145303816 \\ 0.019195996 \\ 0.543016375 \end{bmatrix}$
10	$\begin{bmatrix} 0.198215044 \\ 0.249230304 \\ 0.730838029 \end{bmatrix}$	$\begin{bmatrix} 0.093314805 \\ 0.296432213 \\ 0.738973504 \end{bmatrix}$
11	$\begin{bmatrix} -0.006468417 \\ 0.2479848 \\ 0.478072393 \end{bmatrix}$	$\begin{bmatrix} -0.011035147 \\ 0.179899884 \\ 0.498391952 \end{bmatrix}$
12	$\begin{bmatrix} -0.109884211 \\ 0.127610427 \\ -0.115487142 \end{bmatrix}$	$\begin{bmatrix} -0.066307091 \\ 0.12689688 \\ -0.091311798 \end{bmatrix}$

Table 6.14: The CRPs for the first 12 well-conditioned frames for Dataset 2 are presented. The initialization values computed by Homography are juxtaposed with the optimized values for comparison. Brown's distortion model is employed in the optimization process.

CRP Vector		
Frame Number	Initial Values	Optimized Values
13	$\begin{bmatrix} -0.053582332 \\ 0.514803771 \\ 0.600251658 \end{bmatrix}$	$\begin{bmatrix} -0.03311101 \\ 0.414189807 \\ 0.62336618 \end{bmatrix}$
14	$\begin{bmatrix} 0.176968006 \\ 0.675453608 \\ 0.650675591 \end{bmatrix}$	$\begin{bmatrix} 0.134747726 \\ 0.544924675 \\ 0.647264577 \end{bmatrix}$
15	$\begin{bmatrix} -0.12278011 \\ 0.233038911 \\ 0.500634354 \end{bmatrix}$	$\begin{bmatrix} -0.155163736 \\ 0.123486213 \\ 0.533846145 \end{bmatrix}$
16	$\begin{bmatrix} -0.37415309 \\ 0.239915419 \\ 0.663019815 \end{bmatrix}$	$\begin{bmatrix} -0.330574461 \\ 0.30375158 \\ 0.72649196 \end{bmatrix}$
17	$\begin{bmatrix} -0.140803108 \\ 0.269869612 \\ 1.37446713 \end{bmatrix}$	$\begin{bmatrix} -0.226694821 \\ 0.290536665 \\ 1.426889678 \end{bmatrix}$
18	$\begin{bmatrix} -2.389296895 \\ 1.122891705 \\ 10.07276728 \end{bmatrix}$	$\begin{bmatrix} -1.92389689 \\ 2.042616973 \\ 11.17832054 \end{bmatrix}$
19	$\begin{bmatrix} -0.916000444 \\ -0.537866052 \\ 5.855210757 \end{bmatrix}$	$\begin{bmatrix} -1.321795693 \\ -0.141367841 \\ 6.727622842 \end{bmatrix}$
20	$\begin{bmatrix} 2.155307255 \\ 1.543846229 \\ -5.983510756 \end{bmatrix}$	$\begin{bmatrix} 1.218184582 \\ 1.138483038 \\ -4.728791547 \end{bmatrix}$

Table 6.15: The CRPs for the remaining well-conditioned frames for Dataset 2 are presented. The initialization values computed by Homography are juxtaposed with the optimized values for comparison.Brown's distortion model is employed in the optimization process.

Translation Vector in inches		
Frame Number	Initial Values	Optimized Values
1	$\begin{bmatrix} -22.91213256 \\ 10.13699501 \\ 50.95590504 \end{bmatrix}$	$\begin{bmatrix} -14.60062355 \\ 5.377916916 \\ 42.33123481 \end{bmatrix}$
2	$\begin{bmatrix} -13.76017336 \\ 1.862474092 \\ 46.8322836 \end{bmatrix}$	$\begin{bmatrix} -7.133416182 \\ -2.861381054 \\ 43.74299226 \end{bmatrix}$
3	$\begin{bmatrix} -34.84511547 \\ 19.48051736 \\ 47.88078406 \end{bmatrix}$	$\begin{bmatrix} -24.59079438 \\ 14.33024014 \\ 35.25689021 \end{bmatrix}$
4	$\begin{bmatrix} -19.35607239 \\ 7.417978234 \\ 38.99625166 \end{bmatrix}$	$\begin{bmatrix} -13.01873448 \\ 3.785808448 \\ 32.64917864 \end{bmatrix}$
5	$\begin{bmatrix} -11.79251225 \\ 12.50048442 \\ 39.05398083 \end{bmatrix}$	$\begin{bmatrix} -5.504787716 \\ 8.72760568 \\ 32.61413295 \end{bmatrix}$
6	$\begin{bmatrix} -28.66816462 \\ -0.413190441 \\ 37.49291084 \end{bmatrix}$	$\begin{bmatrix} -22.24107244 \\ -3.629367014 \\ 29.36982385 \end{bmatrix}$
7	$\begin{bmatrix} -19.78021146 \\ 9.156074279 \\ 32.71146966 \end{bmatrix}$	$\begin{bmatrix} -13.99630461 \\ 6.074798399 \\ 26.56143254 \end{bmatrix}$
8	$\begin{bmatrix} -11.4836863 \\ 3.25105537 \\ 31.6456562 \end{bmatrix}$	$\begin{bmatrix} -6.915629087 \\ 0.216694655 \\ 29.60781105 \end{bmatrix}$
9	$\begin{bmatrix} -16.07468759 \\ 17.14336632 \\ 48.01391502 \end{bmatrix}$	$\begin{bmatrix} -8.806835552 \\ 13.81241485 \\ 43.95680161 \end{bmatrix}$
10	$\begin{bmatrix} -29.06942799 \\ 3.067385513 \\ 47.59662329 \end{bmatrix}$	$\begin{bmatrix} -20.16925345 \\ -0.881799101 \\ 36.02169892 \end{bmatrix}$
11	$\begin{bmatrix} -9.732224091 \\ 6.521310406 \\ 46.80621636 \end{bmatrix}$	$\begin{bmatrix} -3.001938366 \\ 2.186421724 \\ 40.88879264 \end{bmatrix}$
12	$\begin{bmatrix} -21.94303433 \\ 5.931324118 \\ 46.25400783 \end{bmatrix}$	$\begin{bmatrix} -14.59124978 \\ 1.417172533 \\ 38.5417268 \end{bmatrix}$

Table 6.16: The Translation vectors (in inches) corresponding to the first 12 well-conditioned frames for Dataset 2 is presented. The initialization values computed by Homography are shown along with the optimized values for comparison. Brown's distortion model is employed in the optimization process.

Translation Vector in inches		
Frame Number	Initial Values	Optimized Values
13	$\begin{bmatrix} -7.279594303 \\ 11.15538191 \\ 51.17166444 \end{bmatrix}$	$\begin{bmatrix} 0.250291932 \\ 6.412338138 \\ 43.62932422 \end{bmatrix}$
14	$\begin{bmatrix} -16.36206795 \\ 7.538784817 \\ 34.34940734 \end{bmatrix}$	$\begin{bmatrix} -11.31453 \\ 4.585013908 \\ 30.46824505 \end{bmatrix}$
15	$\begin{bmatrix} -11.26995873 \\ 1.732523249 \\ 42.33063579 \end{bmatrix}$	$\begin{bmatrix} -5.303713232 \\ -2.516820249 \\ 39.72653371 \end{bmatrix}$
16	$\begin{bmatrix} -26.87498887 \\ 12.48631918 \\ 35.39855055 \end{bmatrix}$	$\begin{bmatrix} -20.74000226 \\ 9.576731271 \\ 27.76402814 \end{bmatrix}$
17	$\begin{bmatrix} -19.06327875 \\ 11.51153051 \\ 33.70168147 \end{bmatrix}$	$\begin{bmatrix} -13.18208824 \\ 8.487059576 \\ 27.50446632 \end{bmatrix}$
18	$\begin{bmatrix} 9.31088737 \\ 24.40987856 \\ 47.2477564 \end{bmatrix}$	$\begin{bmatrix} 16.61723659 \\ 20.57868484 \\ 37.77418241 \end{bmatrix}$
19	$\begin{bmatrix} -11.15330922 \\ 28.75480968 \\ 52.18094678 \end{bmatrix}$	$\begin{bmatrix} -2.619017473 \\ 23.95295717 \\ 42.07785777 \end{bmatrix}$
20	$\begin{bmatrix} 14.07458808 \\ -1.447254709 \\ 57.92300964 \end{bmatrix}$	$\begin{bmatrix} 22.4161842 \\ -7.058758014 \\ 50.62701069 \end{bmatrix}$

Table 6.17: The Translation vectors (in inches) corresponding to the remaining well-conditioned frame for Dataset 2 is presented. The initialization values computed by Homography are shown along with the optimized values for comparison. Brown's distortion model is employed in the optimization process.

The converged intrinsics and extrinsics are slightly different as compared to the corresponding values computed using Homography. However, the converged extrinsics remain close enough to the extrinsics as computed using Homography to be just as justifiable.

The combined extrinsic projections of all frames is shown in Figure 6.11.

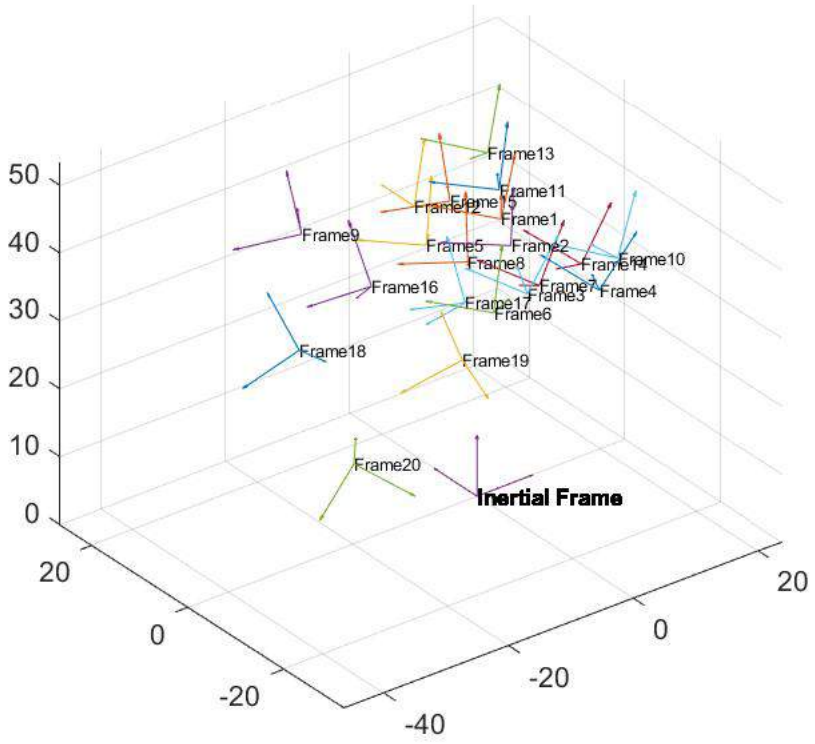

Figure 6.11: Extrinsic projections of all frames for Dataset 2 are shown together with respect to the inertial frame. Brown's distortion model is employed in the optimization process.

The camera is held in the upright position for this experiment as well, so the nearly $\pi/4$ angle shift between both the planar axes of the inertial and image plane will bean additive affect on the final CRPs. There is no noticeable difference in the calculation of intrinsics or extrinsics, although it is believed that there is an improvement in the accuracy of the extrinsics on addition of more beacons.

The plots of the translation vector elements and CRP vector elements against frame number are shown in Figures 6.12 and 6.13.

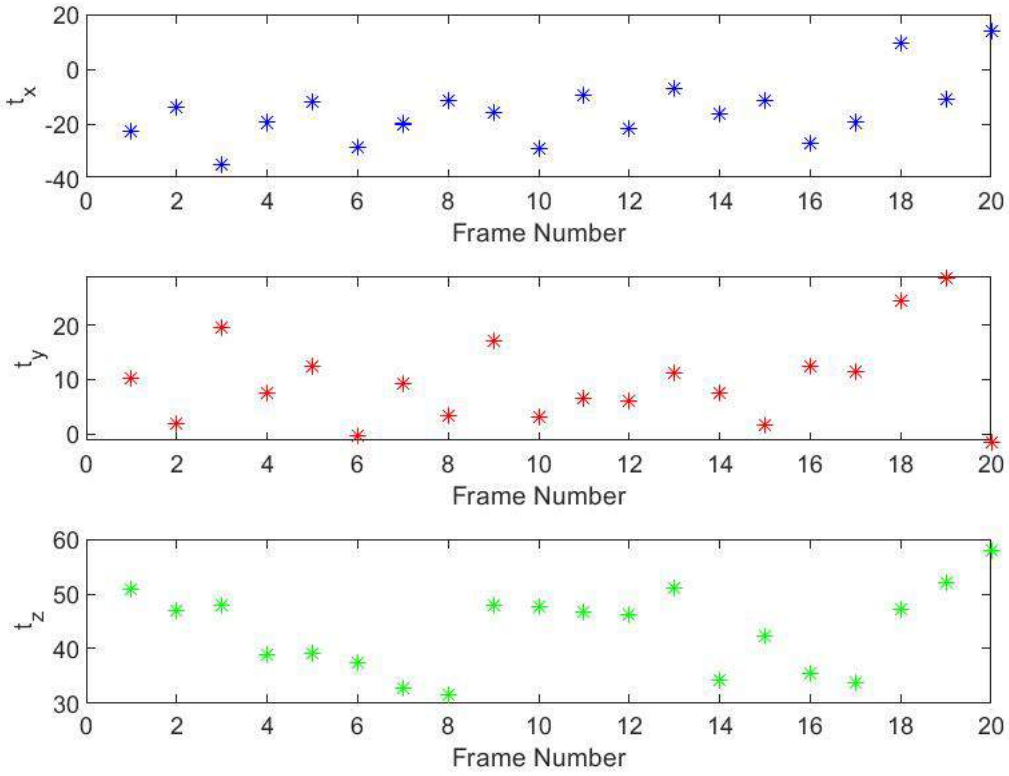

Figure 6.12: Plots of translation vector elements in inches against frame number for Dataset 2. Brown's distortion model is employed in the optimization process.

6.2.2 Geometric Distortion model

The combined estimation approach was employed using the Geometric distortion model to compute the modified intrinsics and extrinsics, along with the distortion coefficients. Table 6.18 shows the values of the intrinsics and the distortion coefficients used to initialize the optimization (computed by the Homography algorithm) along with the optimized values.

Tables 6.19 and 6.20 show the values of the CRPs for each of the viable frames, used to ini-

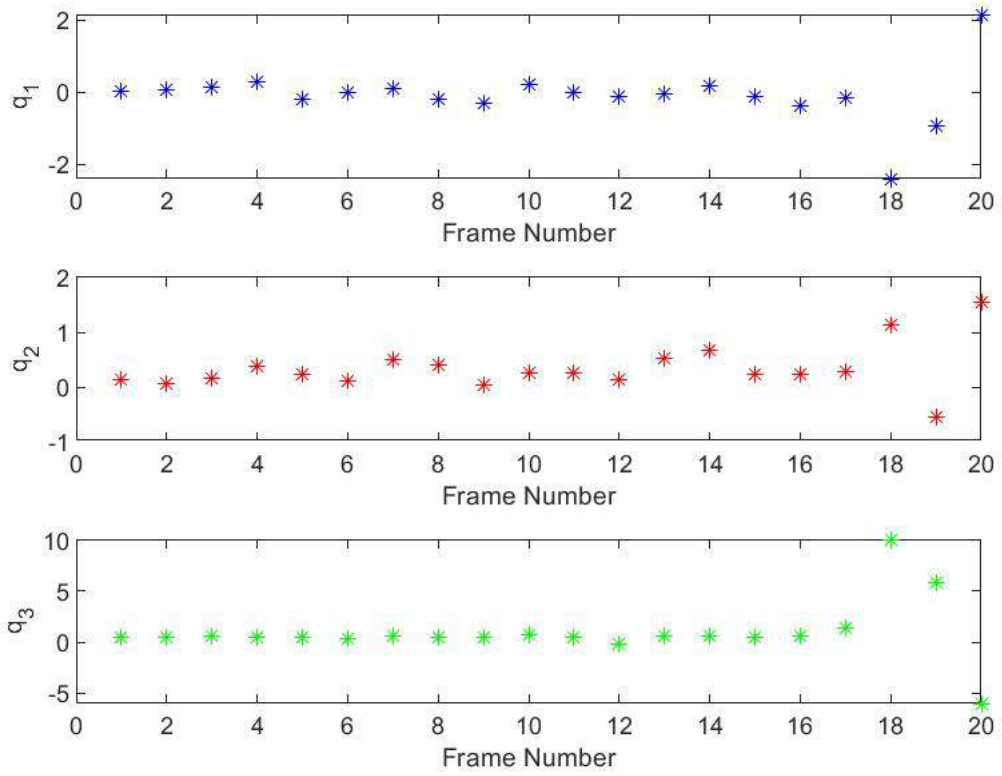

Figure 6.13: Plots of CRP vector elements against frame number for Dataset 2. Brown's distortion model is employed in the optimization process.

tialize the optimization algorithm along with the optimized values. Tables 6.21 and 6.22 show the values of the translation vectors for each of the viable frames, used to initialize the optimization algorithm along with the optimized values.

The extrinsic projections of the 20 frames are shown in Figure D.4 in Appendix D for aesthetic purposes.

Parameter	Initial Values	Optimized Values
α	1.157687557	1.102711539
β	1.228225441	1.207412578
c	0.038390921	0.001792144
u_0	0.74216295	0.805518249
v_0	0.372623487	0.524512571
k_{x1}	0	0.598824241
k_{x2}	0	-0.140608444
k_{x3}	0	0.912536353
k_{y1}	0	3.132509035
k_{y2}	0	-0.009073492
k_{y3}	0	3.641362372

Table 6.18: The intrinsic parameters and the distortion coefficients for Dataset 2, as computed by the Homography algorithm and optimized are shown. Geometric distortion model is employed in the optimization process.

CRP Vector		
Frame Number	Initial Values	Optimized Values
1	$\begin{bmatrix} 0.023347867 \\ 0.134875443 \\ 0.469764129 \end{bmatrix}$	$\begin{bmatrix} 0.022509811 \\ 0.187493521 \\ 0.492346957 \end{bmatrix}$
2	$\begin{bmatrix} 0.058589106 \\ 0.064839454 \\ 0.471290649 \end{bmatrix}$	$\begin{bmatrix} 0.048942135 \\ 0.021197516 \\ 0.480009984 \end{bmatrix}$
3	$\begin{bmatrix} 0.157898381 \\ 0.164745831 \\ 0.548605368 \end{bmatrix}$	$\begin{bmatrix} 0.146626167 \\ 0.289017271 \\ 0.572680143 \end{bmatrix}$
4	$\begin{bmatrix} 0.273106239 \\ 0.377291341 \\ 0.512009173 \end{bmatrix}$	$\begin{bmatrix} 0.173598315 \\ 0.402313711 \\ 0.54013001 \end{bmatrix}$
5	$\begin{bmatrix} -0.192482166 \\ 0.239400098 \\ 0.437794263 \end{bmatrix}$	$\begin{bmatrix} -0.141084963 \\ 0.249380807 \\ 0.467309496 \end{bmatrix}$
6	$\begin{bmatrix} -0.0128827 \\ 0.11925558 \\ 0.327708288 \end{bmatrix}$	$\begin{bmatrix} -0.084830102 \\ 0.211267883 \\ 0.343767638 \end{bmatrix}$
7	$\begin{bmatrix} 0.110680406 \\ 0.503884266 \\ 0.613505727 \end{bmatrix}$	$\begin{bmatrix} 0.018809304 \\ 0.520697692 \\ 0.650062084 \end{bmatrix}$
8	$\begin{bmatrix} -0.177197626 \\ 0.403946394 \\ 0.458456281 \end{bmatrix}$	$\begin{bmatrix} -0.238628256 \\ 0.369377816 \\ 0.495277975 \end{bmatrix}$
9	$\begin{bmatrix} -0.288518115 \\ 0.041790808 \\ 0.49816919 \end{bmatrix}$	$\begin{bmatrix} -0.26317117 \\ 0.070512326 \\ 0.517414286 \end{bmatrix}$
10	$\begin{bmatrix} 0.198215044 \\ 0.249230304 \\ 0.730838029 \end{bmatrix}$	$\begin{bmatrix} 0.028820257 \\ 0.363811712 \\ 0.765328171 \end{bmatrix}$
11	$\begin{bmatrix} -0.006468417 \\ 0.2479848 \\ 0.478072393 \end{bmatrix}$	$\begin{bmatrix} -0.060738505 \\ 0.224981472 \\ 0.507694416 \end{bmatrix}$
12	$\begin{bmatrix} -0.109884211 \\ 0.127610427 \\ -0.115487142 \end{bmatrix}$	$\begin{bmatrix} -0.108510971 \\ 0.214768342 \\ -0.111305497 \end{bmatrix}$

Table 6.19: The CRPs corresponding to the first 12 well-conditioned frames for Dataset 2 is presented. The initialization values computed by Homography are shown along with the optimized values for comparison. Geometric distortion model is employed in the optimization process.

CRP Vector		
Frame Number	Initial Values	Optimized Values
13	$\begin{bmatrix} -0.053582332 \\ 0.514803771 \\ 0.600251658 \end{bmatrix}$	$\begin{bmatrix} -0.100515237 \\ 0.496452113 \\ 0.653110194 \end{bmatrix}$
14	$\begin{bmatrix} 0.176968006 \\ 0.675453608 \\ 0.650675591 \end{bmatrix}$	$\begin{bmatrix} 0.06447531 \\ 0.651408456 \\ 0.697320569 \end{bmatrix}$
15	$\begin{bmatrix} -0.12278011 \\ 0.233038911 \\ 0.500634354 \end{bmatrix}$	$\begin{bmatrix} -0.241552024 \\ 0.190660546 \\ 0.528003283 \end{bmatrix}$
16	$\begin{bmatrix} -0.37415309 \\ 0.239915419 \\ 0.663019815 \end{bmatrix}$	$\begin{bmatrix} -0.418099447 \\ 0.379806059 \\ 0.715189515 \end{bmatrix}$
17	$\begin{bmatrix} -0.140803108 \\ 0.269869612 \\ 1.37446713 \end{bmatrix}$	$\begin{bmatrix} -0.33749925 \\ 0.327208424 \\ 1.441512183 \end{bmatrix}$
18	$\begin{bmatrix} -2.389296895 \\ 1.122891705 \\ 10.07276728 \end{bmatrix}$	$\begin{bmatrix} -3.296954558 \\ 2.098295467 \\ 13.48125977 \end{bmatrix}$
19	$\begin{bmatrix} -0.916000444 \\ -0.537866052 \\ 5.855210757 \end{bmatrix}$	$\begin{bmatrix} -1.590631214 \\ -0.359257966 \\ 5.876606185 \end{bmatrix}$
20	$\begin{bmatrix} 2.155307255 \\ 1.543846229 \\ -5.983510756 \end{bmatrix}$	$\begin{bmatrix} 1.848173634 \\ 1.505457715 \\ -5.027503483 \end{bmatrix}$

Table 6.20: The CRPs corresponding to the remaining well-conditioned frame for Dataset 2 is presented. The initialization values computed by Homography are shown along with the optimized values for comparison. Geometric distortion model is employed in the optimization process.

Translation Vector in inches		
Frame Number	Initial Values	Optimized Values
1	$\begin{bmatrix} -22.91213256 \\ 10.13699501 \\ 50.95590504 \end{bmatrix}$	$\begin{bmatrix} -24.61640316 \\ 3.81277377 \\ 46.92329184 \end{bmatrix}$
2	$\begin{bmatrix} -13.76017336 \\ 1.862474092 \\ 46.8322836 \end{bmatrix}$	$\begin{bmatrix} -16.53582712 \\ -4.245012048 \\ 47.08847725 \end{bmatrix}$
3	$\begin{bmatrix} -34.84511547 \\ 19.48051736 \\ 47.88078406 \end{bmatrix}$	$\begin{bmatrix} -33.28912911 \\ 12.5173524 \\ 37.97063787 \end{bmatrix}$
4	$\begin{bmatrix} -19.35607239 \\ 7.417978234 \\ 38.99625166 \end{bmatrix}$	$\begin{bmatrix} -20.59874098 \\ 2.573863361 \\ 35.44361172 \end{bmatrix}$
5	$\begin{bmatrix} -11.79251225 \\ 12.50048442 \\ 39.05398083 \end{bmatrix}$	$\begin{bmatrix} -13.37893901 \\ 7.624698992 \\ 37.46858568 \end{bmatrix}$
6	$\begin{bmatrix} -28.66816462 \\ -0.413190441 \\ 37.49291084 \end{bmatrix}$	$\begin{bmatrix} -29.50340936 \\ -4.872369302 \\ 31.61387198 \end{bmatrix}$
7	$\begin{bmatrix} -19.78021146 \\ 9.156074279 \\ 32.71146966 \end{bmatrix}$	$\begin{bmatrix} -20.57223376 \\ 5.048047039 \\ 29.52569094 \end{bmatrix}$
8	$\begin{bmatrix} -11.4836863 \\ 3.25105537 \\ 31.6456562 \end{bmatrix}$	$\begin{bmatrix} -13.77268792 \\ -0.856644522 \\ 32.91302967 \end{bmatrix}$
9	$\begin{bmatrix} -16.07468759 \\ 17.14336632 \\ 48.01391502 \end{bmatrix}$	$\begin{bmatrix} -18.77215784 \\ 11.76217629 \\ 47.56348402 \end{bmatrix}$
10	$\begin{bmatrix} -29.06942799 \\ 3.067385513 \\ 47.59662329 \end{bmatrix}$	$\begin{bmatrix} -28.90624583 \\ -2.324040768 \\ 39.44627971 \end{bmatrix}$
11	$\begin{bmatrix} -9.732224091 \\ 6.521310406 \\ 46.80621636 \end{bmatrix}$	$\begin{bmatrix} -12.45825899 \\ 0.733707186 \\ 46.88459575 \end{bmatrix}$
12	$\begin{bmatrix} -21.94303433 \\ 5.931324118 \\ 46.25400783 \end{bmatrix}$	$\begin{bmatrix} -23.35915417 \\ -0.103650251 \\ 41.68137299 \end{bmatrix}$

Table 6.21: The Translation vectors (in inches) corresponding to the first 12 well-conditioned frame for Dataset 2 is presented. The initialization values computed by Homography are shown along with the optimized values for comparison. Geometric distortion model is employed in the optimization process.

Translation Vector in inches		
Frame Number	Initial Values	Optimized Values
13	$\begin{bmatrix} -7.279594303 \\ 11.15538191 \\ 51.17166444 \end{bmatrix}$	$\begin{bmatrix} -9.970071203 \\ 4.852246307 \\ 50.94954898 \end{bmatrix}$
14	$\begin{bmatrix} -16.36206795 \\ 7.538784817 \\ 34.34940734 \end{bmatrix}$	$\begin{bmatrix} -18.72289667 \\ 3.4367047 \\ 34.2905939 \end{bmatrix}$
15	$\begin{bmatrix} -11.26995873 \\ 1.732523249 \\ 42.33063579 \end{bmatrix}$	$\begin{bmatrix} -14.07218231 \\ -3.760724253 \\ 43.30017397 \end{bmatrix}$
16	$\begin{bmatrix} -26.87498887 \\ 12.48631918 \\ 35.39855055 \end{bmatrix}$	$\begin{bmatrix} -27.78160665 \\ 8.330539858 \\ 30.26297185 \end{bmatrix}$
17	$\begin{bmatrix} -19.06327875 \\ 11.51153051 \\ 33.70168147 \end{bmatrix}$	$\begin{bmatrix} -20.07781989 \\ 7.395110119 \\ 30.87484063 \end{bmatrix}$
18	$\begin{bmatrix} 9.31088737 \\ 24.40987856 \\ 47.2477564 \end{bmatrix}$	$\begin{bmatrix} 7.721441318 \\ 19.12084373 \\ 46.01582899 \end{bmatrix}$
19	$\begin{bmatrix} -11.15330922 \\ 28.75480968 \\ 52.18094678 \end{bmatrix}$	$\begin{bmatrix} -13.08262226 \\ 22.34071203 \\ 48.78772959 \end{bmatrix}$
20	$\begin{bmatrix} 14.07458808 \\ -1.447254709 \\ 57.92300964 \end{bmatrix}$	$\begin{bmatrix} 11.17801027 \\ -8.84486584 \\ 57.58015521 \end{bmatrix}$

Table 6.22: The Translation vectors (in inches) corresponding to the remaining well-conditioned frame for Dataset 2 is presented. The initialization values computed by Homography are shown along with the optimized values for comparison. Geometric distortion model is employed in the optimization process.

The converged intrinsics and extrinsics are slightly different as compared to the corresponding values computed using Homography. However, the converged extrinsics remain close enough to the extrinsics as computed using Homography to be just as justifiable.

The combined extrinsic projections of all frames is shown in Figure 6.14.

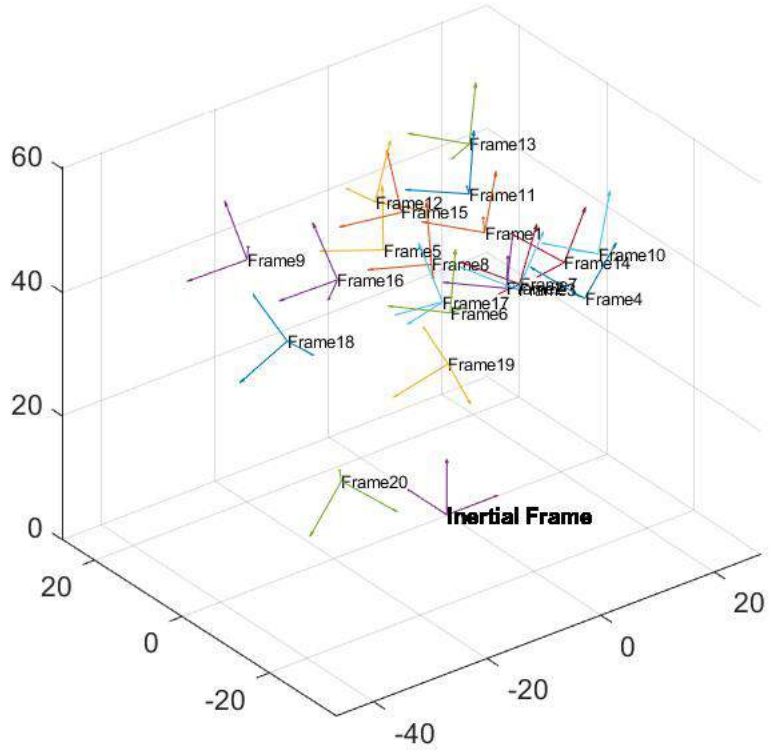

Figure 6.14: Extrinsic projections of all frames for Dataset 2 are shown together with respect to the inertial frame. Geometric Distortion Model is employed to obtain these results

The camera is held in the upright position for this experiment as well, so the nearly $\pi/4$ angle shift between both the planar axes of the inertial and image plane will be an additive effect in the final CRPs. There is no noticeable difference in the calculation of intrinsics or extrinsics, although it is believed that there is an improvement in the accuracy of the extrinsics on addition of more beacons.

The plots of the translation vector elements and CRP vector elements against frame number are shown in Figures 6.15 and 6.16.

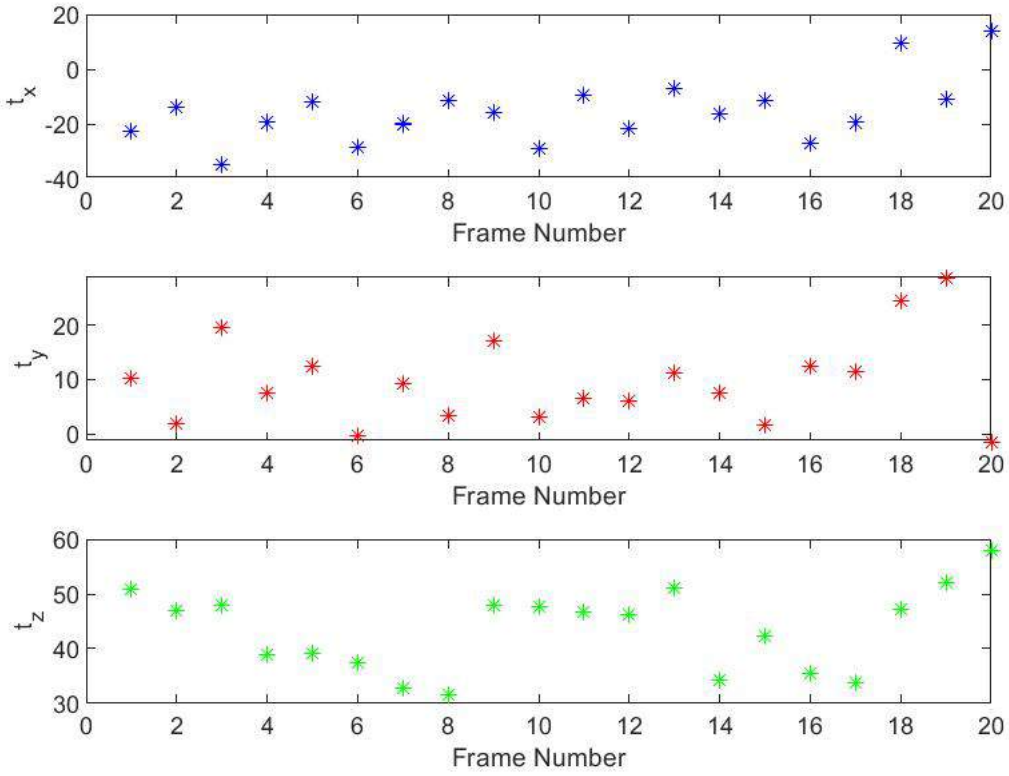

Figure 6.15: Plots of translation vector elements in inches against frame number for Dataset 2. Geometric distortion model is employed in the optimization process.

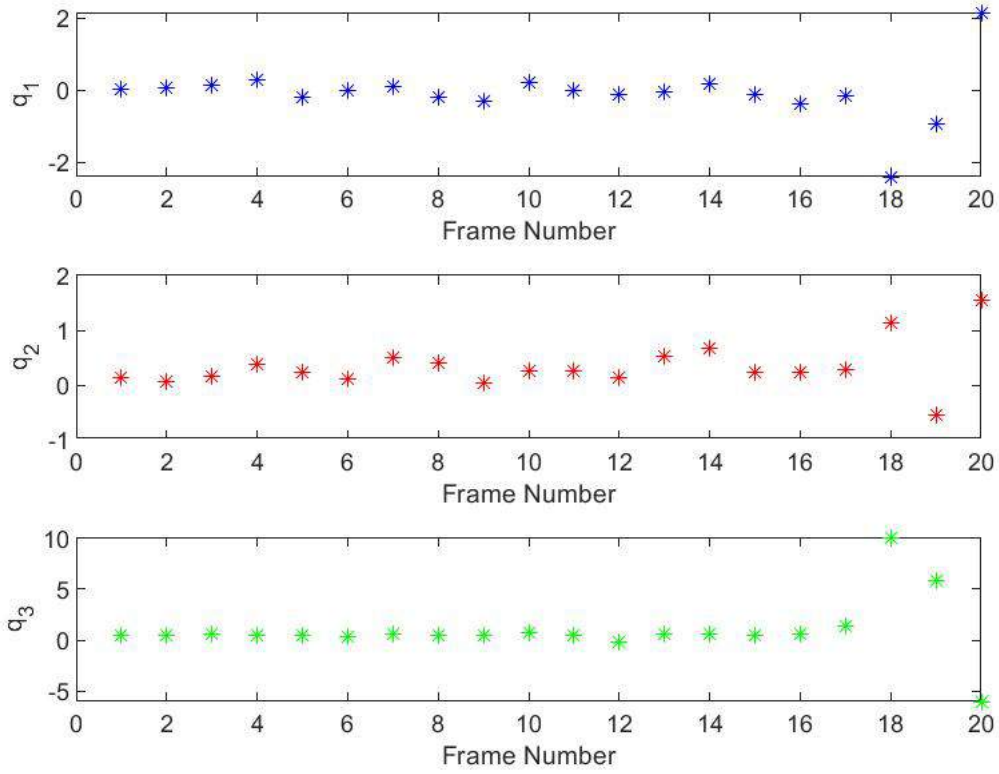

Figure 6.16: Plots of CRP vector elements against frame number for Dataset 2. Geometric distortion model is employed in the optimization process.

6.3 Dataset 3

The setup used was the same as Dataset 2, so the same beacon positions and inertial coordinates apply as shown in Figure 6.9 and Table 6.12 respectively.

All 19 frames satisfied the criterion of the difference in order to last two singular values of the L matrix being two or greater. So no frames were eliminated as noisy.

The image plane projections of the 19 frames as seen from the Phasespace Viewer are shown in Figure 6.17.

The checkerboard was hand held at various poses in order to leverage the full extent of all three available rotational degrees of freedom. The physical alignment images are omitted here.

The intrinsic parameters and distortion coefficients will be shown at a later section to highlight

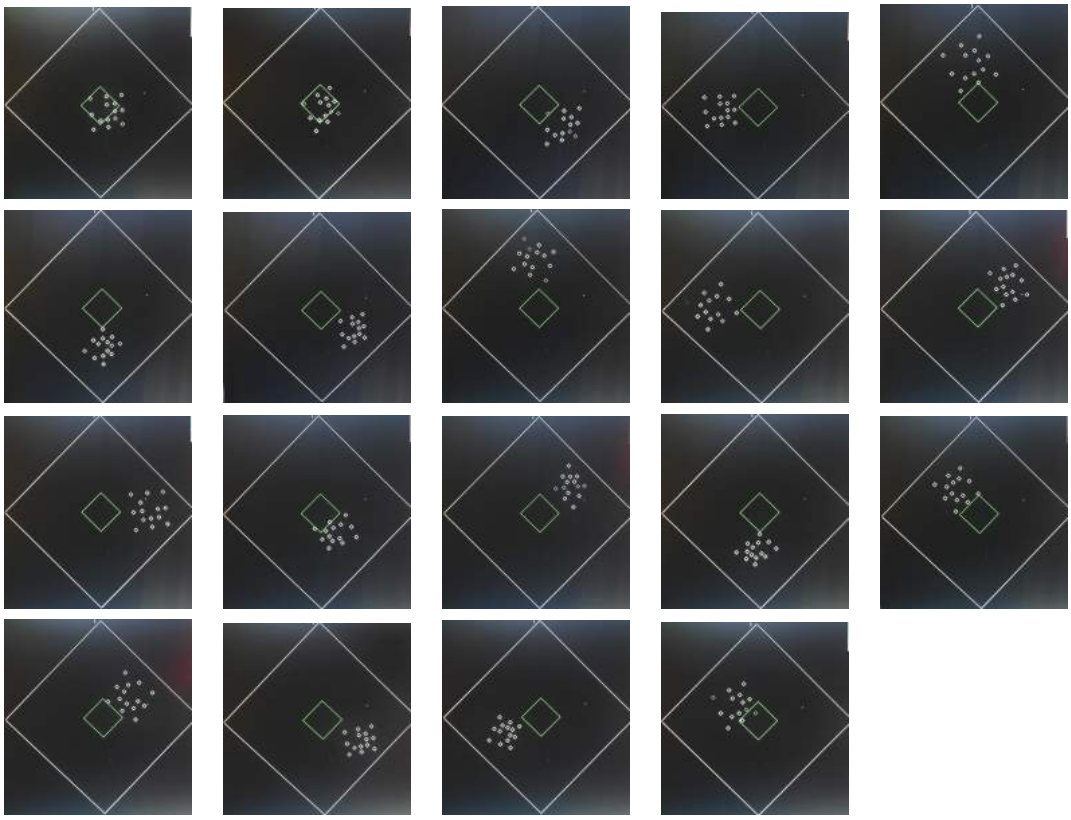

Figure 6.17: Image plane projections of each pose of the board as seen through the Phasespace Viewer. The frames are ordered from the top left to the bottom right.

a different noteworthy point.

6.3.1 Brown's Distortion Model

The combined estimation approach was employed using Brown's distortion model to compute the modified intrinsics and extrinsics, along with the distortion coefficients. The initialization values for the nonlinear optimization algorithm, as computed by the Homography algorithm, are shown in the subsequent tables. Table 6.23 shows the values of the intrinsics and the distortion coefficients used to initialize the optimization along with the optimized values.

Tables 6.24 and 6.25 show the values of the CRPs for each of the viable frames, used to initialize the optimization algorithm along with the optimized values. Tables 6.26 and 6.27 show the values of the translation vectors for each of the viable frames, used to initialize the optimization algorithm along with the optimized values.

Parameter	Initial Values	Optimized Values
α	1.136176911	0.933614725
β	1.240234279	0.940498616
c	0.047646686	-0.000748829
u_0	0.791416878	0.536693111
v_0	0.418736274	0.473476283
k_1	0	-0.183942693
k_2	0	0.164119565
k_3	0	-0.060467711
p_1	0	0.005690797
p_2	0	-0.009347019

Table 6.23: The intrinsic parameters and the distortion coefficients for Dataset 3, as computed by the Homography algorithm and optimized are shown. Brown's distortion model is employed in the optimization process.

The extrinsic projections of the 19 frames are shown in Figure D.5 in Appendix D for aesthetic purposes.

CRP Vector		
Frame Number	Initial Values	Optimized Values
1	$\begin{bmatrix} 0.758547534 \\ 0.094100396 \\ -1.333076525 \end{bmatrix}$	$\begin{bmatrix} 0.587140881 \\ 0.048661986 \\ -1.353395839 \end{bmatrix}$
2	$\begin{bmatrix} 0.96314922 \\ 0.375388791 \\ -2.359973574 \end{bmatrix}$	$\begin{bmatrix} 0.633686539 \\ 0.220753093 \\ -2.244775879 \end{bmatrix}$
3	$\begin{bmatrix} 0.711417294 \\ 0.078850934 \\ -2.285252821 \end{bmatrix}$	$\begin{bmatrix} 0.664270734 \\ -0.006480545 \\ -2.248905688 \end{bmatrix}$
4	$\begin{bmatrix} 0.037660009 \\ 0.227939966 \\ -1.506908042 \end{bmatrix}$	$\begin{bmatrix} 0.093368047 \\ 0.24369272 \\ -1.432611863 \end{bmatrix}$
5	$\begin{bmatrix} 0.309028655 \\ 0.224796215 \\ -0.969381606 \end{bmatrix}$	$\begin{bmatrix} 0.316585173 \\ 0.081259621 \\ -0.964679794 \end{bmatrix}$
6	$\begin{bmatrix} 0.789126453 \\ -0.128721835 \\ -1.750009631 \end{bmatrix}$	$\begin{bmatrix} 0.539059276 \\ -0.069761675 \\ -1.777279076 \end{bmatrix}$
7	$\begin{bmatrix} 0.203457955 \\ 0.087375023 \\ 0.245928901 \end{bmatrix}$	$\begin{bmatrix} 0.090781584 \\ 0.140002693 \\ 0.236381182 \end{bmatrix}$
8	$\begin{bmatrix} -0.280284624 \\ 0.320660536 \\ 0.674658857 \end{bmatrix}$	$\begin{bmatrix} -0.214134745 \\ 0.338459116 \\ 0.701529419 \end{bmatrix}$
9	$\begin{bmatrix} 0.15118898 \\ 0.289710785 \\ 0.681328005 \end{bmatrix}$	$\begin{bmatrix} 0.088023195 \\ 0.223243671 \\ 0.664789101 \end{bmatrix}$
10	$\begin{bmatrix} -0.179611547 \\ 0.63131627 \\ 2.966108078 \end{bmatrix}$	$\begin{bmatrix} 0.006068842 \\ 0.228165478 \\ 2.88106427 \end{bmatrix}$
11	$\begin{bmatrix} -0.50194005 \\ 0.127488768 \\ 0.659966444 \end{bmatrix}$	$\begin{bmatrix} -0.357282028 \\ 0.097631812 \\ 0.731076327 \end{bmatrix}$
12	$\begin{bmatrix} 0.205875134 \\ 0.357345698 \\ 0.080292483 \end{bmatrix}$	$\begin{bmatrix} 0.145722086 \\ 0.250765873 \\ 0.068896081 \end{bmatrix}$

Table 6.24: The CRPs corresponding to the first 12 well-conditioned frame for Dataset 3 is presented. The initialization values computed by Homography are shown along with the optimized values for comparison. Brown's distortion model is employed in the optimization process.

CRP Vector		
Frame Number	Initial Values	Optimized Values
13	$\begin{bmatrix} -0.538461481 \\ 0.233773301 \\ 0.848744048 \end{bmatrix}$	$\begin{bmatrix} -0.336933688 \\ 0.237133184 \\ 0.911610646 \end{bmatrix}$
14	$\begin{bmatrix} 0.158867822 \\ 0.371436232 \\ 0.898188113 \end{bmatrix}$	$\begin{bmatrix} 0.057227542 \\ 0.343853612 \\ 0.869206866 \end{bmatrix}$
15	$\begin{bmatrix} -0.128278076 \\ 0.179402721 \\ 1.222455949 \end{bmatrix}$	$\begin{bmatrix} -0.047232287 \\ 0.141631375 \\ 1.238143841 \end{bmatrix}$
16	$\begin{bmatrix} 0.0929669 \\ 0.222673614 \\ -1.729404845 \end{bmatrix}$	$\begin{bmatrix} 0.031646155 \\ 0.218287488 \\ -1.630618635 \end{bmatrix}$
17	$\begin{bmatrix} 0.498263553 \\ 0.197490781 \\ -0.716999306 \end{bmatrix}$	$\begin{bmatrix} 0.423967126 \\ 0.117580942 \\ -0.72887371 \end{bmatrix}$
18	$\begin{bmatrix} 0.513597284 \\ 0.100111325 \\ -1.407198456 \end{bmatrix}$	$\begin{bmatrix} 0.484250008 \\ 0.121313501 \\ -1.401287771 \end{bmatrix}$
19	$\begin{bmatrix} 0.500583177 \\ -0.189774666 \\ -1.497960464 \end{bmatrix}$	$\begin{bmatrix} 0.325848726 \\ -0.103901706 \\ -1.543819743 \end{bmatrix}$

Table 6.25: The CRPs corresponding to the remaining well-conditioned frame for Dataset 3 is presented. The initialization values computed by Homography are shown along with the optimized values for comparison. Brown's distortion model is employed in the optimization process.

Translation Vector in inches		
Frame Number	Initial Values	Optimized Values
1	$\begin{bmatrix} -6.205458809 \\ -1.586128991 \\ 72.25987044 \end{bmatrix}$	$\begin{bmatrix} 9.322264308 \\ -4.858886131 \\ 56.05038541 \end{bmatrix}$
2	$\begin{bmatrix} 7.450754495 \\ 0.726922386 \\ 67.46792526 \end{bmatrix}$	$\begin{bmatrix} 21.55064032 \\ -2.25475939 \\ 51.92833128 \end{bmatrix}$
3	$\begin{bmatrix} -17.67785724 \\ 15.59139825 \\ 79.49812657 \end{bmatrix}$	$\begin{bmatrix} 0.705326689 \\ 11.57937835 \\ 57.59245551 \end{bmatrix}$
4	$\begin{bmatrix} -9.518870641 \\ -10.52179483 \\ 48.93490264 \end{bmatrix}$	$\begin{bmatrix} 1.041024352 \\ -13.22742004 \\ 38.74005001 \end{bmatrix}$
5	$\begin{bmatrix} 0.405829738 \\ 5.410229951 \\ 79.37401584 \end{bmatrix}$	$\begin{bmatrix} 17.03832158 \\ 2.173214102 \\ 60.47337617 \end{bmatrix}$
6	$\begin{bmatrix} 9.053839434 \\ -2.765982395 \\ 76.36623225 \end{bmatrix}$	$\begin{bmatrix} 26.07221085 \\ -6.531078101 \\ 61.61247516 \end{bmatrix}$
7	$\begin{bmatrix} -43.95329837 \\ -11.08117544 \\ 59.71962914 \end{bmatrix}$	$\begin{bmatrix} -28.70634864 \\ -13.36060602 \\ 41.79031817 \end{bmatrix}$
8	$\begin{bmatrix} -37.55054397 \\ 22.05526897 \\ 50.12388385 \end{bmatrix}$	$\begin{bmatrix} -22.89606141 \\ 19.50844877 \\ 33.28668836 \end{bmatrix}$
9	$\begin{bmatrix} -23.84598366 \\ -3.610008807 \\ 51.82073386 \end{bmatrix}$	$\begin{bmatrix} -11.61580954 \\ -5.833889532 \\ 39.23650173 \end{bmatrix}$
10	$\begin{bmatrix} 2.393589601 \\ 5.500250228 \\ 51.21574812 \end{bmatrix}$	$\begin{bmatrix} 13.56708478 \\ 3.213954849 \\ 40.46461603 \end{bmatrix}$
11	$\begin{bmatrix} -16.84175948 \\ 13.07570972 \\ 53.89670374 \end{bmatrix}$	$\begin{bmatrix} -4.208453701 \\ 11.60591278 \\ 44.19883791 \end{bmatrix}$
12	$\begin{bmatrix} -24.44874148 \\ -18.90325306 \\ 58.54380367 \end{bmatrix}$	$\begin{bmatrix} -11.82326804 \\ -22.80298791 \\ 46.31345947 \end{bmatrix}$

Table 6.26: The Translation vectors (in inches) corresponding to the first 12 well-conditioned frame for Dataset 3 is presented. The initialization values computed by Homography are shown along with the optimized values for comparison. Brown's distortion model is employed in the optimization process.

Translation Vector in inches		
Frame Number	Initial Values	Optimized Values
13	$\begin{bmatrix} -15.18856609 \\ 25.46510009 \\ 60.78919229 \end{bmatrix}$	$\begin{bmatrix} -0.619125755 \\ 24.35123813 \\ 46.93726878 \end{bmatrix}$
14	$\begin{bmatrix} -35.71578218 \\ 11.0943303 \\ 52.23092979 \end{bmatrix}$	$\begin{bmatrix} -22.26529174 \\ 9.128599626 \\ 38.2132221 \end{bmatrix}$
15	$\begin{bmatrix} -19.56423501 \\ 5.020779307 \\ 56.59213804 \end{bmatrix}$	$\begin{bmatrix} -5.863605806 \\ 2.677733405 \\ 40.72107367 \end{bmatrix}$
16	$\begin{bmatrix} 14.30873772 \\ -7.321424438 \\ 72.93111453 \end{bmatrix}$	$\begin{bmatrix} 29.52392697 \\ -10.93669959 \\ 56.91359197 \end{bmatrix}$
17	$\begin{bmatrix} -29.06231785 \\ 11.8281216 \\ 92.62288731 \end{bmatrix}$	$\begin{bmatrix} -7.113886152 \\ 7.626050867 \\ 69.40483095 \end{bmatrix}$
18	$\begin{bmatrix} -14.8955691 \\ -2.044728032 \\ 65.95063732 \end{bmatrix}$	$\begin{bmatrix} -0.233052545 \\ -4.879727627 \\ 50.33975413 \end{bmatrix}$
19	$\begin{bmatrix} 2.579369054 \\ -15.04801757 \\ 68.68800025 \end{bmatrix}$	$\begin{bmatrix} 17.01688283 \\ -19.1207319 \\ 54.27518228 \end{bmatrix}$

Table 6.27: The Translation vectors (in inches) corresponding to the remaining well-conditioned frame for Dataset 3 is presented. The initialization values computed by Homography are shown along with the optimized values for comparison. Brown's distortion model is employed in the optimization process.

The converged intrinsics and extrinsics are slightly different as compared to the corresponding values computed using Homography. However, the converged extrinsics remain close enough to the extrinsics as computed using Homography to be just as justifiable.

The combined extrinsic projections of the frames is shown in Figure 6.18.

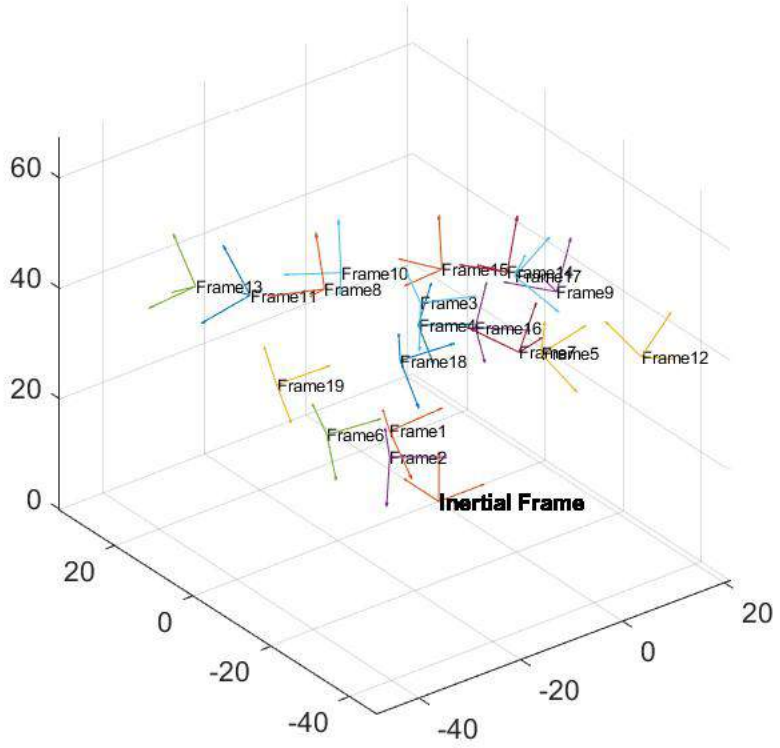

Figure 6.18: Extrinsic projections of all frames for Dataset 3 are shown together with respect to the inertial frame. Brown's Distortion Model is employed to obtain these results

The CRPs for each frame were computed from the Rotation Matrix by first converting to quaternions using Sheppard's Algorithm and then converting the quaternions to CRPs. The plots of the translation vector elements and CRP vector elements against frame number are shown in Figures 6.19 and 6.20.

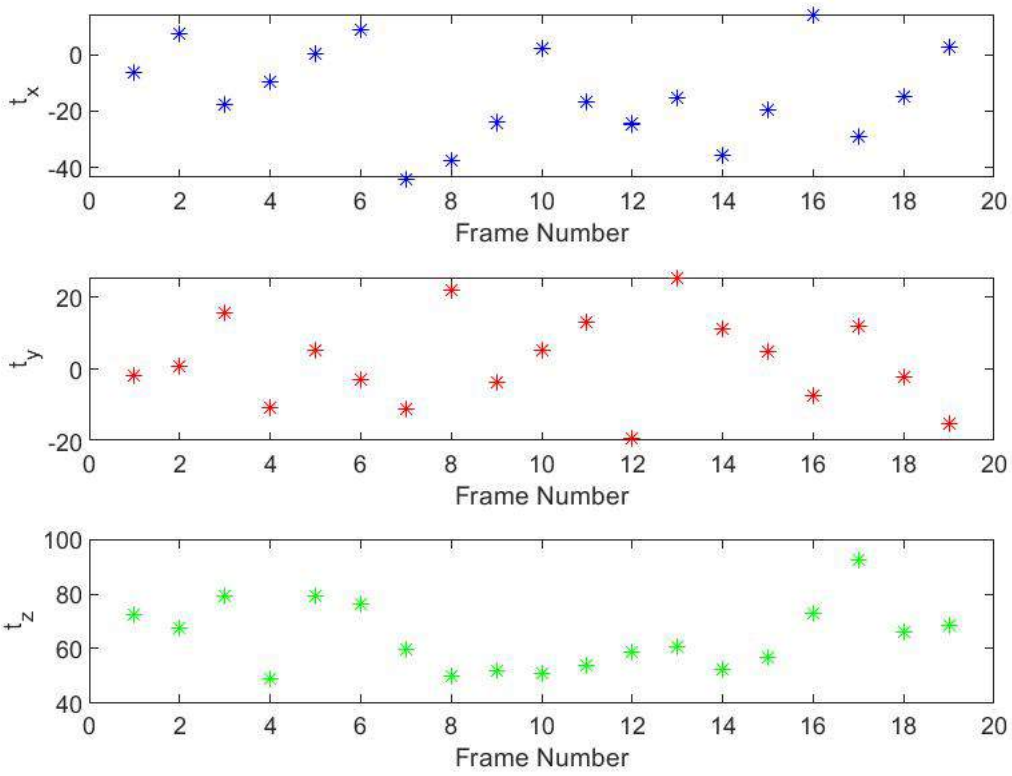

Figure 6.19: Plots of translation vector elements in inches against frame number for Dataset 3. Brown's distortion model is employed in the optimization process.

6.3.2 Geometric Distortion model

The combined estimation approach was employed using the Geometric distortion model to compute the modified intrinsics and extrinsics, along with the distortion coefficients. Table 6.28 shows the values of the intrinsics and the distortion coefficients used to initialize the optimization along with the optimized values.

Tables 6.29 and 6.30 show the values of the CRPs for each of the viable frames, used to initialize the optimization algorithm along with the optimized values. Tables 6.31 and 6.32 show the values of the translation vectors for each of the viable frames, used to initialize the optimization algorithm along with the optimized values. The extrinsic projections of the 19 frames are shown in Figure D.6 in Appendix D for aesthetic purposes.

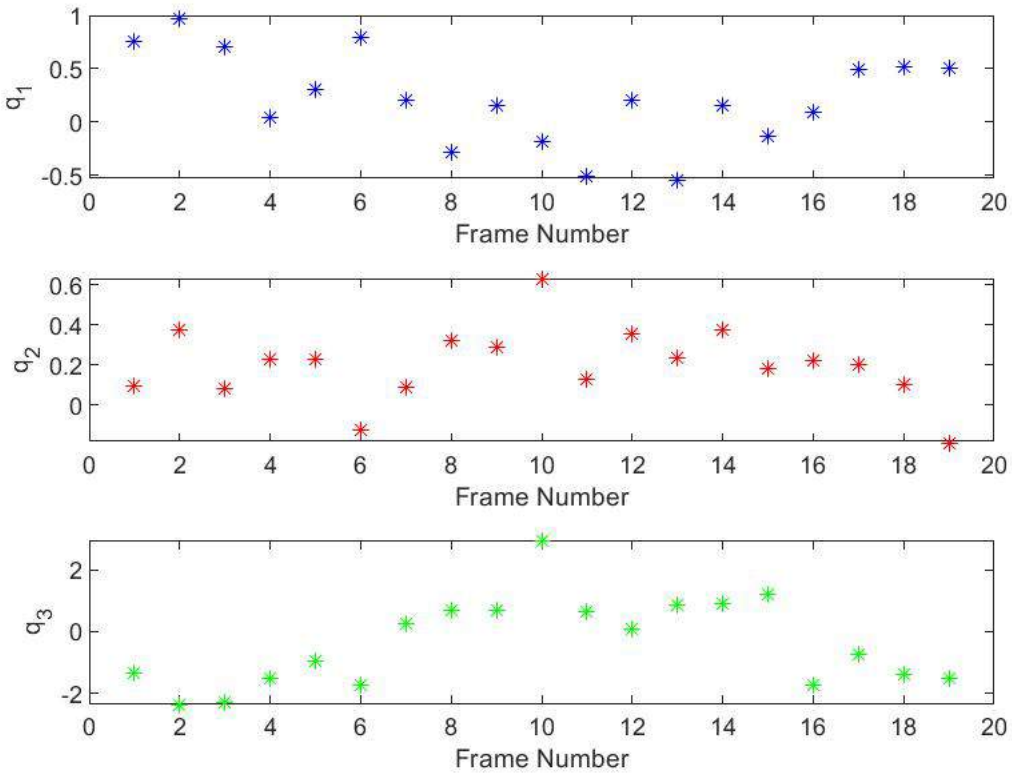

Figure 6.20: Plots of CRP vector elements against frame number for Dataset 3. Brown's distortion model is employed in the optimization process.

Parameter	Initial Values	Optimized Values
α	1.136176911	1.05811654
β	1.240234279	1.14663427
c	0.047646686	0.002806537
u_0	0.791416878	0.771806514
v_0	0.418736274	0.488215565
k_{x1}	0	0.267086201
k_{x2}	0	-0.090530433
k_{x3}	0	0.512177244
k_{y1}	0	3.609937896
k_{y2}	0	-0.043344237
k_{y3}	0	4.201661839

Table 6.28: The intrinsic parameters and the distortion coefficients for Dataset 3, as computed by the Homography algorithm and optimized are shown. Geometric distortion model is employed in the optimization process.

CRP Vector		
Frame Number	Initial Values	Optimized Values
1	$\begin{bmatrix} 0.758547534 \\ 0.094100396 \\ -1.333076525 \end{bmatrix}$	$\begin{bmatrix} 0.707553348 \\ 0.139502697 \\ -1.289304693 \end{bmatrix}$
2	$\begin{bmatrix} 0.96314922 \\ 0.375388791 \\ -2.359973574 \end{bmatrix}$	$\begin{bmatrix} 0.804852924 \\ 0.329939233 \\ -2.222269588 \end{bmatrix}$
3	$\begin{bmatrix} 0.711417294 \\ 0.078850934 \\ -2.285252821 \end{bmatrix}$	$\begin{bmatrix} 0.848655212 \\ 0.064670193 \\ -2.189180769 \end{bmatrix}$
4	$\begin{bmatrix} 0.037660009 \\ 0.227939966 \\ -1.506908042 \end{bmatrix}$	$\begin{bmatrix} 0.142519088 \\ 0.322355327 \\ -1.463738442 \end{bmatrix}$
5	$\begin{bmatrix} 0.309028655 \\ 0.224796215 \\ -0.969381606 \end{bmatrix}$	$\begin{bmatrix} 0.383115048 \\ 0.173975288 \\ -0.936937372 \end{bmatrix}$
6	$\begin{bmatrix} 0.789126453 \\ -0.128721835 \\ -1.750009631 \end{bmatrix}$	$\begin{bmatrix} 0.678459275 \\ -0.020210944 \\ -1.681736426 \end{bmatrix}$
7	$\begin{bmatrix} 0.203457955 \\ 0.087375023 \\ 0.245928901 \end{bmatrix}$	$\begin{bmatrix} 0.078112204 \\ 0.215776086 \\ 0.254012885 \end{bmatrix}$
8	$\begin{bmatrix} -0.280284624 \\ 0.320660536 \\ 0.674658857 \end{bmatrix}$	$\begin{bmatrix} -0.279908963 \\ 0.394840073 \\ 0.699094976 \end{bmatrix}$
9	$\begin{bmatrix} 0.15118898 \\ 0.289710785 \\ 0.681328005 \end{bmatrix}$	$\begin{bmatrix} 0.03734198 \\ 0.330024873 \\ 0.699089407 \end{bmatrix}$
10	$\begin{bmatrix} -0.179611547 \\ 0.63131627 \\ 2.966108078 \end{bmatrix}$	$\begin{bmatrix} -0.168571455 \\ 0.355893487 \\ 3.021477653 \end{bmatrix}$
11	$\begin{bmatrix} -0.50194005 \\ 0.127488768 \\ 0.659966444 \end{bmatrix}$	$\begin{bmatrix} -0.467645929 \\ 0.159095259 \\ 0.692389414 \end{bmatrix}$
12	$\begin{bmatrix} 0.205875134 \\ 0.357345698 \\ 0.080292483 \end{bmatrix}$	$\begin{bmatrix} 0.151443086 \\ 0.358777151 \\ 0.091171695 \end{bmatrix}$

Table 6.29: The CRPs corresponding to the first 12 well-conditioned frame for Dataset 3 is presented. The initialization values computed by Homography are shown along with the optimized values for comparison. Geometric distortion model is employed in the optimization process.

CRP Vector		
Frame Number	Initial Values	Optimized Values
13	$\begin{bmatrix} -0.538461481 \\ 0.233773301 \\ 0.848744048 \end{bmatrix}$	$\begin{bmatrix} -0.469231459 \\ 0.306281381 \\ 0.894510163 \end{bmatrix}$
14	$\begin{bmatrix} 0.158867822 \\ 0.371436232 \\ 0.898188113 \end{bmatrix}$	$\begin{bmatrix} -0.027121014 \\ 0.441687787 \\ 0.897360845 \end{bmatrix}$
15	$\begin{bmatrix} -0.128278076 \\ 0.179402721 \\ 1.222455949 \end{bmatrix}$	$\begin{bmatrix} -0.140098859 \\ 0.229326592 \\ 1.26004091 \end{bmatrix}$
16	$\begin{bmatrix} 0.0929669 \\ 0.222673614 \\ -1.729404845 \end{bmatrix}$	$\begin{bmatrix} 0.063047551 \\ 0.3902326 \\ -1.664095795 \end{bmatrix}$
17	$\begin{bmatrix} 0.498263553 \\ 0.197490781 \\ -0.716999306 \end{bmatrix}$	$\begin{bmatrix} 0.487070564 \\ 0.23013117 \\ -0.701703117 \end{bmatrix}$
18	$\begin{bmatrix} 0.513597284 \\ 0.100111325 \\ -1.407198456 \end{bmatrix}$	$\begin{bmatrix} 0.622961124 \\ 0.221390404 \\ -1.372574435 \end{bmatrix}$
19	$\begin{bmatrix} 0.500583177 \\ -0.189774666 \\ -1.497960464 \end{bmatrix}$	$\begin{bmatrix} 0.468310064 \\ -0.031100019 \\ -1.47185497 \end{bmatrix}$

Table 6.30: The CRPs corresponding to the remaining well-conditioned frame for Dataset 3 is presented. The initialization values computed by Homography are shown along with the optimized values for comparison. Geometric distortion model is employed in the optimization process.

Translation Vector in inches		
Frame Number	Initial Values	Optimized Values
1	$\begin{bmatrix} -6.205458809 \\ -1.586128991 \\ 72.25987044 \end{bmatrix}$	$\begin{bmatrix} -4.896331504 \\ -5.720964602 \\ 66.55064966 \end{bmatrix}$
2	$\begin{bmatrix} 7.450754495 \\ 0.726922386 \\ 67.46792526 \end{bmatrix}$	$\begin{bmatrix} 8.851030757 \\ -3.148060975 \\ 63.69222041 \end{bmatrix}$
3	$\begin{bmatrix} -17.67785724 \\ 15.59139825 \\ 79.49812657 \end{bmatrix}$	$\begin{bmatrix} -14.45215635 \\ 10.75851981 \\ 68.96489082 \end{bmatrix}$
4	$\begin{bmatrix} -9.518870641 \\ -10.52179483 \\ 48.93490264 \end{bmatrix}$	$\begin{bmatrix} -8.923824184 \\ -13.70849318 \\ 45.49350864 \end{bmatrix}$
5	$\begin{bmatrix} 0.405829738 \\ 5.410229951 \\ 79.37401584 \end{bmatrix}$	$\begin{bmatrix} 1.791293655 \\ 0.948024741 \\ 72.77369385 \end{bmatrix}$
6	$\begin{bmatrix} 9.053839434 \\ -2.765982395 \\ 76.36623225 \end{bmatrix}$	$\begin{bmatrix} 10.83895408 \\ -7.477305709 \\ 74.95299518 \end{bmatrix}$
7	$\begin{bmatrix} -43.95329837 \\ -11.08117544 \\ 59.71962914 \end{bmatrix}$	$\begin{bmatrix} -40.20444574 \\ -13.89153874 \\ 46.91381401 \end{bmatrix}$
8	$\begin{bmatrix} -37.55054397 \\ 22.05526897 \\ 50.12388385 \end{bmatrix}$	$\begin{bmatrix} -33.58607921 \\ 18.94603789 \\ 40.16800796 \end{bmatrix}$
9	$\begin{bmatrix} -23.84598366 \\ -3.610008807 \\ 51.82073386 \end{bmatrix}$	$\begin{bmatrix} -21.72584366 \\ -6.258587768 \\ 44.47005733 \end{bmatrix}$
10	$\begin{bmatrix} 2.393589601 \\ 5.500250228 \\ 51.21574812 \end{bmatrix}$	$\begin{bmatrix} 3.357547866 \\ 2.704499728 \\ 47.73891811 \end{bmatrix}$
11	$\begin{bmatrix} -16.84175948 \\ 13.07570972 \\ 53.89670374 \end{bmatrix}$	$\begin{bmatrix} -15.86296827 \\ 10.64470546 \\ 51.57203219 \end{bmatrix}$
12	$\begin{bmatrix} -24.44874148 \\ -18.90325306 \\ 58.54380367 \end{bmatrix}$	$\begin{bmatrix} -23.86460287 \\ -23.32440981 \\ 52.5909421 \end{bmatrix}$

Table 6.31: The Translation vectors (in inches) corresponding to the first 12 well-conditioned frame for Dataset 3 is presented. The initialization values computed by Homography are shown along with the optimized values for comparison. Geometric distortion model is employed in the optimization process.

Translation Vector in inches		
Frame Number	Initial Values	Optimized Values
13	$\begin{bmatrix} -15.18856609 \\ 25.46510009 \\ 60.78919229 \end{bmatrix}$	$\begin{bmatrix} -13.33121674 \\ 23.42533036 \\ 56.61067769 \end{bmatrix}$
14	$\begin{bmatrix} -35.71578218 \\ 11.0943303 \\ 52.23092979 \end{bmatrix}$	$\begin{bmatrix} -33.2095772 \\ 8.39910302 \\ 44.59179245 \end{bmatrix}$
15	$\begin{bmatrix} -19.56423501 \\ 5.020779307 \\ 56.59213804 \end{bmatrix}$	$\begin{bmatrix} -16.35914788 \\ 2.166119856 \\ 46.9990632 \end{bmatrix}$
16	$\begin{bmatrix} 14.30873772 \\ -7.321424438 \\ 72.93111453 \end{bmatrix}$	$\begin{bmatrix} 15.31368889 \\ -11.63984514 \\ 68.53506817 \end{bmatrix}$
17	$\begin{bmatrix} -29.06231785 \\ 11.8281216 \\ 92.62288731 \end{bmatrix}$	$\begin{bmatrix} -24.98145436 \\ 6.289468909 \\ 80.6983535 \end{bmatrix}$
18	$\begin{bmatrix} -14.8955691 \\ -2.044728032 \\ 65.95063732 \end{bmatrix}$	$\begin{bmatrix} -13.30762509 \\ -5.600090395 \\ 59.46352495 \end{bmatrix}$
19	$\begin{bmatrix} 2.579369054 \\ -15.04801757 \\ 68.68800025 \end{bmatrix}$	$\begin{bmatrix} 3.188794374 \\ -19.7234355 \\ 64.9716381 \end{bmatrix}$

Table 6.32: The Translation vectors (in inches) corresponding to the remaining well-conditioned frame for Dataset 3 is presented. The initialization values computed by Homography are shown along with the optimized values for comparison. Geometric distortion model is employed in the optimization process.

The converged intrinsics and extrinsics are slightly different as compared to the corresponding values computed using Homography. However, the converged extrinsics remain close enough to the extrinsics as computed using Homography to be just as justifiable.

The combined extrinsic projections of the frames is shown in Figure 6.21.

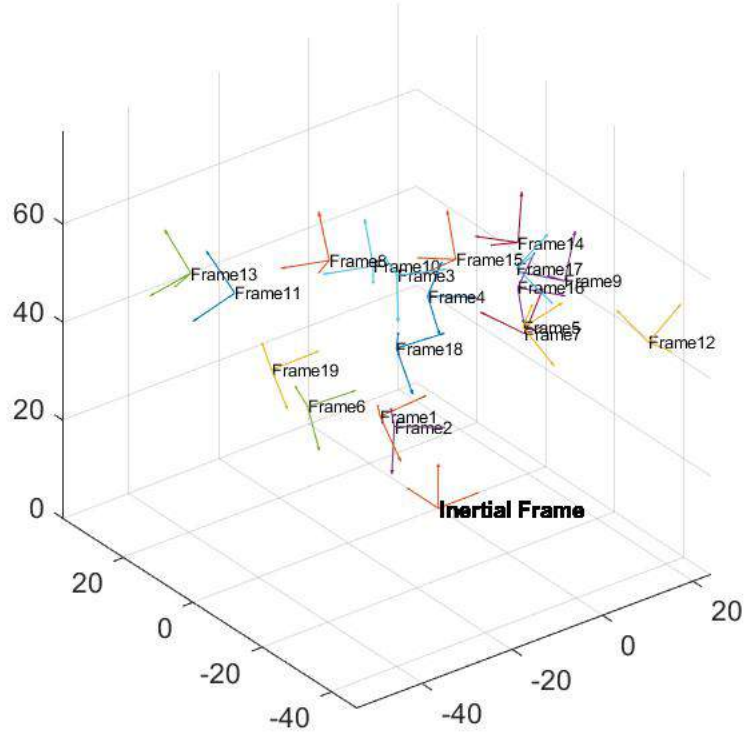

Figure 6.21: Extrinsic projections of all frames are shown together with respect to the inertial frame for Dataset 3. Geometric distortion model is employed in the optimization process.

The plots of the translation vector elements and CRP vector elements against frame number are shown in Figures 6.22 and 6.23.

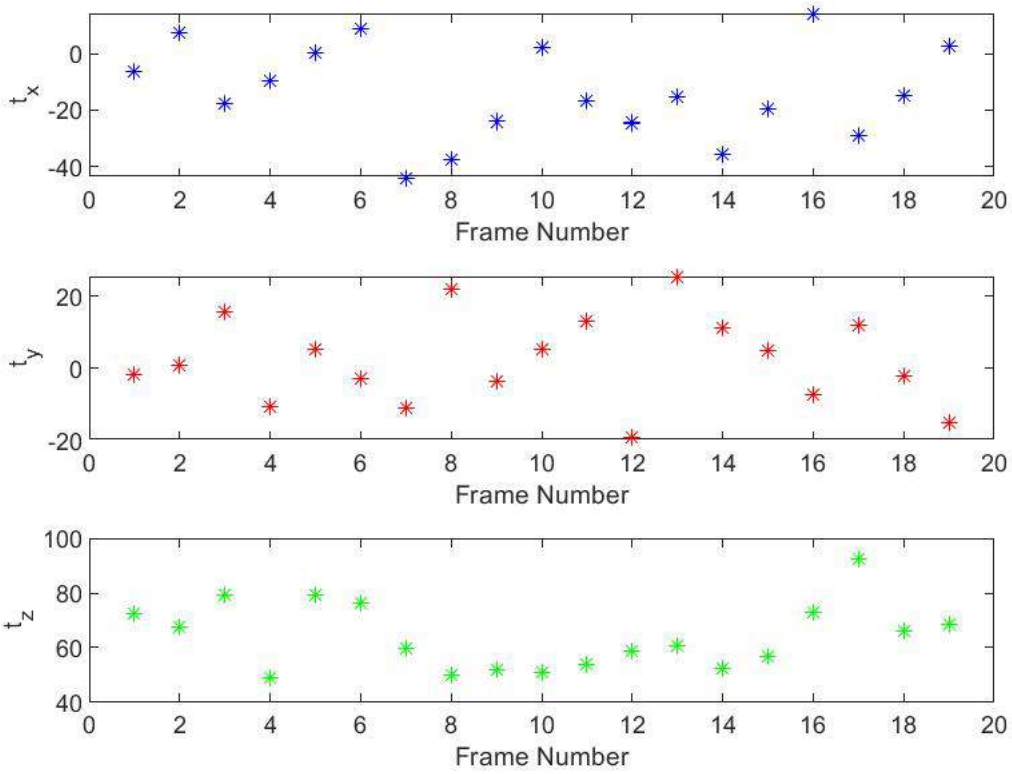

Figure 6.22: Plots of translation vector elements in inches against frame number for Dataset 3. Geometric distortion model is employed in the optimization process.

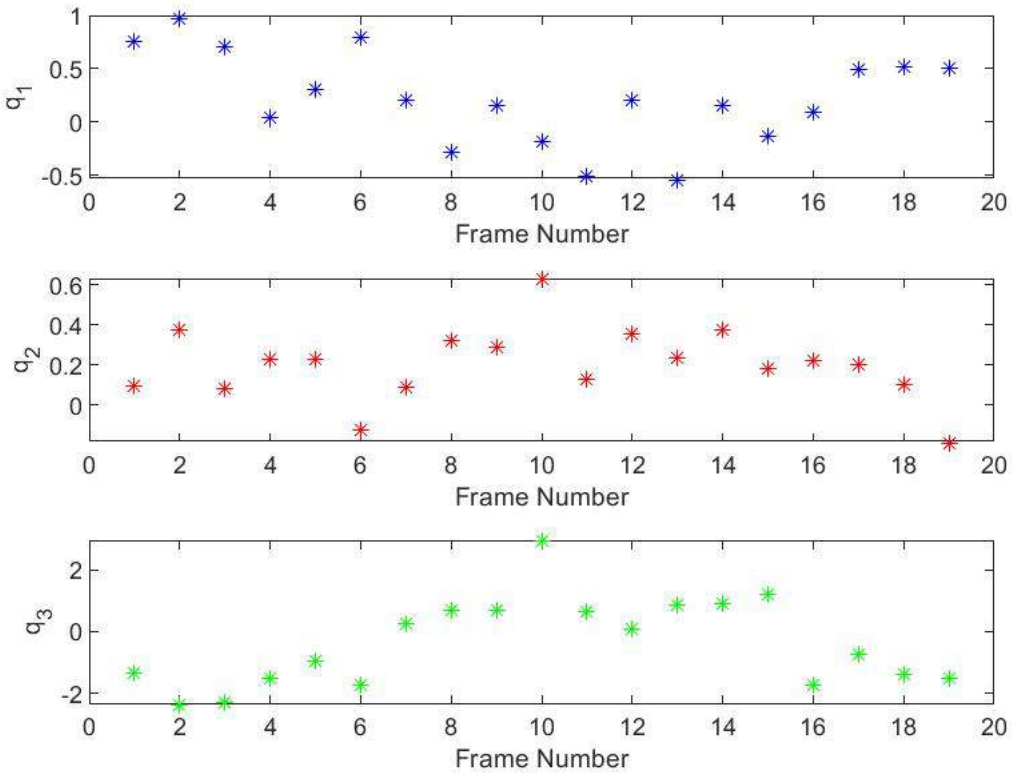

Figure 6.23: Plots of CRP vector elements against frame number for Dataset 3. Geometric distortion model is employed in the optimization process.

6.4 Dataset 4

The main purpose of this experiment is to verify the ability of the algorithm by Wong et al [3] dicussed in Chapter 4 to estimate the relative pose of a body equipped with the LED beacons, assuming a calibrated camera according to a particular distortion model. Here, a dataset is chosen and the intrinsics, distortion coefficients and the extrinsics are estimated using the Combined Estimation approach with Brown's Distortion model. Then, the converged intrinsics and distortion coefficients are fed to Wong's algorithm and the resulting extrinsics are compared with the extrinsics from the Combined Estimation approach.

The arrangement of the 8 beacons on the checkerboard pattern is shown in Figure 6.24.

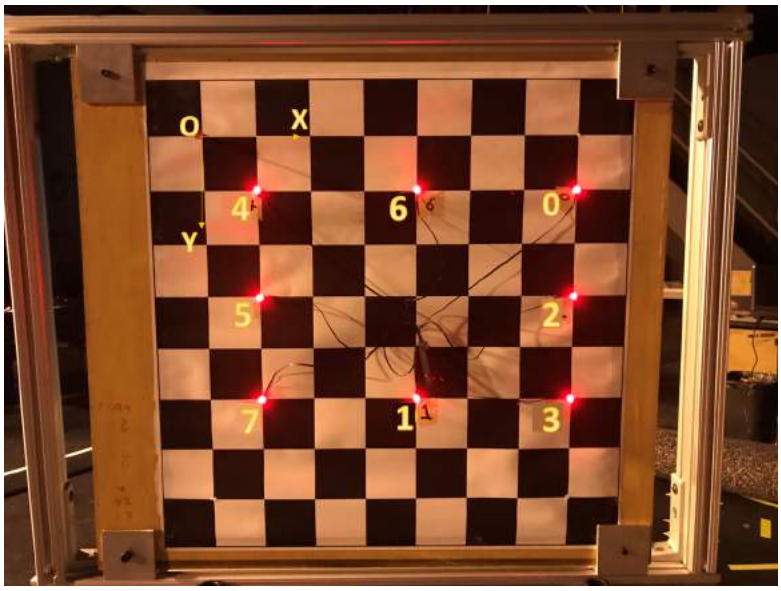

Figure 6.24: Beacon Arrangement on the checkerboard pattern is shown. The numbers next to the beacons indicate their number assignment in the Phasespace system. The origin O, the inertial x-axis X and inertial y-axis Y are also shown.

The inertial coordinates of the beacons are given in Table 6.33.

The image plane projections of the 16 frames as seen from the Phasespace Viewer are shown in Figure 6.25.

Beacon No.	Inertial Position
0	$[7s,s]$
1	$[4s,5s]$
2	$[7s,3s]$
3	$[7s,5s]$
4	$[s,s]$
5	$[s,3s]$
6	$[4s,s]$
7	$[s,5s]$

Table 6.33: Inertial coordinates of each beacon given as [X-coordinate,Y-coordinate], s=49/16 inches

This time a frame was fabricated out of aluminium 80-20 channels in order to support the checkerboard. This frame was mounted onto a rolling table to enable quick translations. The frame has a negligible rotational degree of freedom about the inertial x-axis and z-axis but could achieve significant rotational freedom in the inertial y-axis due to the moving table.

The physical alignment of the board with the camera for each frame (pose) is shown in Figure 6.26.

Using the difference in order of the last two singular values of the L matrix criterion, Frame 13 was eliminated as being noisy.

The CRPs as computed using the Combined Estimation algorithm using Brown's distortion model are shown in Tables 6.34 and 6.35. The corresponding CRPs estimated using the Wong [3] algorithm are presented side-by-side for comparison.

The translations as computed using the Combined Estimation algorithm using Brown's distortion model are shown in Tables 6.36 and 6.37. The corresponding translations estimated using the Wong [3] algorithm are presented side-by-side for comparison.

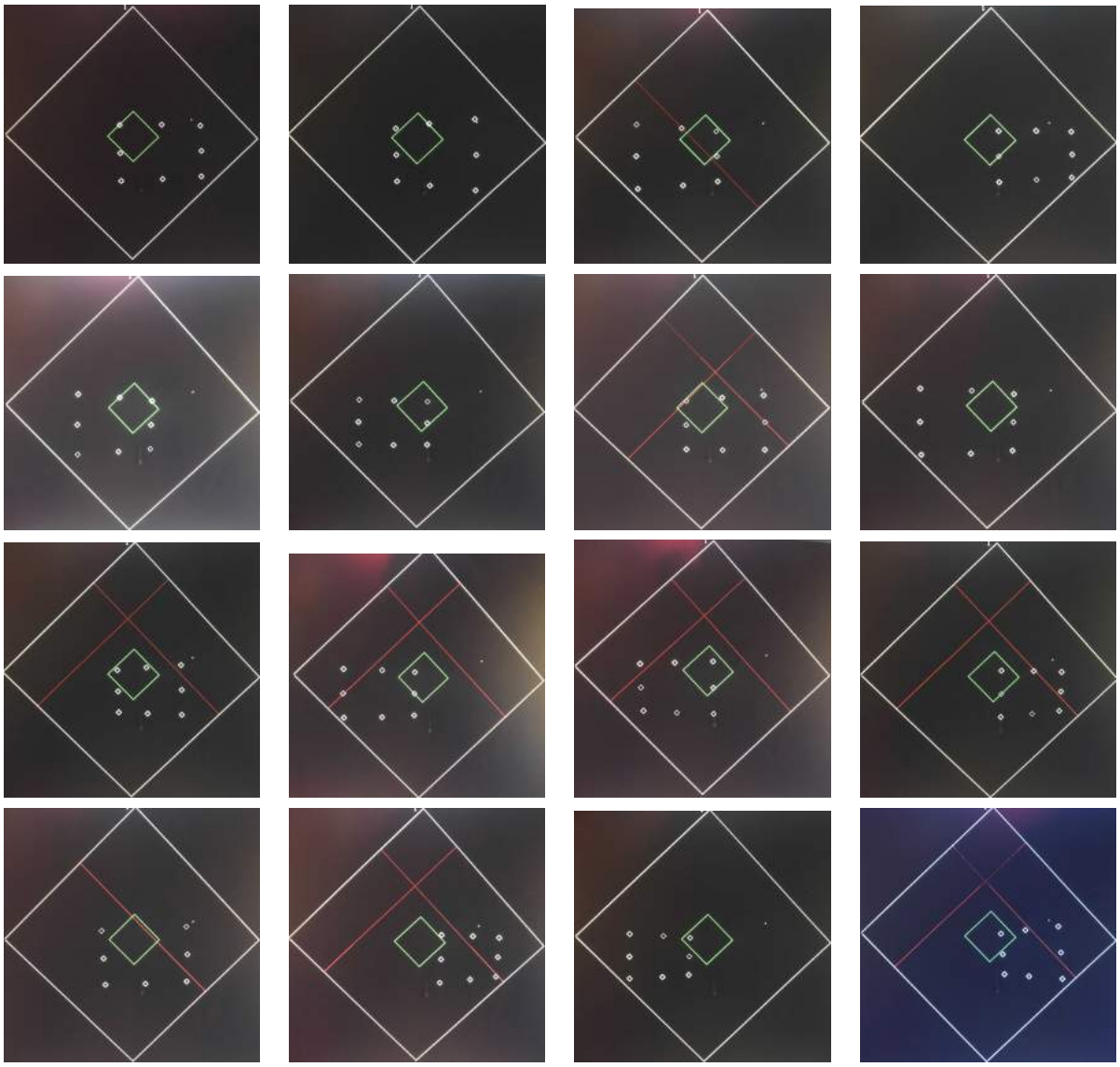

Figure 6.25: Image plane projections of each pose of the board as seen through the Phasespace Viewer. The frames are ordered from the top left to the bottom right.

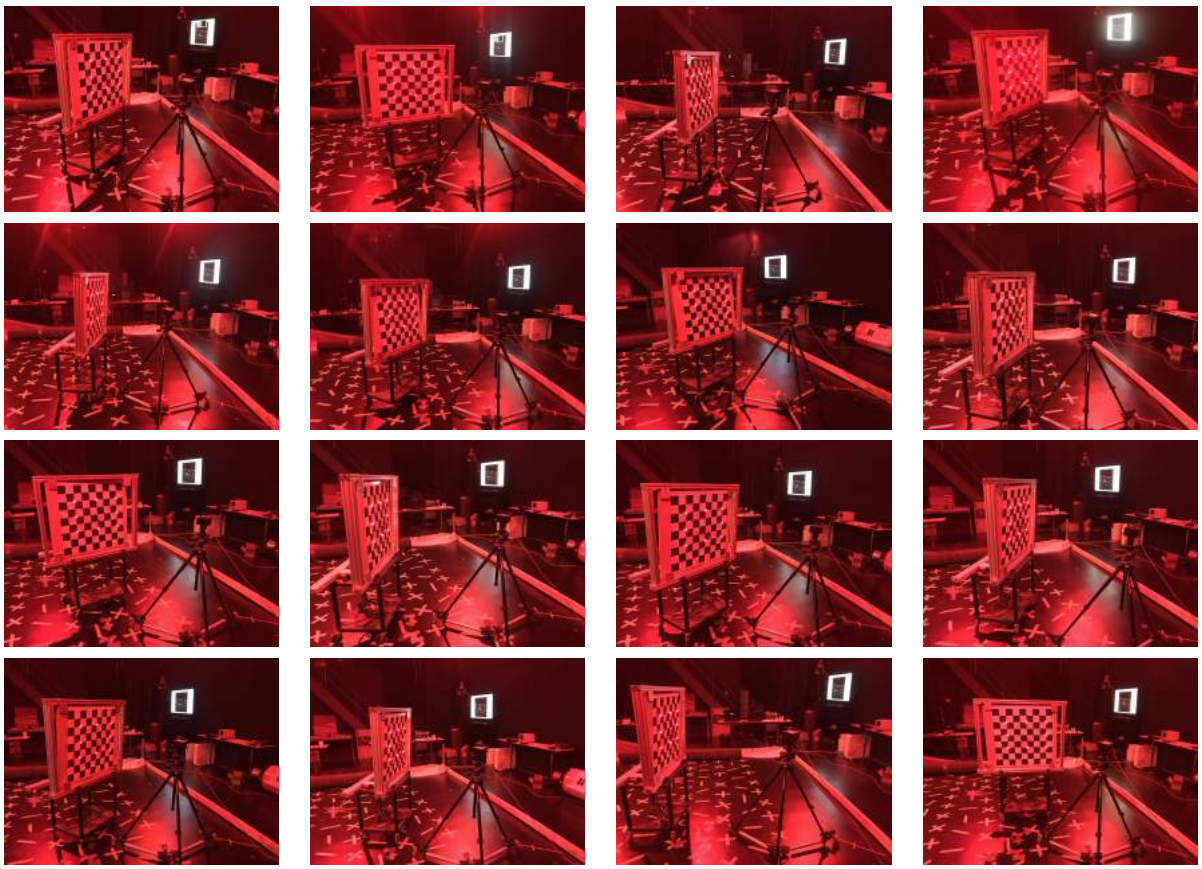

Figure 6.26: Physical alignment of the board with respect to the camera corresponding to each frame in Figure 6.25. The frames are numbered successively starting from the top left frame being numbered as zero.

CRP Vector		
Frame Number	Nonlinear Optimization Values	Wong's Optimization Values
1	$\begin{bmatrix} 0.033359314 \\ 0.030623055 \\ 0.439167102 \end{bmatrix}$	$\begin{bmatrix} 0.033376798 \\ 0.031250795 \\ 0.439254485 \end{bmatrix}$
2	$\begin{bmatrix} -0.129586341 \\ -0.33100283 \\ 0.448308512 \end{bmatrix}$	$\begin{bmatrix} -0.129760678 \\ -0.332531783 \\ 0.448065431 \end{bmatrix}$
3	$\begin{bmatrix} 0.190927207 \\ 0.304283395 \\ 0.436713101 \end{bmatrix}$	$\begin{bmatrix} 0.191853845 \\ 0.306120499 \\ 0.436562647 \end{bmatrix}$
4	$\begin{bmatrix} 0.019914092 \\ 0.021830796 \\ 0.440923613 \end{bmatrix}$	$\begin{bmatrix} 0.018491696 \\ 0.02097715 \\ 0.441352708 \end{bmatrix}$
5	$\begin{bmatrix} 0.141211557 \\ 0.316286425 \\ 0.422454032 \end{bmatrix}$	$\begin{bmatrix} 0.143136108 \\ 0.317456364 \\ 0.422492507 \end{bmatrix}$
6	$\begin{bmatrix} 0.083032971 \\ 0.067534775 \\ 0.434984971 \end{bmatrix}$	$\begin{bmatrix} 0.082102162 \\ 0.06823347 \\ 0.434701419 \end{bmatrix}$
7	$\begin{bmatrix} -0.006134483 \\ -0.192336612 \\ 0.435345539 \end{bmatrix}$	$\begin{bmatrix} -0.006629743 \\ -0.192633167 \\ 0.435323133 \end{bmatrix}$
8	$\begin{bmatrix} 0.095637129 \\ 0.200216239 \\ 0.428417084 \end{bmatrix}$	$\begin{bmatrix} 0.095040001 \\ 0.200213324 \\ 0.428381982 \end{bmatrix}$
9	$\begin{bmatrix} -0.099944555 \\ -0.26118559 \\ 0.449568092 \end{bmatrix}$	$\begin{bmatrix} -0.09978487 \\ -0.261609976 \\ 0.449506747 \end{bmatrix}$
10	$\begin{bmatrix} 0.117475901 \\ 0.218435049 \\ 0.424917738 \end{bmatrix}$	$\begin{bmatrix} 0.11300051 \\ 0.217150759 \\ 0.424542694 \end{bmatrix}$
11	$\begin{bmatrix} -0.079313182 \\ -0.063869603 \\ 0.445981023 \end{bmatrix}$	$\begin{bmatrix} -0.08056309 \\ -0.06242113 \\ 0.445402204 \end{bmatrix}$
12	$\begin{bmatrix} 0.022796146 \\ 0.152887307 \\ 0.436399133 \end{bmatrix}$	$\begin{bmatrix} 0.021964069 \\ 0.151579455 \\ 0.436808985 \end{bmatrix}$

Table 6.34: The CRPs corresponding to the first 12 well-conditioned frames for Dataset 4 is presented. The optimized values are shown along with the values from Wong's algorithm for comparison. Brown's distortion model is used here.

CRP Vector		
Frame Number	Nonlinear Optimization Values	Wong's Optimization Values
14	$\begin{bmatrix} 0.032022859 \\ 0.179180497 \\ 0.43518826 \end{bmatrix}$	$\begin{bmatrix} 0.031968669 \\ 0.178028717 \\ 0.435458152 \end{bmatrix}$
15	$\begin{bmatrix} 0.128422292 \\ 0.36601367 \\ 0.408803928 \end{bmatrix}$	$\begin{bmatrix} 0.130502712 \\ 0.367551211 \\ 0.409104262 \end{bmatrix}$
16	$\begin{bmatrix} -0.221209751 \\ -0.419195734 \\ 0.48566403 \end{bmatrix}$	$\begin{bmatrix} -0.220897028 \\ -0.421539677 \\ 0.485192994 \end{bmatrix}$

Table 6.35: The CRPs corresponding to the remaining well-conditioned frames for Dataset 4 is presented. The optimized values are shown along with the values from Wong's algorithm for comparison. Brown's distortion model is used here.

Translation Vector in inches		
Frame Number	Nonlinear Optimization Values	Wong's Optimization Values
1	$\begin{bmatrix} -10.99786072 \\ 0.403353682 \\ 35.66646035 \end{bmatrix}$	$\begin{bmatrix} -10.99677713 \\ 0.404245837 \\ 35.63909587 \end{bmatrix}$
2	$\begin{bmatrix} -11.87379323 \\ 1.614739633 \\ 39.86347337 \end{bmatrix}$	$\begin{bmatrix} -11.86311416 \\ 1.597673766 \\ 39.86327773 \end{bmatrix}$
3	$\begin{bmatrix} -17.31223252 \\ 6.748851412 \\ 28.0181802 \end{bmatrix}$	$\begin{bmatrix} -17.2908489 \\ 6.721404865 \\ 27.98294982 \end{bmatrix}$
4	$\begin{bmatrix} -7.66362449 \\ -2.84923245 \\ 39.36956872 \end{bmatrix}$	$\begin{bmatrix} -7.65553003 \\ -2.836260225 \\ 39.4208431 \end{bmatrix}$
5	$\begin{bmatrix} -15.96321435 \\ 5.517845396 \\ 29.42188065 \end{bmatrix}$	$\begin{bmatrix} -15.9551982 \\ 5.500277643 \\ 29.3993202 \end{bmatrix}$
6	$\begin{bmatrix} -20.42295585 \\ 11.02824689 \\ 43.0596597 \end{bmatrix}$	$\begin{bmatrix} -20.41911324 \\ 11.02135568 \\ 43.04748637 \end{bmatrix}$
7	$\begin{bmatrix} -11.29286787 \\ 1.381955751 \\ 42.69603972 \end{bmatrix}$	$\begin{bmatrix} -11.29249785 \\ 1.379405033 \\ 42.69596436 \end{bmatrix}$
8	$\begin{bmatrix} -17.40147332 \\ 6.745094455 \\ 26.97406904 \end{bmatrix}$	$\begin{bmatrix} -17.40117485 \\ 6.747586621 \\ 27.00773029 \end{bmatrix}$
9	$\begin{bmatrix} -11.81672734 \\ 2.191294174 \\ 49.27022371 \end{bmatrix}$	$\begin{bmatrix} -11.81142537 \\ 2.190245874 \\ 49.27707577 \end{bmatrix}$
10	$\begin{bmatrix} -22.04873174 \\ 12.13661277 \\ 36.59301094 \end{bmatrix}$	$\begin{bmatrix} -22.05620254 \\ 12.16218982 \\ 36.73773421 \end{bmatrix}$
11	$\begin{bmatrix} -20.31339757 \\ 11.1833679 \\ 40.52428869 \end{bmatrix}$	$\begin{bmatrix} -20.31402129 \\ 11.1769473 \\ 40.50245086 \end{bmatrix}$
12	$\begin{bmatrix} -7.341620153 \\ -2.565477139 \\ 41.27122477 \end{bmatrix}$	$\begin{bmatrix} -7.341720524 \\ -2.548400613 \\ 41.33868661 \end{bmatrix}$

Table 6.36: The Translation elements (in inches) corresponding to the first 12 well-conditioned frames for Dataset 4 is presented. The optimized values are shown along with the values from Wong's algorithm for comparison. Brown's distortion model is used here.

Translation Vector in inches		
Frame Number	Nonlinear Optimization Values	Wong's Optimization Values
14	$\begin{bmatrix} -5.072169309 \\ -5.135343787 \\ 39.03350354 \end{bmatrix}$	$\begin{bmatrix} -5.073582124 \\ -5.130562914 \\ 39.11159264 \end{bmatrix}$
15	$\begin{bmatrix} -21.96685025 \\ 12.78855735 \\ 39.51243335 \end{bmatrix}$	$\begin{bmatrix} -21.95876699 \\ 12.77293626 \\ 39.56517031 \end{bmatrix}$
16	$\begin{bmatrix} -6.173046371 \\ -3.235477819 \\ 51.24032763 \end{bmatrix}$	$\begin{bmatrix} -6.15542398 \\ -3.260943219 \\ 51.2514248 \end{bmatrix}$

Table 6.37: The Translation elements (in inches) corresponding to the remaining well-conditioned frames for Dataset 4 is presented. The optimized values are shown along with the values from Wong's algorithm for comparison. Brown's distortion model is used here.

As can be seen from the above tables, the extrinsics are very well estimated by Wong's algorithm. This reflects on the translations and CRPS of each frame relative to the first frame. This is calculated using Equation 6.1.

$$
\begin{aligned}
R_{b1b2} &= R_{cb1}R_{cb2} \\
\boldsymbol{t_{b1b2}} &= R_{cb1}(t_{cb2} - t_{cb1})
\end{aligned}
\tag{6.1}
$$

where R_{b1b2} and $\boldsymbol{t_{b1b2}}$ are the rotation matrix and translation vector from frame $b1$ to $b2$, $\boldsymbol{t_{b1b2}}$ is expressed in the $b1$ frame, R_{cb1} and $\boldsymbol{t_{cb1}}$ are the rotation matrix and translation vector from the camera frame to frame $b1$, $\boldsymbol{t_{cb1}}$ is expressed in the camera frame and R_{cb2} and $\boldsymbol{t_{cb2}}$ are the rotation matrix and translation vector from the camera frame to frame $b2$, $\boldsymbol{t_{cb2}}$ is expressed in the camera frame.

Using Equation 6.1, the first frame relative projections are computed using the extrinsic projections from both the Homography optimization algorithm and Wong's algorithm. The combined first frame projections corresponding to the Homography optimization algorithm are shown in Figure 6.27 and that corresponding to Wong's algorithm is shown in Figure 6.28.

The differences between the elements of the translation and CRP vectors of each frame with respect to the first frame as computed using the nonlinear least squares algorithm by Wong et al and Phasespace data are shown in Figures 6.29 and 6.30.

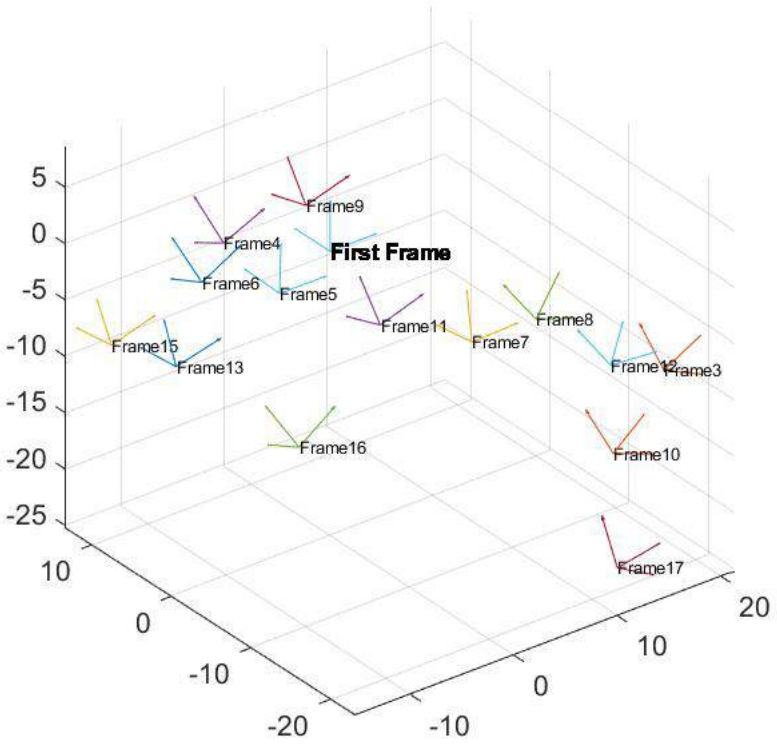

Figure 6.27: Combined Extrinsic Projections with respect to the first frame as computed from the Homography optimization algorithm for Dataset 4

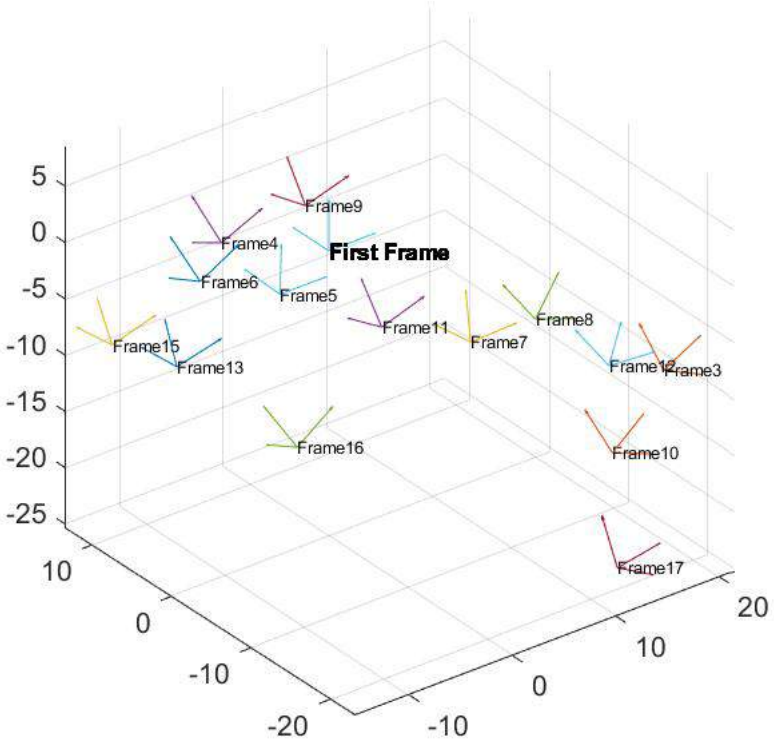

Figure 6.28: Combined Extrinsic Projections with respect to the first frame as computed from Wong's algorithm for Dataset 4

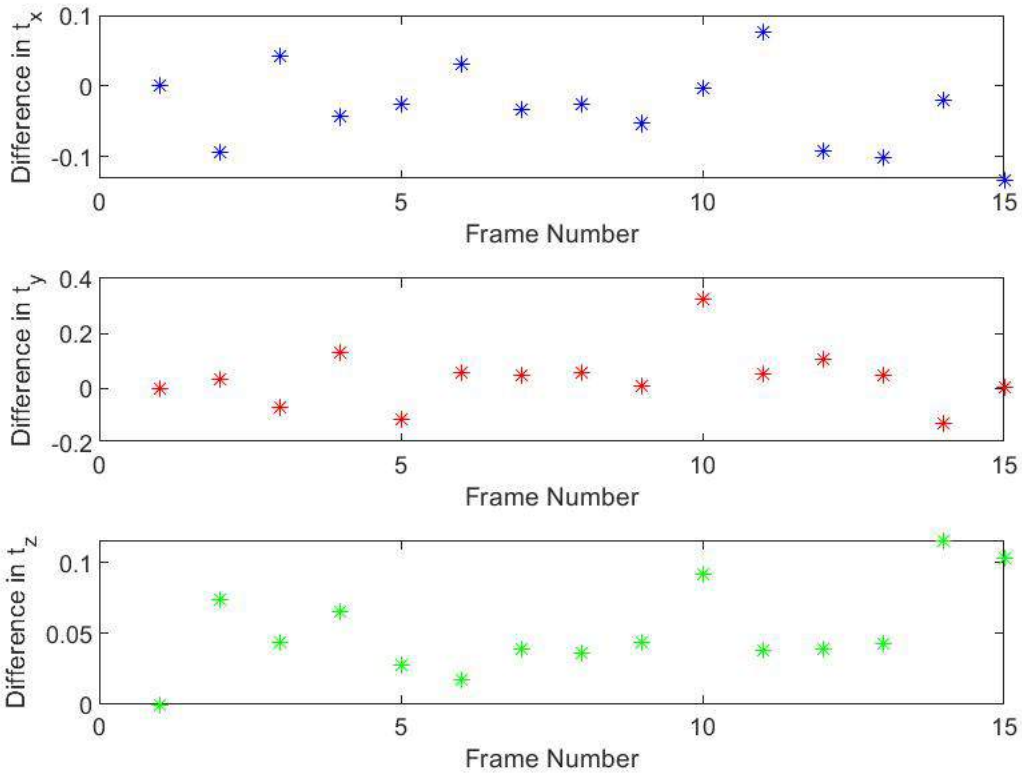

Figure 6.29: Difference between the translation elements of each frame with respect to the first frame, expressed in the first frame, as computed using Wong's algorithm and Homography optimization algorithm for Dataset 4

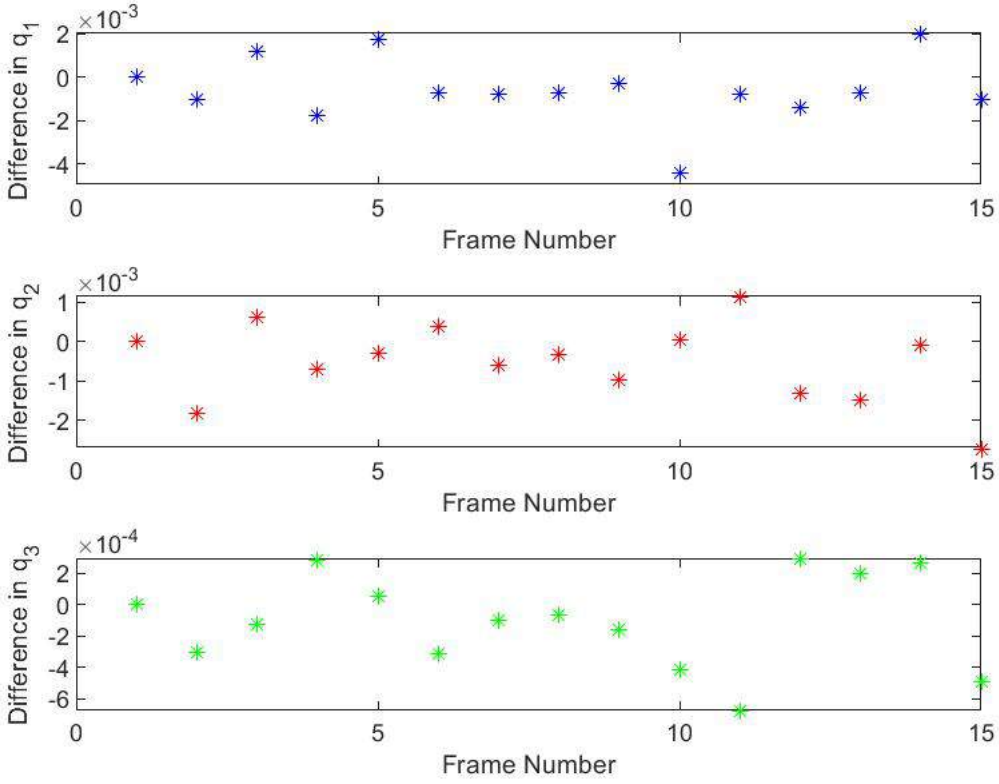

Figure 6.30: Difference between the CRP elements of each frame with respect to the first frame, expressed in the first frame, as computed using Wong's algorithm and Homography optimization algorithm for Dataset 4

The above results prove that Wong's algorithm can reliably estimate the extrinsics. Since the algorithm solves a nonlinear optimization problem for each frame separately to estimate the CRPs using a quadratic function in the CRPs, global optimization is guaranteed. This makes it suitable for real time relative navigation applications.

6.5 Intrinsic Parameter analysis

The various intrinsic parameter matrices computed from the above datasets are shown below. Tables 6.38 and 6.40 show the intrinsics and distortion coefficients as computed from the three datasets. Tables 6.39 and 6.41 show the uncertainty bounds in the intrinsics and distortion coefficients as computed from the three datasets.

Appendix A discusses the computation of the uncertainty bounds for the Combined Estimation approach with Brown's distortion model whereas Appendix C discussed the computation of the uncertainty bounds for the Combined Estimation approach with Geometric distortion model. It must be mentioned that since the standard deviation for the measurements in the each dataset was not available, the average of the standard deviations as discussed in Tables 3.4 and 3.5 in Chapter 3 are utilized. This may have contributed to some errors in the computation.

Similarly for the geometric distortion incorporated estimation.

It is generally expected that, for an ideal imager, the intrinsics and distortion coefficients would not vary significantly across multiple datasets since the intrinsics and distortion coefficients are properties of the imager. However, there is quite some variation in the intrinsic values. This points to the conclusion that both Brown's distortion model and Geometric distortion model (as defined here) are inadequate for modelling the distortions in the linear imager based camera and that a different distortion model is required in order to fully characterize and model this camera made of two linear imagers.

Dataset No.	Intrinsic Parameter Matrix A	Distortion Vector k
1	$\begin{bmatrix} 0.866387157 & -0.005218412 & 0.490403937 \\ 0 & 0.862603651 & 0.525072226 \\ 0 & 0 & 1.0000 \end{bmatrix}$	$\begin{bmatrix} 0.26381864 \\ -2.017524534 \\ 4.043408479 \\ -0.000291855 \\ -0.004889833 \end{bmatrix}$
2	$\begin{bmatrix} 1.033197839 & -0.013443215 & 0.580530016 \\ 0 & 1.049048926 & 0.486606025 \\ 0 & 0 & 1.0000 \end{bmatrix}$	$\begin{bmatrix} -0.26838847 \\ 0.407314863 \\ -0.30403853 \\ 0.0000723 \\ -0.012106003 \end{bmatrix}$
3	$\begin{bmatrix} 0.933614725 & -0.000748829 & 0.536693111 \\ 0 & 0.940498616 & 0.473476283 \\ 0 & 0 & 1.0000 \end{bmatrix}$	$\begin{bmatrix} -0.183942693 \\ 0.164119565 \\ -0.060467711 \\ 0.005690797 \\ -0.009347019 \end{bmatrix}$

Table 6.38: Intrinsic parameter matrices and Distortion Coefficient Vectors computed from datasets 1 to 3 using the combined estimation approach with Brown's Distortion Model

Dataset No.	Intrinsics Parameter Uncertainty	Distortion Coefficient Uncertainty
1	$\begin{bmatrix} 0.060687847 \\ 0.061242848 \\ 0.005525372 \\ 0.028292439 \\ 0.02716402 \end{bmatrix}$	$\begin{bmatrix} 0.418047257 \\ 2.697456412 \\ 5.264047693 \\ 0.013981611 \\ 0.00956818 \end{bmatrix}$
2	$\begin{bmatrix} 0.074166612 \\ 0.08240079 \\ 0.018045583 \\ 0.091293218 \\ 0.069922164 \end{bmatrix}$	$\begin{bmatrix} 0.220330454 \\ 1.170368469 \\ 1.916351421 \\ 0.018345758 \\ 0.012122195 \end{bmatrix}$
3	$\begin{bmatrix} 0.168289227 \\ 0.190832277 \\ 0.026920961 \\ 0.160988539 \\ 0.121934432 \end{bmatrix}$	$\begin{bmatrix} 0.301480745 \\ 1.51767908 \\ 2.313373459 \\ 0.035025965 \\ 0.020629391 \end{bmatrix}$

Table 6.39: Intrinsic parameter matrices and Distortion Coefficient Vectors computed from datasets 1 to 3 using the combined estimation approach with Brown's Distortion model

Dataset No.	Intrinsic Parameter Matrix A	Distortion Vector k_x	Distortion Vector k_y
1	$\begin{bmatrix} 1.0963 & -0.0048 & 0.4998 \\ 0 & 0.9102 & 0.5250 \\ 0 & 0 & 1.0000 \end{bmatrix}$	$\begin{bmatrix} 140.4243 \\ 1.6521 \\ 170.0546 \end{bmatrix}$	$\begin{bmatrix} -3.0629 \\ 0.1170 \\ -3.2673 \end{bmatrix}$
2	$\begin{bmatrix} 1.1027 & 0.0017 & 0.8055 \\ 0 & 1.207 & 0.5250 \\ 0 & 0 & 1.0000 \end{bmatrix}$	$\begin{bmatrix} 0.5988 \\ -0.1406 \\ 0.9125 \end{bmatrix}$	$\begin{bmatrix} 3.1325 \\ -0.0091 \\ 3.6413 \end{bmatrix}$
3	$\begin{bmatrix} 1.0581 & 0.0028 & 0.7718 \\ 0 & 1.1466 & 0.4882 \\ 0 & 0 & 1.0000 \end{bmatrix}$	$\begin{bmatrix} 0.2670 \\ -0.0905 \\ 0.5121 \end{bmatrix}$	$\begin{bmatrix} 3.6099 \\ -0.0433 \\ 4.2016 \end{bmatrix}$

Table 6.40: Intrinsic parameter matrices and Distortion Coefficient Vectors computed from datasets 1 to 3 using the combined estimation approach with Geometric Distortion Model

Dataset No.	Intrinsics Parameter Uncertainty	Uncertainty in k_x	Uncertainty in k_y
1	$\begin{bmatrix} 2.020131878 \\ 0.04794347 \\ 0.005723225 \\ 0.022404945 \\ 0.025610263 \end{bmatrix}$	$\begin{bmatrix} 1636.928306 \\ 16.96154426 \\ 2293.286971 \end{bmatrix}$	$\begin{bmatrix} 2293.286971 \\ 12.83852394 \\ 0.252974375 \end{bmatrix}$
2	$\begin{bmatrix} 0.128345809 \\ 0.151502376 \\ 0.02181624 \\ 0.081149127 \\ 0.077461218 \end{bmatrix}$	$\begin{bmatrix} 1.681538998 \\ 0.252611835 \\ 1.983449448 \end{bmatrix}$	$\begin{bmatrix} 1.983449448 \\ 6.781770652 \\ 0.371800737 \end{bmatrix}$
3	$\begin{bmatrix} 0.212716701 \\ 0.286222168 \\ 0.040492438 \\ 0.160116505 \\ 0.087860199 \end{bmatrix}$	$\begin{bmatrix} 1.793141866 \\ 0.29600319 \\ 2.164310509 \end{bmatrix}$	$\begin{bmatrix} 2.164310509 \\ 10.01248092 \\ 0.482133905 \end{bmatrix}$

Table 6.41: Intrinsic parameter matrices and Distortion Coefficient Vectors computed from datasets 1 to 3 using the combined estimation approach with Geometric Distortion Model

7. CONCLUSIONS AND FUTURE WORK

The Phasespace Motion Capture camera was considered for investigating the viability of two existing distortion models, namely Brown's distortion model and the Geometric distortion model, on linear imager cameras. To establish the credibility of the author's implementation of the non-linear Homography optimization algorithm two reference datasets were considered, the Bouguet Toolbox dataset and Zhang's dataset. The Homography optimization was carried out using both distortion models and the results were verified with the known results of the reference datasets. The Homography optimization algorithm was then tested on three datasets acquired from the Phasespace camera with the two distortion models employed one after the other. Although justifiable extrinsics were obtained for all three datasets, the intrinsics and the distortion parameters were found to vary across the datasets. This is contrary to the expectation that the intrinsics and distortion coefficients must remain the same throughout multiple datasets acquired by the same camera. As a result, both distortion models were deemed inadequate to represent the distortion effects in the Phasespace camera's imager. In addition, a nonlinear optimization algorithm for relative pose estimation proposed by Wong et al [3] was presented with the motive of employing this algorithm for real time relative navigation using the Phasespace camera. It was tested with a dataset acquired from the Phasespace camera. The results were then compared with the results of the Homography optimization algorithm and were found to be verified.

As per the results of this research, the obvious direction to proceed in the future is the formulation of a dedicated distortion model for linear imager cameras that leverages the knowledge of cylindrical lens optics. The relaxation of some of the assumptions in the existing image distortion models can also lead to an acceptable distortion function. Once the distortion function is found and verified with test datasets, the Wong algorithm presented here can be employed for efficient real time relative pose estimation.

REFERENCES

[1] Z. Zhang, "A flexible new technique for camera calibration," *IEEE Transactions on pattern analysis and machine intelligence*, vol. 22, no. 11, pp. 1330–1334, 2000.

[2] "Phasespace vision camera." http://phasespace.com/vision-cameras.html. Accessed: 2018-04-13.

[3] X. I. Wong and M. Majji, "A structured light system for relative navigation applications," *IEEE Sensors Journal*, vol. 16, no. 17, pp. 6662–6679, 2016.

[4] L. Ma, Y. Chen, and K. L. Moore, "A family of simplified geometric distortion models for camera calibration," *arXiv preprint cs/0308003*, 2003.

[5] A. A. Magill, "Variation in distortion with magnification," *JOSA*, vol. 45, no. 3, pp. 148–152, 1955.

[6] A. Cox, *Optics, the technique of definition*. Focal Press, 1945.

[7] C. B. Duane, "Close-range camera calibration," *Photogramm. Eng*, vol. 37, no. 8, pp. 855–866, 1971.

[8] J. Kenefick, "Ultra-precise analytical stereotriangulation for structural measurements," in *Presented paper on Symposium on Close-Range Photogrammetry, Illinois*, 1971.

[9] J. Heikkila and O. Silven, "A four-step camera calibration procedure with implicit image correction," in *cvpr*, p. 1106, IEEE, 1997.

[10] R. Tsai, "A versatile camera calibration technique for high-accuracy 3d machine vision metrology using off-the-shelf tv cameras and lenses," *IEEE Journal on Robotics and Automation*, vol. 3, no. 4, pp. 323–344, 1987.

[11] Z. Zhang, "Microsoft kinect sensor and its effect," *IEEE multimedia*, vol. 19, no. 2, pp. 4–10, 2012.

[12] S. Olufs and M. Vincze, "A simple inexpensive interface for robots using the nintendo wii controller," in *Intelligent Robots and Systems, 2009. IROS 2009. IEEE/RSJ International Conference on*, pp. 473–479, IEEE, 2009.

[13] M. K. Dobrzynski, R. Pericet-Camara, and D. Floreano, "Vision tapeâĂŤa flexible compound vision sensor for motion detection and proximity estimation," *IEEE Sensors Journal*, vol. 12, no. 5, pp. 1131–1139, 2012.

[14] M. Placer and S. Kovačič, "Enhancing indoor inertial pedestrian navigation using a shoe-worn marker," *Sensors*, vol. 13, no. 8, pp. 9836–9859, 2013.

[15] T. N. Hung and Y. S. Suh, "Inertial sensor-based two feet motion tracking for gait analysis," *Sensors*, vol. 13, no. 5, pp. 5614–5629, 2013.

[16] T. N. Do and Y. S. Suh, "Gait analysis using floor markers and inertial sensors," *Sensors*, vol. 12, no. 2, pp. 1594–1611, 2012.

[17] J. Valasek, K. Gunnam, J. Kimmett, J. L. Junkins, D. Hughes, and M. D. Tandale, "Vision-based sensor and navigation system for autonomous air refueling," *Journal of Guidance, Control, and Dynamics*, vol. 28, no. 5, pp. 979–989, 2005.

[18] A. Fosbury and J. Crassidis, "Relative navigation of air vehicles," *Journal of Guidance, Control, and Dynamics*, vol. 31, no. 4, pp. 824–834, 2008.

[19] S.-G. Kim, J. L. Crassidis, Y. Cheng, A. M. Fosbury, and J. L. Junkins, "Kalman filtering for relative spacecraft attitude and position estimation," *Journal of Guidance, Control, and Dynamics*, vol. 30, no. 1, pp. 133–143, 2007.

[20] O. De Silva, G. K. Mann, and R. G. Gosine, "An ultrasonic and vision-based relative positioning sensor for multirobot localization," *IEEE Sensors Journal*, vol. 15, no. 3, pp. 1716–1726, 2015.

[21] C. F. Olson, L. H. Matthies, J. R. Wright, R. Li, and K. Di, "Visual terrain mapping for mars exploration," *Computer Vision and Image Understanding*, vol. 105, no. 1, pp. 73–85, 2007.

[22] N. Trawny, A. I. Mourikis, S. I. Roumeliotis, A. E. Johnson, and J. F. Montgomery, "Vision-aided inertial navigation for pin-point landing using observations of mapped landmarks," *Journal of Field Robotics*, vol. 24, no. 5, pp. 357–378, 2007.

[23] M. Majji, J. Davis, J. Doebbler, J. Junkins, B. Macomber, M. Vavrina, and J. Vian, "Terrain mapping and landing operations using vision based navigation systems," in *AIAA Guidance, Navigation, and Control Conference*, p. 6581, 2011.

[24] K. K. Gunnam, D. C. Hughes, J. L. Junkins, and N. Kehtarnavaz, "A vision-based dsp embedded navigation sensor," *IEEE Sensors Journal*, vol. 2, no. 5, pp. 428–442, 2002.

[25] J. L. Junkins, D. Hughes, and H. Schaub, "Noncontact position and orientation measurement system and method," July 24 2001. US Patent 6,266,142.

[26] J. Shan and X. Wang, "Experimental study on mobile robot navigation using stereo vision," in *Robotics and Biomimetics (ROBIO), 2013 IEEE International Conference on*, pp. 1958–1965, IEEE, 2013.

[27] J. L. Crassidis and J. L. Junkins, *Optimal estimation of dynamic systems*. Chapman and Hall/CRC, 2011.

[28] J. J. Moré, "The levenberg-marquardt algorithm: implementation and theory," in *Numerical analysis*, pp. 105–116, Springer, 1978.

[29] "Bouguet camera calibration toolbox." http://www.vision.caltech.edu/bouguetj/calib_doc/. Accessed: 2018-11-30.

APPENDIX A

COMBINED DISTORTION INCORPORATED ESTIMATION PROCEDURE

This section describes the development of the combined estimation approach for the estimation of the intrinsics and extrinsics, along with the distortion coefficients.

We know that

$$\boldsymbol{p_i^C} = R_j \boldsymbol{p_i^W} + \boldsymbol{t_j} \tag{A.1}$$

where $\boldsymbol{p_i^W} = \begin{bmatrix} x_i^W & y_i^W & z_i^W \end{bmatrix}^T$ is the inertial frame coordinate of the ith beacon, $\boldsymbol{p_i^C} = \begin{bmatrix} x_i^C & y_i^C & z_i^C \end{bmatrix}^T$ is the 3D camera frame coordinate of $\boldsymbol{p_i^W}$, the rotation matrix and translation vector for the jth frame are written as $R_j = \begin{bmatrix} r_{11} & r_{12} & r_{13} \\ r_{21} & r_{22} & r_{23} \\ r_{31} & r_{32} & r_{33} \end{bmatrix}$ and $\boldsymbol{t_j} = \begin{bmatrix} t_1 \\ t_2 \\ t_3 \end{bmatrix}$

The undistorted normalised camera frame coordinates $\begin{bmatrix} x_u & y_u \end{bmatrix}^T$ are obtained by normalising $\boldsymbol{p_i^C}$ by z_i^C. We thus obtain the relations

$$\begin{aligned} x_u &= \frac{x_i^C}{z_i^c} \\ y_u &= \frac{y_i^C}{z_i^C} \end{aligned} \tag{A.2}$$

In terms of the elements of the rotation matrix and translation vector, x_u and y_u can be described as follows.

$$\begin{aligned} x_u &= \frac{r_{11}x_i^W + r_{12}y_i^W + t_1}{r_{31}x_i^W + r_{32}y_i^W + t_3} \\ y_u &= \frac{r_{21}x_i^W + r_{22}y_i^W + t_2}{r_{31}x_i^W + r_{32}y_i^W + t_3} \end{aligned} \tag{A.3}$$

Using Brown's distortion model, the distorted normalised camera space coordinates can be computed based on the estimate of the distortion coefficients $\hat{\boldsymbol{k}} = \begin{bmatrix} k_1 & k_2 & k_3 & p_1 & p_2 \end{bmatrix}^T$.

$$\begin{aligned} x_d &= x_u + x_u(k_1 r^2 + k_2 r^4 + ...) + (p_1(r^2 + 2x_u^2) + 2p_2 x_u y_u)(1 + p_3 r^2 + p_4 r^4 + ...) \\ y_d &= y_u + y_u(k_1 r^2 + k_2 r^4 + ...) + (2p_1 x_u y_d + u_2(r^2 + 2y_u^2))(1 + p_3 r^2 + p_4 r^4 + ...) \end{aligned} \tag{A.4}$$

Here, $r^2 = x_u^2 + y_u^2$.

The distorted image plane coordinates $\begin{bmatrix} x_d & y_d \end{bmatrix}^T$ are then obtained using the intrinsic camera matrix $A = \begin{bmatrix} \alpha & c & u_0 \\ 0 & \beta & v_0 \\ 0 & 0 & 1 \end{bmatrix}$.

Here, α and β are the focal lengths in the directions of the two basis vectors of the image plane, c is the skew coefficient and $\begin{bmatrix} u_0 & v_0 \end{bmatrix}^T$ is the principal offset.

The distorted image plane coordinates are computed as follows.

$$\begin{bmatrix} u_d \\ v_d \\ 1 \end{bmatrix} = A \begin{bmatrix} x_d \\ y_d \\ 1 \end{bmatrix} \tag{A.5}$$

The estimated distorted image plane coordinates of the ith beacon coordinate in the jth frame $\hat{\boldsymbol{m}}_{\boldsymbol{ij}} = \begin{bmatrix} u_d & v_d \end{bmatrix}$ are computed and the $2mn$ equations are then stacked to create a vector $\hat{\boldsymbol{m}}$, where m is the number of beacons and n is the number of frames.

Then, a nonlinear least squares formulation is employed to estimate the $6n + 10$ parameters (10 intrinsic parameters, including the distortion coefficients and $6n$ extrinsic parameters must be estimated, given that the rotation matrix is parameterized in terms of the CRPs).

The nonlinear least squares is implemented as the Levenberg Marquardt [28] algorithm and is carried out using the $lsqnonlin$ function in MatLab. The formal problem statement is written as follows.

$$min_{\boldsymbol{x}} \boldsymbol{e}^T W \boldsymbol{e} + \lambda \Delta \boldsymbol{x}^T W_y \Delta \boldsymbol{x} \tag{A.6}$$

where $\boldsymbol{e} = \tilde{\boldsymbol{m}} - \hat{\boldsymbol{m}}$, W is a weight matrix taken as $I_{2mn \times 2mn}$, W_y is a weight matrix taken as $I_{6n+10 \times 6n+10}$, $\tilde{\boldsymbol{m}}$ is the vector of the measured image plane coordinates, stacked in a similar manner to $\hat{\boldsymbol{m}}$ and $\boldsymbol{x} = \begin{bmatrix} \boldsymbol{x_{int}} & \boldsymbol{x_{ext}} \end{bmatrix}^T$ is the vector of parameters to estimate, $\boldsymbol{x_{int}} = \begin{bmatrix} \alpha & \beta & c & u_0 & v_0 & k_1 & k_2 & k_3 & p_1 & p_2 \end{bmatrix}^T$ and $\boldsymbol{x_{ext}} = \begin{bmatrix} q_{1i} & q_{2i} & q_{3i} & t_{1i} & t_{2i} & t_{3i} \end{bmatrix}^T$
$i = 1, 2, 3, 4.....n$

The initial guess for the parameters is taken to be the estimated intrinsics and extrinsics from the Homography algorithm in Zhang[1], with the distortion coefficients initialized as zeros. The differential correction for the parameters is given by

$$\Delta \boldsymbol{x} = (H^T W H + \lambda W_y)^{-1} H^T W \boldsymbol{e} \tag{A.7}$$

where $H = \frac{\partial \boldsymbol{f}}{\partial \boldsymbol{x}}_{\boldsymbol{x_c}}$ is the Jacobian matrix evaluated at the current estimate of the parameters
$H \in I\!R^{2mn \times (6n+10)}$

Convergence is said to be achieved when the change in the cost function J for successive iterations is less than 10^{-6}. This statement can be written mathematically as

$$\left| \frac{J_{k+1} - J_k}{J_{k+1}} \right| < 10^{-6} \tag{A.8}$$

where $J_k = \boldsymbol{e_k}^T W \boldsymbol{e_k} + \lambda \Delta \boldsymbol{x_k}^T W_y \Delta \boldsymbol{x_k}$

Given the standard deviation of the measured image plane coordinates, the covariance matrix for the measurement error vector R_y can be constructed. This covariance matrix can be utilized to compute the parameter error covariance. Starting from Equation A.7, the steps outlined by Equation A.9 can be employed to compute the state error covariance.

$$
\begin{aligned}
\delta\boldsymbol{x}\delta\boldsymbol{x}^T &= (H^TWH + \lambda W_y)^{-1}H^TW\delta\boldsymbol{y}\delta\boldsymbol{y}^TW^TH(H^TWH + \lambda W_y)^{-T} \\
E[\delta\boldsymbol{x}\delta\boldsymbol{x}^T] &= E[(H^TWH + \lambda W_y)^{-1}H^TW\delta\boldsymbol{y}\delta\boldsymbol{y}^TW^TH(H^TWH + \lambda W_y)^{-T}] \\
E[\delta\boldsymbol{x}\delta\boldsymbol{x}^T] &= (H^TWH + \lambda W_y)^{-1}H^TWE[\delta\boldsymbol{y}\delta\boldsymbol{y}^T]W^TH(H^TWH + \lambda W_y)^{-T} \\
E[\delta\boldsymbol{x}\delta\boldsymbol{x}^T] &= (H^TWH + \lambda W_y)^{-1}H^TWR_yW^TH(H^TWH + \lambda W_y)^{-T}
\end{aligned}
\tag{A.9}
$$

Here, H is the Jacoban Matrix computed at the converged states, W is the weighting matrix which is taken as $I^{2mn\times 2mn}$, m being the number of beacons and n being the number of well conditioned frames.

However, since λ is not readily available, the Gauss-Newton equivalent of the expression for $E[\delta\boldsymbol{x}\delta\boldsymbol{x}^T]$ is used which is

$$
E[\delta\boldsymbol{x}\delta\boldsymbol{x}^T] = (H^TWH)^{-1}H^TWR_yW^TH(H^TWH)^{-T}
$$

No significant error will be incurred with the above assumption assuming that λ is sufficiently small. Using $E[\delta\boldsymbol{x}\delta\boldsymbol{x}^T]$ the uncertainty bounds on each parameter can be estimated as $\sigma_{x,i} = 3\sqrt{R_{ii}}$. In the first 3 experimental datasets, the uncertainty bounds on the intrinsic parameters are computed using the average of the measured standard deviations for each beacon from Tables 3.4 and 3.5.

The various partials involved in the computation of the Jacobian Matrix at an estimate of the parameters are shown below.

We first look at the computation of the Jacobian with respect to the intrinsics and distortion coefficients.

$$
\begin{aligned}
\frac{\partial u_d}{\partial \alpha} &= x_d \\
\frac{\partial u_d}{\partial \beta} &= 0 \\
\frac{\partial u_d}{\partial c} &= y_d \\
\frac{\partial u_d}{\partial u_0} &= 1 \\
\frac{\partial u_d}{\partial v_0} &= 0
\end{aligned}
\tag{A.10}
$$

$$
\begin{aligned}
\frac{\partial v_d}{\partial \alpha} &= 0 \\
\frac{\partial v_d}{\partial \beta} &= y_d \\
\frac{\partial v_d}{\partial c} &= 0 \\
\frac{\partial v_d}{\partial u_0} &= 0 \\
\frac{\partial v_d}{\partial v_0} &= 1
\end{aligned}
\tag{A.11}
$$

$$
\begin{aligned}
\frac{\partial u_d}{\partial k_1} &= \alpha \frac{\partial x_d}{\partial k_1} + c \frac{\partial y_d}{\partial k_1} \\
\frac{\partial u_d}{\partial k_2} &= \alpha \frac{\partial x_d}{\partial k_2} + c \frac{\partial y_d}{\partial k_2} \\
\frac{\partial u_d}{\partial k_3} &= \alpha \frac{\partial x_d}{\partial k_3} + c \frac{\partial y_d}{\partial k_3} \\
\frac{\partial u_d}{\partial p_1} &= \alpha \frac{\partial x_d}{\partial p_1} + c \frac{\partial y_d}{\partial p_1} \\
\frac{\partial u_d}{\partial p_2} &= \alpha \frac{\partial x_d}{\partial p_2} + c \frac{\partial y_d}{\partial p_2}
\end{aligned}
\tag{A.12}
$$

$$
\begin{aligned}
\frac{\partial v_d}{\partial k_1} &= \beta \frac{\partial y_d}{\partial k_1} \\
\frac{\partial v_d}{\partial k_2} &= \beta \frac{\partial y_d}{\partial k_2} \\
\frac{\partial v_d}{\partial k_3} &= \beta \frac{\partial y_d}{\partial k_3} \\
\frac{\partial v_d}{\partial p_1} &= \beta \frac{\partial y_d}{\partial p_1} \\
\frac{\partial v_d}{\partial p_2} &= \beta \frac{\partial y_d}{\partial p_2}
\end{aligned}
\tag{A.13}
$$

The partials of x_d and y_d with respect to the distortion coefficients can be computed using Equation A.4.

$$
\begin{aligned}
\frac{\partial x_d}{\partial k_1} &= x_u r^2 \\
\frac{\partial x_d}{\partial k_2} &= x_u r^4 \\
\frac{\partial x_d}{\partial k_3} &= x_u r^6 \\
\frac{\partial x_d}{\partial p_1} &= r^2 + 2x_u^2 \\
\frac{\partial x_d}{\partial p_2} &= 2x_u y_u
\end{aligned}
\tag{A.14}
$$

$$
\begin{aligned}
\frac{\partial y_d}{\partial k_1} &= y_u r^2 \\
\frac{\partial y_d}{\partial k_2} &= y_u r^4 \\
\frac{\partial y_d}{\partial k_3} &= y_u r^6 \\
\frac{\partial y_d}{\partial p_1} &= 2x_u y_u \\
\frac{\partial y_d}{\partial p_2} &= r^2 + 2y_u^2
\end{aligned}
\tag{A.15}
$$

These can be plugged back in to the Equations A.12 and A.13.

$$\begin{aligned}
\frac{\partial u_d}{\partial k_1} &= \alpha x_u r^2 + c y_u r^2 \\
\frac{\partial u_d}{\partial k_2} &= \alpha x_u r^4 + c y_u r^4 \\
\frac{\partial u_d}{\partial k_3} &= \alpha x_u r^6 + c y_u r^6 \\
\frac{\partial u_d}{\partial p_1} &= \alpha(r^2 + 2x_u^2) + c(2x_u y_u) \\
\frac{\partial u_d}{\partial p_2} &= \alpha(2x_u y_u) + c(r^2 + 2y_u^2)
\end{aligned} \tag{A.16}$$

$$\begin{aligned}
\frac{\partial v_d}{\partial k_1} &= \beta y_u r^2 \\
\frac{\partial v_d}{\partial k_2} &= \beta y_u r^4 \\
\frac{\partial v_d}{\partial k_3} &= \beta y_u r^6 \\
\frac{\partial v_d}{\partial p_1} &= \beta(2x_u y_u) \\
\frac{\partial v_d}{\partial p_1} &= \beta(r^2 + 2y_u^2)
\end{aligned} \tag{A.17}$$

Now, we look at the computation of the Jacobian with respect to the extrinsics which is slightly more involved.

$$\begin{aligned}
\frac{\partial u_d}{\partial q_1} &= \alpha \frac{\partial x_d}{\partial q_1} + c \frac{\partial y_d}{\partial q_1} \\
\frac{\partial u_d}{\partial q_2} &= \alpha \frac{\partial x_d}{\partial q_2} + c \frac{\partial y_d}{\partial q_2} \\
\frac{\partial u_d}{\partial q_3} &= \alpha \frac{\partial x_d}{\partial q_3} + c \frac{\partial y_d}{\partial q_3}
\end{aligned} \tag{A.18}$$

$$\begin{aligned}
\frac{\partial v_d}{\partial q_1} &= \beta \frac{\partial y_d}{\partial q_1} \\
\frac{\partial v_d}{\partial q_2} &= \beta \frac{\partial y_d}{\partial q_2} \\
\frac{\partial v_d}{\partial q_3} &= \beta \frac{\partial y_d}{\partial q_3}
\end{aligned} \tag{A.19}$$

Similarly the partials with respect to the translation vector elements can also be computed.

$$\begin{aligned}
\frac{\partial u_d}{\partial t_1} &= \alpha \frac{\partial x_d}{\partial t_1} + c \frac{\partial y_d}{\partial t_1} \\
\frac{\partial u_d}{\partial t_2} &= \alpha \frac{\partial x_d}{\partial t_2} + c \frac{\partial y_d}{\partial t_2} \\
\frac{\partial u_d}{\partial t_3} &= \alpha \frac{\partial x_d}{\partial t_3} + c \frac{\partial y_d}{\partial t_3}
\end{aligned} \tag{A.20}$$

$$\begin{aligned}
\frac{\partial v_d}{\partial t_1} &= \beta \frac{\partial y_d}{\partial t_1} \\
\frac{\partial v_d}{\partial t_2} &= \beta \frac{\partial y_d}{\partial t_2} \\
\frac{\partial v_d}{\partial t_3} &= \beta \frac{\partial y_d}{\partial t_3}
\end{aligned} \tag{A.21}$$

Since, x_d and y_d are implicit functions of $\boldsymbol{q}$ and $\boldsymbol{t}$ through x_u and y_u, first the partials with respect to x_u and y_u must be computed. This can be done using the Equation A.4.

$$
\begin{aligned}
\frac{\partial x_d}{\partial x_u} &= 1 + k_1 r^2 + k_2 r^4 + k_3 r^6 + x_u(2k_1 r + 4k_2 r^3 + 6k_3 r^5)\frac{\partial r}{\partial x_u} + p_1(2r\frac{\partial r}{\partial x_u} + 4x_u) + 2p_2 y_u \\
\frac{\partial x_d}{\partial y_u} &= x_u(2k_1 r + 4k_2 r^3 + 6k_3 r^5)\frac{\partial r}{\partial y_u} + p_1(2r\frac{\partial r}{\partial y_u} + 2p_2 x_u) \\
\frac{\partial y_d}{\partial x_u} &= y_u(2k_1 r + 4k_2 r^3 + 6k_3 r^5)\frac{\partial r}{\partial x_u} + p_2(2r\frac{\partial r}{\partial x_u} + 2p_1 y_u) \\
\frac{\partial y_d}{\partial y_u} &= 1 + k_1 r^2 + k_2 r^4 + k_3 r^6 + y_u(2k_1 r + 4k_2 r^3 + 6k_3 r^5)\frac{\partial r}{\partial y_u} + p_2(2r\frac{\partial r}{\partial y_u} + 4y_u) + 2p_1 x_u
\end{aligned}
\tag{A.22}
$$

The partials of r with respect to x_u and y_u can be computed using the relation $r^2 = x_u^2 + y_u^2$.

$$
\begin{aligned}
\frac{\partial r}{\partial x_u} &= \frac{x_u}{r} \\
\frac{\partial r}{\partial y_u} &= \frac{y_u}{r}
\end{aligned}
\tag{A.23}
$$

We now use the product rule for partial derivatives to compute the partials of x_d and y_d with respect to $\boldsymbol{q}$ and $\boldsymbol{t}$.

$$
\begin{aligned}
\frac{\partial x_d}{\partial q_1} &= \frac{\partial x_d}{\partial x_u}\frac{\partial x_u}{\partial q_1} + \frac{\partial x_d}{\partial y_u}\frac{\partial y_u}{\partial q_1} \\
\frac{\partial x_d}{\partial q_2} &= \frac{\partial x_d}{\partial x_u}\frac{\partial x_u}{\partial q_2} + \frac{\partial x_d}{\partial y_u}\frac{\partial y_u}{\partial q_2} \\
\frac{\partial x_d}{\partial q_3} &= \frac{\partial x_d}{\partial x_u}\frac{\partial x_u}{\partial q_3} + \frac{\partial x_d}{\partial y_u}\frac{\partial y_u}{\partial q_3} \\
\frac{\partial y_d}{\partial q_1} &= \frac{\partial y_d}{\partial x_u}\frac{\partial x_u}{\partial q_1} + \frac{\partial y_d}{\partial y_u}\frac{\partial y_u}{\partial q_1} \\
\frac{\partial y_d}{\partial q_2} &= \frac{\partial y_d}{\partial x_u}\frac{\partial x_u}{\partial q_2} + \frac{\partial y_d}{\partial y_u}\frac{\partial y_u}{\partial q_2} \\
\frac{\partial y_d}{\partial q_3} &= \frac{\partial y_d}{\partial x_u}\frac{\partial x_u}{\partial q_3} + \frac{\partial y_d}{\partial y_u}\frac{\partial y_u}{\partial q_3}
\end{aligned}
\tag{A.24}
$$

$$
\begin{aligned}
\frac{\partial x_d}{\partial t_1} &= \frac{\partial x_d}{\partial x_u}\frac{\partial x_u}{\partial t_1} + \frac{\partial x_d}{\partial y_u}\frac{\partial y_u}{\partial t_1} \\
\frac{\partial x_d}{\partial t_2} &= \frac{\partial x_d}{\partial x_u}\frac{\partial x_u}{\partial t_2} + \frac{\partial x_d}{\partial y_u}\frac{\partial y_u}{\partial t_2} \\
\frac{\partial x_d}{\partial t_3} &= \frac{\partial x_d}{\partial x_u}\frac{\partial x_u}{\partial q_3} + \frac{\partial x_d}{\partial y_u}\frac{\partial y_u}{\partial t_3} \\
\frac{\partial y_d}{\partial t_1} &= \frac{\partial y_d}{\partial x_u}\frac{\partial x_u}{\partial t_1} + \frac{\partial y_d}{\partial y_u}\frac{\partial y_u}{\partial t_1} \\
\frac{\partial y_d}{\partial t_2} &= \frac{\partial y_d}{\partial x_u}\frac{\partial x_u}{\partial t_2} + \frac{\partial y_d}{\partial y_u}\frac{\partial y_u}{\partial t_2} \\
\frac{\partial y_d}{\partial t_3} &= \frac{\partial y_d}{\partial x_u}\frac{\partial x_u}{\partial t_3} + \frac{\partial y_d}{\partial y_u}\frac{\partial y_u}{\partial t_3}
\end{aligned}
\tag{A.25}
$$

As per the Equation A.3, it can be seen that x_u and y_u are both implicit functions of the CRPs but explicit functions of the translations.

As a result, the explicit partial derivatives of x_u and y_u can be computed readily using the Equation A.3.

$$
\begin{aligned}
\frac{\partial x_u}{\partial t_1} &= \frac{1}{r_{31}x_W + r_{32}y_W + t_3} \\
\frac{\partial x_u}{\partial t_2} &= 0 \\
\frac{\partial x_u}{\partial t_3} &= -\frac{r_{11}x_W + r_{12}y_W + t_1}{(r_{31}x_W + r_{32}y_W + t_3)^2}
\end{aligned}
\tag{A.26}
$$

$$
\begin{aligned}
\frac{\partial y_u}{\partial t_1} &= 0 \\
\frac{\partial y_u}{\partial t_2} &= \frac{1}{r_{31}x_W + r_{32}y_W + t_3} \\
\frac{\partial y_u}{\partial t_3} &= -\frac{r_{21}x_W + r_{22}y_W + t_2}{(r_{31}x_W + r_{32}y_W + t_3)^2}
\end{aligned}
\tag{A.27}
$$

The computation of the partials of x_u and y_u with respect to the CRPs requires the parameterization of the rotation matrix R in terms of the CRPs. Keeping with the same variables as in

Equation A.3, the partials with respect to the CRPs are computed as follows.

$$\frac{\partial x_u}{\partial q_1} = -\frac{r_{11}x_W + r_{12}y_W + t_1}{(r_{31}x_W + r_{32}y_W + t_3)^2}\left(\frac{\partial r_{31}}{\partial q_1}x_w + \frac{\partial r_{32}}{\partial q_1}y_w\right) + \frac{1}{r_{31}x_W + r_{32}y_W + t_3}\left(\frac{\partial r_{11}}{\partial q_1}x_w + \frac{\partial r_{12}}{\partial q_1}y_w\right) \quad \text{(A.28)}$$

$$\frac{\partial x_u}{\partial q_2} = -\frac{r_{11}x_W + r_{12}y_W + t_1}{(r_{31}x_W + r_{32}y_W + t_3)^2}\left(\frac{\partial r_{31}}{\partial q_2}x_w + \frac{\partial r_{32}}{\partial q_2}y_w\right) + \frac{1}{r_{31}x_W + r_{32}y_W + t_3}\left(\frac{\partial r_{11}}{\partial q_2}x_w + \frac{\partial r_{12}}{\partial q_2}y_w\right) \quad \text{(A.29)}$$

$$\frac{\partial x_u}{\partial q_3} = -\frac{r_{11}x_W + r_{12}y_W + t_1}{(r_{31}x_W + r_{32}y_W + t_3)^2}\left(\frac{\partial r_{31}}{\partial q_3}x_w + \frac{\partial r_{32}}{\partial q_3}y_w\right) + \frac{1}{r_{31}x_W + r_{32}y_W + t_3}\left(\frac{\partial r_{11}}{\partial q_3}x_w + \frac{\partial r_{12}}{\partial q_3}y_w\right) \quad \text{(A.30)}$$

$$\frac{\partial y_u}{\partial q_1} = -\frac{r_{21}x_W + r_{22}y_W + t_2}{(r_{31}x_W + r_{32}y_W + t_3)^2}\left(\frac{\partial r_{31}}{\partial q_1}x_w + \frac{\partial r_{32}}{\partial q_1}y_w\right) + \frac{1}{r_{31}x_W + r_{32}y_W + t_3}\left(\frac{\partial r_{21}}{\partial q_1}x_w + \frac{\partial r_{22}}{\partial q_1}y_w\right) \quad \text{(A.31)}$$

$$\frac{\partial y_u}{\partial q_2} = -\frac{r_{21}x_W + r_{22}y_W + t_2}{(r_{31}x_W + r_{32}y_W + t_3)^2}\left(\frac{\partial r_{31}}{\partial q_2}x_w + \frac{\partial r_{32}}{\partial q_2}y_w\right) + \frac{1}{r_{31}x_W + r_{32}y_W + t_3}\left(\frac{\partial r_{21}}{\partial q_2}x_w + \frac{\partial r_{22}}{\partial q_2}y_w\right) \quad \text{(A.32)}$$

$$\frac{\partial y_u}{\partial q_3} = -\frac{r_{21}x_W + r_{22}y_W + t_2}{(r_{31}x_W + r_{32}y_W + t_3)^2}\left(\frac{\partial r_{31}}{\partial q_3}x_w + \frac{\partial r_{32}}{\partial q_3}y_w\right) + \frac{1}{r_{31}x_W + r_{32}y_W + t_3}\left(\frac{\partial r_{21}}{\partial q_3}x_w + \frac{\partial r_{22}}{\partial q_3}y_w\right) \quad \text{(A.33)}$$

The rotation matrix in terms of the CRPs is given below.

$$R = \frac{1}{1 + q_1^2 + q_2^2 + q_3^2}\begin{bmatrix} 1 + q_1^2 - q_2^2 - q_3^2 & 2(q_1q_2 + q_3) & 2(q_1q_3 - q_2) \\ 2(q_2q_1 - q_3) & 1 - q_1^2 + q_2^2 - q_3^2 & 2(q_2q_3 + q_1) \\ 2(q_3q_1 + q_2) & 2(q_2q_3 - q_1) & 1 - q_1^2 - q_2^2 + q_3^2 \end{bmatrix} \quad \text{(A.34)}$$

Now, the partials of the requisite rotation matrix elements with respect to the CRPs can be computed.

$$\begin{aligned}
\frac{\partial r_{11}}{\partial q_1} &= \frac{4q_1(q_2^2 + q_3^2)}{(1 + q_1^2 + q_2^2 + q_3^2)^2} \\
\frac{\partial r_{12}}{\partial q_1} &= \frac{2q_2(1 - q_1^2 + q_2^2 + q_3^2) - 4q_1q_3}{(1 + q_1^2 + q_2^2 + q_3^2)^2} \\
\frac{\partial r_{21}}{\partial q_1} &= \frac{2q_2(1 - q_1^2 + q_2^2 + q_3^2) + 4q_1q_3}{(1 + q_1^2 + q_2^2 + q_3^2)^2} \\
\frac{\partial r_{22}}{\partial q_1} &= -\frac{4q_1(1 + q_2^2)}{(1 + q_1^2 + q_2^2 + q_3^2)^2} \\
\frac{\partial r_{31}}{\partial q_1} &= \frac{2q_3(1 - q_1^2 + q_2^2 + q_3^2) - 4q_1q_2}{(1 + q_1^2 + q_2^2 + q_3^2)^2} \\
\frac{\partial r_{32}}{\partial q_1} &= \frac{-2(1 - q_1^2 + q_2^2 + q_3^2) - 4q_1q_2q_3}{(1 + q_1^2 + q_2^2 + q_3^2)^2}
\end{aligned} \quad \text{(A.35)}$$

$$
\begin{aligned}
\frac{\partial r_{11}}{\partial q_2} &= -\frac{4q_2(1+q_1^2)}{(1+q_1^2+q_2^2+q_3^2)^2} \\
\frac{\partial r_{12}}{\partial q_2} &= \frac{2q_1(1+q_1^2-q_2^2+q_3^2)-4q_2q_3}{(1+q_1^2+q_2^2+q_3^2)^2} \\
\frac{\partial r_{21}}{\partial q_2} &= \frac{2q_1(1+q_1^2-q_2^2+q_3^2)+4q_2q_3}{(1+q_1^2+q_2^2+q_3^2)^2} \\
\frac{\partial r_{22}}{\partial q_2} &= \frac{4q_2(q_1^2+q_3^2)}{(1+q_1^2+q_2^2+q_3^2)^2} \\
\frac{\partial r_{31}}{\partial q_2} &= \frac{2(1+q_1^2-q_2^2+q_3^2)-4q_1q_2q_3}{(1+q_1^2+q_2^2+q_3^2)^2} \\
\frac{\partial r_{32}}{\partial q_2} &= \frac{2q_3(1+q_1^2-q_2^2+q_3^2)+4q_1q_2}{(1+q_1^2+q_2^2+q_3^2)^2}
\end{aligned}
\tag{A.36}
$$

$$
\begin{aligned}
\frac{\partial r_{11}}{\partial q_3} &= -\frac{4q_3(1+q_1^2)}{(1+q_1^2+q_2^2+q_3^2)^2} \\
\frac{\partial r_{12}}{\partial q_3} &= \frac{2(1+q_1^2+q_2^2-q_3^2)-4q_1q_2q_3}{(1+q_1^2+q_2^2+q_3^2)^2} \\
\frac{\partial r_{21}}{\partial q_3} &= \frac{-2(1+q_1^2+q_2^2-q_3^2)-4q_1q_2q_3}{(1+q_1^2+q_2^2+q_3^2)^2} \\
\frac{\partial r_{22}}{\partial q_3} &= -\frac{4q_3(1+q_2^2)}{(1+q_1^2+q_2^2+q_3^2)^2} \\
\frac{\partial r_{31}}{\partial q_3} &= \frac{2q_1(1+q_1^2+q_2^2-q_3^2)-4q_2q_3}{(1+q_1^2+q_2^2+q_3^2)^2} \\
\frac{\partial r_{32}}{\partial q_3} &= \frac{2q_2(1+q_1^2+q_2^2-q_3^2)+4q_1q_3}{(1+q_1^2+q_2^2+q_3^2)^2}
\end{aligned}
\tag{A.37}
$$

We now have all the ingredients required to compute the full Jacobian Matrix H of the distorted image frame coordinates with respect to the intrinsics, distortion coefficients and the extrinsics.

The form of the H matrix can be described in the following manner.

$$
H = \begin{bmatrix} H_{int} & H_{ext} \end{bmatrix} \tag{A.38}
$$

where H_{int} is the portion of the Jacobian matrix strictly associated with the differential corrections in the intrinsics and the distortion coefficients, whereas H_{ext} is the portion of the Jacobian

matrix strictly associated with the differential corrections in the extrinsics.

As a result, $H_{int} \in IR^{2mn \times 10}$ and $H_{ext} \in IR^{2mn \times 6n}$.

$$H_{int} = \begin{bmatrix} \frac{\partial u_d^{11}}{\partial \alpha} & \frac{\partial u_d^{11}}{\partial \beta} & \frac{\partial u_d^{11}}{\partial c} & \frac{\partial u_d^{11}}{\partial u_0} & \frac{\partial u_d^{11}}{\partial v_0} & \frac{\partial u_d^{11}}{\partial k_1} & \frac{\partial u_d^{11}}{\partial k_2} & \frac{\partial u_d^{11}}{\partial k_3} & \frac{\partial u_d^{11}}{\partial p_1} & \frac{\partial u_d^{11}}{\partial p_2} \\ \frac{\partial v_d^{11}}{\partial \alpha} & \frac{\partial v_d^{11}}{\partial \beta} & \frac{\partial v_d^{11}}{\partial c} & \frac{\partial v_d^{11}}{\partial u_0} & \frac{\partial v_d^{11}}{\partial v_0} & \frac{\partial v_d^{11}}{\partial k_1} & \frac{\partial v_d^{11}}{\partial k_2} & \frac{\partial v_d^{11}}{\partial k_3} & \frac{\partial v_d^{11}}{\partial p_1} & \frac{\partial v_d^{11}}{\partial p_2} \\ \frac{\partial u_d^{12}}{\partial \alpha} & \frac{\partial u_d^{12}}{\partial \beta} & \frac{\partial u_d^{12}}{\partial c} & \frac{\partial u_d^{12}}{\partial u_0} & \frac{\partial u_d^{12}}{\partial v_0} & \frac{\partial u_d^{12}}{\partial k_1} & \frac{\partial u_d^{12}}{\partial k_2} & \frac{\partial u_d^{12}}{\partial k_3} & \frac{\partial u_d^{12}}{\partial p_1} & \frac{\partial u_d^{12}}{\partial p_2} \\ \frac{\partial v_d^{12}}{\partial \alpha} & \frac{\partial v_d^{12}}{\partial \beta} & \frac{\partial v_d^{12}}{\partial c} & \frac{\partial v_d^{12}}{\partial u_0} & \frac{\partial v_d^{12}}{\partial v_0} & \frac{\partial v_d^{12}}{\partial k_1} & \frac{\partial v_d^{12}}{\partial k_2} & \frac{\partial v_d^{12}}{\partial k_3} & \frac{\partial v_d^{12}}{\partial p_1} & \frac{\partial v_d^{12}}{\partial p_2} \\ \vdots & \vdots & \vdots & \vdots & \vdots & \vdots & \vdots & \vdots & \vdots & \vdots \\ \frac{\partial u_d^{1m}}{\partial \alpha} & \frac{\partial u_d^{1m}}{\partial \beta} & \frac{\partial u_d^{1m}}{\partial c} & \frac{\partial u_d^{1m}}{\partial u_0} & \frac{\partial u_d^{1m}}{\partial v_0} & \frac{\partial u_d^{1m}}{\partial k_1} & \frac{\partial u_d^{1m}}{\partial k_2} & \frac{\partial u_d^{1m}}{\partial k_3} & \frac{\partial u_d^{1m}}{\partial p_1} & \frac{\partial u_d^{1m}}{\partial p_2} \\ \frac{\partial v_d^{1m}}{\partial \alpha} & \frac{\partial v_d^{1m}}{\partial \beta} & \frac{\partial v_d^{1m}}{\partial c} & \frac{\partial v_d^{1m}}{\partial u_0} & \frac{\partial v_d^{1m}}{\partial v_0} & \frac{\partial v_d^{1m}}{\partial k_1} & \frac{\partial v_d^{1m}}{\partial k_2} & \frac{\partial v_d^{1m}}{\partial k_3} & \frac{\partial v_d^{1m}}{\partial p_1} & \frac{\partial v_d^{1m}}{\partial p_2} \\ \frac{\partial u_d^{21}}{\partial \alpha} & \frac{\partial u_d^{21}}{\partial \beta} & \frac{\partial u_d^{21}}{\partial c} & \frac{\partial u_d^{21}}{\partial u_0} & \frac{\partial u_d^{21}}{\partial v_0} & \frac{\partial u_d^{21}}{\partial k_1} & \frac{\partial u_d^{21}}{\partial k_2} & \frac{\partial u_d^{21}}{\partial k_3} & \frac{\partial u_d^{21}}{\partial p_1} & \frac{\partial u_d^{21}}{\partial p_2} \\ \frac{\partial v_d^{21}}{\partial \alpha} & \frac{\partial v_d^{21}}{\partial \beta} & \frac{\partial v_d^{21}}{\partial c} & \frac{\partial v_d^{21}}{\partial u_0} & \frac{\partial v_d^{21}}{\partial v_0} & \frac{\partial v_d^{21}}{\partial k_1} & \frac{\partial v_d^{21}}{\partial k_2} & \frac{\partial v_d^{21}}{\partial k_3} & \frac{\partial v_d^{21}}{\partial p_1} & \frac{\partial v_d^{21}}{\partial p_2} \\ \vdots & \vdots & \vdots & \vdots & \vdots & \vdots & \vdots & \vdots & \vdots & \vdots \\ \vdots & \vdots & \vdots & \vdots & \vdots & \vdots & \vdots & \vdots & \vdots & \vdots \\ \frac{\partial u_d^{nm}}{\partial \alpha} & \frac{\partial u_d^{nm}}{\partial \beta} & \frac{\partial u_d^{nm}}{\partial c} & \frac{\partial u_d^{nm}}{\partial u_0} & \frac{\partial u_d^{nm}}{\partial v_0} & \frac{\partial u_d^{nm}}{\partial k_1} & \frac{\partial u_d^{nm}}{\partial k_2} & \frac{\partial u_d^{nm}}{\partial k_3} & \frac{\partial u_d^{nm}}{\partial p_1} & \frac{\partial u_d^{nm}}{\partial p_2} \\ \frac{\partial v_d^{nm}}{\partial \alpha} & \frac{\partial v_d^{nm}}{\partial \beta} & \frac{\partial v_d^{nm}}{\partial c} & \frac{\partial v_d^{nm}}{\partial u_0} & \frac{\partial v_d^{nm}}{\partial v_0} & \frac{\partial v_d^{nm}}{\partial k_1} & \frac{\partial v_d^{nm}}{\partial k_2} & \frac{\partial v_d^{nm}}{\partial k_3} & \frac{\partial v_d^{nm}}{\partial p_1} & \frac{\partial v_d^{nm}}{\partial p_2} \end{bmatrix} \tag{A.39}$$

Here, n is the number of frames and m is the number of beacons.

$$H_{ext} \in IR^{2mn \times 6n}$$

H_{ext} has the following form.

$$H_{ext} = \begin{bmatrix}
\frac{\partial u_d^{11}}{\partial \boldsymbol{q_1}}^T & \frac{\partial u_d^{11}}{\partial \boldsymbol{t_1}}^T & 0 & \cdots & \cdots & \cdots & \cdots & \cdots & \cdots & 0 \\
\frac{\partial v_d^{11}}{\partial \boldsymbol{q_1}}^T & \frac{\partial v_d^{11}}{\partial \boldsymbol{t_1}}^T & 0 & \cdots & \cdots & \cdots & \cdots & \cdots & \cdots & 0 \\
\frac{\partial u_d^{12}}{\partial \boldsymbol{q_1}}^T & \frac{\partial u_d^{12}}{\partial \boldsymbol{t_1}}^T & 0 & \cdots & \cdots & \cdots & \cdots & \cdots & \cdots & 0 \\
\frac{\partial v_d^{12}}{\partial \boldsymbol{q_1}}^T & \frac{\partial v_d^{12}}{\partial \boldsymbol{t_1}}^T & 0 & \cdots & \cdots & \cdots & \cdots & \cdots & \cdots & 0 \\
\vdots & \vdots & \vdots & \vdots & \vdots & \vdots & \vdots & \vdots & \vdots & \vdots \\
\frac{\partial u_d^{1m}}{\partial \boldsymbol{q_1}}^T & \frac{\partial u_d^{1m}}{\partial \boldsymbol{t_1}}^T & 0 & \cdots & \cdots & \cdots & \cdots & \cdots & \cdots & 0 \\
\frac{\partial v_d^{1m}}{\partial \boldsymbol{q_1}}^T & \frac{\partial v_d^{1m}}{\partial \boldsymbol{t_1}}^T & 0 & \cdots & \cdots & \cdots & \cdots & \cdots & \cdots & 0 \\
0 & \cdots & 0 & \frac{\partial u_d^{21}}{\partial \boldsymbol{q_2}}^T & \frac{\partial u_d^{21}}{\partial \boldsymbol{t_2}}^T & 0 & \cdots & \cdots & \cdots & 0 \\
0 & \cdots & 0 & \frac{\partial v_d^{21}}{\partial \boldsymbol{q_2}}^T & \frac{\partial v_d^{21}}{\partial \boldsymbol{t_2}}^T & 0 & \cdots & \cdots & \cdots & 0 \\
\vdots & \vdots & \vdots & \vdots & \vdots & \vdots & \vdots & \vdots & \vdots & \vdots \\
\vdots & \vdots & \vdots & \vdots & \vdots & \vdots & \vdots & \vdots & \vdots & \vdots \\
0 & \cdots & \cdots & \cdots & \cdots & \cdots & \cdots & 0 & \frac{\partial u_d^{nm}}{\partial \boldsymbol{q_n}}^T & \frac{\partial u_d^{nm}}{\partial \boldsymbol{t_n}}^T \\
0 & \cdots & \cdots & \cdots & \cdots & \cdots & \cdots & 0 & \frac{\partial v_d^{nm}}{\partial \boldsymbol{q_n}}^T & \frac{\partial v_d^{nm}}{\partial \boldsymbol{t_n}}^T
\end{bmatrix} \tag{A.40}$$

Since all $6n + 10$ parameters are being estimated together, the high dimensionality of the nonlinear estimation process may often result in longer iterations for convergence. For this reason, and also for ease of troubleshooting, the uncoupled estimation procedure discussed in Appendix B is usually preferred for the estimation of the intrinsics, distortion coefficients and the extrinsics.

APPENDIX B

EXTRINSICS ESTIMATION USING NONLINEAR LEAST SQUARES - JACOBIAN

This section describes the derivation and form of the Jacobian Matrix for nonlinear optimization algorithm for the estimation of the extrinsics, described in Chapter 5. The extrinsics are estimation process continues iteratively till the relative change in the cost function between successive iterations is less than 10^{-6}.

$$\begin{bmatrix} x_d^{ij} \\ y_d^{ij} \\ 1 \end{bmatrix} = A^{-1} \begin{bmatrix} u_d^{ij} \\ v_d^{ij} \\ 1 \end{bmatrix} \tag{B.1}$$

The variables u_i' and v_i', as defined in Chapter 5, are the undistorted normalised camera frame coordinates. They are computed from the measured image plane coordinates using the Equations B.1 and Brown's distortion model Equation 5.2.

The rotation matrix, parameterised in terms of the CRPs, is shown below.

$$R = \frac{1}{1+q_1^2+q_2^2+q_3^2} \begin{bmatrix} 1+q_1^2-q_2^2-q_3^2 & 2(q_1q_2+q_3) & 2(q_1q_3-q_2) \\ 2(q_2q_1-q_3) & 1-q_1^2+q_2^2-q_3^2 & 2(q_2q_3+q_1) \\ 2(q_3q_1+q_2) & 2(q_2q_3-q_1) & 1-q_1^2-q_2^2+q_3^2 \end{bmatrix} \tag{B.2}$$

The vector $\boldsymbol{r}(\boldsymbol{q})$, which is the columns of R stacked to form a column vector will have the

following form.

$$\boldsymbol{r}(\boldsymbol{q}) = \frac{1}{1+q_1^2+q_2^2+q_3^2}\begin{bmatrix} 1+q_1^2-q_2^2-q_3^2 \\ 2(q_2q_1-q_3) \\ 2(q_3q_1+q_2) \\ 2(q_1q_2+q_3) \\ 1-q_1^2+q_2^2-q_3^2 \\ 2(q_2q_3-q_1) \\ 2(q_1q_3-q_2) \\ 2(q_2q_3+q_1) \\ 1-q_1^2-q_2^2+q_3^2 \end{bmatrix} \tag{B.3}$$

The CRP estimate $\hat{\boldsymbol{q}}$ must be found so as to satisfy the function expression $K\boldsymbol{r}(\hat{\boldsymbol{q}}) = \mathbf{0}$ as closely as possible.

Let us denote $K\boldsymbol{r}(\boldsymbol{q})$ as $\boldsymbol{f}(\boldsymbol{q})$. $K \in IR^{2mn\times 9}$ and $\boldsymbol{f}(\boldsymbol{q}) \in IR^{2mn\times 1}$ where m is the number of beacons and n is the number of frames.

If $f_i(\boldsymbol{q})$ denotes the ith row of $\boldsymbol{f}(\boldsymbol{q})$ and $K_{i,j}$ denotes the element of K in the ith row and jth column, we obtain.

$$\begin{aligned} f_i(\boldsymbol{q}) = (K_{i,1}-K_{i,5}-K_{i,9})q_1^2+(K_{i,5}-K_{i,1}-K_{i,9})q_2^2+(K_{i,9}-K_{i,5}-K_{i,1})q_3^2+2(K_{i,2}+K_{i,4})q_1q_2 \\ +2(K_{i,3}+K_{i,7})q_1q_3+2(K_{i,6}+K_{i,8})q_2q_3+2(K_{i,8}-K_{i,6})q_1+2(K_{i,3}-K_{i,7})q_2+2(K_{i,4}-K_{i,2})q_3 \\ +K_{i,1}+K_{i,5}+K_{i,9} \end{aligned} \tag{B.4}$$

We also know, from the development in Chapter 4, that $f_i(\boldsymbol{q}) = 0$.

The Jacobian Matrix (lets call it H_q) can be computed by individually evaluating the columns in the following manner.

$$\frac{\partial \boldsymbol{f}(\boldsymbol{q})}{\partial \boldsymbol{q}} = \begin{bmatrix} \frac{\partial \boldsymbol{f}}{\partial q_1} & \frac{\partial \boldsymbol{f}}{\partial q_2} & \frac{\partial \boldsymbol{f}}{\partial q_3} \end{bmatrix} \tag{B.5}$$

$$\begin{aligned}
\frac{\partial \boldsymbol{f}}{\partial q_1} &= 2(K_{i,1} - K_{i,5} - K_{i,9})q_1 + 2(K_{i,2} + K_{i,4})q_2 + 2(K_{i,3} + K_{i,7})q_3 + 2(K_{i,8} - K_{i,6}) \\
\frac{\partial \boldsymbol{f}}{\partial q_2} &= 2(K_{i,5} - K_{i,1} - K_{i,9})q_2 + 2(K_{i,2} + K_{i,4})q_1 + 2(K_{i,6} + K_{i,8})q_3 + 2(K_{i,3} - K_{i,7}) \\
\frac{\partial \boldsymbol{f}}{\partial q_3} &= 2(K_{i,9} - K_{i,5} - K_{i,1})q_3 + 2(K_{i,3} + K_{i,7})q_1 + 2(K_{i,6} + K_{i,8})q_2 + 2(K_{i,4} - K_{i,2})
\end{aligned} \tag{B.6}$$

H_q is evaluated at the current estimates of the CRPs and the process continues iteratively till convergence is reached.

The translation vectors for each frame are then computed using the linear algebra problem shown in Chapter 4.

$$\boldsymbol{t} = -(A_2^T A_2)^{-1} A_2^T A_1 \boldsymbol{r}(\boldsymbol{q}) \tag{B.7}$$

Here, A_1 and A_2 depend on the inertial frame coordinates and the undistorted normalised camera frame coordinates.

APPENDIX C

GEOMETRIC DISTORTION INCORPORATED ESTIMATION

This section discusses the derivation and form of the Jacobian Matrix for the Geometric Distortion Incorporated Estimation algorithm. The algorithm itself is discussed in Chapter 4.

The Geometric Distortion Incorporated Estimation procedure follows the Combined Estimation algorithm for the complete optimization of the intrinsic parameters, distortion coefficients and the extrinsic parameters. The key difference is the incorporation of the requisite expressions pertinent to the geometric distortion model.

The rigid body motion and pinhole projection model equations remain the same as in the Combined Estimation procedure with Brown's Distortion Model.

$$\boldsymbol{p_i^C} = R_j \boldsymbol{p_i^W} + \boldsymbol{t_j} \tag{C.1}$$

where $\boldsymbol{p_i^W} = \begin{bmatrix} x_i^W & y_i^W & z_i^W \end{bmatrix}^T$ is the inertial frame coordinate of the ith beacon, $\boldsymbol{p_i^C} = \begin{bmatrix} x_i^C & y_i^C & z_i^C \end{bmatrix}^T$ is the 3D camera frame coordinate of $\boldsymbol{p_i^W}$, the rotation matrix and translation vector for the jth frame are written as $R_j = \begin{bmatrix} r_{11} & r_{12} & r_{13} \\ r_{21} & r_{22} & r_{23} \\ r_{31} & r_{32} & r_{33} \end{bmatrix}$ and $\boldsymbol{t_j} = \begin{bmatrix} t_1 \\ t_2 \\ t_3 \end{bmatrix}$

The undistorted normalised camera frame coordinates $\begin{bmatrix} x_u & y_u \end{bmatrix}^T$ are obtained by normalising $\boldsymbol{p_i^C}$ by z_i^C. We thus obtain the relations

$$\begin{aligned} x_u &= \frac{x_i^C}{z_i^c} \\ y_u &= \frac{y_i^C}{z_i^C} \end{aligned} \tag{C.2}$$

In terms of the elements of the rotation matrix and translation vector, x_u and y_u can be described

as follows.

$$\begin{aligned} x_u &= \frac{r_{11}x_i^W + r_{12}y_i^W + t_1}{r_{31}x_i^W + r_{32}y_i^W + t_3} \\ y_u &= \frac{r_{21}x_i^W + r_{22}y_i^W + t_2}{r_{31}x_i^W + r_{32}y_i^W + t_3} \end{aligned} \tag{C.3}$$

Using the Geometric distortion model, the distorted normalised camera space coordinates can be computed based on the estimate of the distortion coefficients $\hat{\boldsymbol{k}_{\boldsymbol{x}}} = \begin{bmatrix} k_{x1} & k_{x2} & k_{x3} \end{bmatrix}^T$ and $\hat{\boldsymbol{k}_{\boldsymbol{y}}} = \begin{bmatrix} k_{y1} & k_{y2} & k_{y3} \end{bmatrix}^T$

Recall that the distortion functions were defined in Chapter 4 in the following manner.

$$\begin{aligned} x_d &= x_u f(r, \boldsymbol{k_x}) \\ y_d &= y_u f(r, \boldsymbol{k_y}) \end{aligned} \tag{C.4}$$

where

$$f(r, \boldsymbol{k}) = \frac{1 + k_1 r^2}{1 + k_2 r + k_3 r^2}$$

and $r^2 = x_u^2 + y_u^2$.

Note that two different sets of distortion coefficients have been defined for the two basis directions in the image plane.

Here, $r^2 = x_u^2 + y_u^2$.

The distorted image plane coordinates $\begin{bmatrix} x_d & y_d \end{bmatrix}^T$ are then obtained using the intrinsic camera matrix $A = \begin{bmatrix} \alpha & c & u_0 \\ 0 & \beta & v_0 \\ 0 & 0 & 1 \end{bmatrix}$.

Here, α and β are the focal lengths in the directions of the two basis vectors of the image plane, c is the skew coefficient and $\begin{bmatrix} u_0 & v_0 \end{bmatrix}^T$ is the principal offset.

The distorted image plane coordinates are computed as follows.

$$\begin{bmatrix} u_d \\ v_d \\ 1 \end{bmatrix} = A \begin{bmatrix} x_d \\ y_d \\ 1 \end{bmatrix} \tag{C.5}$$

The estimated distorted image plane coordinates of the ith beacon coordinate in the jth frame $\hat{\boldsymbol{m}}_{\boldsymbol{ij}} = \begin{bmatrix} u_d & v_d \end{bmatrix}$ are computed and the $2mn$ equations are then stacked to create a vector $\hat{\boldsymbol{m}}$, where m is the number of beacons and n is the number of frames.

Then, a nonlinear least squares formulation is employed to estimate the $6n + 11$ parameters (11 intrinsic parameters, including the distortion coefficients and $6n$ extrinsic parameters must be estimated, given that the rotation matrix is parameterized in terms of the CRPs).

The nonlinear least squares is implemented as the Levenberg Marquardt [28] algorithm and is carried out using the $lsqnonlin$ function in MatLab. The formal problem statement is written as follows.

$$min_{\boldsymbol{x}} \boldsymbol{e}^T W \boldsymbol{e} + \lambda \Delta \boldsymbol{x}^T W_y \Delta \boldsymbol{x} \tag{C.6}$$

where $\boldsymbol{e} = \tilde{\boldsymbol{m}} - \hat{\boldsymbol{m}}$, W is a weight matrix taken as $I_{2mnx2mn}$, W_y is a weight matrix taken as $I_{6n+11 \times 6n+11}$, $\tilde{\boldsymbol{m}}$ is the vector of the measured image plane coordinates, stacked in a similar manner to $\hat{\boldsymbol{m}}$ and $\boldsymbol{x} = \begin{bmatrix} \boldsymbol{x_{int}} & \boldsymbol{x_{ext}} \end{bmatrix}^T$ is the vector of parameters to estimate, $\boldsymbol{x_{int}} = \begin{bmatrix} \alpha & \beta & c & u_0 & v_0 & k_1 & k_2 & k_3 & p_1 & p_2 \end{bmatrix}^T$ and $\boldsymbol{x_{ext}} = \begin{bmatrix} q_{1i} & q_{2i} & q_{3i} & t_{1i} & t_{2i} & t_{3i} \end{bmatrix}^T$
$i = 1, 2, 3, 4.....n$

The nonlinear least squares is implemented in accordance with the Gaussian Least Squares Differential Correction (GLSDC) approach outlined in the Crassidis and Junkins[27].

The initial guess for the parameters is taken to be the estimated intrinsics and extrinsics from the Homography algorithm in Zhang[1], with the distortion coefficients initialized as zeros. As per

the GLSDC algorithm, the differential correction for the parameters is given by

$$\Delta x = (H^T W H)^{-1} H^T W \boldsymbol{e} \tag{C.7}$$

where $H = \frac{\partial \boldsymbol{f}}{\partial \boldsymbol{x}\, \boldsymbol{x_c}}$ is the Jacobian matrix evaluated at the current estimate of the parameters.

$H \in IR^{2mn \times (6n+10)}$

Convergence is said to be achieved when the change in the cost function J for successive iterations is less than 10^{-6}. This statement can be written mathematically as

$$\left| \frac{J_{k+1} - J_k}{J_{k+1}} \right| < 10^{-6} \tag{C.8}$$

where $J_k = \boldsymbol{e_k}^T W \boldsymbol{e_k} + \lambda \Delta \boldsymbol{x_k}^T W_y \Delta \boldsymbol{x_k}$

Given the standard deviation of the measured image plane coordinates, the covariance matrix for the measurement error vector R_y can be constructed. This covariance matrix can be utilized to compute the parameter error covariance. Starting from Equation C.7, the steps outlined by Equation C.9 can be employed to compute the state error covariance.

$$\begin{aligned}
\delta \boldsymbol{x} \delta \boldsymbol{x}^T &= (H^T W H + \lambda W_y)^{-1} H^T W \delta \boldsymbol{y} \delta \boldsymbol{y}^T W^T H (H^T W H + \lambda W_y)^{-T} \\
E[\delta \boldsymbol{x} \delta \boldsymbol{x}^T] &= E[(H^T W H + \lambda W_y)^{-1} H^T W \delta \boldsymbol{y} \delta \boldsymbol{y}^T W^T H (H^T W H + \lambda W_y)^{-T}] \\
E[\delta \boldsymbol{x} \delta \boldsymbol{x}^T] &= (H^T W H + \lambda W_y)^{-1} H^T W E[\delta \boldsymbol{y} \delta \boldsymbol{y}^T] W^T H (H^T W H + \lambda W_y)^{-T} \\
E[\delta \boldsymbol{x} \delta \boldsymbol{x}^T] &= (H^T W H + \lambda W_y)^{-1} H^T W R_y W^T H (H^T W H + \lambda W_y)^{-T}
\end{aligned} \tag{C.9}$$

Here, H is the Jacoban Matrix computed at the converged states, W is the weighting matrix which is taken as $I^{2mn \times 2mn}$, m being the number of beacons and n being the number of well conditioned frames.

However, since λ is not readily available, the Gauss-Newton equivalent of the expression for

$E[\delta \boldsymbol{x} \delta \boldsymbol{x}^T]$ is used which is

$$E[\delta \boldsymbol{x} \delta \boldsymbol{x}^T] = (H^T W H)^{-1} H^T W R_y W^T H (H^T W H)^{-T}$$

No significant error will be incurred with the above assumption assuming that λ is sufficiently small. Using $E[\delta \boldsymbol{x} \delta \boldsymbol{x}^T]$ the uncertainty bounds on each parameter can be estimated as $\sigma_{x,i} = 3\sqrt{R_{ii}}$. In the first 3 experimental datasets, the uncertainty bounds on the intrinsic parameters are computed using the average of the measured standard deviations for each beacon from Tables 3.4 and 3.5.

The various partials involved in the computation of the Jacobian Matrix at an estimate of the parameters are shown below.

We first look at the computation of the Jacobian with respect to the intrinsics and distortion coefficients.

The partials with respect to the intrinsic parameters remain the same as in the Combined Estimation procedure, shown in Equations A.10 and A.11.

We know that the distorted image plane coordinates are related to the distorted normalised camera coordinates according to Equations C.10 andC.11.

$$\begin{aligned}
\frac{\partial u_d}{\partial k_{x1}} &= \alpha \frac{\partial x_d}{\partial k_{x1}} + c \frac{\partial y_d}{\partial k_{x1}} \\
\frac{\partial u_d}{\partial k_{x2}} &= \alpha \frac{\partial x_d}{\partial k_{x2}} + c \frac{\partial y_d}{\partial k_{x2}} \\
\frac{\partial u_d}{\partial k_{x3}} &= \alpha \frac{\partial x_d}{\partial k_{x3}} + c \frac{\partial y_d}{\partial k_{x3}} \\
\frac{\partial u_d}{\partial k_{y1}} &= \alpha \frac{\partial x_d}{\partial k_{y1}} + c \frac{\partial y_d}{\partial k_{y1}} \\
\frac{\partial u_d}{\partial k_{y2}} &= \alpha \frac{\partial x_d}{\partial k_{y2}} + c \frac{\partial y_d}{\partial k_{y2}} \\
\frac{\partial u_d}{\partial k_{y3}} &= \alpha \frac{\partial x_d}{\partial k_{y3}} + c \frac{\partial y_d}{\partial k_{y3}}
\end{aligned} \tag{C.10}$$

$$
\begin{aligned}
\frac{\partial v_d}{\partial k_{x1}} &= \beta \frac{\partial y_d}{\partial k_{x1}} \\
\frac{\partial v_d}{\partial k_{x2}} &= \beta \frac{\partial y_d}{\partial k_{x2}} \\
\frac{\partial v_d}{\partial k_{x3}} &= \beta \frac{\partial y_d}{\partial k_{x3}} \\
\frac{\partial v_d}{\partial k_{y1}} &= \beta \frac{\partial y_d}{\partial k_{y1}} \\
\frac{\partial v_d}{\partial k_{y2}} &= \beta \frac{\partial y_d}{\partial k_{y2}} \\
\frac{\partial v_d}{\partial k_{y3}} &= \beta \frac{\partial y_d}{\partial k_{y3}}
\end{aligned}
\tag{C.11}
$$

The partials of x_d and y_d with respect to the distortion coefficients can be computed using Equation C.4.

$$
\begin{aligned}
\frac{\partial x_d}{\partial k_{x1}} &= x_u \left(\frac{r^2}{1 + k_{x2} r + k_{x3} r^2} \right) \\
\frac{\partial x_d}{\partial k_{x2}} &= -x_u \left(\frac{(1 + k_{x1} r^2) r}{(1 + k_{x2} r + k_{x3} r^2)^2} \right) \\
\frac{\partial x_d}{\partial k_{x3}} &= -x_u \left(\frac{(1 + k_{x1} r^2) r^2}{(1 + k_{x2} r + k_{x3} r^2)^2} \right) \\
\frac{\partial x_d}{\partial k_{y1}} &= 0 \\
\frac{\partial x_d}{\partial k_{y2}} &= 0 \\
\frac{\partial x_d}{\partial k_{y3}} &= 0
\end{aligned}
\tag{C.12}
$$

$$
\begin{aligned}
\frac{\partial y_d}{\partial k_{y1}} &= y_u\left(\frac{r^2}{1+k_{y2}r+k_{y3}r^2}\right) \\
\frac{\partial y_d}{\partial k_{y2}} &= -y_u\left(\frac{(1+k_{y1}r^2)r}{(1+k_{y2}r+k_{y3}r^2)^2}\right) \\
\frac{\partial y_d}{\partial k_{y3}} &= -y_u\left(\frac{(1+k_{y1}r^2)r^2}{(1+k_{y2}r+k_{y3}r^2)^2}\right) \\
\frac{\partial y_d}{\partial k_{x1}} &= 0 \\
\frac{\partial y_d}{\partial k_{x2}} &= 0 \\
\frac{\partial y_d}{\partial k_{x3}} &= 0
\end{aligned}
\tag{C.13}
$$

These can be plugged back in to the Equations C.10 and C.11.

The computation of the Jacobian with respect to the extrinsics follows the same procedure as that outlined in Appendix A. The only difference is the partial differential expressions of the distorted normalised camera coordinates with respect to the undistorted normalised camera coordinates, provided in Equation C.14.

$$
\begin{aligned}
\frac{\partial x_d}{\partial x_u} &= \frac{1+k_{x1}r^2}{1+k_{x2}r+k_{x3}r^2} + x_u\left(\frac{1+2k_{x1}r\frac{\partial r}{\partial x_u}}{1+k_{x2}r+k_{x3}r^2} - \frac{(1+k_{x1}r^2)(k_{x2}\frac{\partial r}{\partial x_u}+2k_{x3}r\frac{\partial r}{\partial x_u})}{(1+k_{x2}r+k_{x3}r^2)^2}\right) \\
\frac{\partial x_d}{\partial y_u} &= x_u\left(\frac{1+2k_{x1}r\frac{\partial r}{\partial y_u}}{1+k_{x2}r+k_{x3}r^2} - \frac{(1+k_{x1}r^2)(k_{x2}\frac{\partial r}{\partial y_u}+2k_{x3}r\frac{\partial r}{\partial y_u})}{(1+k_{x2}r+k_{x3}r^2)^2}\right) \\
\frac{\partial y_d}{\partial x_u} &= y_u\left(\frac{1+2k_{y1}r\frac{\partial r}{\partial x_u}}{1+k_{y2}r+k_{y3}r^2} - \frac{(1+k_{y1}r^2)(k_{y2}\frac{\partial r}{\partial x_u}+2k_{y3}r\frac{\partial r}{\partial x_u})}{(1+k_{y2}r+k_{y3}r^2)^2}\right) \\
\frac{\partial y_d}{\partial y_u} &= \frac{1+k_{y1}r^2}{1+k_{y2}r+k_{y3}r^2} + y_u\left(\frac{1+2k_{y1}r\frac{\partial r}{\partial y_u}}{1+k_{y2}r+k_{y3}r^2} - \frac{(1+k_{y1}r^2)(k_{y2}\frac{\partial r}{\partial y_u}+2k_{y3}r\frac{\partial r}{\partial y_u})}{(1+k_{y2}r+k_{y3}r^2)^2}\right)
\end{aligned}
\tag{C.14}
$$

The partials of r with respect to x_u and y_u can be computed using the relation $r^2 = x_u^2 + y_u^2$.

$$\begin{aligned} \frac{\partial r}{\partial x_u} &= \frac{x_u}{r} \\ \frac{\partial r}{\partial y_u} &= \frac{y_u}{r} \end{aligned} \tag{C.15}$$

We now have all the ingredients required to compute the full Jacobian Matrix H of the distorted image frame coordinates with respect to the intrinsics, distortion coefficients and the extrinsics.

The form of the H matrix can be described in the following manner.

$$H = \begin{bmatrix} H_{int} & H_{ext} \end{bmatrix} \tag{C.16}$$

where H_{int} is the portion of the Jacobian matrix strictly associated with the differential corrections in the intrinsics and the distortion coefficients, whereas H_{ext} is the portion of the Jacobian matrix strictly associated with the differential corrections in the extrinsics.

As a result, $H_{int} \in I\!R^{2mn \times 11}$ and $H_{ext} \in I\!R^{2mn \times 6n}$.

$$H_{int} = \begin{bmatrix}
\frac{\partial u_d^{11}}{\partial \alpha} & \frac{\partial u_d^{11}}{\partial \beta} & \frac{\partial u_d^{11}}{\partial c} & \frac{\partial u_d^{11}}{\partial u_0} & \frac{\partial u_d^{11}}{\partial v_0} & \frac{\partial u_d^{11}}{\partial k_{x1}} & \frac{\partial u_d^{11}}{\partial k_{x2}} & \frac{\partial u_d^{11}}{\partial k_{x3}} & \frac{\partial u_d^{11}}{\partial k_{y1}} & \frac{\partial u_d^{11}}{\partial k_{y2}} & \frac{\partial u_d^{11}}{\partial k_{y3}} \\
\frac{\partial v_d^{11}}{\partial \alpha} & \frac{\partial v_d^{11}}{\partial \beta} & \frac{\partial v_d^{11}}{\partial c} & \frac{\partial v_d^{11}}{\partial u_0} & \frac{\partial v_d^{11}}{\partial v_0} & \frac{\partial v_d^{11}}{\partial k_{x1}} & \frac{\partial v_d^{11}}{\partial k_{x2}} & \frac{\partial v_d^{11}}{\partial k_{x3}} & \frac{\partial v_d^{11}}{\partial k_{y1}} & \frac{\partial v_d^{11}}{\partial k_{y2}} & \frac{\partial v_d^{11}}{\partial k_{y3}} \\
\frac{\partial u_d^{12}}{\partial \alpha} & \frac{\partial u_d^{12}}{\partial \beta} & \frac{\partial u_d^{12}}{\partial c} & \frac{\partial u_d^{12}}{\partial u_0} & \frac{\partial u_d^{12}}{\partial v_0} & \frac{\partial u_d^{12}}{\partial k_{x1}} & \frac{\partial u_d^{12}}{\partial k_{x2}} & \frac{\partial u_d^{12}}{\partial k_{x3}} & \frac{\partial u_d^{12}}{\partial k_{y1}} & \frac{\partial u_d^{12}}{\partial k_{y2}} & \frac{\partial u_d^{12}}{\partial k_{y3}} \\
\frac{\partial v_d^{12}}{\partial \alpha} & \frac{\partial v_d^{12}}{\partial \beta} & \frac{\partial v_d^{12}}{\partial c} & \frac{\partial v_d^{12}}{\partial u_0} & \frac{\partial v_d^{12}}{\partial v_0} & \frac{\partial v_d^{12}}{\partial k_{x1}} & \frac{\partial v_d^{12}}{\partial k_{x2}} & \frac{\partial v_d^{12}}{\partial k_{x3}} & \frac{\partial v_d^{12}}{\partial k_{y1}} & \frac{\partial v_d^{12}}{\partial k_{y2}} & \frac{\partial v_d^{12}}{\partial k_{y3}} \\
\vdots & \vdots & \vdots & \vdots & \vdots & \vdots & \vdots & \vdots & \vdots & \vdots & \vdots \\
\frac{\partial u_d^{1m}}{\partial \alpha} & \frac{\partial u_d^{1m}}{\partial \beta} & \frac{\partial u_d^{1m}}{\partial c} & \frac{\partial u_d^{1m}}{\partial u_0} & \frac{\partial u_d^{1m}}{\partial v_0} & \frac{\partial u_d^{1m}}{\partial k_{x1}} & \frac{\partial u_d^{1m}}{\partial k_{x2}} & \frac{\partial u_d^{1m}}{\partial k_{x3}} & \frac{\partial u_d^{1m}}{\partial k_{y1}} & \frac{\partial u_d^{1m}}{\partial k_{y2}} & \frac{\partial u_d^{1m}}{\partial k_{y3}} \\
\frac{\partial v_d^{1m}}{\partial \alpha} & \frac{\partial v_d^{1m}}{\partial \beta} & \frac{\partial v_d^{1m}}{\partial c} & \frac{\partial v_d^{1m}}{\partial u_0} & \frac{\partial v_d^{1m}}{\partial v_0} & \frac{\partial v_d^{1m}}{\partial k_{x1}} & \frac{\partial v_d^{1m}}{\partial k_{x2}} & \frac{\partial v_d^{1m}}{\partial k_{x3}} & \frac{\partial v_d^{1m}}{\partial k_{y1}} & \frac{\partial v_d^{1m}}{\partial k_{y2}} & \frac{\partial v_d^{1m}}{\partial k_{y3}} \\
\frac{\partial u_d^{21}}{\partial \alpha} & \frac{\partial u_d^{21}}{\partial \beta} & \frac{\partial u_d^{21}}{\partial c} & \frac{\partial u_d^{21}}{\partial u_0} & \frac{\partial u_d^{21}}{\partial v_0} & \frac{\partial u_d^{21}}{\partial k_{x1}} & \frac{\partial u_d^{21}}{\partial k_{x2}} & \frac{\partial u_d^{21}}{\partial k_{x3}} & \frac{\partial u_d^{21}}{\partial k_{y1}} & \frac{\partial u_d^{21}}{\partial k_{y2}} & \frac{\partial u_d^{21}}{\partial k_{y3}} \\
\frac{\partial v_d^{21}}{\partial \alpha} & \frac{\partial v_d^{21}}{\partial \beta} & \frac{\partial v_d^{21}}{\partial c} & \frac{\partial v_d^{21}}{\partial u_0} & \frac{\partial v_d^{21}}{\partial v_0} & \frac{\partial v_d^{21}}{\partial k_{x1}} & \frac{\partial v_d^{21}}{\partial k_{x2}} & \frac{\partial v_d^{21}}{\partial k_{x3}} & \frac{\partial v_d^{21}}{\partial k_{y1}} & \frac{\partial v_d^{21}}{\partial k_{y2}} & \frac{\partial v_d^{21}}{\partial k_{y3}} \\
\vdots & \vdots & \vdots & \vdots & \vdots & \vdots & \vdots & \vdots & \vdots & \vdots & \vdots \\
\vdots & \vdots & \vdots & \vdots & \vdots & \vdots & \vdots & \vdots & \vdots & \vdots & \vdots \\
\frac{\partial u_d^{nm}}{\partial \alpha} & \frac{\partial u_d^{nm}}{\partial \beta} & \frac{\partial u_d^{nm}}{\partial c} & \frac{\partial u_d^{nm}}{\partial u_0} & \frac{\partial u_d^{nm}}{\partial v_0} & \frac{\partial u_d^{nm}}{\partial k_{x1}} & \frac{\partial u_d^{nm}}{\partial k_{x2}} & \frac{\partial u_d^{nm}}{\partial k_{x3}} & \frac{\partial u_d^{nm}}{\partial k_{y1}} & \frac{\partial u_d^{nm}}{\partial k_{y2}} & \frac{\partial u_d^{nm}}{\partial k_{y3}} \\
\frac{\partial v_d^{nm}}{\partial \alpha} & \frac{\partial v_d^{nm}}{\partial \beta} & \frac{\partial v_d^{nm}}{\partial c} & \frac{\partial v_d^{nm}}{\partial u_0} & \frac{\partial v_d^{nm}}{\partial v_0} & \frac{\partial v_d^{nm}}{\partial k_{x1}} & \frac{\partial v_d^{nm}}{\partial k_{x2}} & \frac{\partial v_d^{nm}}{\partial k_{x3}} & \frac{\partial v_d^{nm}}{\partial k_{y1}} & \frac{\partial v_d^{nm}}{\partial k_{y2}} & \frac{\partial v_d^{nm}}{\partial k_{y3}}
\end{bmatrix} \tag{C.17}$$

Here, n is the number of frames and m is the number of beacons.

$$H_{ext} \in IR^{2mn \times 6n}$$

H_{ext} has the same form as that in Appendix A.

$$H_{ext} = \begin{bmatrix}
\frac{\partial u_d^{11}}{\partial \boldsymbol{q_1}}^T & \frac{\partial u_d^{11}}{\partial \boldsymbol{t_1}}^T & 0 & \cdots & \cdots & \cdots & \cdots & \cdots & \cdots & 0 \\
\frac{\partial v_d^{11}}{\partial \boldsymbol{q_1}}^T & \frac{\partial v_d^{11}}{\partial \boldsymbol{t_1}}^T & 0 & \cdots & \cdots & \cdots & \cdots & \cdots & \cdots & 0 \\
\frac{\partial u_d^{12}}{\partial \boldsymbol{q_1}}^T & \frac{\partial u_d^{12}}{\partial \boldsymbol{t_1}}^T & 0 & \cdots & \cdots & \cdots & \cdots & \cdots & \cdots & 0 \\
\frac{\partial v_d^{12}}{\partial \boldsymbol{q_1}}^T & \frac{\partial v_d^{12}}{\partial \boldsymbol{t_1}}^T & 0 & \cdots & \cdots & \cdots & \cdots & \cdots & \cdots & 0 \\
\vdots & \vdots & \vdots & \vdots & \vdots & \vdots & \vdots & \vdots & \vdots & \vdots \\
\frac{\partial u_d^{1m}}{\partial \boldsymbol{q_1}}^T & \frac{\partial u_d^{1m}}{\partial \boldsymbol{t_1}}^T & 0 & \cdots & \cdots & \cdots & \cdots & \cdots & \cdots & 0 \\
\frac{\partial v_d^{1m}}{\partial \boldsymbol{q_1}}^T & \frac{\partial v_d^{1m}}{\partial \boldsymbol{t_1}}^T & 0 & \cdots & \cdots & \cdots & \cdots & \cdots & \cdots & 0 \\
0 & \cdots & 0 & \frac{\partial u_d^{21}}{\partial \boldsymbol{q_2}}^T & \frac{\partial u_d^{21}}{\partial \boldsymbol{t_2}}^T & 0 & \cdots & \cdots & \cdots & 0 \\
0 & \cdots & 0 & \frac{\partial v_d^{21}}{\partial \boldsymbol{q_2}}^T & \frac{\partial v_d^{21}}{\partial \boldsymbol{t_2}}^T & 0 & \cdots & \cdots & \cdots & 0 \\
\vdots & \vdots & \vdots & \vdots & \vdots & \vdots & \vdots & \vdots & \vdots & \vdots \\
\vdots & \vdots & \vdots & \vdots & \vdots & \vdots & \vdots & \vdots & \vdots & \vdots \\
0 & \cdots & \cdots & \cdots & \cdots & \cdots & \cdots & 0 & \frac{\partial u_d^{nm}}{\partial \boldsymbol{q_n}}^T & \frac{\partial u_d^{nm}}{\partial \boldsymbol{t_n}}^T \\
0 & \cdots & \cdots & \cdots & \cdots & \cdots & \cdots & 0 & \frac{\partial v_d^{nm}}{\partial \boldsymbol{q_n}}^T & \frac{\partial v_d^{nm}}{\partial \boldsymbol{t_n}}^T
\end{bmatrix} \tag{C.18}$$

Since all $6n + 11$ parameters are being estimated together, the high dimensionality of the nonlinear estimation process may often result in longer iterations for convergence.

APPENDIX D

EXTRINSIC PROJECTIONS FOR ALL DATASETS

The extrinsic projections of all the well-conditioned frames for all four datasets are provided in this section. They were separated from the main text to focus on the results and for aesthetic purposes. For each dataset, the frames progress sequentially from the top left and end at the bottom right. For reference the inertial frame is shown at the bottom of each projection.

Figure D.1: Extrinsic Projections as computed using the Homography optimization algorithm corresponding to each image plane projection shown in Figure 6.2 for Dataset 1. The distances are provided in inches. Brown's distortion is employed in the optimization process. The frames are ordered from the top left to the bottom right.

Figure D.2: Extrinsic Projections as computed using the Homography optimization algorithm corresponding to each image plane projection shown in Figure 6.2 for Dataset 1. The distances are provided in inches. Geometric distortion is employed in the optimization process. The frames are ordered from the top left to the bottom right.

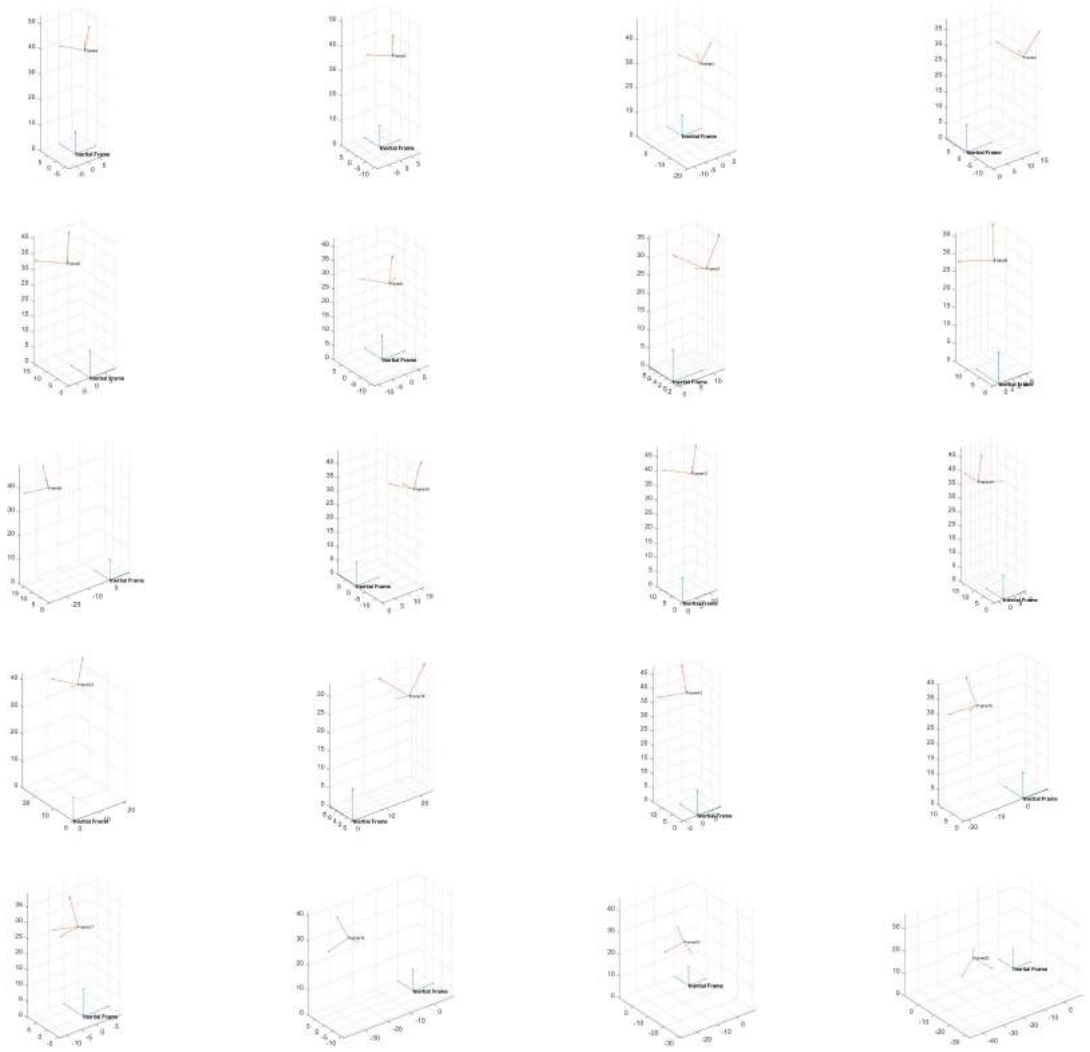

Figure D.3: Extrinsic Projections as computed using the Homography optimization algorithm corresponding to each image plane projection shown in Figure 6.10 for Dataset 2. The distances are provided in inches. Brown distortion is employed in the optimization process. The frames are ordered from the top left to the bottom right.

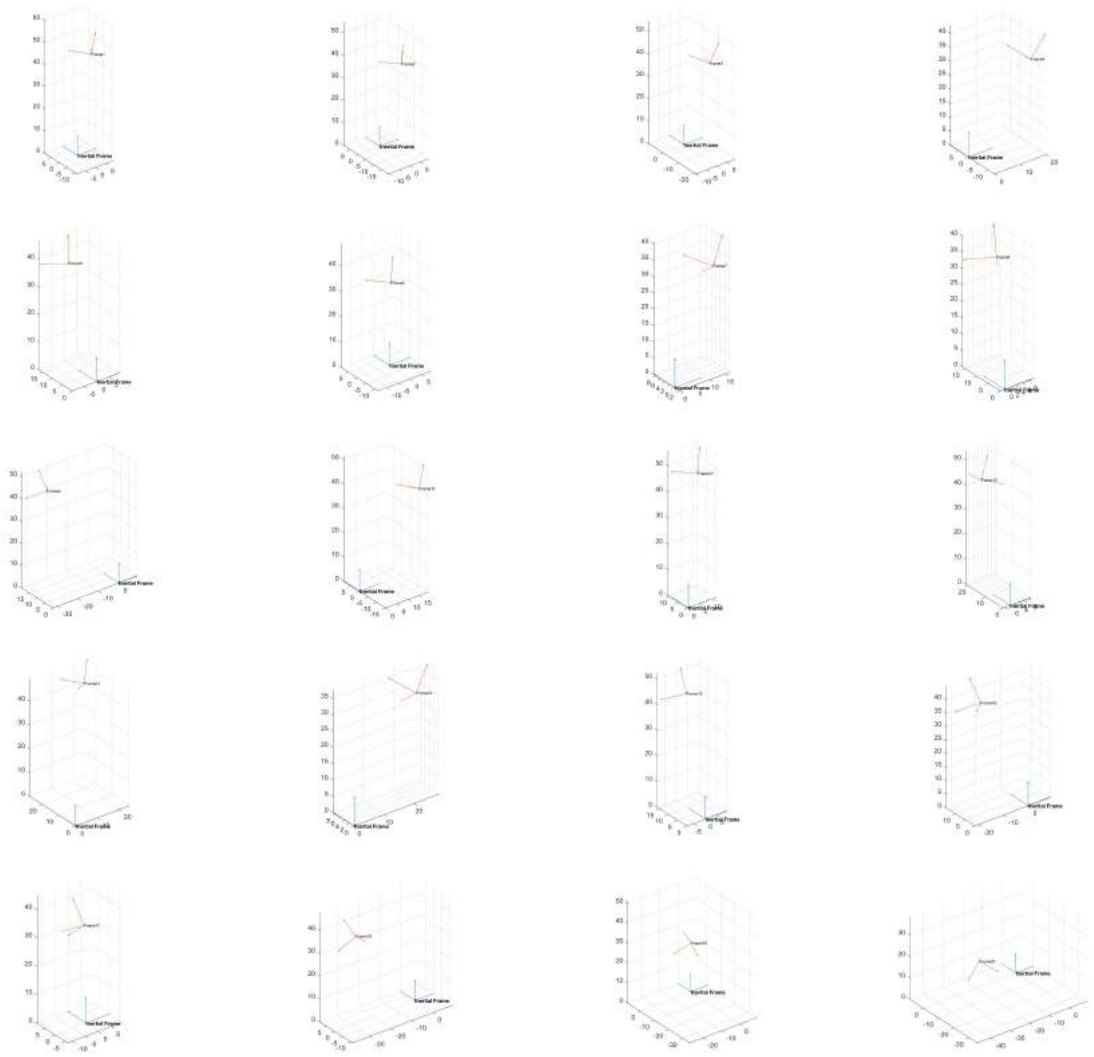

Figure D.4: Extrinsic Projections as computed using the Homography optimization algorithm corresponding to each image plane projection shown in Figure 6.10 for Dataset 2. The distances are provided in inches. Geometric distortion is employed in the optimization process. The frames are ordered from the top left to the bottom right.

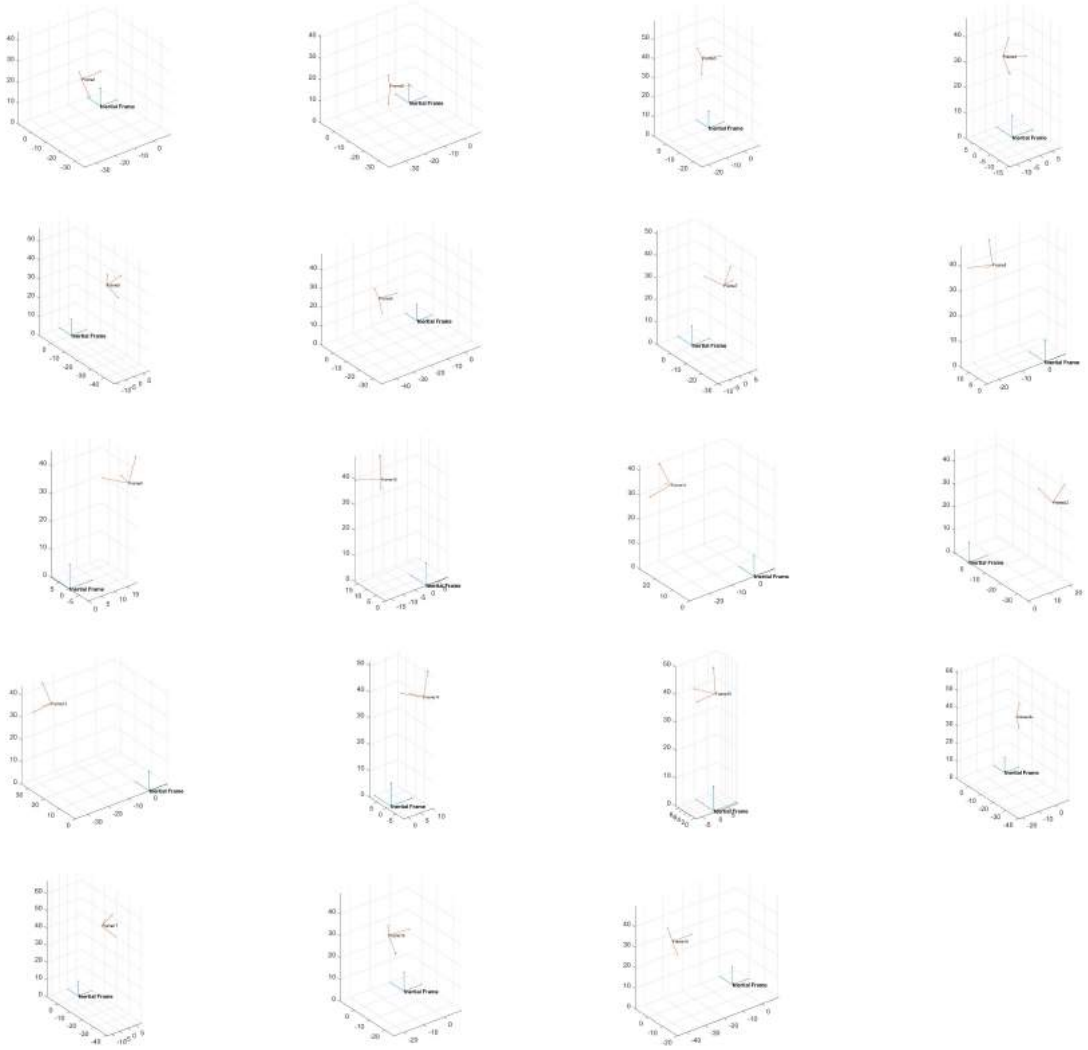

Figure D.5: Extrinsic Projections as computed using the Homography optimization algorithm corresponding to each image plane projection shown in Figure 6.17 for Dataset 3. The distances are provided in inches. Brown's distortion is employed in the optimization process. The frames are ordered from the top left to the bottom right.

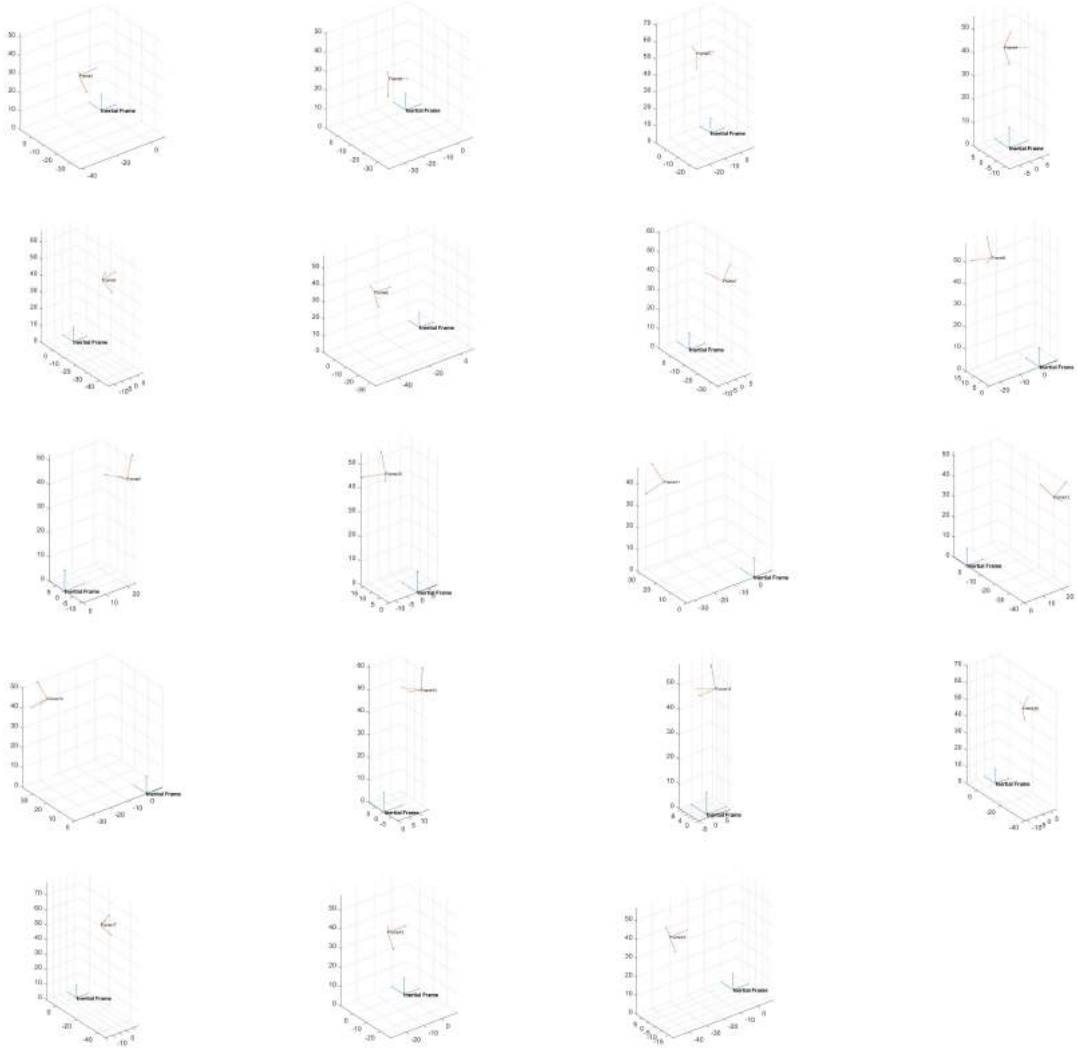

Figure D.6: Extrinsic Projections as computed using the Homography optimization algorithm corresponding to each image plane projection shown in Figure 6.17 for Dataset 3. The distances are provided in inches. Geometric distortion is employed in the optimization process. The frames are ordered from the top left to the bottom right.